INFORMATION TO USERS

This manuscript has been reproduced from the microfilm master. UMI films the text directly from the original or copy submitted. Thus, some thesis and dissertation copies are in typewriter face, while others may be from any type of computer printer.

The quality of this reproduction is dependent upon the quality of the copy submitted. Broken or indistinct print, colored or poor quality illustrations and photographs, print bleedthrough, substandard margins, and improper alignment can adversely affect reproduction.

In the unlikely event that the author did not send UMI a complete manuscript and there are missing pages, these will be noted. Also, if unauthorized copyright material had to be removed, a note will indicate the deletion.

Oversize materials (e.g., maps, drawings, charts) are reproduced by sectioning the original, beginning at the upper left-hand corner and continuing from left to right in equal sections with small overlaps. Each original is also photographed in one exposure and is included in reduced form at the back of the book.

Photographs included in the original manuscript have been reproduced xerographically in this copy. Higher quality 6" x 9" black and white photographic prints are available for any photographs or illustrations appearing in this copy for an additional charge. Contact UMI directly to order.

UMI

A Bell & Howell Information Company
300 North Zeeb Road, Ann Arbor MI 48106-1346 USA
313/761-4700 800/521-0600

FUNCTIONAL ORGANIZATION AND NEUROMODULATION OF ENTORHINAL CORTEX LAYER II NEURONS

by
Ruby Klink
Department of Neurology and Neurosurgery
McGill University, Montreal
September, 1996

A thesis submitted to the Faculty of
Graduate Studies and Research
in partial fulfilment of the requirements
for the degree of
Doctor of Philosophy

TABLE OF CONTENTS

ABSTRACT

Morphological and electrophysical properties of layer II neurons from the medial entorhinal cortex were investigated in a rat brain slice preparation to enhance our understanding of the role the entorhinal cortex plays in the gating of afferent stimuli to the hippocampal formation.

Morphological characterization revealed that layer II projection neurons fell into two distinct categories. 65% of neurons were identified as the stellate cells described previously. The remaining 35% had, for the most, a pyramidal-like morphology, and were referred to as non-stellates.

Electrophysiological characterization revealed that stellates and non-stellates had distinct electroresponsive properties. Notably, stellates, upon d.c. depolarization, generated subthreshold, sinusoidal-like, membrane potential oscillations at a mean frequency of 8.6 Hz and a 1-3 Hz repetitive bursting pattern, referred to as clustering. Non-stellates, when d.c. depolarized, never generated subthreshold oscillations nor spike clusters; instead they readily went into tonic firing.

Investigation of the main ionic mechanisms endowing stellates and non-stellates with their differential electroresponsiveness revealed that stellates exclusively possessed a fast, low threshold, Ba^{2+}-sensitive outward rectifier, which, in interplay with the persistent Na^{+} conductance, generated the membrane potential oscillations.

The cholinergic agonist carbachol caused a depolarization in both stellates and non-stellates, associated with no change or a slight increase in apparent input resistance. In stellates, carbachol caused a decrease in the dominant frequency of the subthreshold membrane potential oscillations from 9.2 to 6.3 Hz. In non-stellates, carbachol transformed tonic firing into a slow voltage-dependent bursting discharge.

Investigation of the ionic mechanisms of the carbachol-induced depolarization in stellates and non-stellates revealed that it resulted mainly from activation of a Ca^{2+}

dependent cationic conductance largely carried by Na^+, mediated predominantly through m1 muscarinic receptor subtype activation.

Serotonin, in stellates, caused a variable response consisting of a hyperpolarization and/or depolarization, associated with a decrease in apparent input resistance, while in non-stellates, only the hyperpolarizing response was observed. In stellates, serotonin increased the frequency of subthreshold oscillations from 8.5 to 14.0 Hz. In non-stellates, serotonin did not affect spike-train adaptation nor the slow afterhyperpolarization following the train of spikes while it reduced both in stellates.

These results attest to the presence, in layer II of the medial entorhinal cortex, of two parallel information processing channels, both projecting to the hippocampal formation, and differentially modulated by the cholinergic and serotoninergic systems. One of these, the stellate channel, is endowed with robust rhythmic properties whose fundamental frequency can vary widely, depending on the relative tone of these two major neurotransmitter systems.

RESUME

Les propriétés morphologiques et electrophysiques des neurones de la couche II du cortex entorhinal median ont été investiguées dans des tranches de rat en vue d'accroitre notre comprehension du role que le cortex entorhinal pourrait jouer dans l'acheminement des stimuli afférents à l'hippocampe.

L'analyse morphologique a révelé que les neurones principaux de la couche II pouvaient etre rangés en deux categories distinctes. 65% des neurones étaient identiques aux cellules stellées précedemment décrites. Les 35% restants possedaient, pour la plupart, une morphologie pyramidale, et ont été classées comme cellules non-stellées.

L'analyse electrophysiologique a révélé que les cellules stellées et non-stellées étaient characterisées par des réponses distinctes. Notamment, les stellées, après une dépolarisation par injection maintenue de courant, pouvaient générer des oscillations infraliminaires sinusoidales du potentiel de la membrane à une fréquence moyenne de 8,6 Hz, et une décharge rythmique de potentiels d'action par salves, à une fréquence dc 1 a 3 Hz, appelés "spike clusters". Les non-stellées, suivant une dépolarization maintenue, ne produisaient jamais d'oscillations persistantes ni de "spike clusters", mais déchargeaient régulierement de façon tonique.

L'investigation des principaux mécanismes ioniques dotant les cellules stellées et non-stellées de leurs réponses differentielles a révélé que les stellées exclusivement possédaient un courant rectificateur sortant, sensitif au Ba^{2+} et dependant du potential de le membrane, activé sous le seuil d'activation des potentials d'action, qui en action reciproque avec la conductance Na^{+} persistente générait les oscillations de la membrane.

L'agoniste cholinergique carbachol a causé, chez les cellules stellées et non-stellées, une dépolarization associée à aucune ou une légère augmentation de la résistance d'entrée apparente. Chez les stellées, le carbachol a produit une baisse de la fréquence des oscillations de la membrane de 9,2 a 6,3 Hz. Chez les non-stellées, le carbachol a

transformé la décharge tonique en une lente décharge par salves dépendant du potentiel de membrane.

L'investigation des mécanismes ioniques responsables de la dépolarization induite par le carbachol chez les cellules stellées et non-stellées a révélé que cette dépolarization résultait principalement de l'activation d'une conductance cationique dépendant du Ca^{2+} et largement due a un flux de Na^{+}, médiée principalement par l'activation du sous-type m1 de récepteurs muscariniques.

La sérotonine, chez les stellées a causé une réponse variable consistant en une hyperpolarization et/ou dépolarization, associée à une diminution de la résistance d'entrée apparente, alors que chez les non-stellées, uniquement la réponse hyperpolarizante a été observée. Chez les stellées, la sérotonine a produit une hausse de la fréquence des oscillations de la membrane de 8,5 a 14,0 Hz. Chez les non-stellées, la sérotonine n'a affecté ni l'adaptation pendant un train ni l'après-hyperpolarization suivant un train de potentiels d'action alors qu'elle a réduit les deux chez les stellées.

Ces resultats indiquent la présence, dans la couche II du cortex entorhinal median, de deux voies parallèles pour le traitement de l'information afférente, tous deux projettant à la formation hippocampale, et differentiellement modulés par les systèmes cholinergiques et sérotoninergiques. Un de ces canaux, celui constitué par les cellules stellées, est doté de propriétés rhytmiques robustes dont la fréquence propre pourrait largement varier, dépendant de la tonicité relative de ces deux systèmes majeurs de neurotransmetteurs.

ACKNOWLEDGEMENTS

I owe to my supervisor, Dr. Angel Alonso, the completion of this work since he believed in me at times when I did not. For this I will remain in permanent debt. His unfaltering enthusiasm towards all things oscillating has been, for me, a constant source of inspiration, and the occasion of many therapeutic laughs.

I would like to thank the "lab-next-door", Dr. Edith Hamel and all her students-collaborators for the assistance and answers provided concerning pharmacology questions; the "lab-upstairs", Dr Barbara Jones, Linda Mainville for assistance with processing and drawing of intracellularly labelled cells; Janet Green for help with the animals; and specially my collegues Armando-Rene Mena, Adriana Galue, and Dr Clayton Dickson for sharing with me the joy as well as the anguish of being a "science grad student"; additional thanks go to Dr Dickson for his edotorial help and inspiring discussions.

Very special thanks go to Monique Lederman, whose most incredible sweetness has made sailing through graduate school a comfortable journey.

Last but foremost, thank you husband for the patience and understanding throughout this endeavor.

PREFACE

This thesis exposes a series of experiments conducted to explore the intrinsic mechanisms by which layer II neurons of the entorhinal cortex may contribute to information processing within the medial temporal lobe. It is presented in accordance with the guidelines for presentation of a doctoral thesis of the Faculty of Graduate Studies and Research of McGill University. The material is organized into 6 chapters (Chap. II-VII), two of which have been published (Chap. III and IV; *J. Neurophysiol.*), and two of which are in press (Chap.V and VI; *J. Neurophysiol.*), supplemented with a general introduction (Chap. I) and a general conclusion (Chap. VIII). Chapters published or in press conform to journal specifications. In accordance with the regulations for manuscript-based theses, the following quote is reproduced from *Guidelines for Thesis Preparation* issued by the Faculty of Graduate Studies and Research:

> Candidates have the option of including, as part of the thesis, the text of one or more papers submitted or to be submitted for publication, or the clearly-duplicated text of one or more published papers. These texts must be bound as an integral part of the thesis.
>
> If this option is chosen, connecting texts that provide logical bridges between the different papers are mandatory. The thesis must be written in such a way that it is more than a mere collection of manuscripts; in other words, results of a series of papers must be integrated.
>
> The thesis must still conform to all other requirements of the "Guidelines for Thesis Preparation". The thesis must include: a Table of Contents, an abstract in English and French, an introduction which clearly states the rationale and objectives of the study, a review of the literature, a final conclusion and summary, and a thorough bibliography or reference list.
>
> Additional material must be provided where appropriate (e.g. in appendices) and in sufficient detail to allow a clear and precise judgement to be made of the importance and originality of the research reported in the thesis.
>
> In the case of manuscripts co-authored by the candidate and others, the candidate is required to make an explicit statement in the thesis as to who contributed to such work and to what extent. Supervisors must attest to the accuracy of such

statements at the doctoral oral defense. Since the task of the examiners is made more difficult in these cases, it is in the candidate's interest to make perfectly clear the responsibilities of all the authors of the co-authored papers.

In accordance with university regulations I hereby clearly state my original contribution to the work presented in this thesis:

Chapter II entitled "Morphological characterization of medial entorhinal cortex layer II neurons" is a short chapter which has not been published. It describes the morphology of layer II neurons as revealed by intracellular staining with biocytin. Among the 34 cells described and whose parameters were quantified, 6 were stained by Dr A. Alonso while he was a post-doctoral fellow in Dr R. Llinàs laboratory. All the others were filled and stained by myself.

Chapter III entitled "Differential electroresponsiveness of stellate and pyramidal-like cells of medial entorhinal cortex layer II" has been published in *Journal of Neurophysiology* (70: 128-143, 1993), and is co-authored by Dr A. Alonso and myself. It describes the intrinsic electrophysiological properties of layer II neurons. Most of the chapter deals with the rhythmic properties of stellate cells and these were determined by Dr Alonso while he was a post-doctoral fellow in Dr R. Llinàs laboratory, and have been the subject of a short publication in *Nature* (342:175-177, 1989). All the cells constituting the database for this chapter have, however, been characterized by myself.

Chapter IV entitled "Ionic mechanisms for the subthreshold oscillations and differential ectroresponsiveness of medial entorhinal cortex layer II neurons" has been published in *Journal of Neurophysiology* (70: 144-157, 1993), and is co-authored by myself and Dr A. Alonso. **Chapter V** entitled "Muscarinic modulation of the oscillatory and repetitive firing properties of entorhinal cortex layer II neurons", and **chapter VI** entitled "Ionic mechanisms of muscarinic depolarization in entorhinal cortex layer II neurons" are, to date, in press in *Journal of Neurophysiology* and are co-authored by myself and Dr A.

Alonso. All the experiments have been conducted and analyzed by myself, under the supervision of Dr Alonso.

Chapter VII entitled "Serotonergic modulation of intrinsic electroresponsiveness of entorhinal cortex layer II neurons" is a short chapter which has not been published. All the experiments have been conducted and analyzed by myself, under the supervision of Dr Alonso.

CHAPTER I

THE ENTORHINAL CORTEX

ABBREVIATIONS

5-HT	5-hydroxytryptamine (serotonin)
AD	Alzheimer's dementia
EC	entorhinal cortex
EEG	electroencephalographic
HF	hippocampal formation
LEA	lateral entorhinal area
LTP	long term potentiation
MEA	medial entorhinal area
PHR	parahippocampal region
PP	perforant path
REM	rapid eye movement

OVERVIEW

The entorhinal cortex lies at the core of the parahippocampal region, which, together with the adjacent hippocampal formation, constitutes an essential component of the "limbic system". Though rather ill-defined in terms of its constituent elements, the limbic system denotes a functional entity, historically first linked to olfactory function, then later to emotional behavior. Yet, for the past 30 years, the limbic system in general, and the parahippocampal region and hippocampal formation in particular, have been inextricably tied to human mnestic disorders. In addition to cognitive function evaluations in amnesic humans, lesion studies in rodents and primates have lead to the formulation of a "medial temporal lobe memory system", damage to which results in amnesia in humans and learning impairments in animals. The contribution of the entorhinal cortex to such a memory system is presently recognized as substantial; this agrees well with the emerging notion of the central involvement of the entorhinal cortex in high-order cognitive functions, underscored by the pathological changes targeting the entorhinal cortex in conditions such as Alzheimer's dementia and schizophrenia.

The limbic system displays two features, synchronized rhythmic activity and plasticity, commonly linked to the operations in which it is engaged. While plasticity is certainly an attribute of most parts of the nervous system, many elements of the limbic system, particularly the entorhinal cortex and hippocampal formation, exhibit particularly prominent plastic properties. These would be an essential prerequisite for any learning and memory process. An unfortunate outcome of alterations in the functional organization of neuronal networks as occurs with plasticity, would be hyperexcitability, hence epilepsy. Temporal lobe epilepsy, the most common epileptic condition, is increasingly viewed as a disorder involving predominantly pathological entorhinal-hippocampal interactions. Epilepsy, in addition, implies synchronous activity. The limbic system can easily achieve synchrony as seen from its electrographic activity. The most salient EEG activity recorded

over the limbic system in most mammals is the theta rhythm; this rhythm is particularly prominent in the hippocampus and entorhinal cortex. Though the functional significance of theta is still the subject of debate, the occurence of synchronized activity in the theta frequency range has been associated, at the cellular level, with states of hightened plasticity. Irrespective of the particular role attributed to theta rhythmicity, its occurrence should be viewed within the broader issue of the function of temporal correlation in neural activity.

The entorhinal cortex is intimately interrelated with the adjacent hippocampal formation. The superficial layers of the entorhinal cortex, via the perforant path, massively project to the hippocampal formation, the output of which is largely redirected to the deep layers of the entorhinal cortex. Since cortical afferents to the superficial layers arise from widespread sensory association areas, and since cortical efferents of the deep layers remarkably reciprocate those input channels, the entorhinal cortex has been viewed as the gateway to neocortical information flowing to and from the hippocampus. Implicitly, it was assumed that the entorhinal cortex acted as a simple relay station: it would funnel multimodal sensory material to the hippocampal formation considered THE processing power house of the limbic system, and redistribute back, to presumed memory storage sites in the neocortex, the result of hippocampal computations. The outcome of such an assumption for our understanding of the entorhinal cortex was a wealth of anatomical details in regard to connectivity, coupled to a dearth of physiological data in regard to intrinsic information processing.

The present work was undertaken within the framework of clarifying the singular contribution of the entorhinal cortex to information processing and integration within the temporal limbic system. The focus was placed on the intrinsic properties of layer II neurons since these are the cells of origin of the major component of the perforant path. The findings are viewed in terms of their contribution to synchronized rhythmic activity and plasticity.

ANATOMIC ORGANIZATION

DEFINITION

The entorhinal cortex (EC) is an integral component of the limbic forebrain. The term "limbic" was first used by Broca in 1878 to refer to the ring of structures encircling the base of the cerebral hemispheres (cf. Lopes da Silva et al. 1990). Limbic cortex, following Broca's definition, includes the subcallosal, cingulate and parahippocampal gyri, and the underlying hippocampal formation, structures he proposed were related to olfaction. The terminology "limbic system" was introduced by MacLean (1952) to emphasize that the limbic cortex and its interconnected subcortical components constituted a single functional entity subserving emotional behavior. Later definitions have varied according to authors (cf. Kötter and Meyer 1992). In the present work, following MacLean (1952), the limbic system is taken to comprise, in addition to the limbic cortex, the mammillary bodies of the hypothalamus, the anterior nuclei of the thalamus, the septal nuclei, the preoptic area, the amygdala, and the nucleus accumbens.

Some authors (Amaral 1987; Insausti 1993) regard the EC as a component of the hippocampal formation (HF). Here, following Witter et al. (1989), it is considered that the EC forms the core of the parahippocampal region (PHR); the HF comprises the dentate gyrus, the hippocampus proper, and the subiculum, while the presubiculum and parasubiculum would compose the limbic belt of the PHR. The perirhinal cortex is included in the paralimbic belt of the PHR. In this context, "limbic" and "paralimbic" refer to the cytoarchitectural subdivisions described in Lopes da Silva (1990).

The EC, forming Brodman's area 28, is bordered laterally by the perirhinal cortex, medially by the parasubiculum, rostrally by the piriform (olfactory) cortex and amygdaloid complex, and caudally by the posterior part of the parahippocampal gyrus (Fig. 1). This last area, in monkeys is comprised of areas TF and TH of Von Bonin and Bailey, and in rats has recently been referred to as postrhinal (Burwell et al. 1995).

CYTOARCHITECTURE

The EC belongs to the transitional mesocortex designated as periallocortex. It thus exhibits hybrid characteristics between isocortex and archicortex. In all mammals the basic architectural plan is the same (Insausti 1993; Witter et al. 1989): superficial layers, lumped into an external principal lamina with isocortical characteristics (Solodkin and Van Hoesen 1996), are separated from deep layers, lumped into an internal principal lamina with allocortical characteristics, by a cell free or cell poor statum, the lamina dissecans. Ramon y Cajal (1901-1902) first distinguished a 6-layer scheme. While this is widely agreed upon, differences arise in the naming of the deep layers. The following laminar organization follows Lorente de Nó's (1933) description:

- layer I is relatively free of neurons and contains a dense band of transversely oriented fibers
- layer II is prominent and consists mainly of stellate cells, which, in many species and specially in primates, are clustered into cell islands
- layer III is made up of medium sized pyramidal cells
- layer IV forms a dense band of large pyramidal cells. This layer is sharply separated from layer III by the lamina dissecans
- layer V has a stratified appearance and at some levels two sublayers can be distinguished. It is made of small pyramidal cells with arched recurrent axons
- layer VI is clearly multilayered. It is made up of many different morphological types of cells.

Across species, from rat to monkey to human, a trend towards a more developed EC in both number of neurons and laminar organization can be seen (Insausti 1993).

Although the preceding scheme applies to all portions of the EC, some local differences are apparent. The most common subdivision of the EC is into a lateral (LEA) and a medial (MEA) entorhinal area (rat: Blackstad 1956; monkey: Van Hoesen and Pandya 1975), with the provision that, in the monkey, these subdivisions fall on a rostral to

caudal axis instead of a lateral to medial as in the rat. The LEA has a clearly demarcated layer II relative to the MEA, while the MEA is characterized by a clearly delineated lamina dissecans. In addition to cytoarchitectonics, the LEA and MEA differ according to hodological criteria.

CIRCUITRY

The most detailed information concerning connections of the EC is derived from studies in the rat. However, available material from the cat and recent studies in the monkey point to a similar organization in all three species. Fig. 2 summarizes in schematic form the connections of the EC as described in the following paragraphs.

Cortical connections

Afferents. The EC receives input from a variety of cortical domains. In the rat and cat, a large input arises directly from the olfactory areas, and terminates, throughout the LEA and MEA, in layer I and the superficial part of layer II (Haberly and Price 1978; Room et al. 1984). In the monkey, olfactory input is restricted to the rostral EC, however the laminar distribution is the same as for rats and cats (Witter 1993).

The second prominent input comes from the paralimbic portion of the PHR, the perirhinal cortex. This projection distributes to restricted portions of both LEA and MEA, with terminations preferentially in the superficial layers (rat: Witter 1993; cat: Witter et al. 1986; monkey: Suzuki and Amaral 1994). The perirhinal cortex itself receives converging input from widespread cortical domains, conveying unimodal and multimodal sensory information (rat: Burwell et al. 1995; cat: Room and Groenewegen 1986a; monkey: Jones and Powell 1970). In the monkey, the EC receives additional direct input from several multimodal cortical assocation areas, in particular from the superior temporal gyrus (Insausti et al. 1987a). This projection terminates in layer I and II (Amaral et al. 1983).

The third major input originates from the limbic portion of the PHR, the presubiculum and parasubiculum. In all species studied, the presubicular projection terminates exclusively in the MEA, in layers I and III, while the parasubicular projection distributes exclusively to layer II, in both the LEA and the MEA (reviewed in Witter 1993). In turn, the presubiculum and parasubiculum receive sensory input (visual and visuomotor), either directly from primary sensory (Vogt and Miller 1983) and parietal association areas (Seltzer and Van Hoesen 1979), or indirectly through the claustrum (Witter and Groenewegen 1986).

Lastly, a group of projections arises from non-parahippocampal limbic and paralimbic cortices: (cf. Lopes da Silva et al. 1990), including the anterior and posterior cingulate which project to the LEA and MEA respectively, the insular cortex and parts of the orbitofrontal cortex (reviewed in Witter et al. 1989). These terminate in the deep layers of the EC.

Efferents. Cortical efferents of the EC largely reciprocate its cortical inputs (reviewed in: (Witter 1993; Witter et al. 1989). Major output is directed to the olfactory areas (Luskin and Price 1983) and perirhinal cortex (Witter et al. 1986); these projections arise in the LEA, predominantly from cells in layers II, III and IV. Weaker projections, arising mainly from cells in layer IV, go to the orbitofrontal and pre- and para-subiculum. An important issue actively investigated during the last 15 years is whether the EC directly projects to the neocortex. Studies have demonstrated projections from the EC to the temporal cortex in the monkey and rat (Kosel et al. 1982), and even to the entire cortical mantle in the rat (Swanson and Köhler 1986), projections originating mainly from cells in layer IV of the LEA.

Hippocamal formation connections

Perforant path projections. It has been known, since Ramon y Cajal (1901-1902) that, via the perforant path (PP), a prominent EC output is directed to the dentate gyrus of the HF.

Organization of the PP exhibits two major characteristics, which have been analyzed in the most detail in the rat.

The first characteristic is topographical organization. It is such that a lateral to medial gradient in the EC corresponds to a septal to temporal gradient in the HF (Ruth et al. 1982). The projection is not entirely specific since small parts of the EC project to at least 25% of the longitudinal axis of the HF (Amaral and Witter 1989).

The second characteristic concerns cells of origin. It is well known that the PP originates almost exclusively from cells in layers II and III (Steward and Scoville 1976), with a minor component from cells in layers IV-VI (Köhler 1985; Deller et al. 1996). The major component of the PP is from layer II to the dentate gyrus and fields CA3/CA2, with fibers distributing over the full transverse extent of these hippocampal domains (Steward 1976). Axons from the LEA terminate in the outer one third of the stratum moleculare and stratum lacunosum moleculare, while those from the MEA terminate in the middle third of these layers. The projection from layer III is to field CA1 and the subiculum. In contrast to that from layer II, this projection is much more restricted along the transverse extent of the recipient hippocampal fields (Steward 1976). In the monkey, a comparable organization for the PP has been confirmed, except that no marked difference in the terminal fields of the LEA and MEA PP projections from layer II has been detected (Witter and Amaral 1991).

Hippocampal formation projections. The non-fornical output of the HF is mostly directed to the EC. Hippocampo-entorhinal projections originate from the subiculum and CA1, and terminate in layer IV of the EC, over its full transverse extent (Swanson and Cowan 1977). The MEA receives and additional projection directed to the superficial layers I-III. Comparable results have been reported in the monkey (Saunders and Rosene 1988).

Subcortical connections

Summary. The EC receives input from a large number of subcortical nuclei (reviewed in Witter et al. 1989). These comprise, with decreasing importance: the medial septal complex of the basal forebrain, basolateral and lateral nuclei of the amygdala, endopiriform nucleus of the claustrum, supramamillary and tuberomammillary nuclei of the hypothalamus, nucleus reuniens and nucleus centralis medialis of the thalamus, and ventral tegmental area, raphe nuclei, and locus coeruleus of the brainstem. The EC reciprocates most of those inputs, either to the same nuclei or to related nuclei in the same structure they originated from. Inputs that are not reciprocated are the midline and intralaminar thalamic and brainstem projections which can be said to form part of a general cortical afferent system that modulates various brain states. In addition, the EC sends a non-reciprocated projection to the ventral and dorsal striatum of the basal ganglia. In what follows, septal and raphe projections to the EC will be considered in detail.

Septal cholinergic innervation of the EC. The medial septal complex (medial septal nucleus and nucleus of the diagonal band) sends a prominent projection to the EC (rat: Alonso and Köhler 1984; cat: Room and Groenewegen 1986b; monkey: Insausti et al. 1987b). Although acetylcholine is the major transmitter conveyed by this projection, it is recognized that part of it is not cholinergic (Alonso and Köhler 1984) but GABAergic (Köhler et al. 1984). The subsequent account will concentrate on the cholinergic innervation of the EC, which forms part of a larger system arising from magnocellular neurons in the basal forebrain and supplying the entire cortical mantle with a cholinergic input.

Cholinergic innervation of the EC has been extensively investigated in many species, including rat (Alonso and Köhler 1984), cat (Kimura et al. 1981), monkey (Alonso and Amaral 1995) and human (de Lacalle et al. 1994). The general laminar distribution of cholinergic fibers and terminals was similar in the different species considered, and consisted of two distinct bands, one in layer II, and another in layer IV.

Relative innervation densities, however, differed between primates and the small mammals: in the rat and cat, the densest terminal field was over layer IV, while in primates the highest density of fiber labeling was in layer II. Layer II innervation in primates was not uniform; in the human brain, cell islands were more densily stained than the intervening cell sparse zones, while the opposite was true in the monkey.

Raphe serotoninergic innervation. Raphe projections to the EC arise from the dorsal raphe nucleus and the nucleus centralis superior (Room and Groenewegen 1986b). Not all raphe cells projecting to the EC contain serotonin (Köhler and Steinbusch 1982). In the rat (Köhler et al. 1981) serotoninergic (5-HT) fibers were found oriented both parallel and transverse to the longitudinal axis of the EC, in a grid-like arrangement. 5-HT innervation was diffuse over all layers, however it became more pronounced over layers II and III, specially at ventral levels. A dense terminal plexus was observed in layer II of the MEA at the most ventral levels, and in layer III of the LEA.

Intrinsic connections

Intrinsic connections within the EC have been extensively studied in the rat (Köhler 1986; Köhler 1988).

MEA. Striking differences exist between the superficial and deep layers of the MEA in terms of the course and divergence of their projections. Layer II has horizontal projections that innervate most of layer II. These intralaminar projections imply the existence of long horizontal (associational and commissural) connections between cells located relatively far apart within layer II. Horizontal projections of layer III are more restricted than those of layer II, but both layers II and III send a prominent, longitudinally directed projection, from dorsal to more ventral levels. The ventral parts of the MEA layer II are thus massively innervated from every part along the longitudinal axis of the EC. The deep layers have highly divergent projections; most of their axons ascend throughout the

longitudinal axis of the MEA, to innervate all superficial layers, as well as to project to the LEA. Layer IV is the major source of this divergent projection.

LEA. In contrast, the LEA exhibits relatively sparse projections to the MEA. These originate in the deep layers and project to the deep layers of the MEA. Similarly to the pattern observed in the MEA, deep layers of the LEA send vertically oriented projections to the superficial layers. All layers of the LEA, but particularly layers II, III and IV send numerous projections by a lateral route, running past the lateral border of the LEA, to the piriform and perirhinal cortices.

FUNCTIONAL CONSIDERATIONS

The anatomical organization of the EC suggests the following functional implications. In all species studied, the superficial layers of the EC would gate, via the PP, cortical input to the HF. Comparative studies suggest that there is a correlation between the increase in size of the neocortex and the extent of its projections to the EC (Insausti 1993). Thus in the rat, in which olfactory domains occupy a large portion of the cortical mantle, the EC has strong connections with these areas. Other sensory modalities communicate indirectly with the EC, through the paralimbic and limbic belt of the PHR. By contrast, in the monkey, olfactory input to the EC is reduced, and the well developed and well differentiated multimodal association cortices project directly to the EC. Intrinsic connections within the EC would enable the output of the HF, directed to the deep layers of the EC, to monitor its input at the level of the superficial layers. Cholinergic innervation of the superficial layers, which in humans is particularly dense, would further modulate this cortical flow. Considering that the output of the EC remarkably reciprocates all of its input channels, the outcome of this circuitry is thus a cortico-entorhino-hippocampal loop in which the EC is in a strategic position to control information flow. Whether the EC is a simple relay station or an active component generating a combined representation of incoming stimuli (Witter et al. 1989) has yet to be precisely determined.

PHYSIOLOGY

In contrast to the wealth of knowledge about anatomical organization, physiological data on the EC is still fragmentary. Most data about the electrophysiology of the EC was obtained *in vivo* by means of field recordings of slow activity and unit activity; synaptic properties were mainly investigated in relation to the connection with the HF. Contrary to the situation in the HF, no systematic attempt has been made to understand the specific electroresponsive characteristics of neurons in the EC.

SYNAPTIC PROPERTIES

Analysis of sensory input reaching the EC is particularly well documented for the olfactory modality. Stimulation of olfactory areas leads to characteristic field evoked potentials whose amplitude corresponds to the density of terminations of the olfactory input (rat: Vaysettes-Courchay and Clugnet 1982; cat: Boeijinga and Van Groen 1984). Inputs from the olfactory bulb and piriform cortex induce increases in the firing rate of EC units most of which lie in layer II. Beside olfactory stimuli, a large number of units respond to auditory, gustatory, and somasthetic modalities, although with long latencies (Vaysettes-Courchay and Sessler 1983).

Amygdalar inputs to the EC have also been physiologically demonstrated (Colino and Fernández de Molina 1986; Finch et al. 1986). These were excitatory, followed by a longer latency inhibition, and observed mostly in cells of layers II and III. Spontaneous discharges occurring in the amygdala during certain EEG-synchronized states were recorded in the EC as sharp, large amplitude population events which were abolished with amygdalar lesions (Paré et al. 1995).

Entorhino-hippocampal connections were investigated with the most detail. Topographically organized, reciprocal excitatory connections between the superficial layers of the EC and the subiculum were demonstrated (Van Groen and Lopes da Silva

1986). After subicular stimulation, the response in the superficial layers of the EC followed that in the deep layers, suggesting relay of subicular inputs from deep to superficial layers by intrinsic EC circuitry (Bartesaghi et al. 1989). Synaptic responses in the deep layers consisted of prolonged NMDA mediated depolarizations (Jones 1987). Functional connectivity of the entire entorhino-hippocampo-entorhinal loop was studied in guinea pigs. In response to lateral olfactory tract stimulation, reverberant activation of the entorhino-hippocampo-entorhinal circuit was often observed. Thus, following a single volley, a sequential activation that arose in the EC, reactivated the EC after having travelled through the hippocampal circuit (de Curtis et al. 1991). Input-output relations constructed from responses simultaneously recorded from different stations along the loop suggested that the whole loop is designed to operate in an explosive manner (Bartesaghi et al. 1995).

The EC, similarly to the HF, exhibits particularly prominent plastic properties in its neuronal networks. Long term potentiation (LTP), the most extensively studied form of synaptic plasticity, was discovered in the PP projection to the dentate gyrus (Bliss and Lømo 1973). LTP has been demonstrated in the projections from the amygdala to the EC (Racine et al. 1983), from the claustrum to the EC (Wilhite et al. 1986), and from the piriform cortex to the EC (de Curtis and Llinás 1993). In this last instance, LTP induction was NMDA dependent, as in the hippocampus; LTP expression, however, exhibited both NMDA and non-NMDA components. In addition to classical, Hebbian-like LTP, neurons of layer II can exhibit a non-Hebbian form of LTP (Alonso et al. 1990) implemented by postsynaptic subthreshold rhythmic membrane potential manipulations not paired to presynaptic activation.

RHYTHMIC ACTIVITY

The EC exhibits several types of electroencephalographic (EEG) activities common to the entire limbic cortex. Of these, the theta rhythm has been the most intensely analyzed, since it is the most prominent electrographic activity recorded from the hippocampus of most mammals. According to the human EEG terminology, theta lies within the 4-7 Hz frequency band, however, in lower mammals, hippocampal theta, also referred to as RSA (rhythmic slow activity; Vanderwolf 1988) may extend up to 10-12 Hz (Lopes da Silva et al. 1990). The EC also exhibits fast activity, higher than 20 Hz. This fast activity has been referred to as beta and meant to cover the frequency range from 20 to 70 Hz (Leung 1992). More recently, the term gamma has been introduced to refer to the range from 30-100 Hz (Eeckman and Freeman 1990) or 40-100 Hz (Bragin et al. 1995). Here, the finer points of the EEG terminology will be ignored and designate the field activity with a frequency above 20 Hz as fast activity. In addition to fast and slow activity, the EC displays the transients referred to as hippocampal sharp waves.

Theta rhythm

General characteristics. Theta is generally associated with the HF, however it has been recorded in other limbic areas, namely the EC and cingulate cortex (Leung and Borst 1987). Other structures of the limbic system participate in theta rhythmicity: discharges at theta frequency have been recorded from the supramammillary nuclei (Kocsis and Vertes 1994), the mammillary bodies (Kocsis and Vertes 1994; Komisaruk 1970; Green and Arduini 1954), the anterior thalamus (Mignard et al. 1987), and the posterior hypothalamus (Bland et al. 1995). The litterature concerning theta rhythm is formidable. Yet, there is still no general agreement (Bland and Colom 1993; Lopes da Silva et al. 1990; Vinogradova 1995; Vanderwolf 1988) on: 1) its origin, whether it is controlled by a single pacemaker or arises from coupling of multiple oscillators in different structures, 2) its cellular generation, since the state of neuronal elements during theta has not been

unequivocally determined, and 3) its relevance for information processing in the brain, given the diversity of behavioral aspects - motivation, attention, learning and memory, motor activity - with which it has been correlated.

The following would be the most "consensual" account of the limbic theta rhythm. In rodents and carnivores, the behavioral correlate of theta is exploratory behavior and rapid eye movement (REM) sleep. Theta is strictly dependent on an intact septal area (Petsche et al. 1962; Stewart and Fox 1990) within which a population of neurons discharge rhythmically in phase with the hippocampal rhythm (Gaztelu and Buño 1982). Cholinergic and GABAergic afferents from septal "pacemaker" neurons (Alonso et al. 1996) would play distinct and complementary roles in theta generation (Stewart and Fox 1990). Theta is modulated by ascending fibers from the brainstem that influence the septal pacemaker (Vertes 1982). Limbic cortex neurons need not be considered simple passive followers of the septal pacemaker; the idea that local mechanisms may also contribute to theta has prompted the study of "thetalike" field potential waveforms in hippocampal (Konopacki et al. 1992a) and entorhinal (Konopacki et al. 1992b) brain slices, and intrinsic rhythmic activity in limbic neurons (Alonso and Llinás 1989; Alonso and Llinás 1992). It seems certain that different network and cellular mechanisms underlie theta generation in different limbic areas.

The occurrence of theta in primates is still a point of controversy. In monkeys, theta homologous, but not identical, to that of rodents has been recorded (Stewart and Fox 1991), while in humans, spectral analysis was necessary to demonstrate theta in the hippocampus of epileptic patients (Arnolds et al. 1980). In this last study, the theta rhythm was reported to be modulated with processing of a cognitive task as well as with the type of behavior commonly described in lower mammals.

Theta in the EC. After hippocampal theta, EC theta is the most prominent within limbic system structures. Locally generated theta in the EC has been recorded in freely movings rats (Mitchell and Ranck 1980) and cats (Boeijinga and Lopes da Silva 1988). The

generator for this activity was centered on layer II of the EC (Alonso and García-Austt 1987a). Rhythmic units, most of them located in layer II, were detected, that fired in a constant phase relationship with, but not at every cycle of, the field theta rhythm (Alonso and García-Austt 1987b). Neuronal sources of EC theta seem therefore located in the superficial layers and mostly in layer II. A comparison of EC and hippocampal theta (Dickson et al. 1994) demonstrated that EC theta activity was produced coïncidently and coherently with that of the HF, and was affected by the same sensory and pharmacologic manipulations. EC and HF theta rhythms would thus be promoted in a parallel fashion from a common source.

Theta and synaptic plasticity. Speculation about the possible role of theta in memory encoding has led to investigate its relationship to synaptic plasticity. Patterned stimulation, consisting of a short train of high frequency pulses delivered at an interpulse frequency of 5 Hz, a characteristic theta frequency, was found to preferentially induce LTP in the hippocampus (Larson et al. 1986) and in the PP pathway to the dentate gyrus (Greenstein et al. 1988). Other forms of synaptic plasticity were also preferentially induced at theta frequency stimulation (Christie and Abraham 1992; Larson et al. 1993). A different, though perhaps more interesting, link between theta and plasticity was drawn when it was realized that, during theta *in vivo* (Pavlides et al. 1988), and "thetalike" slow activity in *vitro* (Huerta and Lisman 1996), synaptic plasticity was increased, and different portions of the theta oscillation were associated with different plastic states.

Fast activity

Fast rhythms in the brain, described more than 50 years ago (reviewed in Bressler 1990), are presently under intense scrutiny. In mammals they have always been associated with increased alertness (Steriade et al. 1990); in humans they have been proposed as the necessary correlate of consciousness (Llinás and Paré 1991). Most commonly recorded over primary sensory and motor cortices (reviewed in Jefferys et al. 1996) in response to

optimal stimuli in animals and humans (reviewed in Steriade et al. 1996), they are also present during REM sleep. Fast rhythms likewise occur in the HF (Bragin et al. 1995; Leung 1992) and EC (Boeijinga and Lopes da Silva 1988; Charpak et al. 1992; Eeckman and Freeman 1990), where they coexist with theta.

In the EC, fast activity coherent with that of the olfactory areas was observed over the LEA (Boeijinga and Lopes da Silva 1988). Depth profiles indicated that it was generated locally, in layer II. Other studies suggested that EC fast activity is linked to that of the HF (Charpak et al. 1992). In fact, the largest power fast activity in the HF, found in the dentate gyrus, was found to be mainly driven by entorhinal input (Bragin et al. 1995).

Since in the HF of behaving animals fast activity was modulated by the slow theta rhythm and covaried with it in several respects (Bragin et al. 1995), this suggests that fast rhythmic activity nested within oscillations of the slow rhythm could be an important aspect of limbic cortex processing related to memory storage as proposed in a recent neural network model (Lisman and Idiart 1995).

Sharp waves

Sharp wave activity may appear in the HF when the EEG is characterized by irregular activity, during consumatory behaviors and slow wave sleep (Buzsàki 1986). The sharp wave is a transient, large amplitude field potential lasting from 40 to 100 ms, recorded throughout stratum radiatum of CA1, in response to a population burst in CA3. It is associated with a 200 Hz oscillatory field potential (ripple) recorded within stratum pyramidale of CA1. It was recently shown (Chrobak and Buzsàki 1996) that high frequency ripples were also observed throughout the hippocampo-entorhinal output pathway. In the EC, ripples were associated with entorhinal sharp waves, suggesting a synchronized field potential in the apical dendrites of layer IV-VI neurons reflecting the hippocampal sharp wave related discharge of CA1 and subicular neurons that synapse in this region. Synchronization of the circuitry associated with each sharp wave burst is

suggested to play a fundamental role in the memory consolidation process (Chrobak and Buzsàki 1996) thought to occur mainly during sleep periods (Skaggs and McNaughton 1996; Wilson and McNaughton 1994).

FUNCTIONAL ASPECTS WITH EMPHASIS ON THE HUMAN EC

MEMORY

Attaching a single, specific function to the EC has been notoriously difficult. The reason probably lies in the fact that the EC functions in close unity with the adjacent structures of the medial temporal lobe, namely the HF and other components of the PHR. Ever since the description, in 1957, by Scoville and Milner (Scoville and Milner 1957), of the induction of a profound amnesic syndrome following bilateral removal of the medial temporal lobe in patient H. M., studies have sought to determine exactly which component of the medial temporal lobe would be the critical one in mediating human declarative memory function. For over 30 years attention was mostly focused on the hippocampus; yet, only 10 years ago was it established that a lesion confined to the hippocampus was sufficient to result in amnesia in patient R. B. (Zola-Morgan et al. 1986). However, R. B.'s amnesia was mild compared to H. M.'s. So although the hippocampus appears critical, other structures within the medial temporal lobe must also contribute to human memory function.

During the past 10 years, lesion studies in monkeys have tried to ascertain the contribution of each component of the medial temporal lobe to memory (Alvarez et al. 1995; Leonard et al. 1995; Meunier et al. 1993; Suzuki et al. 1993; Zola-Morgan et al. 1989; Zola-Morgan et al. 1993; Zola-Morgan et al. 1994). Lesions confined to the hippocampus produced mild memory impairments. These increased when the adjacent cortex of the PHR was included in the lesion, and deficit severity correlated with the locus

and extent of cortical damage within the PHR. Lesions confined to the PHR without involvement of the hippocampus resulted in severe memory impairment. The conclusion was reached that each of the cortical regions of the PHR (the entorhinal, perirhinal and posterior parahippocampal areas) make qualitatively different and important contributions to memory function and that information need not reach the hippocampus itself for some memory storage to occur.

Compared to a complete lesion of the medial temporal lobe (HF+PHR), bilateral lesions of the EC produced a transient, mild memory impairment in a visual recognition task (Leonard et al. 1995; Meunier et al. 1993), which was, however, more severe than that due to pure hippocampal lesions (Alvarez et al. 1995). It has been argued by Vnek et al. (1995) that the delayed-nonmatching-to-sample tests used in monkey studies are simply a measure of acquisition (learning) and not of long term retention (memory), and therefore cannot assess the equivalent of human amnesia. Following these principles, it was found that rats with lesions of the EC (Levisohn and Isacson 1991) or with disruption of entorhino-hippocampal connections (Vnek et al. 1995) demonstrated close to normal performance in the acquisition of various visual discrimination tasks, but severe deficits in retaining these tasks over a 2 week interval. In line with the preceding, in a PET study designed to measure visual associative recall (recognition of a cue picture and subsequent recall of a paired associate from long term memory), the human entorhinal cortex and presubiculum were found to be selectively activated (Klingberg et al. 1994). The involvement of the EC in associative memory agrees well with the observation that, in the early stages of Alzheimer's disease which selectively target the EC, deficits in associative retrieval occur (Parasuraman and Martin 1994). More generally, this could explain the proposed role of the medial temporal lobe memory system in memory consolidation. Alvarez and Squire (1994) have proposed that, during consolidation, the medial temporal lobe memory system is required to establish and maintain associations between the multiple neocortical representations that together constitute a complete memory.

EPILEPSY

Temporal lobe epilepsy is the most common human epileptic condition. Analysis of spontaneous seizures has revealed that some syndromes of medial temporal lobe epilepsy involve complex interactions between entorhinal and hippocampal regions (Spencer and Spencer 1994a) and that the hippocampus does not act alone in the genesis of temporal lobe epilepsy (Spencer and Spencer 1994b). In many patients, onset of ictal events could first be recorded in the EC, which could explain why successful seizure control was dependent on EC resection (Feindel et al. 1996).

A number of animal models of epilepsy (Nagao et al. 1996; Paré et al. 1992) have suggested a role for the closed hippocampal-entorhinal loop in shaping hippocampal epileptic discharges. Sustained, reverberant loop activity in the hippocampal entorhinal circuit was found to be the central event in the organization of epileptic discharges.

DEMENTIA AND SCHIZOPHRENIA

Dementia and schizophrenia might be considered diseases "of the most uniquely human portions of the brain" (Ross and Pearlson 1996). Both those pathologic conditions exhibit temporal lobe abnormalitites, expressed mostly in the EC.

In Alzheimer's Dementia (AD) the EC shows gross morphological changes; it is markedly atrophied in a high percentage of cases (Van Hoesen et al. 1991), probably in correlation with the massive neuronal loss from the superficial layers. In AD, changes in the EC are an invariant and early feature of the pathology. Although extensive and variable cortical areas are ultimately affected, the EC remains the most heavily damaged of all cortical areas. The most dominant type of pathology in AD is the neurofibrillary tangle; neurons in layer II of the EC are heavily invested by neurofibrillary tangles and massively die, while other layers of the EC, such as layer IV, are affected to a much lesser extent. A profound loss (up to 60%) of layer II neurons has been detected in individual exhibiting very mild AD (Gómez-Isla et al. 1996). That layer II neurons of the EC are the first to be

touched by tangle formation has been shown recently (Braak and Braak 1991). In the initial stage of AD, severe deposition of neurofibrillary tangles in layer II coupled to a surprisingly small number of changes in both hippocampal formation and isocortex were observed. Since the early memory changes in AD are characterized by confusion and an inability to recall new and changing daily episodes, the disfunctionality of layer II can be viewed as the structural basis for these early memory impairments (Van Hoesen et al. 1991).

Parkinson's disease, progressive supranuclear palsy, and Huntington's disease all involve various subcortical nuclei pathologies. In the severe forms, personality changes and dementia are observed. It is interesting that, in these diseases, cortical changes restricted to the EC are only seen in demented individuals exhibiting overt cognitive decline (Braak and Braak 1992). While in Parkinson's disease and progressive supranuclear palsy, neurofibrillary tangle related destruction of layer II takes place, in Huntington's disease, the deep layers are the most affected.

In schizophrenia, temporal lobe atrophy is sometimes observed. More often, MRI studies reveal smaller parahippocampal areas. Schizophrenic brains exhibit atypical cytoarchitecture of the EC, with disorganization mostly apparent in the superficial layers. Clusters of layer II neurons are poorly formed and located heterotypically, deep in layer III (Arnold et al. 1991). This abnormal architecture most likely results from faulty neuronal migration due to altered brain development (Ross and Pearlson 1996). It is proposed that this structural defect will induce the EC to operate abnormally and cause inappropriate retroactivation of fragmentary experience with commensurate impairment of reality testing (Arnold et al. 1991).

OBJECTIVES OF THE PRESENT STUDY

From what precedes it is seen that the EC has been studied in greatest detail from an anatomic point of view. EC physiology has mostly been investigated as it relates to the adjacent hippocampal formation. The aim of the present work is thus to initiate the understanding of the intrinsic mechanisms used by the EC for information processing. The specific objective is to determine the functional - electrophysiological and morphological - properties of layer II neurons, the cells of origin of the PP, which as seen from the preceeding account of normal and pathological function, play a pivotal role in neocortical-hippocampal interactions. This study will deal exclusively with neurons in the MEA.

Using an *in vitro* rat brain slice preparation, the following will be determined by intracellular recordings from layer II neurons:

- intrinsic electroresponsive properties
- morphological characteristics and relation to electrophysiological types
- ionic mechanisms that endow layer II neurons with their basic electroresponsive properties
- modulation of electroresponsive properties by the two major neurotransmitter systems, the cholinergic and serotoninergic.

It is hoped that understanding the functional organization of layer II neurons will clarify the unique contribution of the EC to information processing within the limbic system.

REFERENCES

Alonso, A., de Curtis, M., and Llinás, R. Postsynaptic Hebbian and non-Hebbian long-term potentiation of synaptic efficacy in the entorhinal cortex in slices and in the isolated adult guinea pig brain. *Proc. Natl. Acad. Sci. USA.* 87: 9280-9284, 1990.

Alonso, A. and García-Austt, E. Neuronal sources of theta rhythm in the entorhinal cortex. I. Laminar distribution of theta field potentials. *Exp. Brain Res.* 67: 493-501, 1987a.

Alonso, A. and García-Austt, E. Neuronal sources of theta rhythm in the entorhinal cortex of the rat. II. Phase relations between unit discharges and theta field potentials. *Exp. Brain Res.* 67: 502-509, 1987b.

Alonso, A., Khateb, A., Fort, P., Jones, B. E., and Mühlethaler, M. Differential oscillatory properties of cholinergic and non-cholinergic nucleus basalis neurons in guinea pig brain slice. *Eur. J. Neurosci.* 8: 169-182, 1996.

Alonso, A. and Köhler, C. A study of the reciprocal connections between the septum and the entorhinal area using anterograde and retrograde axonal transport methods in the rat brain. *J. Comp. Neurol.* 225: 327-343, 1984.

Alonso, A. and Llinas, R. R. Subthreshold Na^+-dependent theta-like rhythmicity in stellate cells of entorhinal cortex layer II. *Nature.* 342: 175-177, 1989.

Alonso, A. and Llinás, R. R. Electrophysiology of the mammillary complex in vitro. II. Medial mammillary neurons. *J. Neurophysiol.* 68: 1321-31, 1992.

Alonso, J. R. and Amaral, D. G. Cholinergic innervation of the primate hippocampal formation. I. Distribution of choline acetyltransferase immunoreactivity in the *Macaca fascicularis* and *Macaca mulatta* monkeys. *J. Comp. Neurol.* 355: 135-170, 1995.

Alvarez, P. and Squire, L. R. Memory consolidation and the medial temporal lobe: a simple network model. *Proc. Natl. Acad. Sci. USA.* 91: 7041-7045, 1994.

Alvarez, P., Zola-Morgan, S., and Squire, L. R. Damage limited to the hippocampal region produces long-lasting memory impairment in monkeys. *J. Neurosci.* 15: 3796-3807, 1995.

Amaral, D. G. Memory: anatomical organization of candidate brain regions. In: *Handbook of Physiology,* edited by Bethesda, MD.: American Physiological society, 1987, 211-294

Amaral, D. G., Insausti, R., and Cowan, W. M. Evidence for a direct projection from the superior temporal gyrus to the entorhinal cortex in the monkey. *Brain Res.* 275: 263-277, 1983.

Amaral, D. G. and Witter, M. P. The three-dimensional organization of the hippocampal formation: a review of anatomical data. *Neuroscience.* 31: 571-591, 1989.

Arnold, E. S., Hyman, B. T., Van Hoesen, G. W., and Damasio, A. Some cytoarchitectural abnormalities of the entorhinal cortex in schizophrenia. *Arch. Gen. Psychiatry.* 48: 625-632, 1991.

Arnolds, D. E. A. T., Lopes da Silva, F. H., Aitink, J. W., Kamp, A., and Boeijinga, P. The spectral properties of hippocampal EEG related to behavior in man. *Electroencephalogr. Clin. Neurophysiol.* 50: 324-328, 1980.

Bartesaghi, R., Gessi, T., and Migliore, M. Input-output relations in the entorhinal-hippocampal-entorhinal loop: entorhinal cortex and dentate gyrus. *Hippocampus.* 5: 440-451, 1995.

Bartesaghi, R., Gessi, T., and Sperti, L. Electrophysiological analysis of the hippocampal projections to the entorhinal area. *Neuroscience.* 30: 51-62, 1989.

Blackstad, T. W. Commissural connections of the hippocampal region in the rat, with special reference to their mode of termination. *J. Comp. Neurol.* 105: 417-537, 1956.

Bland, B. H. and Colom, L. V. Extrinsic and intrinsic properties underlying oscillation and synchrony in limbic cortex. *Prog. Neurobiol.* 4: 157-208, 1993.

Bland, B. H., Konopacki, J., Kirk, I. J., Oddie, S. D., and Dickson, C. T. Discharge patterns of hippocampal theta-related cells in the caudal diencephalon of the urethan-anesthetized rat. *J. Neurophysiol.* 74: 322-333, 1995.

Bliss, T. V. P. and Lømo, T. Long-lasting potentiation of synaptic transmission in the dentate area of the anesthetized rabbit, following stimulation of the perforant path. *J. Physiol. (Lond.).* 232: 331-356, 1973.

Boeijinga, P. H. and Lopes da Silva, F. H. Differential distribution of β and θ EEG activity in the entorhinal cortex of the cat. *Brain Res.* 448: 272-286, 1988.

Boeijinga, P. H. and Van Groen, T. Inputs from the olfactory bulb and olfactory cortex to the entorhinal cortex in the cat. II. physiological studies. *Exp. Brain Res.* 57: 40-48, 1984.

Braak, H. and Braak, E. Neuropathological stageing of Alzheimer-related changes. *Acta Neuropathol.* 82: 239-259, 1991.

Braak, H. and Braak, E. The human entorhinal cortex: normal morphology and lamina-specific pathology in various diseases. *Neurosci. Research.* 15: 6-31, 1992.

Bragin, A., Jandó, G., Nádasdy, Z., Hetke, J., Wise, K., and Buzsáki, G. Gamma (40-100 Hz) oscillation in the hippocampus of the behaving rat. *J. Neurosci.* 15: 47-60, 1995.

Bressler, S. L. The gamma wave: a cortical information carrier. *Trends Neurosci.* 13: 161-163, 1990.

Burwell, R. D., Witter, M. P., and Amaral, D. G. Perirhinal and postrhinal cortices of the rat: a review of the neuroanatomical literature and comparison with findings from the monkey brain. *hippocampus.* 5: 390-408, 1995.

Buzsàki, G. Hippocampal sharp waves: their origin and significance. *Brain Res.* 398: 242-252, 1986.

Charpak, S., Paré, D., and Llinás, R. R. Entorhinal cortex (EC) generates 40 Hz hippocampal oscillations. *Soc. Neurosci. Abstr.* 18: 386.5, 1992.

Christie, B. R. and Abraham, W. C. Priming of associative long term depression in the dentate gyrus by θ frequency synaptic activity. *Neuron.* 9: 79-84, 1992.

Chrobak, J. J. and Buzsàki, G. High-frequency oscillations in the output networks of the hippocampal-entorhinal axis of the freely behaving rat. *J. Neurosci.* 16: 3056-3066, 1996.

Colino, A. and Fernández de Molina, A. Inhibitory response in entorhinal and subicular cortices after electrical stimulation of the lateral and basolateral amygdala of the rat. *Brain Res.* 378: 416-419, 1986.

de Curtis, M. and Llinás, R. R. Entorhinal cortex long-term potentiation evoked by theta-patterned stimulation of associative fibers in the isolated in vitro guinea pig brain. *Brain Res.* 600: 327-330, 1993.

de Curtis, M., Paré, D., and Llinás, R. R. The electrophysiology of the olfactory-hippocampal circuit in the isolated and perfused adult mammalian brain *in vitro*. *Hippocampus.* 1: 341-354, 1991.

de Lacalle, S., Lim, C., Sobreviella, T., Mufson, E. J., Hersh, L. B., and Saper, C. B. Cholinergic innervation in the human hippocampal formation including the entorhinal cortex. *J. Comp. Neurol.* 345: 321-344, 1994.

Dickson, C. T., Trepel, C., and Bland, B. H. Extrinsic modulation of theta field activity in the entorhinal cortex of the anesthetized rat. *Hippocampus.* 4: 37-52, 1994.

Eeckman, F. H. and Freeman, W. J. Correlations between unit firing and EEG in the rat olfactory system. *Brain Res.* 528: 238-244, 1990.

Feindel, W., Leonard, G., Caramanos, Z., Li, M., Harrison, J., and Kuchela, A. Role of the amygdala and entorhinal cortex in the surgery of temporal lobe seizures. *31st meeting of the canadian congress of neurological sciences.* 1996.

Finch, D. M., Wong, E. E., Derian, E. L., Chen, X.-H., Nowlin-Finch, N. L., and Brothers, L. A. Neurophysiology of limbic system pathways in the rat: projections from the amygdala to he entorhinal cortex. *Brain Res.* 370: 273-284, 1986.

Gaztelu, J. M. and Buño, W. Septo-hippocampal relationships during EEG theta rhythm. *Electroencephalogr. Clin. Neurophysiol.* 54: 375-387, 1982.

Gómez-Isla, T., Price, J. L., McKeel Jr., D. W., Morris, J. C., Growdon, J. H., and Hyman, B. T. Profound loss of layer II entorhinal cortex neurons occurs in very mild Alzheimer's disease. *J. Neurosci.* 16: 4491-4500, 1996.

Green, J. D. and Arduini, A. Hippocampal electrical activity in arousal. *J. Neurophysiol.* 17: 533-557, 1954.

Greenstein, Y. J., Pavlides, C., and Winson, J. Long-term potentiation in the dentate gyrus is preferentially induced at theta rhythm periodicity. *Brain Res.* 438: 331-334, 1988.

Haberly, L. B. and Price, J. L. Association and commissural fiber systems of the olfactory cortex in the rat. I. Systems originating in the piriform cortex and adjacent areas. *J. Comp. Neurol.* 178: 711-740, 1978.

Huerta, P. T. and Lisman, J. E. Synaptic plasticity during the cholinergic theta-frequency oscillation in vitro. *Hippocampus.* 6: 58-61, 1996.

Insausti, R. Comparative anatomy of the entorhinal cortex and hippocampus in mammals. *Hippocampus.* 3, special issue: 19-26, 1993.

Insausti, R., Amaral, D. G., and Cowan, W. M. The entorhinal cortex of the monkey. II. Cortical afferents. *J. Comp. Neurol.* 264: 356-395, 1987a.

Insausti, R., Amaral, D. G., and Cowan, W. M. The entorhinal cortex of the monkey. III. Subcortical afferents. *J. Comp. Neurol.* 264: 396-408, 1987b.

Jefferys, J. G. R., Traub, R. D., and Whittington, M. A. Neuronal networks for induced '40 Hz' rhythms. *Trends Neurosci.* 19: 202-207, 1996.

Jones, E. G. and Powell, T. P. S. An anatomical study of converging sensory pathways within the cerebral cortex of the monkey. *Brain.* 93: 793-820, 1970.

Jones, R. S. G. Complex synaptic responses of entorhinal cortical cells in the rat to subicular stimulation in vitro: demonstration of an NMDA receptor-mediated component. *Neurosci. Lett.* 81: 209-214, 1987.

Kimura, H., McGeer, P. L., Peng, J. H., and McGeer, E. G. The central cholinergic system studied by choline acetyltransferase immunohistochemistry in the cat. *J. Comp. Neurol.* 200: 151-201, 1981.

Klingberg, T., Roland, P. E., and Kawashima, R. The human entorhinal cortex participates in associative memory. *Neureport.* 6: 57-60, 1994.

Kocsis, B. and Vertes, R. P. Characterization of neurons in the supamammillay nucleus and mammillary body that discharge rhythmically with the hippocampal theta rhythm in the rat. *J. Neurosci.* 14: 7040-7052, 1994.

Köhler, C. A projection from the deep layers of the entorhinal area to the hippocampal formation in the rat. *Neurosci. Lett.* 56: 13-19, 1985.

Köhler, C. Intrinsic connections of the retrohippocampal region in the rat brain. II. the medial entorhinal area. *J. Comp. Neurol.* 246: 149-169, 1986.

Köhler, C. Intrinsic connections of the retrohippocampal region in the rat brain: III. the lateral entorhinal area. *J. Comp. Neurol.* 271: 208-228, 1988.

Köhler, C., Chan-Palay, V., and Steinbusch, H. The distribution and orientation of serotonin fibers in the entorhinal and other retrohippocampal areas. An immunohistochemical study with anti-serotonin antibodies in the rat's brain. *Anat. Embryol.* 161: 237-264, 1981.

Köhler, C., Chan-Palay, V., and Wu, J.-Y. Septal neurons containing glutamic acid decarboxylase immunoreactivity project to the hippocampal region in the rat brain. *Anat. Embriol.* 169: 41-44, 1984.

Köhler, C. and Steinbusch, H. Identification of serotonin and non-serotonin containing neurons of the midbrain raphe projecting to the entorhinal area and the hippocampal formation. A combined immunohistochemical and fluorescent retrograde tracing study in the rat brain. *Neuroscience.* 7: 951-975, 1982.

Komisaruk, B. R. Synchrony between limbic system theta activity and rhythmical behavior in rats. *J. Comp. Physiol. Psychol.* 70: 482-492, 1970.

Konopacki, J., Golebiewski, H., and Eckersdorf, B. Carbachol-induced rhythmic slow activity (theta) in cat hippocampal formation slices. *Brain Res.* 578: 13-16, 1992a.

Konopacki, J., Golebiewski, H., and Eckersdorf, B. Carbachol-induced theta-like activity in entorhinal cortex slices. *Brain Res.* 572: 76-90, 1992b.

Kosel, K. C., Van Hoesen, G. W., and Rosene, D. L. Non-hippocampal cortical projections from the entorhinal cortex in the rat and rhesus monkey. *Brain Res.* 244: 201-213, 1982.

Kötter, R. and Meyer, N. The limbic system: a review of its empirical foundation. *Behav. Brain Res.* 52: 105-127, 1992.

Larson, J., Wong, D., and Lynch, G. Patterned stimulation at the theta frequency is optimal for the induction of hippocampal long-term potentiation. *Brain Res.* 165: 210-218, 1986.

Larson, J., Xiao, P., and Lynch, G. Reversal of LTP by theta frequency stimulation. *Brain Res.* 600: 97-102, 1993.

Leonard, B. W., Amaral, D. G., Squire, L. R., and Zola-Morgan, S. Transient memory impairment in monkeys with bilateral lesions of the entorhinal cortex. *J. Neurosci.* 15: 5637-5659, 1995.

Leung, L. S. Fast (beta) rhythms in the hippocampus: a review. *Hippocampus.* 2: 93-98, 1992.

Leung, L.-W. S. and Borst, J. G. G. Electrical activity of the cingulate cortex. I. Generating mechanisms and relations to behavior. *Brain Res.* 407: 68-80, 1987.

Levisohn, L. F. and Isacson, O. Excitotoxic lesions of the rat entorhinal cortex. Effects of selective neuronal damage on acquisition and retention of non-spatial reference memory task. *Brain Res.* 564: 230-244, 1991.

Lisman, J. E. and Idiart, M. A. P. Storage of 7 ± 2 short term memories in oscillatory subcycles. *Science.* 267: 1512-1515, 1995.

Llinás, R. R. and Paré, D. Of dreaming and wakefulness. *Neuroscience.* 44: 521-535, 1991.

Lopes da Silva, F. H., Witter, M. P., Boeijinga, P. H., and Lohman, H. M. Anatomic organization and physiology of the limbic cortex. *Physiol. Rev.* 70: 453-511, 1990.

Lorente de Nó, R. Studies on the structure of the cerebral cortex. I. The area entorhinalis. *J. Psychol. Neurol.* 45: 381-438, 1933.

Luskin, M. B. and Price, J. L. The topographic organization of associational fibers of the olfactrory system in the rat, including centrifugal fibers to the olfactory bulb. *J. Comp. Neurol.* 216: 264-291, 1983.

MacLean, P. D. Some psychiatric implications of physiological studies on frontotemporal portion of limbic system (visceral brain). *Electroencephalogr. Clin. Neurophysiol.* 4: 407-418, 1952.

Meunier, M., Bachevalier, J., Mishkin, M., and Murray, E. A. Effects on visual recognition of combined and separate ablations of the entorhinal and perirhinal cortex in rhesus monkeys. *J. Neurosci.* 13: 5418-5432, 1993.

Mignard, M., Bentzinger, D., Bender, N., and Grabiel, M. Type I and type II theta-like unit activity in structures of the Papez circuit during differential avoidance conditioning in rabbits. *Soc. Neurosci. Abstr.* 13: 305.15, 1987.

Mitchell, S. J. and Ranck, J. B. J. Generation of theta rhythm in medial entorhinal cortex of freely moving rats. *Brain Res.* 189: 49-66, 1980.

Nagao, T., Alonso, A., and Avoli, M. Epileptiform activity induced by pilocarpine in the rat hippocampal-entorhinal slice prepatation. *Neuroscience.* 72: 399-408, 1996.

Parasuraman, R. and Martin, A. Cognition in Alzheimer's disease: disorders of attention and semantic knowledge. *Curr. Opin. Neurobiol.* 4: 237-244, 1994.

Paré, D., Dong, J., and Gaudreau, H. Amygdalo-entorhinal relations and their reflection in the hippocampal formation: generation of sharp sleep potentials. *J. Neurosci.* 15: 2482-2503, 1995.

Paré, D., de Curtis, M., and Llinás, R. Role of the hippocampal-entorhinal loop in temporal lobe epilepsy: extra- and intracellular study in the isolated guinea pig brain *in vitro*. *J. Neurosci.* 12: 1867-1881, 1992.

Pavlides, C., Greenstein, Y. J., and Goudman, M. Long term potentiation in the dentate gyrus is induced preferentially on the positive phase of theta-thythm. *Brain Res.* 439: 383-387, 1988.

Petsche, H., Stumpf, C., and Gogolák, G. The significance of the rabbit's septum as a relay station between the midbrain and the hippocampus. I. The control of hippocampus arousal activity by the septum cells. *Electroenceph. Clin. Neurophysiol.* 14: 202-211, 1962.

Racine, R. J., Milgram, N. W., and Hafner, S. Long term potentiation phenomena in the rat limbic forebrain. *Brain Res.* 260: 217-231, 1983.

Ramon y Cajal, S. Estudios sobre la corteza cerebral humana. *Trab. Inst. Cajal. Invest. Biol.* 1: 1-227, 1901-1902.

Room, P. and Groenewegen, H. J. Connections of the parahippocampal cortex. I. Cortical afferents. *J. Comp. Neurol.* 251: 415-450, 1986a.

Room, P. and Groenewegen, H. J. Connections of the parahippocampal cortex in the cat. II. Subcortical afferents. *J. Comp. Neurol.* 251: 451-473, 1986b.

Room, P., Groenewegen, H. J., and Lohman, A. H. M. Inputs from the olfactory bulb and olfactory cortex to the entorhinal cortex in the cat. I. Anatomical observations. *Exp. Brain Res.* 56: 488-496, 1984.

Ross, C. A. and Pearlson, G. D. Schizophrenia, the heteromodal association neorcortex and development: potential for a neurogenetic approach. *Trends Neurosci.* 19: 171-176, 1996.

Ruth, R. E., Collier, T. J., and Routtenberg, A. Topography between the entorhinal cortex and the dentate septotemporal axis in rats: I. Medial and intermediate entorhinal projection cells. *J. Comp. Neurol.* 209: 69-78, 1982.

Saunders, R. C. and Rosene, D. L. A comparison of the efferents of the amygdala and the hippocampal formation in the rhesus monkey. I. Convergence in the entorhinal, prorhinal and perirhinal cortices. *J. Comp. Neurol.* 271: 153-184, 1988.

Scoville, W. B. and Milner, B. Loss of recent memory after bilateral hippocampal lesions. *J. Neurol. Neurosurg. Psychiat.* 20: 11-21, 1957.

Seltzer, B. and Van Hoesen, G. W. A direct inferior parietal lobule projection to the presubiculum in the rhesus monkey. *Brain Res.* 179: 157-161, 1979.

Skaggs, W. E. and McNaughton, B. L. Replay of neuronal firing sequences in rat hippocampus during sleep following spatial experience. *Science.* 271: 1870-1873, 1996.

Solodkin, A. and Van Hoesen, G. W. Entorhinal cortex modules of the human brain. *J. Comp. Neurol.* 365: 610-627, 1996.

Spencer, D. D. and Spencer, S. S. Entorhinal-hippocampal interactions in medial temporal lobe epilepsy. *Epilepsia.* 35: 721-727, 1994a.

Spencer, D. D. and Spencer, S. S. Hippocampal resections and the use of human tissue in defining temporal lobe epilepsy syndromes. *Hippocampus.* 4: 242-249, 1994b.

Steriade, M., Amzica, F., and Contreras, D. Synchronization of fast (30-40 Hz) spontaneous cortical rhythms during brain activation. *J. Neurosci.* 16: 392-417, 1996.

Steriade, M., Gloor, P., Llinás, R. R., Lopes da Silva, F. H., and Mesulam, M.-M. Basic mechanisms of cerebral rhythmic activities. *Electroencephalogr. Clin. Neurophysiol.* 76: 481-508, 1990.

Steward, O. Topographic organization of the projections from the entorhinal area to the hippocampal formation of the rat. *J. Comp. Neurol.* 167: 285-314, 1976.

Steward, O. and Scoville, S. A. Cells of origin of entorhinal cortical afferents to the hippocampus and fascia dentata of the rat. *J. Comp. Neurol.* 169: 347-370, 1976.

Stewart, M. and Fox, S. E. Do septal neurons pace the hippocampal theta rhythm? *Trends Neurosci.* 13: 163-168, 1990.

Stewart, M. and Fox, S. E. Hippocampal theta activity in monkeys. *Brain Res.* 538: 59-63, 1991.

Suzuki, W. A. and Amaral, D. G. Topographic organization of the reciprocal connections between the monkey entorhinal cortex and the perirhinal and parahippocampal cortices. *J. Neurosci.* 14: 1856-1877, 1994.

Suzuki, W. A., Zola-Morgan, S., Squire, L. R., and Amaral, D. G. Lesions of the perirhinal and parahippocampal cortices in the monkey produce long-lasting memory impairment in the visual and tactual modalities. *J. Neuorosci.* 13: 2430-2451, 1993.

Swanson, L. W. and Cowan, W. M. An autoradiographic study of the organization of the efferent connections of the hippocampal formation in the rat. *J. Comp. Neurol.* 172: 49-84, 1977.

Swanson, L. W. and Köhler, C. Anatomical evidence for direct projections from the entorhinal area to the entire cortical mantle in the rat. *J. Neurosci.* 6: 3010-3023, 1986.

Vanderwolf, C. H. Cerebral activity and behavior: control by central cholinergic and serotoninergic systems. *Int. Rev. Neurobiol.* 30: 225-340, 1988.

Van Groen, T. and Lopes da Silva, F. H. Organization of the reciprocal connections between the subiculum and the entorhinal cortex in the cat. II. An electrophysiological study. *J. Comp. Neurol.* 251: 111-120, 1986.

Van Hoesen, G. W., Hyman, B. T., and Damasio, A. R. Entorhinal cortex pathology in Alzheimer's disease. *Hippocampus.* 1: 1-8, 1991.

Van Hoesen, G. W. and Pandya, D. N. Some connections of the entorhinal (area 28) and perirhinal (area 35) cortices of the rhesus monkey. I. Temporal lobe afferents. *Brain Res.* 95: 1-24, 1975.

Vaysettes-Courchay, C. and Clugnet, M. C. Mise en évidence de projections et de réponses olfactives au sein du cortex entorhinal du rat. *C. R. Soc. Biol.* 176: 828-833, 1982.

Vaysettes-Courchay, C. and Sessler , F. M. Mise en évidence de convergences sensorielles dans le cortex entorhinal du rat. *C. R. Acad. Sci. Paris.* 296: 877-880, 1983.

Vertes, R. P. Brain stem generation of the hippocampal EEG. *Prog. Neurobiol.* 19: 159-186, 1982.

Vinogradova, O. S. Expression, control, and probable functional significance of the neuronal theta-rhythm. *Prog. Neurobiol.* 45: 523-583, 1995.

Vnek, N., Gleason, T. C., Kromer, L. F., and Rothblat, L. A. Entorhinal-hippocampal connections and object memory in the rat: acquisition versus retention. *J. Neurosci.* 15: 3193-3199, 1995.

Vogt, B. A. and Miller, M. W. Cortical connections between rat cingulate cortex and visual, motor and postsubicular cortices. *J. Comp. Neurol.* 216: 192-210, 1983.

Wilhite, B. L., Teyler, T. J., and Hendricks, C. Functional relations of the rodent claustral-entorhinal -hippocampal system. *Brain Res.* 365: 54-60, 1986.

Wilson, M. and McNaughton, B. L. Reactivation of hippocampal ensemble memories during sleep. *Science.* 265: 676-679, 1994.

Witter, M. Organization of the entorhinal-hippocampal system: a review of current anatomical data. *Hippocampus.* 3, special issue: 33-44, 1993.

Witter, M. P. and Amaral, D. G. Entorhinal cortex of the monkey. V. Projections to the dentate gyrus, hippocampus, and subicular complex. *J. Comp. Neurol.* 307: 437-459, 1991.

Witter, M. P. and Groenewegen, H. J. Connections of the parahippocampal cortex in the cat. IV. Subcortical efferents. *J. Comp. Neurol.* 251: 51-77, 1986.

Witter, M. P., Groenewegen, H. J., and Lohman, A. H. M. Connections of the parahippocampal cortex in the cat. V. Intrinsic connections: comments on input/output connections with the hippocampus. *J. Comp. Neurol.* 252: 78-94, 1986.

Witter, M. P., Groenewegen, H. J., Lopes da Silva, F. H., and Lohman, A. H. M. Functional organization of the extrinsic and intrinsic circuitry of the parahippocampal region. *Progr. Neurobiol.* 33: 161-253, 1989.

Zola-Morgan, S., Squire, L. R., and Amaral, D. G. Human amnesia and the medial temporal region: enduring memory impairment following a bilateral lesion limited to field CA1 of the hippocampus. *J. Neurosci.* 6: 2950-2967, 1986.

Zola-Morgan, S., Squire, L. R., and Amaral, D. G. Lesions of the amygdala that spare the adjacent cortical regions do not impair memory or exacerbate the impairment following lesions of the hippocampal formation. *J. Neurosci.* 9: 1922-1936, 1989.

Zola-Morgan, S., Squire, L. R., Clower, R. P., and Rempel, N. L. Damage to the perirhinal cortex exarcerbates memory impairment following lesions of the hippocampal formation. *J. Neurosci.* 13: 251-265, 1993.

Zola-Morgan, S., Squire, L. R., and Ramus, S. J. Severity of memory impairment in monkeys as a function of locus and extent of damage within the medial temporal lobe memory system. *Hippocampus.* 4: 483-495, 1994.

Figure 1. Lateral view of the rat brain showing the borders of the EC. Rs, rhinal sulcus; Pir, piriform cortex; EC, entorhinal cortex (area 28); PC, perirhinal cortex (rostral areas 35 and 36); PoC, postrhinal cortex (caudal areas 35 and 36). Definitions of perirhinal and postrhinal cortices follow Burwell et al. (1995).

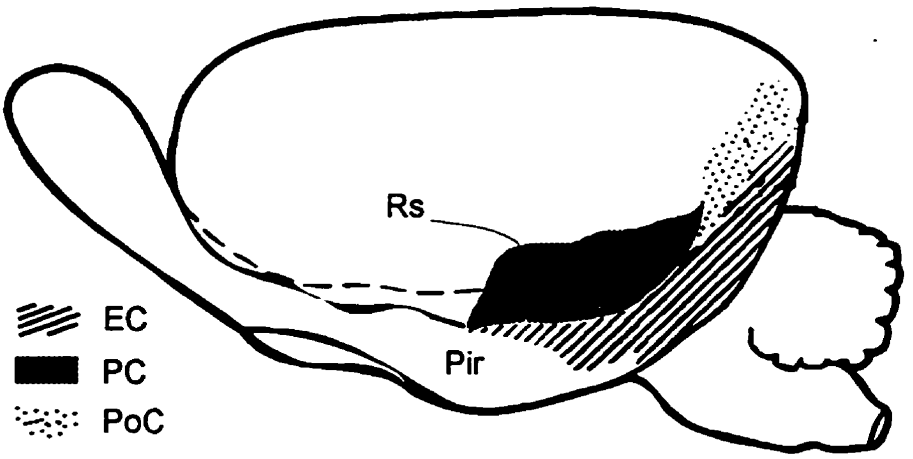

Adapted from Burwell et al. (1995), p. 393

Figure 2. Major connections of the EC with emphasis on the cortico-entorhino-hippocampal loop. Among subcortical afferents, only those from the septal complex and raphe nuclei are shown. See text for details.

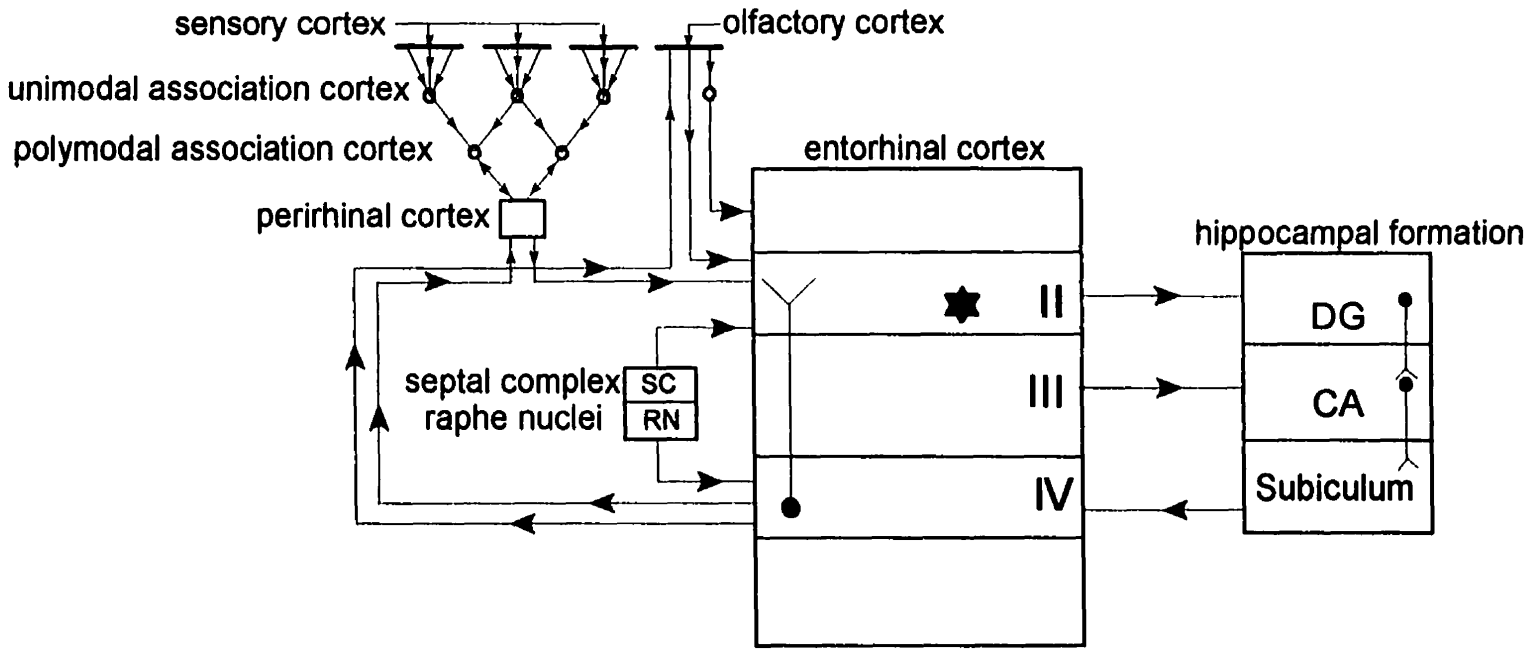
sensory cortex
olfactory cortex
unimodal association cortex
polymodal association cortex
perirhinal cortex
entorhinal cortex
hippocampal formation
II
III
IV
DG
CA
Subiculum
septal complex
raphe nuclei
SC
RN

CHAPTER II

MORPHOLOGICAL CHARACTERIZATION OF MEDIAL ENTORHINAL CORTEX LAYER II NEURONS

ABBREVIATIONS

EC	entorhinal cortex
HF	hippocampal formation
HRP	horseradish peroxidase
LEC	lateral entorhinal cortex
MEC	medial enrorhinal cortex
non-SC	non-stellate cell
PP	perforant path
SC	stellate cell

INTRODUCTION

The pathway between the entorhinal cortex (EC) and hippocampal formation (HF) was described as early as the beginning of the century by Ramon y Cajal (1901-1902) who dubbed it the perforant path (PP) since it perforated all cortical layers in the region of the presubiculum and subiculum while ascending from the entorhinal area to the dentate gyrus. Much later studies showed that axons of layer II neurons contributing to the PP - which comprise the vast majority of PP fibers - extend ipsilaterally to the dentate gyrus and regio inferior of the hippocampus, with those from the medial entorhinal cortex (MEC) terminating at mid proximo-distal dendritic segments, and those from the lateral entorhinal cortex (LEC) terminating at distal segments, as determined in the rat (Hjorth-Simonsen and Jeune 1972; Steward 1976; Steward and Scoville 1976). However, unequivocal identification of neurons of origin of the PP was not possible until the development of fine forms of retrograde transport material capable of giving Golgi-type resolution of cell bodies and dendrites (Schwartz and Coleman 1981).

The classical studies of the EC (Lorente de Nó 1933; Ramon y Cajal 1901-1902), using Golgi labelling, had described several types of cells in layer II. Only one type was identified as hippocampally projecting with "long-axon cylinders projecting to the white matter". This was the spiny "stellate cell" of Ramon y Cajal or "star cell" of Lorente de Nó which was so abundant in layer II that the latter termed this layer the "star cell layer". Other neuronal types in layer II were described as having "short axon cylinders" and included various spindle-like and multipolar neurons, and interestingly enough, pyramidal cells found in lower layer II. More recently, Schwartz and Coleman (1981) using a fine form of the retrogradely transported product horseradish peroxidase (HRP) established that layer II neurons contributing to the PP were of several kinds, including pyramids, stellates, fusiforms, and horizontal tripolar and bipolar cells. Interestingly, they noted that the proportion of the differently labelled cell types was strikingly different between the

MEC and LEC. Inasmuch as retrogradely transported HRP does not stain the entire dendritic tree, subsequent studies, using *in vivo* intracellular injection of HRP (Lingenhöhl and Finch 1991) or neurobiotin (Tamamaki and Nojyo 1993), or combined retrograde tracing and intracellular injection of Lucifer Yellow (Germroth et al. 1989a; Germroth et al. 1991; Schwerdtfeger et al. 1990) attempted to refine the morphological identification of the neuronal types contributing to the PP.

With the recognition that layer II neurons are involved in several neurological and neuropsychiatric disorders (summarized in Chap. I), renewed interest was sparked in the various cell types of layer II, specially in primates, with emphasis on ultrastructural morphology (Goldenberg et al. 1995) and histochemical (Beall and Lewis 1992; Carboni et al. 1990; Peterson et al. 1996) or metabolic identity (Hevner and Wong-Riley 1992; Solodkin and Van Hoesen 1996). Interestingly, comparative studies between primates and nonprimates revealed that few interspecies differences in the dendritic geometry was encountered in the EC, while a lot of differences were demonstrated in the hippocampus proper (Belichenko 1993).

The present series of experiments was undertaken to bridge the gap between cellular morphology and physiology of layer II neurons of the MEC. The tracer biocytin (Horikawa and Armstrong 1988) was used because it affords - in a Golgi-like manner - complete labelling of dendritic domains and fine features such as dendritic spines and axon collaterals, while still allowing complete electrophysiological characterization of labelled neurons. It was found that the two electophysiologically different types encountered in layer II of the MEC, were, in addition, morphologically distinct. The following chapter deals with the electroresponsive properties of the two classes of neurons, while this chapter describes in detail the morphological characteristics of each class.

METHODS

Brain slices were derived from male Wistar rats (125-250 g.) using the following procedure. After Nembutal (30 mg/Kg) anesthesia, rats were transcarcardially perfused with cold (6-10 °C) oxygenated Ringer solution for one minute to eliminate red blood cells that obscure neuronal morphology demonstrated by peroxidase histochemistry. Rats were then decapitated, the brain was rapidly removed, and a block of tissue containing the retrohippocampal region was glued to a plexiglass support and placed in cold oxygenated Ringer. Horizontal slices were sectioned at 350 μm using a vibratome, then allowed to recover in incubation chambers for at least two hours, in Ringer solution at room temperature.

At the time of recording, a single slice was transferred to a submerged recording chamber, held in place with small silver wires, and perfused with normal oxygenated Ringer at 35±1 °C. Slices consisted of the EC, medial and lateral, the HF and portions of the perirhinal cortex. Layer II of the MEC was visually identified as a distinct dark band extending from the parasubiculum to the transition zone with the LEC (Fig. 1), as defined by Blackstad (Blackstad 1956).

Intracellular glass electrodes were filled with a 2% biocytin (Sigma) solution in 3 M potassium acetate or 3 M potassium chloride (tip resistance 100-200 MΩ). Cells were labeled by running the protocol for electrophysiological characterization (see Chapter III), which required at least 30 minutes of stable impalement. Following injections, slices were fixed in 4% paraformaldehyde in a potassium phosphate buffer solution (KPBS) for 2 hours, then transferred to a 30% sucrose solution and left overnight.

Slices were sectioned at 50-100 μm with a freezing microtome, washed several times in KPBS, then incubated for 2 hours in a 1% Triton X-100 and an avidin-biotin-horseradish-peroxidase complex (Vectastain Elite ABC kit, Vector Laboratories). Following several washes in KPBS, sections were reacted with diaminobenzidine (DAB,

Sigma; 0.1% DAB, 0.003% hydrogen peroxide in KPBS), mounted on slides, dehydrated and covered.

Intracellularly stained neurons with their entire dendritic arborization and axonal projections were reconstructed by camera lucida 2-dimensional tracing at a 500 X magnification. Morphometric analysis was done automatically by the Biocom software system (Biocom 200, France) from thin slices visualized on a monitor screen. Morphometric parameters included perimeter, surface area, long and short dimension of neuronal somata, and diameter of proximal processes. Extent of dendritic fields was estimated from the camera lucida reconstructions.

Solutions. Ringer solution consisted of (in mM): 124 NaCl; 5 KCl; 1.2 KH_2PO_4; 2.4 $CaCl_2$; 2.6 $MgSO_4$; 26 $NaHCO_3$; and 10 glucose. pH was adjusted to 7.4 by saturating with 95% O_2 and 5% CO_2. KPBS consisted of (in mM): 50 K_2HPO_4; 50 KH_2PO_4. pH adjusted to 7.2-7.4.

RESULTS

The results described here are based on 34 biocytin-injected neurons in layer II of the MEC (Fig.1), in which detailed electrophysiological characterization was performed. As described in the following chapter, these cells fell into two categories as defined on the basis of their electroresponsive properties. One category included those neurons (n=22) that exhibited sustained, sinusoidal like, subthreshold membrane potential oscillations around -54 mV, and a pronounced slow voltage peak (Fig. 2A) that determined early firing upon current pulse injection from rest. The other category included those neurons (n=12) that never developed sustained subthreshold oscillatory activity and which displayed a slowly rising ramp potential (Fig. 2B) that culminated with the generation of an action potential at a long latency upon current pulse injection fom rest. Neurons in the first and second category will be referred to temporarily as Type I and Type II neurons.

Intracellular labelling revealed that Type I and Type II neurons belonged to clearly distinct morphological classes, whose attributes will be described in detail in the remaining text.

TYPE I NEURONS

All Type I neurons (22/34) were identified morphologically as the stellate cells of Ramon y Cajal (1901-1902), on the basis of soma shape and dendritic tree. The cell body within layer II was preferentially located in the superficial (towards the pia; n=10) or middle (n=9) third; only 3 neurons were located in the deepest third of layer II (Figs 3A, 4, 7).

The soma shape was ovoid or trapezoid, with elongation always oriented perpendicular to the pial surface (Fig. 7); some circular outlines were encountered (n=3). The average somatic dimensions were 23.0±4.4 μm (n=22; range 16-30 μm) by 12.9±2.2 (n=22; range 10-16 μm).

The majority of neurons had 5 (n=16) or 6 (n=3) thick primary dendrites. Usually, the primary dendrites arising from the top (pial) surface (2 or 3) where the thickest, reaching 5.6-7.5 μm as measured at the base, while the lower dendrites were thinner (2.3-4.5 μm) (Figs 3, 4, 7). Occasionnaly, primary dendrites were of uniform thickness (5.0-5.9 μm) and these belonged to perikarya located only in the superficial third of layer II. Among the 3 neurons encountered in the deep third of layer II, 2 had one primary dendrite substantially thicker than the rest, rising vertically before branching into two secondary dendrites, well below the boundary between layers I and II (Figs 4, 7 far right). Dendrites tapered slowly, and still appeared relatively thick far from the soma (Figs 5A, 5B). They were commonly very sinuous and undulatory, sometimes forming spirals (Fig. 3B). When dendrites thinned down they became beaded, and this was seen mostly on distal lower dendrites.

Primary dendrites emerged most frequently from the top and bottom poles of the cell, giving neurons a bi-tufted appearance after multiple branching. When dendrites

originated from the sides of the cell, they mostly curved upwards, coursing obliquely in layer I towards the pial surface. Upper, superficially directed dendrites, were very long and diverged widely, forming a V-shaped dendritic domain in which the distal processes frequently reached the pial surface and could run parallel to it (Figs 3A, 4). The medio-lateral expanse (distance between the two most diverging dendrites) of the upper dendritic field ranged from 310 to 720 μm (average: 497±154 μm; n=20). Lower dendrites were also widely divergent and extended over the superficial part of layer III; since, however, they were shorter than the upper ones, the medio-lateral expanse of the lower dendritic field was, for each cell, about half that of the upper one (Figs 3A, 4) and ranged from 120 to 350 μm (average: 231±69 μm; n=20). Because few dendrites arose from the sides of the cell (and when they did they bent upwards, or more rarely, downwards), the densest dendritic coverage did not occur in the bulk of layer II. The full dendritic domain thus appeared bitriangular with the soma sitting on the apices.

Dendritic spines were abundant and evenly distributed throughout the dendritic tree. Spines had a delicate appearance with a distinct head and a long and very thin stalk (Figs 5B, 5C). Dendrites most frequently ended with a bouquet of 3-6 spines with a stalk typically longer than the rest (Fig. 5E). In addition to spines, a few thin and long dendritic appendages were observed in most cells (Fig. 5D).

In 16 of the cells, the axon was seen coursing radially down towards the angular bundle, and, in 12 of those cells, the origin could be visualized. The axon arose from a primary dendrite, close to the soma (Figs 4, 6A, 7), except in one instance where the axon appeared to emerge from the base of the cell (Fig. 3A). The axon was relatively thick, as measured about 40 μm away from the soma (1.4±0.2 μm; n=10), and was generally smooth, rarely beaded. The axon followed a very straight course and in most cases (n=9) could be traced to the deep layers (V/VI). In two other neurons the axon could be seen entering the angular bundle and giving off a branch in the subiculum. Within its initial 200-400 μm (deep layer II/superficial layer III), the axon always gave off several (3-5) very

thin recurrent collaterals that bent upwards and branched repeateadly, forming a delicate net over the entire dendritic domain of the labeled cell (Fig. 6A). Some of the ascending branches extended also beyond the dendritic field, medially and laterally, in layers II and I (Fig. 6C). In addition, the axon gave off a few (1-3) collaterals in deep layer III and layers IV-VI (Fig. 6B). Axon collaterals were always beaded, with evenly distributed round swellings, and frequently terminated in a flower-like manner, with several long appendages capped by boutons.

TYPE II NEURONS.

None of the labelled type II cells (n=12) had a stellate morphology. 11 of them had a pyramidal-like appearance, while the remaining neuron was classified as a horizontal tripolar cell. The cell body of the pyramidal-like neurons was preferentially located in the deepest third of layer II (n=6); only 3 neurons were encountered in the middle third, and 2 in the superficial third of the layer (Figs 8A, 11). The tripolar cell was located superficially in layer II (Figs 10A, 11 far right). The following deals with the pyramidal-like neurons while a description of the horizontal tripolar cell will be left to the end.

The soma shape of the pyramidal-like neurons was ovoid or triangular, with elongation oriented perperdicularly to the pial surface (n=9) or oblique to it (n=2). The average somatic dimensions were 20.8±3.9 μm (n=11; range 16-26 μm) by 11.1±2.0 μm (n=11; range 8-15 μm). The majority of cells (n=7) had one prominent thick (4.3±1.5 μm) apical dendrite that branched at or above the border with layer I (Fig. 8). The apical dendrite rose vertically, except for the 2 cells with perikarya oriented oblique to the pial surface, in which the apical dendrite (as well as the whole dendritic tree) had an oblique orientation (Fig. 9A). In fact, these 2 cells were perfectly identical to the previous ones except that they were tilted. Secondary branches to this apical dendrite were almost perpendicular to it (Figs 8, 9A, 9B). The remaining cells (n=4) had two thick apical dendrites rising vertically prarallel to each other or diverging slightly. One of these two

apical dendrites always advanced further in layer I, and branched more profusely, than the other (Fig 9C). In all neurons, the basal dendrites were thin, relatively short and straight, and commonly beaded distally; they arose all around the soma and branched extensively, thus forming a basal skirt surrounding the soma (Figs 8, 9A, 9C).

In all pyramidal-like cells, very few superficial dendrites reached the pial surface, and basal dendrites were confined to the most superficial portion of layer III. The medio-lateral expanse of the upper dendritic field ranged from 100 to 360 μm (average 184±75 μm; n=11) and was thus about one third of that of Type I neurons. The lower dendritic field was equivalent in extent to the upper one (average 185±35 μm; n=11). The overall dendritic domain had thus a rectangular appearance (obliquely oriented for the tilted cells) with the soma sitting towards the base.

In general, cells were more densily covered with dendritic spines than Type I neurons (Figs 8B, 9B, 9D). Spines were particularly dense on the apical dendrite and some cells were so heavily populated with spines that these almost completely concealed the dendritic trunk. Spines appeared to have a shorter stalk and a larger head than those of Type I neurons (Figs 9B and D).

In 5 neurons the axon could be visualized, and in those 5 cells, always originated from the soma (Fig. 11). The axon was relatively thin (0.6±0.2 μm; n=5) and smooth. The axon followed a sinuous route before it took a radial course towards the angular bundle. The tortuosity was particularly evident in the dorso-ventral extent since, in 4 out of the 5 neurons, the axon was frequently lost from the horizontal plane containing the soma and the main dendritic field, and reappeared 100-150 μm above or below. In one neuron, the axon was seen penetrating the angular bundle, and in 2 other cells, could be followed down to layer VI. Axon collaterals branched repeateadly, giving off very thin and beaded fibers that had a similar aspect and distribution to those observed in Type I neurons.

The horizontal tripolar cell. This cell had a distincly different appearance from the pyramidal-like neurons. It was very elongated (26 by 12 μm), with elongation parallel to

the pial surface (Fig. 10A). It had 3 primary dendrites, with the 2 emerging from the lateral poles much thicker than the remaining one emerging from the basal pole (Fig. 11, far right). The dendritic field of this cell was almost circular with a diameter of 230 μm, and extended mainly over layer II and the bottom part of layer I. Dendrites were very heavily populated with short spines capped with a thick head (Fig. 10C). The axon (0.8 μm) originated from the soma (Figs 10A, 10B, 11 far right) and could be traced to deep layer III. Axonal collateralisation was extensive; beaded collaterals ascended and descended to cover layers I, II and III (Fig. 10C), medially extending as far as the parasubiculum.

DISCUSSION

The results described show that layer II neurons of the MEC, classified into Type I or Type II neurons on the basis of their electroresponsive properties, could also be distinguished according to their morphological characteristics. Type I neurons were morphologically homogenous and were all alike to the spiny stellate cells described by Ramon y Cajal (1901-1902) and Lorente de Nó (1933). Type II neurons appeared less homogenous morphologically, and consisted of pyramidal-like neurons and a horizontal tripolar cell. Both Type I and Type II neurons were principal neurons since the axon could be seen projecting to the angular bundle. From now on, in view of the clear-cut morphological differences between the two types of electrophysiologically defined classes, Type I neurons will be referred to as stellate cells (SCs), and Type II neurons as non-stellate cells (non-SCs).

SCs and non-SCs were found to constitute 65% and 35% of sampled neurons respectively. Schwartz and Coleman (1981), in a study of retrogradely labeled neurons, report a figure of 81% for the stellate morphology in layer II of the MEC. The discrepancy might reflect, in the present study, a selective vulnerability to impalement of SCs *versus* non-SCs. With regard to the non-SCs, the identification of a single tripolar cell (3% of

sampled neurons) agrees well with the figure of 2% reported by the same authors for this type of cell.

STELLATE CELLS

The features most clearly distinguishing SCs from the pyramidal-like non-SCs were the presence, in SCs, of multiple, thick, primary dendrites and of a widely diverging dendritic tree. In addition, the axon in SCs was consistently observed to emerge from a primary dendrite, a feature never observed in the non-SCs. Consistent with Schwartz and Coleman's (1981) observation that the cell body orientation and dendritic tree of layer II MEC stellate cells were, in general, different from those of LEC stellate cells, the SCs described here were perfectly identical to stellate cells described elsewhere in the MEC (Lingenhöhl and Finch 1991; Schwartz and Coleman 1981; Tamamaki and Nojyo 1993) but slightly different from those reported for the LEC (Carboni et al. 1990; Germroth et al. 1989a; Germroth et al. 1991; Lingenhöhl and Finch 1991).

SCs were preferentially located superficially in layer II (14% only in the bottom third) while non-SCs were preferentially located towards the bottom of layer II (17% only in the superficial third for pyramidal-like cells). For the SCs located towards the bottom of layer II and exhibiting a thick vertical dendrite (thus superficially resembling pyramidal cells), these could still be distinguished from the non-SCs since the "apical" dendrite branched well below the layer I/layer II boundary, and secondary branches diverged widely as in all other SCs.

The dendritic tree of SCs was very characteristic, diverging widely to reach its maximum medio-lateral expanse (up to more than 700 μm) in the most superficial portions of layer I, in agreement with Tamamaki and Nojyo (1993). The characteristics of the dendrite branching were such that the densest dendritic coverage did not occur in the bulk of layer II, but in layer I for the upper dendritic field, and in the superficial portion of layer III for the lower dendritic field.

Dendritic spines of SCs appeared more complex than those of non-SCs, in agreement with the ultrastructural study of Germroth et al. (1991). The dendritic appendages observed in most SCs were also reported in stellate cells described by Lingenhöhl and Finch (1991) and suggested to represent transynaptically stained axonal processes.

In SCs, the axon, which characteristically arose from a primary dendrite, had a diameter more than double that of the non-SCs. As reported in this study, axonal branches in the subiculum, and axonal collaterals extending over all layers but mostly over the superficial ones, have been described for stellate cells in the MEC (Lingenhöhl and Finch 1991; Tamamaki and Nojyo 1993).

NON-STELLATE CELLS

Pyramidal-like cells. These cells had a classical pyramidal morphology, or slight variants of it. Layer II pyramids, as described in this study and observed by others (Carboni et al. 1990; Germroth et al. 1989a; Germroth et al. 1991; Schwartz and Coleman 1981) have a short apical dendritic shaft that bifurcates close to (but always above) the border with layer I. In the few cells characterized by 2 apical dendrites, the upper and basal dendritic trees were similar to those with a single apical dendrite. As to the obliquely oriented pyramidal cells, these have been noted in layer III as well as layer II (Carboni et al. 1990).

Horizontal tripolar cell. In addition to stellate cells and pyramidal like cells, other spiny and sparsely spiny neuronal types have been described in layer II including fusiform, horizontal and multipolar neurons (Germroth et al. 1989a; Germroth et al. 1989b; Schwartz and Coleman 1981). The spiny horizontal tripolar cell described here is identical to the horizontal tripolar cell reported in Schwartz and Coleman (1981). The horizontal tripolar cell of Schwartz and Coleman has been classified as a type of stellate cell (second type of stellate cell of Germroth et al. 1989a). In the present study, a constellation of

features, including the horizontal orientation of the soma, the dendritic tree, and the axon emerging from the base of the soma, clearly distinguish this type of cell from the described SCs.

FUNCTIONAL CONSIDERATIONS

Both SCs and non-SCs may collect input from layers I, II and III. However, SCs appear to do so from a much larger medio-lateral expanse of the EC than non-SCs. While SCs can integrate input from a large horizontal band reaching its maximum extent in superficial layer I, non-SCs integrate input from a horizontally restricted vertical column (oblique column for the oblique pyramidal-like cells). SCs as well as non-SCs have extrinsic axons projecting outside the EC. In addition, they are also characterized by extensive recurrent axon collateralization and therefore substantially contribute to the local intrinsic circuitry. This dual feature makes them function both as local circuit and projection neurons. As already suggested (Germroth et al. 1991), this may be a widespread, and hence functionally significant feature of principal neurons, since it has been described in other cortical areas (Gabbott et al. 1987). However, in layer II of the MEC, it appears that long, horizontal connections between cells located relatively far apart are particularly prominent (Köhler 1986). Asymmetric synapses of layer II spiny neurons on dendritic spines within the local surrounding (Germroth et al. 1991) imply that local excitatory connections with other excitatory neurons are established. Considering that the vast majority of MEC layer II neurons (the SCs) are intrinsic oscillators in the subthreshold range (described in detail in chapter III), recurrent connections would rapidly generate and amplify a synchronous oscillatory wave triggered by a relatively small original input (König et al. 1992; Williams 1992). As discussed later in this work, this could have far reaching implications for information processing within the EC.

In addition to electrophysiological and morphological heterogeneity, layer II neurons display a high degree of chemical diversity (Beall and Lewis 1992; Solodkin and

Van Hoesen 1996), which has been proposed to underlie the selective targeting of neuronal populations in the various neuropsychiatirc disorders affecting layer II. In an EC layer II neuronal degeneration model, glutamatergic calbindin-positive neurons in layer II were found to be selectively resistant to axotomy-induced death (Peterson et al. 1996), with calbindin-positivity detected in pyramidal and other non-stellate types (Beall and Lewis 1992). Cell islands in primate layer II, where stellate cells are selectively clustered (Carboni et al 1990), were found to be darkly reactive to staining for cytochrome oxydase (Hevner and Wong-Riley 1992), an enzyme closely related to the level of functional activity in neuronal pathways (Wong-Riley 1989). It is therefore tempting to speculate that the intrinsic electroresponsive properties of SCs, and particularly their ability to generate sustained rhythmic behavior, exert a high metabolic demand which might lead to selective degeneration because SCs do not seem to posess the protective mechanins that non-SCs are endowed with.

REFERENCES

Beall, M. J. and Lewis, D. A. Heterogeneity of layer II neurons in human entorhinal cortex. *J. Comp. Neurol.* 321: 241-266, 1992.

Belichenko, P. Neuronal cell types in entorhinal cortex and hippocampal formation of man and other mammalia: an interspecies comparison. *Hippocampus.* 3: 3-10, 1993.

Blackstad, T. W. Commissural connections of the hippocampal region in the rat, with special reference to their mode of termination. *J. Comp. Neurol.* 105: 417-537, 1956.

Carboni, A. A., Lavelle, W. G., Barnes, C. L., and Cipolloni, P. B. Neurons of the lateral entorhinal cortex of the rhesus monkey: a Golgi, histochemical, and immunocytochemical characterization. *J. Comp. Neurol.* 291: 583-608, 1990.

Gabbott, P. L. A., Martin, K. A. C., and Whitteridge, D. Connections between pyramidal neurons in layer 5 of cat visual cortex (area 17). *J. Comp. Neurol.* 259: 364-381, 1987.

Germroth, P., Schwerdtfeger, W. K., and Buhl, E. H. Morphology of identified entorhinal neurons projecting to the hippocampus. A light microscopical study combining retrograde tracing and intracellular injection. *Neuroscience.* 30: 683-691, 1989a.

Germroth, P., Schwerdtfeger, W. K., and Buhl, E. H. GABAergic neurons in the entorhinal cortex project to the hippocampus. *Brain Res.* 494: 187-192, 1989b.

Germroth, P., Schwerdtfeger, W. K., and Buhl, E. H. Ultrastructure and aspects of functional organization of pyramidal and nonpyramidal entorhinal projection neurons contributing to the perforant path. *J. Comp. Neurol.* 305: 215-231, 1991.

Goldenberg, T. M., Bakay, R. A. E., and Ribak, C. E. Electron microscopy of cell islands in layer II of the primate entorhinal cortex. *J. Comp. Neurol.* 355: 51-66, 1995.

Hevner, R. F. and Wong-Riley, M. T. T. Entorhinal cortex of the human, monkey, and rat: metabolic map as revealed by cytochrome oxidase. *J. Comp. Neurol.* 326: 451-469, 1992.

Hjorth-Simonsen, A. and Jeune, B. Origin and termination of the hippocampal perforant path in the rat studied by silver impregnation. *J. Comp. Neurol.* 144: 215-232, 1972.

Horikawa, K. and Armstrong, W. E. A versatile means of intracellular labeling: injection of biocytin and its detection with avidin conjugates. *J. Neurosci. Methods.* 25: 1-11, 1988.

Köhler, C. Intrinsic connections of the retrohippocampal region in the rat brain. II. the medial entorhinal area. *J. Comp. Neurol.* 246: 149-169, 1986.

König, P., Janosch, B., and Schillen, T. B. Stimulus-dependent assembly formation of oscillatory responses: III learning. *Neural Comput.* 4: 666-681, 1992.

Lingenhöhl, K. and Finch, D. M. Morphological characterization of rat entorhinal neurons in vivo: soma-dendritic structure and axonal domains. *Exp. Brain Res.* 84: 57-74, 1991.

Lorente de Nó, R. Studies on the structure of the cerebral cortex. I. The area entorhinalis. *J. Psychol. Neurol.* 45: 381-438, 1933.

Peterson, D. A., Lucidi-Phillipi, C. A., Murphy, D. P., Ray, J., and Gage, F. H. Fibroblast growth factor-2 protects entorhinal layer II glutamatergic neurons from axotomy-induced death. *J. Neurosci.* 16: 886-898, 1996.

Ramon y Cajal, S. Estudios sobre la corteza cerebral humana. *Trab. Inst. Cajal. Invest. Biol.* 1: 1-227, 1901-1902.

Schwartz, S. P. and Coleman, P. D. Neurons of origin of the perforant path. *Exp. Neurol.* 74: 305-312, 1981.

Schwerdtfeger, W. K., Buhl, E. H., and Germroth, P. Disynaptic olfactory input to the hippocampus mediated by stellate cells in the entorhinal cortex. *J. Comp. Neurol.* 292: 163-177, 1990.

Solodkin, A. and Van Hoesen, G. W. Entorhinal cortex modules of the human brain. *J. Comp. Neurol.* 365: 610-627, 1996.

Steward, O. Topographic organization of the projections from the entorhinal area to the hippocampal formation of the rat. *J. Comp. Neurol.* 167: 285-314, 1976.

Steward, O. and Scoville, S. A. Cells of origin of entorhinal cortical afferents to the hippocampus and fascia dentata of the rat. *J. Comp. Neurol.* 169: 347-370, 1976.

Swanson, L. W. and Köhler, C. Anatomical evidence for direct projections from the entorhinal area to the entire cortical mantle in the rat. *J. Neurosci.* 6: 3010-3023, 1986.

Tamamaki, N. and Nojyo, Y. Projection of the entorhinal layer II neurons in the rat as revealed by intracellular pressure-injection of neurobiotin. *Hippocampus.* 3: 471-480, 1993.

Williams, T. L. Phase coupling by synaptic spread in chains of coupled neuronal oscillators. *Science.* 258: 662-665, 1992.

Wong-Riley, M. T. T. Cytochrome oxidase: an endogenous metabolic marker for neuronal activity. *Trends Neurosci.* 12: 94-101, 1989.

Figure 1. Horizontal section of the retrohippocampal area in a rat brain. MEC, medial entorhinal cortex; LEC, lateral entorhinal cortex; PAR, parasubiculum; PRE, presubiculum; PERI, perirhinal cortex. Layer II of the MEC is shown in grey.

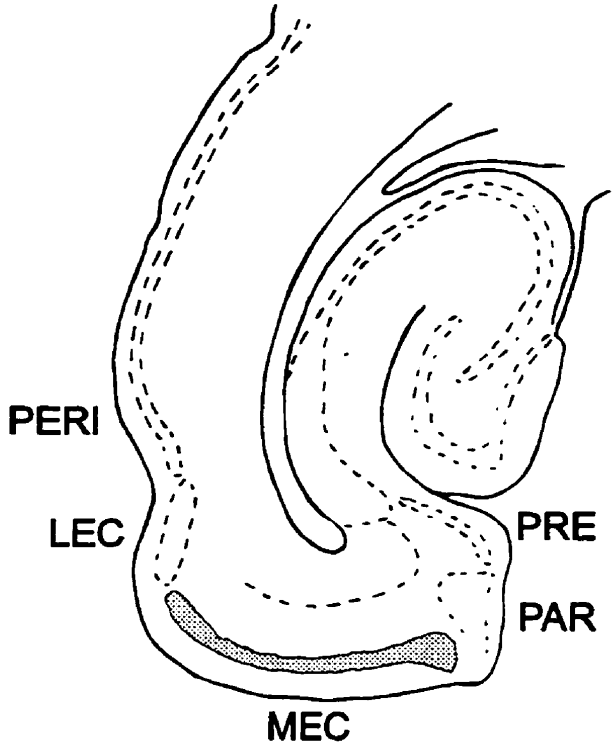

Adapted from Swanson and Köhler 1986, p. 3018

Figure 2. Characteristic electroresponsive properties of Type I (*A*) and Type II neurons (*B*). *A*: subthreshold rhythmic membrane potential oscillations exhibited by a Type I neuron in response to d.c current (0.31 nA) injection (top). In another Type I neuron, voltage response to a subthreshold depolarizing current pulse (0.23 nA). Note the sagging of the membrane potential, which determines that a Type I neuron will always fire early during the pulse, at the peak of the voltage response (bottom). *B*: in a Type II neuron d.c current injection (0.21 nA) does not elicit any rhythmic activity (top). In the same Type II neuron, voltage response to a subthreshold depolarizing current pulse (0.17 nA). The membrane potential charges slowly in a ramp-like manner (bottom), which determines that a Type II neuron will fire late during the pulse.

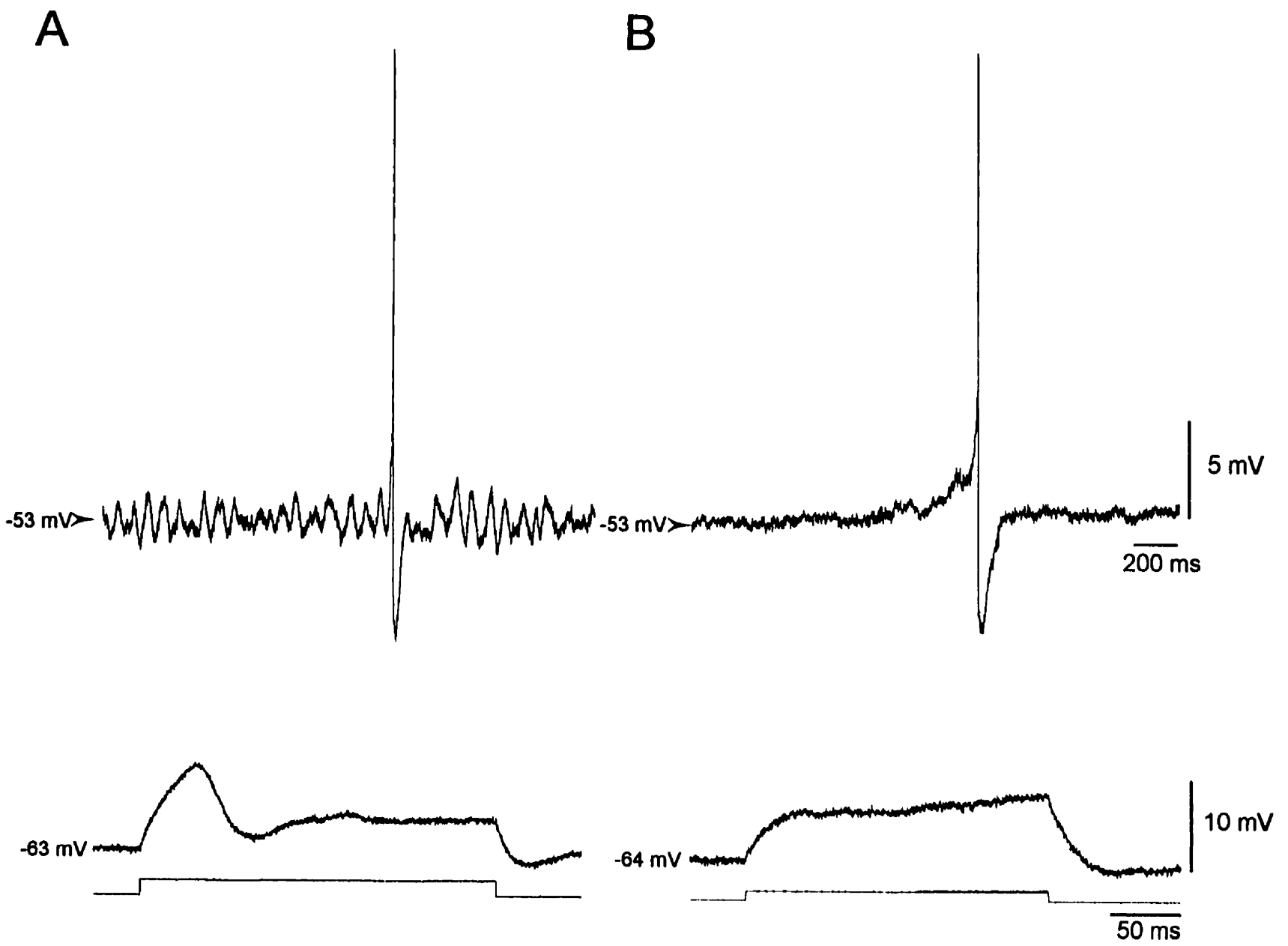
A
B
-53 mV
-53 mV
5 mV
200 ms
-63 mV
-64 mV
10 mV
50 ms

Figure 3. Type I neuron exhibiting the typical stellate morphology. *A*: camera lucida reconstruction of cell Ia. Note the multiple thick primary dendrites, the widely diverging upper and lower dendritic trees, with superficially directed dendrites reaching the topmost portion of layer I. Cell Ia was located in the superficial third of layer II and its axon (arrows) appeared to emerge from the base of the soma. Axon trunctated. *B*: photomicrograph of cell Ia showing the slowly tapering, long and sinuous dendrites, and the thick axon (arrow) emanating from the base of the cell.

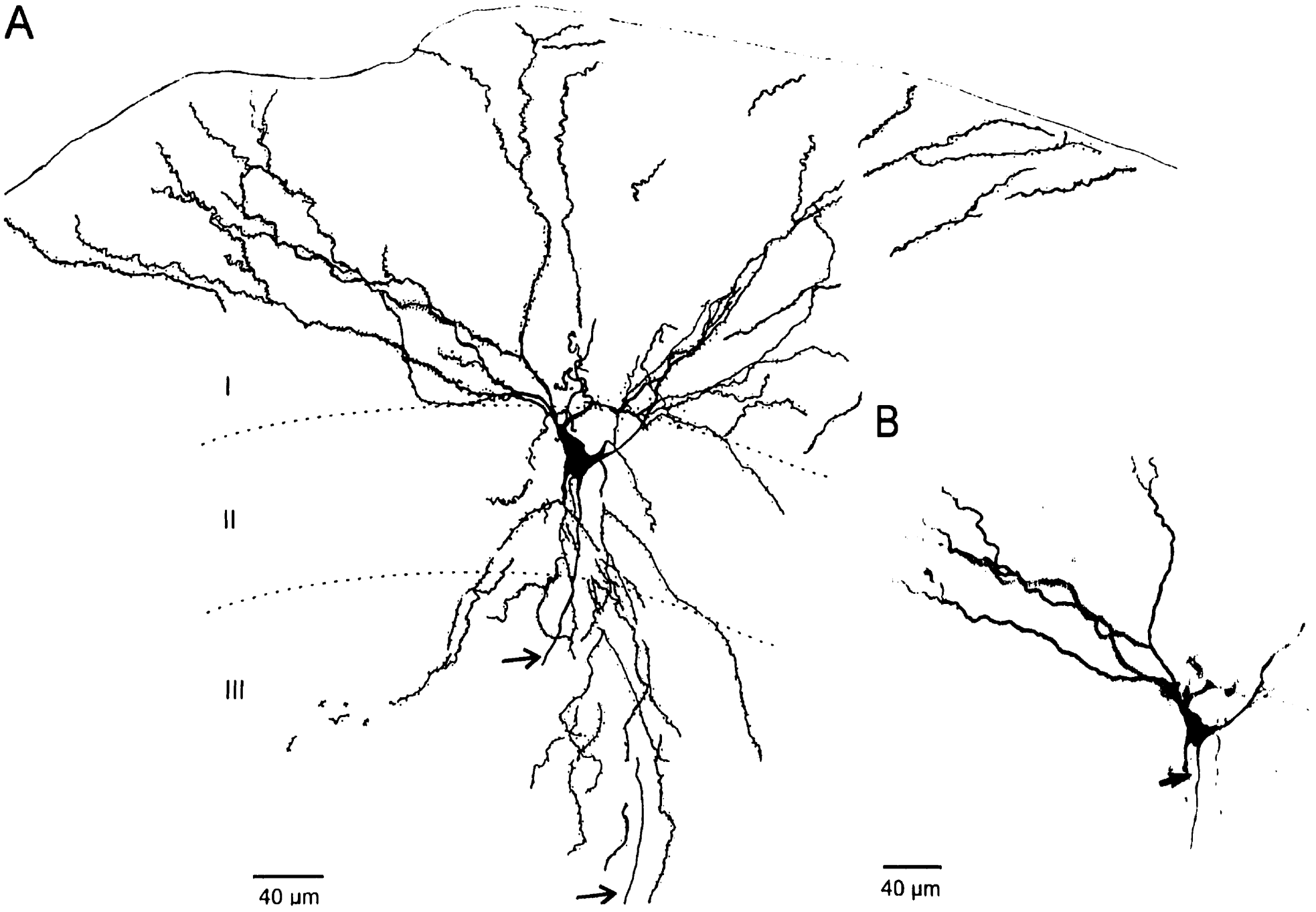
A
I
II
III
40 µm
B
40 µm

Figure 4. Camera lucida reconstruction of a Type I neuron (cell Ib) located in the deep third of layer II. Note the short "apical" dendrite which branches well below the border with layer I. Secondary dendrites then diverge widely as in other Type I neurons. The axon (large and small arrows) emerges from a thin dendrite 11 μm away from the soma. Axon truncated.

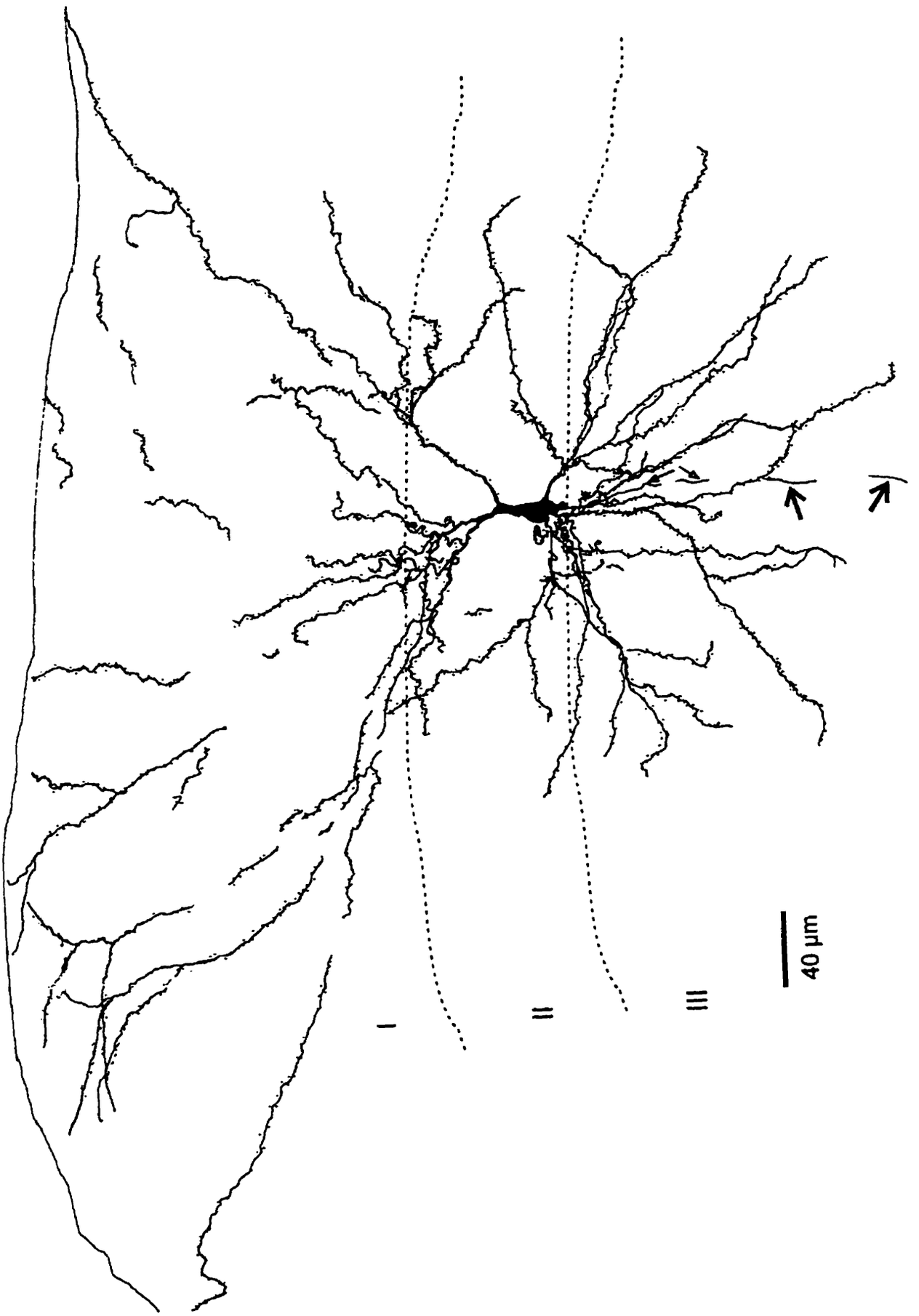
40 µm

Figure 5. Dendrites of Type I neurons. *A*: photomicrograph of cell Ic. *B*: detail of cell Ic showing thick dendrites covered witrh evenly distributed spines. *C*: detail of dendrite of cell Ic showing spines with a long and thin stalk and a distinct head (arrows). *D*: dendritic appendage (arrow) in cell Ic. *E*: bouquet of long spines (arrows) terminating a dendrite in cell Ic. Calibration bar in *C* applies also to *D* and *E*.

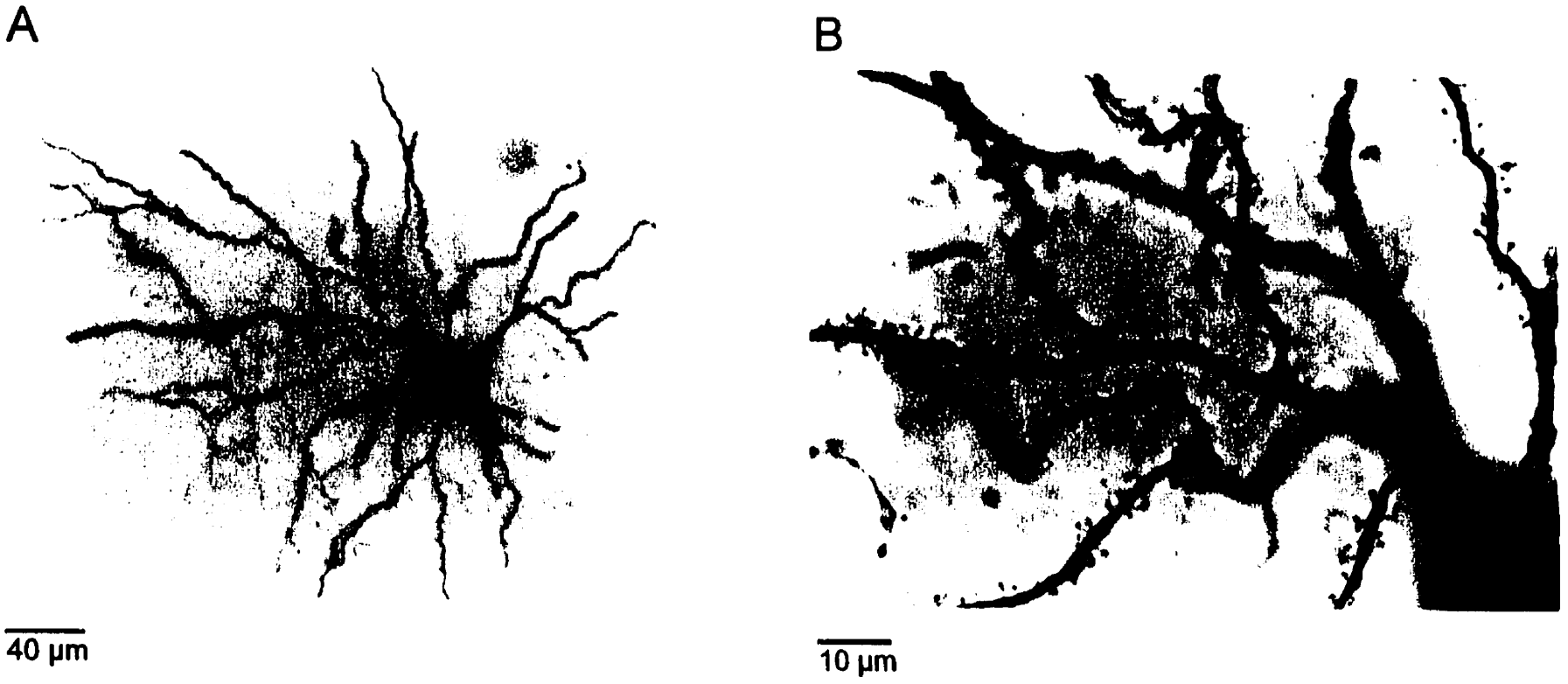
A
40 µm
B
10 µm
C
10 µm
D
E

Figure 6. Axon collaterals in Type I neurons. *A*: photomicrograph of lower dendritic field in cell Id showing beaded axon collaterals branching at right angles from the axon (arrow), and covering the dendritic field with a delicate net. *B*: Detail showing a collateral emerging from the axon in layer IV. *C*: beaded collaterals in layer II extending beyond the dendritic field.

A

B

C

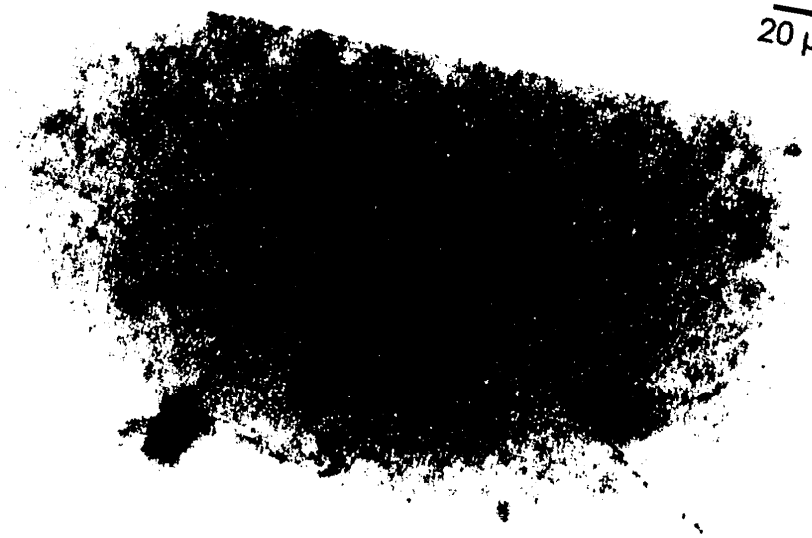

Figure 7. Camera lucida reconstructions of 4 Type I neurons (cells Ie, If, Ig, and Ih) showing details of soma shape, proximal processes (truncated; axon in red) and location within layer II. Note the multiple thick primary dendrites that emerge preferentially from the top and bottom poles of the cells, and the axon that emerges from a primary dendrite. Cell Ih (far right), located in the deep third of layer II and characterized by a thick vertically rising dendrite, was attributed a stellate morphology because of its dendritic tree which was similar to that of cell Ib in Fig. 4.

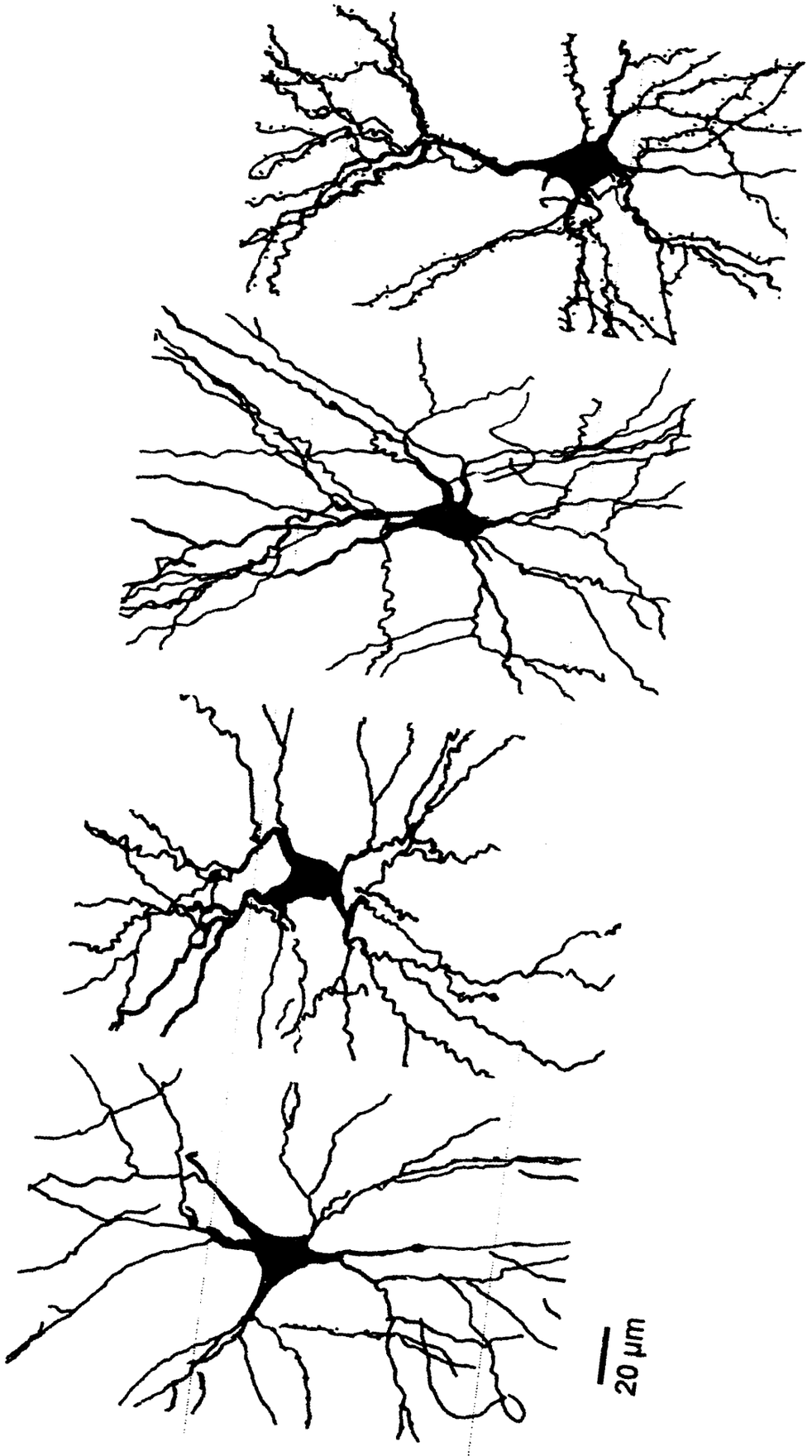
20 µm

Figure 8. Type II neuron exhibiting the typical pyramidal morphology. *A*: camera lucida reconstruction of cell IIa. Note the thick apical dendrite branching above the border with layer I, the thin basal dendrites arising radially from the soma, and the limited extent of the upper dendritic tree. The axon (arrows) emerges from the base of the soma, and branches in layer III. Axon trucated. *B*: photomicrograph of cell IIa. The apical dendrite is heavily populated with spines (arrows).

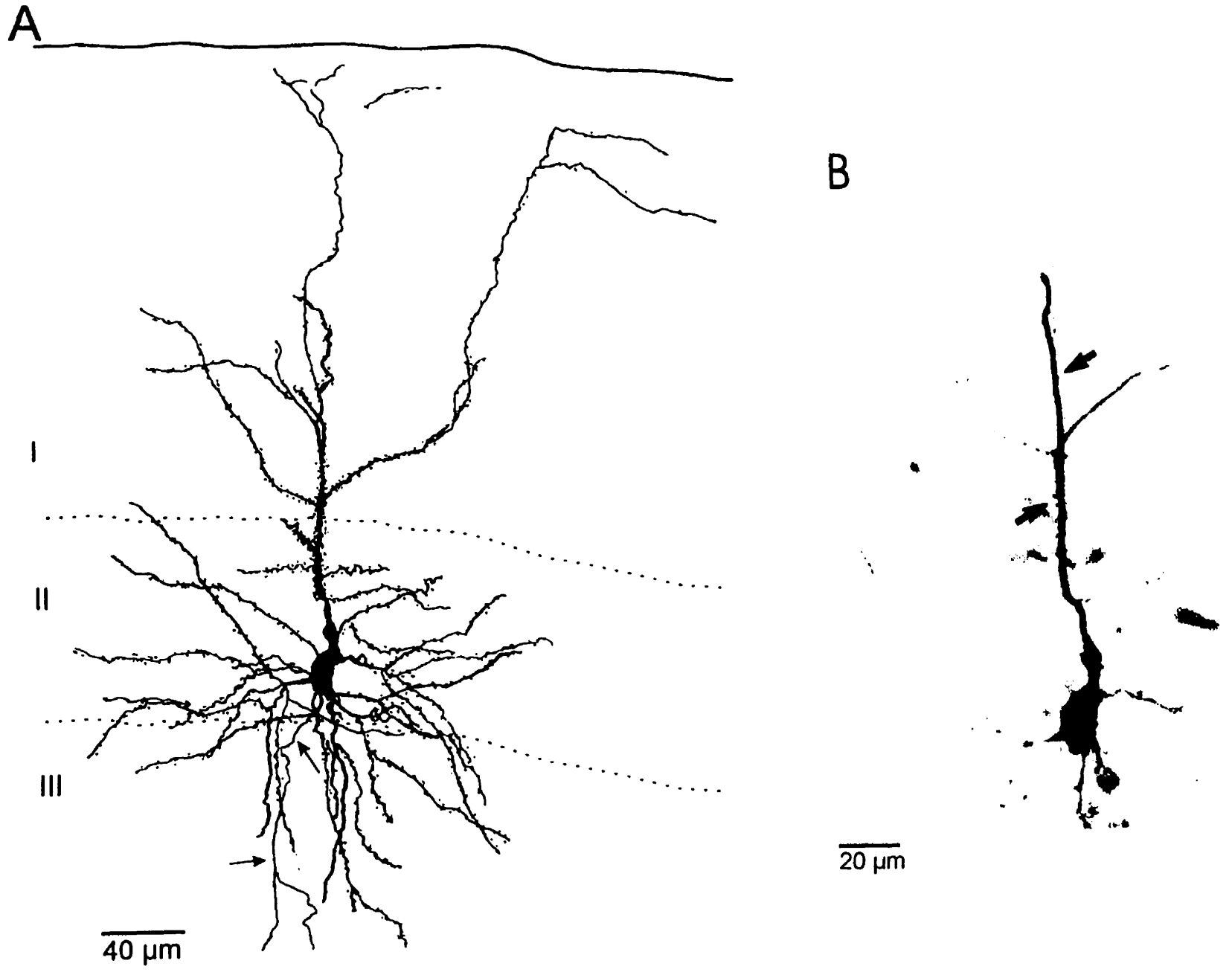
A
I
II
III
40 µm
B
20 µm

Figure 9. Other pyramidal-like morphologies of Type II neurons. *A*: photomicrograph of an obliquely oriented pyramidal-like neuron (cell IIb). *B*: detail of cell IIb showing apical dendrite covered with short spines (arrow). *C*: photomicrograph of a pyramidal-like neuron (cell IIc) with 2 apical dendrites. Note that only one of them extends to layer I. *D*: detail of cell IIc showing dendrites densely covered with short spines (arrows).

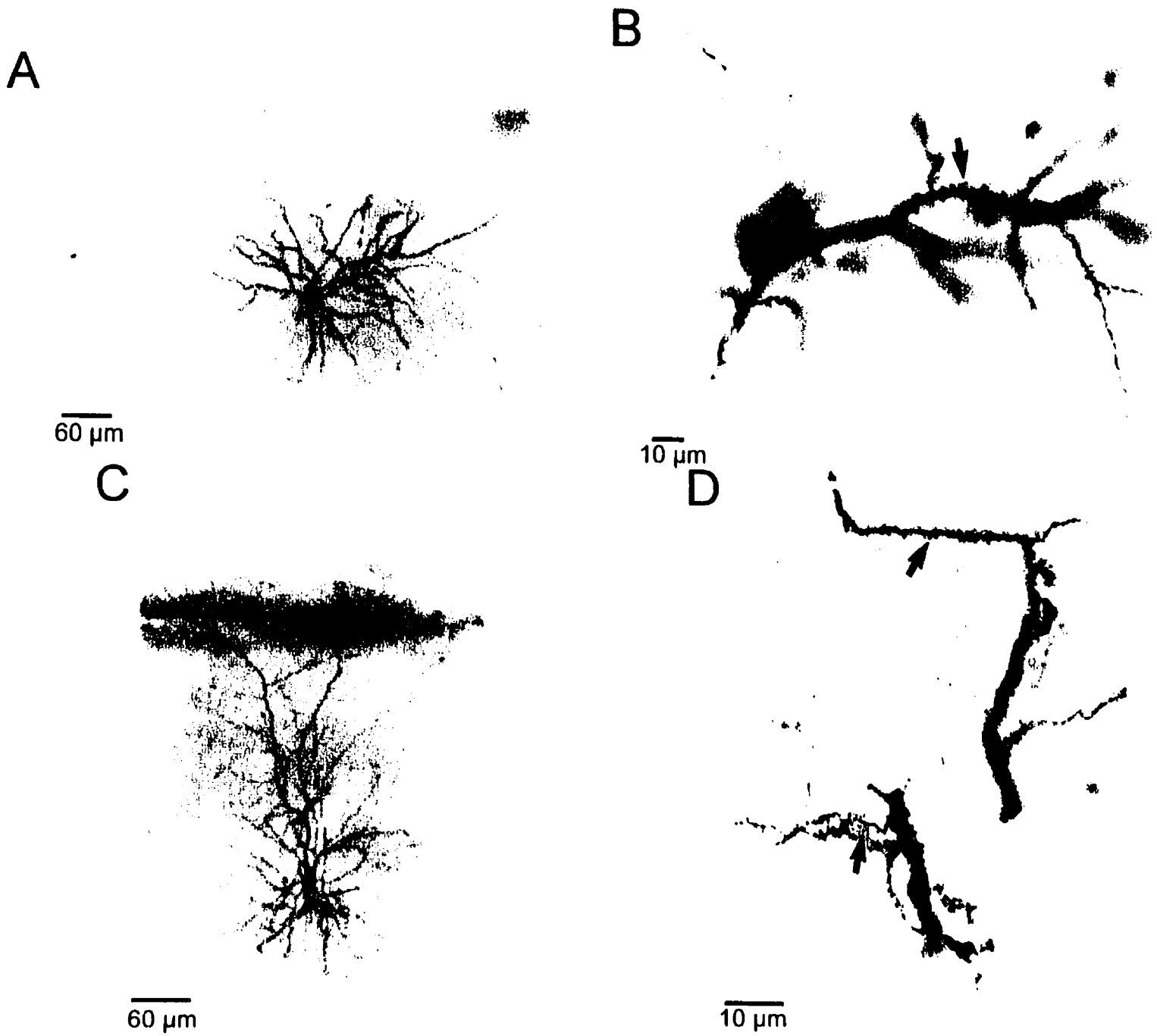
A
60 µm
B
10 µm
C
60 µm
D
10 µm

Figure 10. Type II neuron exhibiting a horizontal-cell morphology. *A*: camera lucida reconstruction of the horizontal tripolar neuron (cell IId). Note the orientation of the cell body with elongation parallel to the pial surface, the triangular soma shape with dendrites emerging from the apices, and the axon arising from the base of the soma (arrow). Axon truncated. *B*: photomicrograph of cell IId showing axon collaterals arising from the axon (arrow) and extending over the lower dendritic field. *C*: detail of cell IId showing dendrites very heavily covered with short spines.

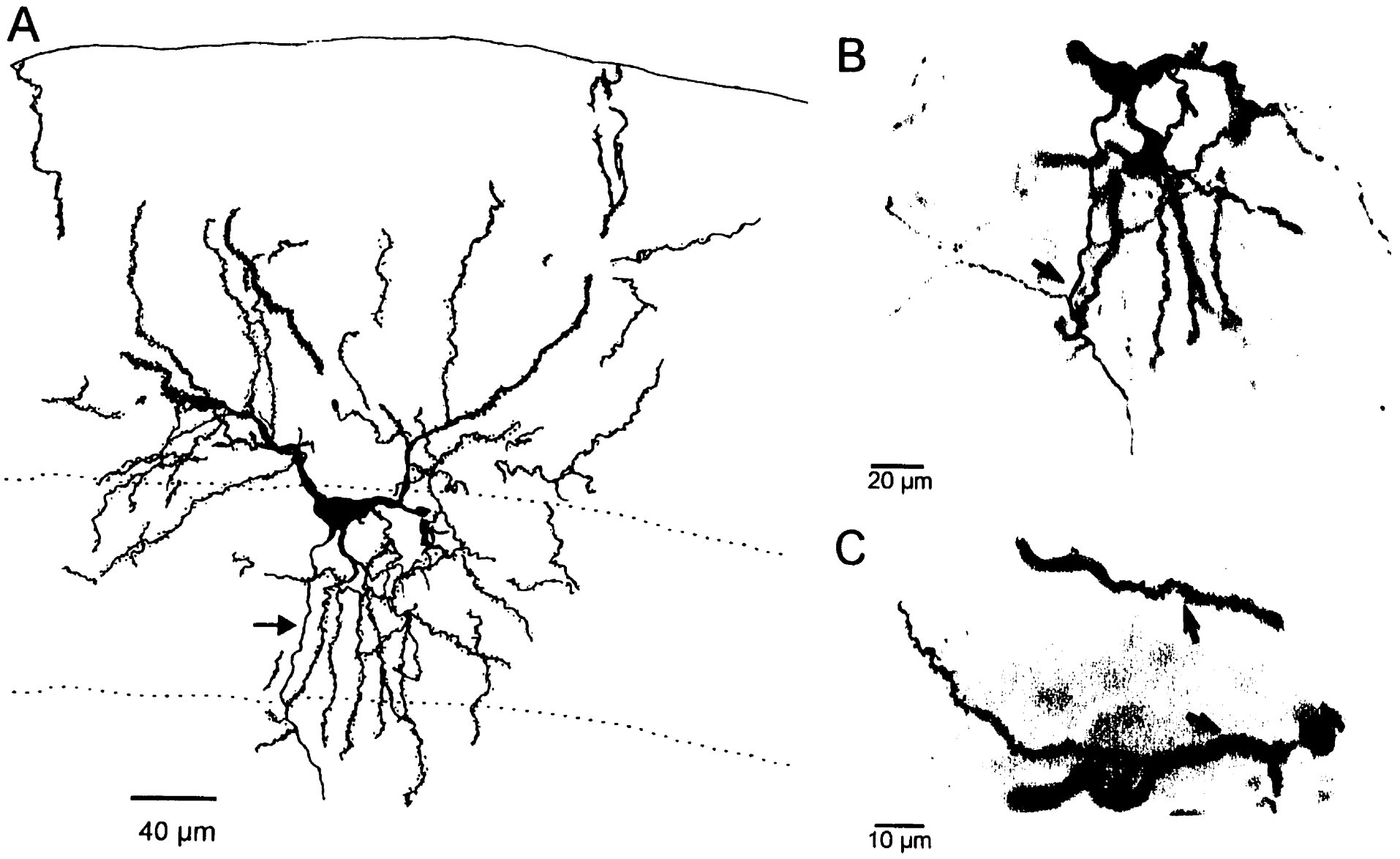
A
B
C
40 µm
20 µm
10 µm

Figure 11. Camera lucida reconstructions of the 4 Type II neurons shown previously (cells IIa, IIb, IIc and IId) showing details of soma shape, proximal processes (truncated; axon in red) and location within layer II. Note that in the obliquely oriented pyramidal cell (IIb) the axon runs perpendicular to the pial surface and does not follow the oblique orientation of the cell.

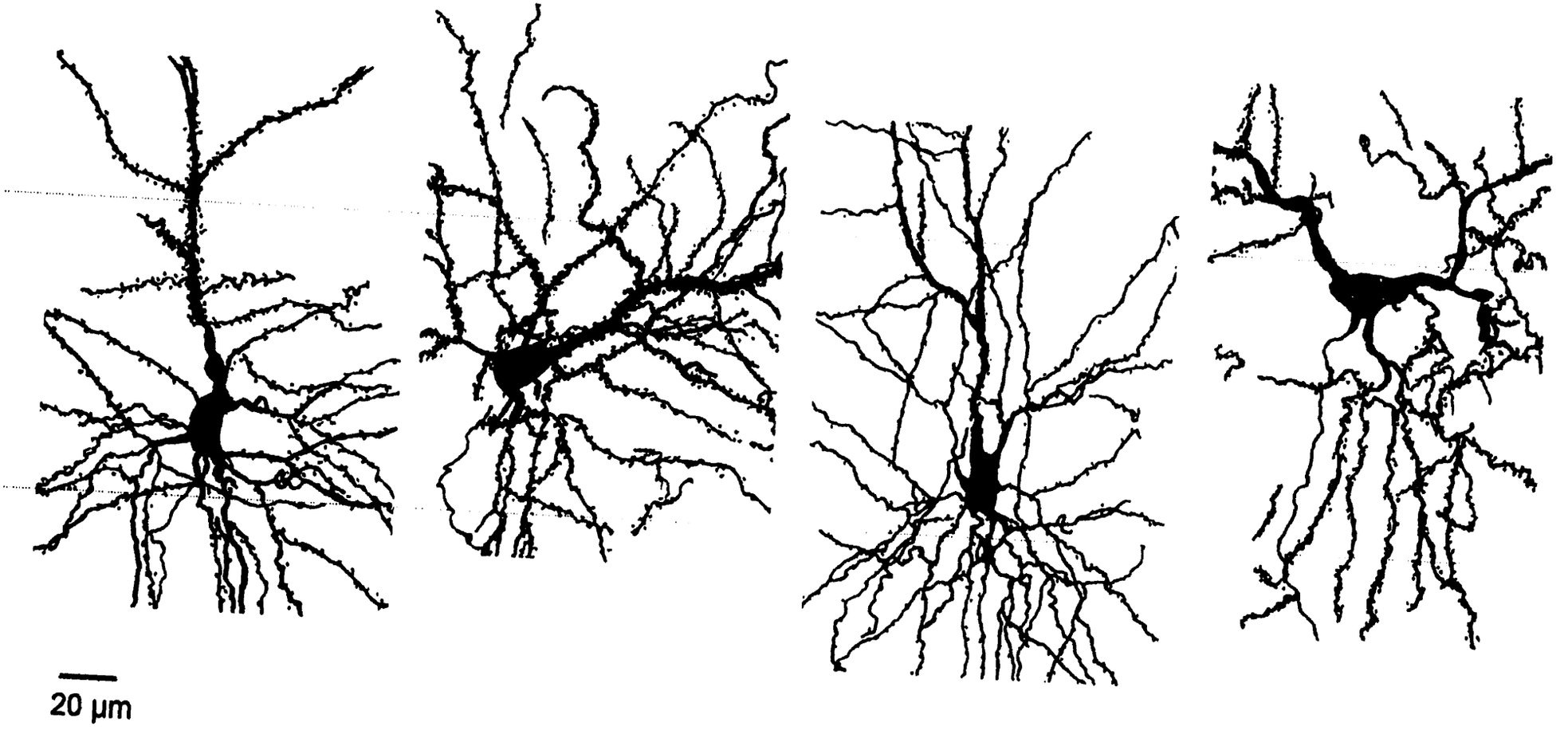
20 µm

CHAPTER III

DIFFERENTIAL ELECTRORESPONSIVENESS OF STELLATE AND PYRAMIDAL-LIKE CELLS OF MEDIAL ENTORHINAL CORTEX LAYER II

Angel Alonso and Ruby Klink

ABBREVIATIONS

AHP Afterhyperpolarization

DS Depolarization induced sag

DAP Depolarizing afterpotential

EC Entorhinal cortex

HS Hyperpolarization induced sag

ISI Interspike interval

MEC Medial entorhinal cortex

NS Number of spikes

SC Stellate cell

SUMMARY AND CONCLUSIONS

1. The electroresponsive properties of neurons from layer II of the rat medial entorhinal cortex (MEC) were studied by intracellular recording under current clamp in an *in vitro* brain slice preparation. From a total of 184 cells that fulfilled our criteria for recording stability, two groups of projection neurons were distinguished on the basis of their intrinsic biophysical properties and morphological characteristics (demonstrated by intracellular biocytin injection; n=34).

2. Stellate cells (SCs) were the most abundant (69%). They were highly electroresponsive and minimal changes (1-3mV) of membrane potential generated an active response. Subthreshold depolarizing or hyperpolarizing current pulse injection always caused the membrane potential to attain an early peak and then sag to a lower level. Depolarization-induced "sags" were larger and determined early firing in all cells. The voltage-current relationship of SCs was markedly non-linear demonstrating robust inward rectification in the hyperpolarizing and depolarizing range.

3. SCs generated persistent rhythmic subthreshold voltage oscillations upon d.c. depolarization positive to -60mV. The mean frequency of the oscillations was 8.6Hz (theta range) at a membrane potential of ~ -55mV at which level occasional single spiking also occurred. At slightly more positive potentials, a striking 1-3Hz repetitive bursting pattern emerged. This consisted of non-adapting trains of spikes ("clusters") interspersed with subthreshold oscillations which had a mean frequency of 21.7Hz (beta range).

4. Non-stellate cells (39%; mostly pyramidal-like) displayed time-dependent inward rectification, which was less pronounced than that of SCs, and minimal depolarization-induced sags. Upon threshold depolarization, firing was always preceded by a slowly rising ramp depolarization and thus occurred with a long delay. Inward rectification in the depolarizing range was very pronounced. However, non-SCs did not generate persistent rhythmic subthreshold oscillatory activity nor spike clusters.

5. Of the electrophysiological parameters quantified, spike threshold, spike duration, depolarizing afterpotential amplitude and apparent membrane time constant demonstrated statistically significant differences between SCs and non-SCs.

6. The repetitive firing properties in response to square current pulses of short duration (<500ms) were also different between SCs and non-SCs. First, most SCs displayed a bilinear f-I relationship for only the first inter-spike interval, while most non-SCs displayed a bilinear relationship for all intervals. Second, SCs had a much steeper primary f-I slope for early intervals than non-SCs. Finally, SCs displayed more pronounced and faster spike frequency adaptation than non-SCs. Moreover, current pulse triggered spike trains were followed by an afterhyperpolarization of larger amplitude and more complex waveform in the SCs than in the non-SCs.

7. Changes in spike trajectory during current-pulse triggered spike trains also followed a different pattern in SCs and non-SCs. In SCs, the action potential duration increased during the first three spikes and then progressively decreased to the initial value, although pronounced adaptation continued. Non-SCs behaved more similarly to other cortical neurons with a progressive increase in spike duration during the adapting train.

8. Thus, fundamental differences exist in the intrinsic electrophysiological architecture of SCs and non-SCs and therefore in the way these neurons transduce synaptic input into spike output towards the hippocampal formation via the perforant path. Accordingly, two parallel channels of information processing with different integrative properties may exist in layer II of the MEC. The SC channel would constitute a highly rhythmic processing system with striking pace-maker properties that may participate in the generation of theta and/or beta rhythmicities in the limbic system.

INTRODUCTION

There is at present a rapidly growing interest in understanding the functional significance of the entorhinal cortex (EC). This interest has been largely motivated by anatomical studies demonstrating that the EC occupies a central position in the limbic forebrain by providing bi-directional interconnections for the hippocampal formation with the rest of the cerebral cortex (Amaral 1987). Animal experimentation and clinical observations in humans have demonstrated that the neocortical-hippocampal-neocortical circuit is fundamental in some forms of memory (Milner 1970; Murray and Mishkin 1986; Squire and Zola-Morgan 1983; Van Hoesen 1982). Indeed, some aspects of memory impairment in Alzheimer's patients have been attributed to damage of the EC which is the earliest and most severely damaged of all cortical areas in this disease (Braak and Braak 1991; Van Hoesen et al. 1991). Focus in understanding EC physiology is also of great interest because this area expresses a high degree of synaptic plasticity which may relate not only to learning and memory but also to epileptogenesis (Alonso et al. 1990). Several electrophysiological investigations in animals and humans have indeed pointed out that the EC may play a crucial role in temporal lobe epilepsy (Jones and Heinemann 1988; Jones and Lambert 1990; Paré et al. 1992; Rutecki et al. 1989; Stanton et al. 1987).

Via a remarkable cascade of cortico-cortical projections (Amaral et al. 1983; Insausti et al. 1987a; Jones and Powell 1970; Room and Groenewegen 1986a; Van Hoesen and Pandya 1975), input from the entire cortical mantle converges upon the superficial layers (II and III) of the EC which are also targets of important subcortical limbic centers (particularly the amygdala) (Insausti et al. 1987b; Krettek and Price 1974; Room and Groenewegen 1986b). In turn, EC layers II and III are the origin of the perforant path which constitutes the major cortical afferent projection to the hippocampal formation (Ramón y Cajal 1902) . In fact, neurons from layer II are actually those which give rise to the most prominent component of the perforant path which terminates primarily on the

molecular layer of the dentate gyrus and also on the stratum lacunosum-moleculare of CA3 (Schwartz and Coleman 1981; Steward 1976; Steward and Scoville 1976). Surprisingly, in spite of all anatomical evidence indicating that neurons from EC layer II occupy a key position for the gating of afferent hippocampal information, very little is known about their electrophysiological characteristics (Alonso and García-Austt 1987b; Finch et al. 1988), which would ultimately be responsible for the activity of perforant path fibers under physiological conditions. Perhaps the reason is that they were regarded as simple relay neurons without important processing capabilities since, on anatomical grounds, the importance of the EC has been viewed as that of an "interface" between the hippocampal formation and neocortex (c.f., Amaral et al. 1987).

Here we report investigations on the intrinsic electroresponsiveness of projection neurons from layer II of the medial subdivision of the EC in a rat brain slice preparation. The medial EC (MEC) was primarily selected as it is better known electrophysiologically than the lateral EC (Alonso and García-Austt 1987a,b; Jones and Heinemann 1988; Quirk et al. 1992). The results indicate that neurons from layer II play a more dynamic computational role in the transduction of afferent input towards the hippocampal formation than previously thought. Two morphologically distinct groups of MEC layer II projection neurons displayed different non-linear membrane properties. We propose that the two groups of neurons indeed represent two parallel input channels to the hippocampal formation. Stellate cells of EC layer II possess a particularly rich intrinsic excitability that endows them with striking oscillatory properties that may implement synchronizing mechanisms in the limbic forebrain. Some of the ionic mechanisms underlying the differential electroresponsiveness between stellate cells (SCs) and non-stellate cells (non-SCs) will be presented in the accompanying paper (Klink and Alonso 1992b). Some of the material presented in these papers has been previously published as preliminary reports (Alonso and Klink 1991; Alonso and Llinás 1989, 1990).

METHODS

Brain slices were derived from male Wistar rats (125-200 g) following standard procedures. Briefly, after Nembutal (30mg/Kg) or ether anesthesia animals were decapitated, the brain was rapidly removed and a block of tissue containing the retrohippocamapl region was placed in a cold (6-10°C) oxygenated Ringer solution (see below). Horizontal slices (350μm) were cut using a vibratome and then allowed to recover at room temperature for at least 2 hours in oxygenated incubation chambers. For recording, a single slice was transferred to a recording chamber, submerged at 35 ± 1°C and superfused with a solution containing (in mM) 124 NaCl; 5 KCl; 1.2 KH_2PO_4; 2.4 $CaCl_2$; 2.6 $MgSO_4$; 26 $NaHCO_3$; and 10 glucose. pH was adjusted to 7.4 by saturating with 95% O_2 and 5% CO_2. Slices normally consisted of the EC (medial and lateral), the hippocampal formation and portions of the perirhinal cortex. Layer II of the medial EC was easily visually identified by transillumination as a distinct dense band of cells extending from the parasubiculum to the transition zone with the lateral EC, as defined by Blackstad (1956). Intracellular glass electrodes were filled with 2-3M potassium acetate (tip resistance 40-120 MΩ), 2-3M potassium chloride (40-80 MΩ) or 1-2% biocytin in 2-3M potassium acetate (100-200 MΩ). Signals were amplified (Axoclamp 2A used in bridge mode), digitized (Neuro-Corder), visualized on line on a digital storage oscilloscope (Tektronix) as well as stored on videotape for subsequent analysis on a 386-based computer. Slices with neurons filled with biocytin were fixed in 4% paraformaldehyde in 30% sucrose and then sectioned at 50-100μm with a freezing microtome. Sections were incubated for 2 hours in 1% Triton X-100 and Avidin-biotin-horseradish peroxidase (Vector) complex. After washing several times in potassium phosphate buffer solution (KPBS), sections were reacted with DAB (0.1%, 0.003% hydrogen peroxide) in KPBS, mounted on slides, dehydrated and covered. Intracellularly stained neurons were drawn with the help of a camera lucida, and dimensions were measured by the Biocom software

system. Electrophysiological parameters were measured as follows: apparent input resistance was measured at the peak of the voltage deflection following a 0.1nA hyperpolarizing pulse from rest. The time constant was taken as the time to reach 63% of the peak voltage deflection for a 0.1nA hyperpolarizing pulse. The hyperpolarization-induced sag (HS) was the percent change in membrane potential during decay from peak to steady state following a hyperpolarizing pulse which caused a peak voltage deflection of about 20 mV. The depolarization-induced sag (DS) was the percent change in membrane potential from peak to steady state after a threshold depolarizing pulse (measurement taken when no action potential was fired) , which generally caused a peak voltage deflection of 8-15 mV. The maximum spike latency was the maximum latency to firing that could be induced following finely graded depolarizing constant current pulses of 300-500 ms. Spike duration was measured at threshold, and spike amplitude and fast and medium AHP amplitudes were measured relative to threshold. The amplitude of the depolarizing afterpotential (DAP) was measured from the peak of the fast AHP to the depolarizing peak. Medium and slow spike train AHP amplitudes were measured from base-line potential to peak. The rhythmic character of the subthreshold oscillations and its dominant frequency were estimated by computing the autocorrelation function and power spectra of, typically, 3-6 sec segments of subthreshold intracellular data digitized at 1-3Khz. Rhyhtmic membrane potential oscillations contributed to rhythmic autocorrelograms and to a spectral peak at the dominant oscillatory frequency. Parameter means were tested for differences according to the two-tailed Student t-test, at a significance level of 0.001.

The data base for the results presented in this and the following paper comprised 184 neurons recorded from layer II of the MEC held for at least 15 min with a minimum resting potential of -55 mV, an input resistance of at least 15 MΩ and an action potential of at least 60 mV (threshold to peak) when recorded with K-acetate or KCl-only containing electrodes (no differences were observed in the electrophysiological characteristics of the cells using either type of electrode).

RESULTS

Two categories of neurons were defined on the basis of their electrical membrane properties. One category included those cells (69%) which developed sustained rhythmic subthreshold oscillatory activity upon d.c. depolarization and a very pronounced "sag" response following an early voltage peak upon subthreshold outward current pulse injection (Stafstrom et al. 1984b). This sag response (hereafter called "depolarization-induced sag"; DS) always determined early firing upon threshold depolarizations. The neurons from the first group also displayed pronounced sag responses to inward current pulses (hyperpolarization-induced sags; HS).

The other category of cells included all those neurons (31%) which did not develop a sustained rhythmic subthreshold oscillatory activity and which always displayed delayed firing upon threshold depolarizations. These neurons always presented weak or no-sag responses to subthreshold current pulse injection.

With regard to the morphology, a total of 34 neurons were intracellularly injected with biocytin after determining the effects of intracellular current injection. This intracellular labeling technique (Horikawa and Armstrong 1988) afforded a detailed morphological investigation of these neurons which will be reported in full elsewhere (Klink and Alonso, in preparation). However, it is relevant to mention here that all those cells that belonged electrophysiologically to the first group were identified morphologically as stellate cells (n=22). As is the case for the cell illustrated in figure 1A, this identification was made mainly on the basis of the spiny dendritic tree formed by multiple, roughly equally sized, primary dendrites. It was also very characteristic of these neurons that after a few branchings their long upper dendrites run over layer I forming an extensive dendritic domain that spreads medially and laterally to usually cover about one half of the medio-lateral extent of the medial entorhinal cortex. The averaged largest soma diameter of the stellate cells was 23.0 ± 4.4 μm (mean ± SD) and the maximal medio-

lateral expanse of the upper dendritic field was 497± 154 μm . None of the 12 biocytin-labeled non-SCs had stellate morphology. As the cell shown in figure 1B, eleven of the non-SCs were classified as pyramidal-like cells and one as a horizontal multipolar cell. The averaged largest soma diameter of these neurons was 21.9 μm ± 4.3 μm and the maximal medio-lateral expanse of the upper dendritic field was 184 ± 75 μm which was highly significantly smaller from that of the SCs. Axons of both SCs and non-SCs could be traced running radially down to the angular bundle, thus allowing the identification of both groups of neurons as projection cells (not shown) (Schwartz and Coleman 1981).

(Fig. 1 near here)

Several electrophysiological properties including voltage-current (V-I) relations, membrane time constants, action potential wave form, repetitive firing properties and afterhyperpolarizations were analyzed to characterize SCs and non-SCs. The mean value of several membrane parameters for the two groups is given in Table 1. We will now describe in parallel their differential electroresponsiveness.

(Table 1 near here)

SUBTHRESHOLD RESPONSES TO CURRENT PULSES

Stellate cells. In all SCs recorded, the voltage response to subthreshold constant current pulses exhibited pronounced time- and voltage-dependence (Fig. 2). In fact, as shown in figure 2A, all subthreshold current pulses in either the depolarizing or hyperpolarizing direction caused the membrane potential to attain an early peak (Vp) and then decay (sag) to a lower level (Vs). In figure 2C this non-linear membrane behavior can be observed in more detail for the responses evoked by the smallest amplitude current pulses applied to the cell in figure 2A that have been plotted at an expanded voltage scale. Note that even voltage changes of only 2-3 mV displayed a marked "sag".

(Fig. 2 near here)

We quantified the sag responses for both close-to-threshold depolarizing (8-15mV peak amplitude) and hyperpolarizing (20mV) pulses as the percent change in membrane potential from Vp to Vs. In all SCs tested (n=49) the DS was larger (57 ± 17%) than the HS (30 ± 7%). The development of a very pronounced DS determined that upon threshold depolarization firing always occurred with a relatively short latency (42 ± 17 ms) and at the peak of the voltage response.

In correlation with the time dependence of the voltage response to subthreshold current pulse injection, on termination of the pulse, the membrane response always transiently overshot the resting level (Fig. 2A and D). The amplitude of the rebound potential was dependent on the amplitude of the voltage response during the current pulse. Figure 2D illustrates rebound potentials to inward current pulses of increasing amplitude from figure 2A at an expanded voltage and time scale. Note the pronounced increase in the amplitude and rate of rise of the rebound potentials (which nonetheless had a similar duration) to increasing levels of hyperpolarization. Following moderate hyperpolarizations (5-10mV), the rebound potentials always reached firing threshold. Stronger hyperpolarizations always elicited burst firing (doublets of spikes) at the end of the current pulse (Fig. 2D, dots).

The V-I relationship for the cell in figure 2A is depicted graphically in figure 2B. The graph illustrates the plots of both the "peak" and "steady state" voltage (measured towards the end of the current pulse) versus injected current. As in this case, in all SCs both peak and steady-state V-I plots displayed a marked concavity over the whole range, the rectification being greater at both the positive and negative ends of the plots. Thus, SCs exhibit inward rectification in both subthreshold depolarizing and hyperpolarizing directions. In fact, inward rectification becomes very apparent when comparing the amplitude of the voltage response (particularly at the peak) evoked by a depolarizing current pulse to that evoked by an equal hyperpolarizing current pulse which was always

smaller (Fig. 2C). Since the V-I curve of SCs is markedly non-linear, the cells' input resistance (Ri) is strongly voltage-dependent (Klink and Alonso 1992b).

(Fig. 3 near here)

Non-stellate cells. The voltage responses of non-SCs to the injection of constant current pulses presented clear differences to those displayed by SCs. As is the case in the cell illustrated in figure 3A, sags in response to hyperpolarizing current pulses developed in all but one of the non-SCs recorded, though this time-dependent membrane behavior was less prominent (sag percentage of 17 ± 8%, n=26) than that displayed by SCs. The difference in the HS percentage between the two groups of neurons was statistically significant (two-tailed t-test, $p<0.001$). The amplitude of the HS was not, however, a clear cut distinction between SCs and non-SCs as some SCs displayed HSs the magnitude of which overlapped with those of the non-SCs (Fig. 8).

Any non-SC could, however, be easily distinguished from a SC by its voltage responses to subthreshold outward current pulses. For a small outward current, an electrotonic potential with a smooth charging trajectory and no or small sag response was always observed. For slightly larger outward current injections, the initial electrotonic potential was followed by a slowly rising ramp potential that usually culminated with the generation of an action potential at a relatively long latency (Fig. 3C). Thus, with respect to the voltage responses to current pulses, the main distinctive characteristics of SCs versus non-SCs were: a) their much smaller DSs (maximum sag percentage=10 ± 9%; Table 1 and Fig. 7A); and b) the presence of delayed firing upon threshold depolarization. The DS was, in fact, smaller for all non-SCs with respect to any SC (Fig. 7A). Also, the maximum spike latency to firing upon threshold depolarization was larger in all non-SCs (180 ± 67ms) with respect to any SC.

In non-SCs, the membrane potential always transiently overshot the resting level at the break of hyperpolarizing current pulses. However, these rebound responses were less prominent than those observed in SCs. Even following large hyperpolarizations, in most

non-SCs the rebound potentials failed to reach firing threshold and, when they did, burst firing (which occurred in the SCs, Fig 2) was never generated. In addition, when prominent rebound was observed, spikes did not arise from the early peak of the rebound potential but after a delay from the top of a plateau depolarization triggered by the initial rebound (Fig. 3D, arrow).

The peak and steady-state V-I plots of non-SCs demonstrated inward rectification in both the hyperpolarizing and depolarizing direction (Fig. 3B), hyperpolarizing inward rectification being, however, less pronounced than in SCs.

(Fig. 4 near here)

SUBTHRESHOLD OSCILLATIONS AND SPIKE "CLUSTERS"

Stellate cells. The most remarkable electrophysiological characteristic of SCs was their ability to generate a persistent rhythmic subthreshold oscillatory activity when these cells were depolarized positive to about -60 mV. The development of this oscillatory phenomenon by a SC upon increasing levels of d.c. depolarization is illustrated in figure 4A. At the resting level (-64 mV), the membrane potential did not display any rhythmic oscillation. At a membrane potential of -58 mV (0.28nA level), a very low-amplitude sinusoidal-like membrane potential oscillation initially emerged. With further depolarization, the membrane potential oscillation became more apparent (0.36 and 0.47nA levels) increasing in amplitude, and firing could then eventually occur at the peak of some of the oscillatory waves. The autocorrelogram in Fig. 4B clearly demonstrates the rhythmic character of the subthreshold oscillation at a frequency of about 8Hz. Rhythmic autocorrelograms of the subthreshold membrane potential behaviour were obtained in all SCs investigated. At the most prominent oscillatory level (about -55 mV), the mean amplitude of the oscillation was 2.6 ± 0.5 mV (range 0.5-9.7 mV; n=49). As illustrated graphically in Fig. 4C, it was a consistent observation that the amplitude of the oscillation

first grew with d.c. depolarization reaching a maximum at about -55mV and then decreased at more positive membrane potential levels.

(Fig. 5 near here)

It was also a characteristic feature of all SCs that constant current depolarization did not readily induce tonic firing. Instead, when these cells were depolarized positive to the membrane potential level dominated by the subthreshold oscillations, a low-frequency (1-3Hz) repetitive bursting ("clustering") pattern always emerged. The tendency to the formation of "clusters" of spikes can be observed for the highest depolarizing level illustrated in figure 4. The development of this clustering phenomenon is illustrated in more detail for a different neuron in figure 5. As the cell is depolarized from its most prominent oscillatory level (Fig. 5A), a conspicuous tendency to form of clusters of spikes in short trains of action potentials separated by subthreshold oscillations developed (Fig. 5B). Further depolarizing current injection did not readily induce tonic firing, but a more prominent repetitive clustering pattern (Fig. 5C) with an increase in both the number of spikes per cluster and the intra-cluster firing frequency, as well as an increase in the frequency of the subthreshold oscillations (D). Note also in Fig. 5C and D that the spike clusters were not followed by a slow afterhyperpolarization. It was also a peculiarity of d.c.-driven spike clusters that the spike and interspike membrane potential trajectories remained unchanged (Fig. 5F and G) with the exception of minor, rather random, fluctuations in the interspike interval. In all SCs tested, rather strong d.c. depolarizations (0.6-1.0nA) always induced tonic firing with occasional spike failures (Fig. 6).

(Fig. 6 near here)

The plot shown in Fig. 5F illustrates that the relationship between subthreshold oscillation frequency and membrane potential was not linear. The oscillation underwent a small increase in frequency in the voltage range of -60 to -55 mV, where no or occasional spikes were triggered by the oscillations, but then displayed a pronounced increase at more positive membrane potential levels. This frequency increase was coincident with the

pronounced development of the clustering pattern. The frequency of the subthreshold oscillations measured at the most prominent voltage oscillatory level (with no or occasional firing) ranged from 5.5-14.5 Hz (mean 8.6 ± 2.1 Hz; n=49). The frequency of the oscillation almost doubled (21.7 ± 2.7 Hz; n=7) during the inter-cluster intervals at more depolarized potentials.

(Fig. 7 near here)

Non-stellate cells. The voltage response of non-SCs to constant current injection was clearly distinct to that of SCs. Upon d.c. depolarization, non-SC cells never displayed the characteristic spike-clustering phenomenon of the SCs, but readily went into tonic firing (Fig. 7). With regard to the subthreshold voltage behaviour, though some membrane potential oscillations of low frequency (2-6Hz) and amplitude could also be observed in these neurons (Fig. 7, 0.18nA) they never displayed a rhythmic character, as assessed by the non-rhythmic autocorrelograms (Fig. 7, right panel).

GENERAL ELECTROPHYSICAL PARAMETERS

The SCs and non-SCs were also different according to several basic electrophysiological parameters (Table 1). The histograms presented in Fig. 8 illustrate the distributions of those membrane parameters that demonstrated statistically significant differences (two-tailed t-test, $p<0.001$) between the two groups of neurons. As already mentioned, both DS and HS percentages were larger in the SCs than in the non-SCs (Fig.8A and B). In addition, action potential duration was shortest and the spike arose from a more negative membrane potential level in SCs as compared to non-SCs (Fig. 8C and D).

(Fig.8 near here)

As shown in Fig. 8E, the action potential of SCs (upper trace) and non-SCs (lower trace) was followed by both a fast afterhyperpolarization (AHP) and a medium AHP. In addition, a distinctive depolarizing afterpotential (DAP) was present in the large majority

of SCs (86%) and in most non-SCs (54%). We did not detect a statistically significant difference in the peak amplitude of either the fast or medium AHP between the two groups of neurons. However, the DAP (when measurable) was significantly larger in SCs than in non-SCs (Fig. 8F).

Resting membrane potential and apparent input resistance did not vary with cellular type. However, the apparent membrane time constant was found to be significantly shorter in SCs than in non-SCs (Fig. 8G).

Repetitive Firing

In order to further compare the current sensitivity between SCs and non-SCs, the firing properties of twenty-two SCs and eleven non-SCs to the injection of 150-500ms square outward current pulses were examined in detail.

(Fig. 9 near here)

Stellate cells. The firing behavior of SCs to outward current steps of increasing amplitude is illustrated in Fig. 9. Larger current steps always resulted in faster firing rates and firing frequency always markedly decreased with time (adapted) (Fig. 9A). In most cells (80%), for current pulses of 0.4-0.8nA, firing ceased after 100-200 ms of pulse onset (Fig. 9A, middle trace). However, when our standard pulse duration was eventually increased, the cells always resumed the repetitive "cluster" pattern described above.

Frequency current (f-I) plots were constructed for early and late interspike intervals (ISIs) (Fig. 9B). All f-I plots showed a continuously graded increase in firing frequency with increasing current intensity. With respect to the first ISI, the f-I relation was bilinear in most cells (95%). In contrast, the f-I relation for the second and subsequent intervals was simply linear in most cells (range: 75-90% from second to eighth ISI) and bilinear in the rest. For bilinear f-I relations, the slope of the primary linear segment was steeper than that of the secondary segment. For the first ISI, the mean

primary f-I curve slope was 338.8 ± 121.9 Hz/nA. The mean secondary f-I slope sharply decreased by 60% to 138.6 ± 56.8 Hz/nA.

Reflecting the strong adaptation of SCs, the f-I slope for the second ISI was 140.7 ± 39.9 Hz/nA, much smaller than that of the first ISI (Fig. 9B). In fact, the ratio of first to second ISI f-I slope was 2.5 ± 0.6 (range: 1.6-3.9). The f-I slope for the third ISI was 82.8 ± 19.7 Hz/nA with a corresponding ratio of second to third ISI f-I slope of 1.7 ± 0.2. The f-I slope for subsequent intervals declined at an increasingly smaller rate particularly after the sixth ISI (Fig. 9B).

In order to further characterize adaptation, plots of instantaneous firing rate versus time were also constructed (Fig. 9D). For small current steps of 0.2-0.4 nA the decline in firing rate was regular (Fig. 9D, triangles). However, for larger current steps there was a distinct break in the firing rate decline with time. During the first three or four intervals, firing rate displayed a fast logarithmic decrease with time, while during subsequent intervals the decrease in firing rate was slower and best fitted by an exponential curve with a mean time constant of 456 ± 240 ms (Fig. 9D, squares). For current steps larger than 0.4 nA there were thus two phases of adaptation, an initial fast and a late slow one. The slow phase began at 51 ± 14 ms after pulse onset for current steps of 0.5-1.0 nA.

We also approached the characterization of input-output relations by plotting the number of spikes (NS) for a given outward current pulse versus current intensity (Fig. 9C). The strong adaptation (that frequently led to cessation of firing) of most SCs caused this plot to present an initial and a late segment with a linear NS/I relation separated by a plateau of no increase in NS with current.

(Fig. 10 near here)

Non-stellate cells. The firing behavior of non-SCs to outward current steps is illustrated in Fig. 10. Firing rate increased with larger current steps and, as compared to SCs, non-SCs showed only moderate levels of adaptation (Fig. 10A). In most neurons, the f-I relation was bilinear for the first ISI (91%) as well as, in contrast to SCs, for subsequent

ISIs (range: 91-62% from second to eighth ISI) (Fig. 10B). For the first ISI, the mean primary f-I slope was 196.2 ± 64.2 Hz/nA, much smaller (58%) than that of SCs. In addition, the ratio of first to second ISIs was 1.4 ± 0.2 (range: 1.1-1.8) also much smaller (56%) than that of SCs, which reflects a smaller degree of adaptation in non-SCs. This caused the f-I slope for late intervals to be in the same range as that of SCs (Fig. 9B and Fig. 10B).

The firing-rate adaptation curves of non-SCs (Fig. 10D) were similar in shape to those of SCs with a monophasic decay for small current steps (0.2-0.5nA) and a biphasic first logarithmic then exponential decay for larger current steps. However, there were significant quantitative differences between the two cell types. The slow exponential phase began at 83 ± 15 ms (for current steps of 0.5-1nA) much later than in SCs. Moreover, the mean time constant of the exponential decline was 2.0 ± 1.0 sec, about four times larger than in SCs.

The plot of number of spikes per current step for non-SCs (Fig. 10C) never displayed the above-described plateau of most SCs (Fig. 9C) thus making it possible to further establish the distinction in firing behavior between the two neuronal cell groups.

SPIKE PARAMETERS DURING REPETITIVE FIRING

We mentioned above that SCs and non-SCs differ in certain spike parameters such as spike threshold and spike duration. In addition, during current pulse-driven repetitive firing these parameters varied differentially in each cell type.

(Fig. 11 near here)

Stellate cells. A conspicuous and remarkable characteristic of these neurons was that spike duration progressively increased for the initial three spikes and then always decreased toward values close to that of the first spike (Fig. 11B and C). Similarly, the peak amplitude of the single-spike AHP was also related to the previous activity of the cell. The first AHP was always deeper than the second and then the AHP amplitude

increased again (concomitantly with the decrease in spike duration) to reach values always larger than those of the first AHP (Fig. 11A and B). In addition, the spike threshold always increased progressively during the current pulse. This increase was rather substantial, reaching 7-10 mV for current steps of 1.0 nA.

Non-stellate cells. The spike duration increased during the initial 3-5 spikes and then, in contrast to SCs, remained rather constant (never decreased) for subsequent spikes during the current pulse (Fig. 12B and C). The AHP amplitude had an inverse relationship to spike duration, being largest for the first spike and remaining rather constant after the 3rd-5th spikes (Fig. 12A and B). As in SCs, the spike threshold progressively increased during the current pulse, though this increase was smaller (only 2-5 mV for current steps of 1.0 nA) than in SCs.

(Fig. 12 near here)

SPIKE-TRAIN AFTERHYPERPOLARIZATION

The characteristic AHP that followed a current-pulse triggered spike train in both SCs and non-SCs is shown in Fig. 13A and B, respectively. In both types of neuron, the spike-train AHP consisted of a medium- (asterisk) and a slow-duration component. However, the amplitude of both components was typically larger in SCs than in non-SCs (Fig. 13C and D). In addition, the total duration of the spike-train AHP was also significantly larger in SCs (2.42 ± 1.1 sec; n=35) than in non-SCs (0.96 ± 0.37 sec; n=19), as measured for current steps of 0.5-0.7 nA. Finally, in SCs, the return of the membrane potential toward the resting level during the slow AHP was distinctly biphasic (Fig. 13A, arrowhead) indicating two different phases of slow repolarization.

(Fig. 13 near here)

DISCUSSION

Knowledge of the basic electrophysiological properties of MEC layer II neurons is essential to assess the characteristics, and degree, of the transduction process performed in this key cortical layer. Our data demonstrate the presence of two electrophysiologically different populations of MEC layer II projection neurons, both displaying a rich intrinsic electroresponsiveness. This richness was particularly manifest in the most abundant cell type shown by intracellular labeling to correspond morphologically to the stellate cells typical of EC layer II (Alonso and Llinás 1989; Germroth et al. 1989; Ramón y Cajal 1902). Non-SCs, the majority of which displayed a pyramidal-like morphology, behaved in a manner electrophysiologically similar to other regular-spiking cortical neurons (Connors and Gutnick 1990; Connors et al. 1982; McCormick et al. 1985; Stafstrom et al. 1984a).

UNIQUENESS OF STELLATE CELL ELECTRORESPONSIVENESS AND MAIN DIFFERENCES FROM NON-STELLATE CELLS.

SCs demonstrated a complex set of electroresponsive properties that caused minimal changes of membrane potential in the subthreshold range to generate an active response. Subthreshold outward current pulse injection always caused the membrane potential to attain a conspicuous early peak and then sag to a lower level. Also, a very pronounced time-dependent inward rectifying response was observed following inward current injection. The voltage versus injected current relationship of the SCs was thus markedly non-linear and demonstrated pronounced inward rectification during polarization on either side of the membrane potential. Further aspects of this membrane behavior and its underlying ionic mechanisms will be presented and discussed in the accompanying paper (Klink and Alonso 1992b). Yet it seems appropriate to mention here that although in general the above properties are not exclusive of the SCs and have been described and

analyzed in detail in other cortical (Halliwell and Adams 1982; Hoston et al. 1979; Spain et al. 1987; Stafstrom et al. 1984b) and subcortical (Kamondi and Reiner 1991; McCormick and Pape 1990; Osmanovic and Shefner 1987; Yarom and Llinás 1987) neurons, it appears to us that the SCs are among those in which a time-dependent inward rectifier has the most pronounced effects on the membrane potential.

The most distinctive electrophysiological signature of the SCs was the presence of rhythmic subthreshold oscillatory activity in the theta or beta range of frequencies depending on the membrane potential. That this was a self-sustained intrinsic membrane phenomenon was indicated by the characteristics of its voltage dependence. Subthreshold oscillations were not present at the resting potential, or below, and gradually developed, growing in amplitude and frequency when the cells were depolarized positive to -60 mV. In addition, this intrinsic oscillatory phenomenon, as opposed to that in many other brain neurons (Llinás 1988), is not Ca^{2+}-dependent but depends instead upon the activation of a persistent Na-conductance (Alonso and Llinás 1989; Klink and Alonso 1992a). Subthreshold oscillations of the membrane potential with a high degree of rhythmicity similar to those of the EC SCs have also been described in other cortical (Llinás et al. 1991; Silva et al. 1991) and subcortical structures (Steriade et al. 1991; Deschenes et al, 1992) and shown to be both Na^{+}- and Ca^{2+}-dependent in layer V neocortical neurons pyramidal cells (Silvaet al. 1991) and at least Na+-dependent in layer IV sparsely spinous interneurons (Llinás et al. 1991). Also, hippocampal pyramidal cells display subthreshold oscillations of low and rather variable frequency and amplitude (Lanthorn et al. 1984; MacVicar 1985) similar to the EC layer II non-SCs.

Another striking characteristic of the SCs was their ability to generate upon d.c. depolarization a repetitive bursting pattern which consisted of non- (or minimally) adapting trains of action potentials (spike "clusters") separated by subthreshold oscillations and not followed by an apparent slow AHP. Similar complex periodic patterns have been previously described in experimental and modeling studies of several oscillatory systems

(Guevara 1987, 1991; Guevara et al. 1987; Guttman and Barnhill 1970; Holden et al. 1982) but not, to our knowledge, in CNS neurons. The emergence of this spike clustering phenomenon may be explained, at least partially, by the entrainment of regular spiking by the subthreshold oscillations and thus coupling of two, otherwise independent, oscillators (subthreshold oscillations and rhythmic spiking). It is also apparent that once spike threshold is reached by a particular pacemaker wave, the probability of a subsequent firing is increased by the larger rebound oscillation triggered by the first spike AHP. Furthermore, factors such as the spiking-dependent build-up of an outward current (which nonetheless causes no measurable effect on the spike trajectory) may contribute to establish the duration of the spike clusters and the inter-cluster interval. The clustering behavior of the SCs is, however, radically different from that previously described in other "bursting" cortical (Connors and Gutnick 1990; Connors et al. 1982; Wong and Prince 1981) or subcortical neurons (Alonso and Llinás 1992; Avanzini et al. 1989; Gerber et al. 1989; Jahnsen and Llinás 1984; Khateb et al. 1992; Wilcox et al. 1988). In these, firing frequency changes drastically during the burst which is always followed by a pronounced long-lasting AHP. Nonetheless, the repetitive spike "clustering" pattern associated with subthreshold oscillations is not an exclusive property of entorhinal neurons in the CNS. A preliminary electrophysiological study of basal forebrain non-cholinergic neurons has also revealed that the most striking intrinsic property of these cells is their ability to develop 40 Hz rhythmic subthreshold membrane potential oscillations associated with rhythmically repeating spike "clusters" at theta frequency (Mühlethaler et al. 1992).

The above-described characteristics distinguish SCs from non-SCs. The latter group displayed a less pronounced time-dependent inward rectification and, most distinctively, small or no depolarization-induced sags. Indeed, in the non-SC firing upon threshold current-pulse depolarization always occurred with a much longer delay than in the SCs and was preceded by a slowly rising plateau depolarization. In addition, non-SCs did not generate a persistent rhythmic subthreshold oscillatory activity, nor did they

develop the spike clustering phenomenon of the SCs. However, membrane potential oscillations of low and rather variable frequency and amplitude, very much like those reported in CA1 hippocampal pyramidal neurons (Lanthorn et al. 1984; MacVicar 1985), were also generated by the non-SCs.

OTHER ELECTROPHYSICAL PROPERTIES

The two groups of neurons were also found to differ in several other electrophysiological properties.

The SC action potential was rather fast (1.27 ms at the base) and followed by three characteristic afterpotentials: a fast- and a medium-duration AHP separated by an ADP. These are, qualitatively, common properties of other cortical projection neurons (Connors and Gutnick 1990; Schwindt et al. 1988b; Wong and Prince 1981) and were also present in non-SCs. However, the action potential of the non-SCs was slower and the ADP was less manifest (or absent) than that of the SCs. These differences probably arise because of different mechanisms underlying action potential repolarization in SCs and non-SCs as shown in the accompanying paper (Klink and Alonso 1992b).

The analysis of firing frequency versus injected current relationship also made it possible to differentiate between SCs and non-SCs. First, whereas most SCs displayed a bilinear f-I relation for the first ISI and simply linear for subsequent ISIs, most non-SCs displayed a bilinear relation at all times. As in other cortical neurons (Lorenzon and Foehring 1992; Stafstrom et al. 1984a), in both SCs and non-SCs, the secondary range was always the shallowest. Second and more noticeable, SCs had a much steeper f-I slope for early intervals than non-SCs. This implies that the SCs had an early higher gain in the transduction of synaptic input into impulse firing. On the other hand, SCs displayed a more pronounced and faster spike frequency adaptation than non-SCs. This adaptation was associated with a longer duration, larger amplitude and more complex wave form slow AHP than in the non-SCs. Adaptation and slow AHP are related events which have

been described in cortically projecting neurons and to which multiple voltage-and non-voltage-dependent ionic conductances have been shown to contribute (Constanti and Sim 1987; Lancaster and Adams 1986; Madison and Nicoll 1984; Schwindt et al. 1988a). The differences in adaptation and slow AHP between SCs and non-SCs must then relate to fundamental differences in the mechanisms underlying repetitive firing in the cell groups.

The complexity of the intrinsic electroresponsiveness of the SCs was also manifested by the changes in spike trajectory during pulse-triggered spike trains. Spike frequency adaptation in other CNS neurons appears correlated with a spike broadening that leads to an increase in Ca^{2+} entry and the activation of slow Ca^{2+}-dependent K^+ current (Bourque and Renaud 1985; Lancaster and Nicoll 1987; Llinás and Alonso 1992; Schwindt et al. 1992; Schwindt et al. 1988a). An increase in spike duration indeed took place in the SCs for the three initial spikes during a train. However, later spikes always displayed a pronounced progressive decrease in duration while adaptation still proceeded. Also, in spite of this decrease, SC spike trains were followed by a much more prominent slow AHP than non-SC spike trains which, on the other hand, never displayed a spike duration decrease. The decrease displayed by the SCs is a striking phenomenon not previously described, to our knowledge, in other neurons.

FUNCTIONAL IMPLICATIONS

Though stellate cells are the most common cell type in MEC layer II giving rise to perforant path fibers upon the dentate gyrus, previous anatomical studies had already demonstrated that other MEC layer II non-SCs (mainly pyramidal-like neurons) also contribute to this projection (Schwartz and Coleman 1981). Our data demonstrate that SCs and non-SCs have indeed very different intrinsic electroresponsiveness that thus renders the two groups of neurons clearly distinct with regard to input-output relations. This, therefore, suggests the existence in MEC layer II of two parallel channels for information processing, each possessing different integrative properties. The SCs channel

constitutes a highly rhythmic processing system with striking pacemaker properties (further discussed below). Interestingly preliminary results indicate that SCs and non-SCs may also be differentially modulated by cholinergic and serotoninergic inputs (Alonso and Klink 1991; Klink and Alonso 1992a). The similarities/dissimilarities of these neurons' targets and the physiological actions upon them remains to be determined. Equally interesting is whether there is a differential segregation of isocortical inputs upon SCs and non-SCs as well as the synaptic interactions between the two groups of cells.

The presence of subthreshold theta-like rhythmicity in SCs brings up the issue of the limbic theta rhythm and the role of oscillations in entorhinal cortex function. Though the theta rhythm has been extensively investigated in the hippocampus, to the point of being most frequently generically referred to as "hippocampal" theta rhythm, theta rhythm is also characteristic of other limbic structures. In fact, the entire circuit of Papez participates in theta rhythmicity. A prominent theta activity is present in the mammillary bodies (Komisaruk 1970; Mignard et al. 1987), anterior thalamus (Mignard et al. 1987) and cingulate cortex (Holsheimer 1982; Leung and Borst 1987), but is primarily seen in the EC. The presence of theta waves in the EC was first reported thirty years ago (Adey et al. 1957, 1960; Holmes and Adey 1960) and in 1980 a local generator of theta rhythm was shown to exist in the dorsomedial aspect of the EC (Mitchell and Ranck 1980). More recently, Alonso and Garcia-Austt (1987a,b) extended this result to the full extent of the EC and demonstrated that rhythmic single-unit activity is present mainly in the superficial layers and primarily in layer II. In this last study, it was actually found that most theta cells in layer II display a unique firing pattern consisting of spikes or brief bursts separated by silent intervals of variable duration, though always an integer multiple of the theta rhythm period. This firing pattern is thus consistent with the underlying pacemaker mechanism being the intrinsic subthreshold oscillations typical of the SCs. Synchronization, in order to give rise to rhythmic population activity such as that present *in vivo*, may be implemented in the local network via the net of recurrent axonal collaterals that the SCs

demonstrate (Alonso and Llinàs 1989; Lingenhöl and Finch 1991). We have never observed, however, evidence of spontaneous rhythmic population activity in the EC slice under our normal recording conditions. Since it has been shown that the emergence of the limbic theta rhythm needs of an intact medial septal complex of the basal forebrain (Mitchell et al. 1982; Stewart and Fox 1990) neuromodulatory influences from this subcortical area may be essential in order to tune the entorhinal local network into an oscillatory mode.

Our present results have also shown that SCs can intrinsically generate, in addition to theta-like subthreshold oscillations, a low-frequency repetitive bursting pattern consisting of non-accommodating spike trains (clusters) separated by beta frequency subthreshold oscillations. This phenomenon may thereby also relate to the simultaneous generation of slow (low-frequency beta) and fast (beta) rhythmic population activities which the pioneer studies of Stumpf (1965) already demonstrated to coexist in hippocampal cortices. The repetitive bursting frequency of the SCs *in vitro* falls, however, just below theta frequencies and the interburst subthreshold oscillations are actually within the low beta range. In the intact animal, however, under the influence of neuromodulatory systems these frequencies may both be increased. In support of this hypothesis we have recently observed that serotonin does indeed increase the frequency of both the spike-clusters (4-5Hz) and the subthreshold oscillations (up to 40Hz) (Klink and Alonso 1992a).

With regard to the functional role of oscillations, theta bursting rhythmicity in the limbic system is widely believed to underlie synaptic plasticity (Greenstein et al. 1988; Larson and Lynch 1986) and thus relate to learning and memory (Doyère and Laroche 1992). Alonso, de Curtis and Llinás (1990) also recently showed that subthreshold oscillation of the membrane potential in SCs can lead to a non-Hebbian-type of long-term enhancement of synaptic efficacy. They then proposed that prominent oscillations and plasticity of SCs may actually serve to enhance resonance in networks so that neuronal

aggregates are created that fire rhythmically. In pathological situations this could eventually lead to epileptogenesis.

Finally, oscillations in EC layer II may be fundamental to coordinate the processing of incoming information from the cortical mantle. The oscillatory behavior of the EC SCs may ultimately implement a synchronizing mechanism by which the activity patterns of the multiple inputs from sensory and association cortices and the limbic system that converge onto these neurons may be temporarily coordinated for its transmission to the hippocampal processing machinery. In the light of the established role of the EC in memory (Gauthier et al. 1982; Levisohn and Isacson 1991; Mishkin 1982; Murray and Mishkin 1986), it seems appropriate to mention that this coordination appears essential to establish the conjunctional relations between distributed features of a particular event that may be fundamental in the acquisition of memory.

ACKNOWLEDGMENTS

We would like to thank Dr. R. Llinás for many helpful suggestions and support, and Drs. B. Jones, A. Kay and Ch. Bourque for comments on the manuscript. This work was supported by the Canadian Medical Research Council.

REFERENCES

Adey, W.R., Sunderland, S. and Dunlop, C.W. The entorhinal area: electrophysiological studies of its interrelations with rhinencephalic structures and the brainstem. *Electroenceph. clin. Neurophysiol.* 9: 309-324, 1957.

Adey, W.R., Dunlop, C.W. and Hendrix, C.E. Hippocampal slow waves: distribution and phase relationships in the course of approach learning. *Arch. Neurol.* 3: 74-90, 1960.

Alonso, A., de Curtis, M. and Llinás, R. Postsynaptic Hebbian and non-Hebbian long-term potentiation of synaptic efficacy in the entorhinal cortex in slices and in the isolated adult guinea pig brain. *Proc. Natl. Acad. Sci. USA* 87: 9280-9284, 1990.

Alonso, A. and García-Austt, E. Neuronal sources of theta rhythm in the entorhinal cortex. I. Laminar distribution of theta field potentials. *Exp. Brain Res.* 67: 493-501, 1987a.

Alonso, A. and García-Austt, E. Neuronal sources of theta rhythm in the entorhinal cortex of the rat. II. Phase relations between unit discharges and theta field potentials. *Expl. Brain Res.* 67: 502-509, 1987b.

Alonso, A. and Klink, R. Cholinergic modulation of entorhinal cortex layer II neurons' intrinsic excitability. *Soc. Neurosci. Abstr.* 17: 535.10, 1991.

Alonso, A. and Llinás, R.. Subthreshold Na^{+}-dependent theta-like rhythmicity in stellate cells of entorhinal cortex layer II. *Nature* 342: 175-177, 1989.

Alonso, A. and Llinás, R. Different electrophysiological cell types in entorhinal cortex layer II in rat brain slices. *Soc. Neurosci. Abstr.* 16: 536.12, 1990.

Alonso, A. and Llinás, R. Electrophysiology of the mammillary complex in vitro. II. Medial mammillary neurons. *J. Neurophysiol.* 64: 1992.

Amaral, D.G. Memory: anatomical organization of candidate brain regions. In: *Handbook of Physiology*, Bethesda, MD.: American Physiological society, 1987, p. 211-294.

Amaral, D.G., Insausti, R. and Cowan, W.M. Evidence for a direct projection from the superior temporal gyrus to the entorhinal cortex in the monkey. *Brain Res.* 275: 263-277, 1983.

Amaral, D.G., Insausti, R. and Cowan, W.M. The entorhinal cortex of the monkey: I. Cytoarchitectonic organization. *J. Comp. Neurol.* 264: 326-355, 1987.

Avanzini, G., de Curtis, M., Panzica, F. and Sprefacio, R. Intrinsic properties of nucleus reticularis thalami neurones of the rat studied *in vitro*. *J. Physiol. (Lond.)* 416: 111-122, 1989.

Bourque, C.W. and Renaud, L.P. Calcium-dependent action potentials in rat supraoptic neurosecretory neurones recorded *in vitro*. *J. Physiol. (Lond.)* 363: 419-428, 1985.

Braak, H. and Braak, E. Neuropathological stageing of Alzheimer-related changes. *Acta Neuropathol* 82: 239-259, 1991.

Connors, B.W. and Gutnick, M.J. Intrinsic firing patterns of diverse neocortical neurons. *Trends Neurosci.* 13: 99-104, 1990.

Connors, B.W., Gutnick, M.J. and Prince, D. Electrophysiological properties of neocortical neurons in vitro. *J. Neurophysiol.* 48: 1302-1320, 1982.

Constanti, A. and Sim, J.A. Calcium-dependent potassium conductance in guinea-pig olfactory cortex neurones *in vitro*. *J. Physiol. (Lond.)* 387: 173-194, 1987.

Doyère, V. and Laroche, S. Linear relationship between the maintenance of hippocampal long-term potentiation and retention of an associative memory. *Hippocampus* 2: 39-48, 1992.

Finch, D.M., Tan, A.M. and Isokawa-Akesson, M. Feedforward inhibition of the rat entorhinal cortex and subicular complex. *J. Neurosci.* 8: 2213-2226, 1988.

Gauthier, M., Destrade, C. and Soumireu-Mourat, B. Late post-learning participation of entorhinal cortex in memory processes. *Brain Res.* 233: 255-264, 1982.

Gerber, U., Greene, R.W. and McCarley, R.W. Repetitive firing properties of medial pontine reticular formation neurones of the rat recorded *in vitro*. *J. Physiol. (Lond.)* 410: 533-560, 1989.

Germroth, P., Schwerdtfeger, W.K. and Buhl, E.H. Morphology of identified entorhinal neurons projecting to the hippocampus. A light microscopical study combining retrograde tracing and intracellular injection. *Neuroscience* 30: 683-691, 1989.

Greenstein, Y.J., Pavlides, C. and Winson, J. Long-term potentiation in the dentate gyrus is preferentially induced at theta rhythm periodicity. *Brain Res.* 438: 331-334, 1988.

Guevara, M.R. Afterpotentials and pacemaker oscillations in an ionic model of cardiac Purkinje fibres. In: *Temporal Disorder in Human Oscillatory Systems*, Berlin: Springer-Verlag, 1987, p. 126-133.

Guevara, M.R., van Ginneken, A.C.G. and Jongsma, H.J. Patterns of activity in a reduced ionic model of a cell from the rabbit sinoatrial node. In: *Chaos in Biological Systems*, New York: Plenum, 1987, p. 5-12.

Guevara, M.R. Displaced reinjection attractors in an electronic analogue of the membrane of the squid giant axon. In: *A Chaotic Hierarchy*, Singapore: World Scientific Publishing Co. Pte. Ltd., 1991, p. 153-164.

Guttman, R. and Barnhill, R. Oscillation and repetitive firing in squid axons: comparison of experiments with computations. *J. Gen. Physiol.* 55: 104-118, 1970.

Halliwell, J.V. and Adams, P.R. Voltage-clamp analysis of muscarinic excitation in hippocampal neurons. *Brain Res.* 250: 71-92, 1982.

Holden, A.V., Winlow, W. and Haydon, P.G. The induction of periodic and chaotic activity in a molluscan neurone. *Biol. Cybern.* 43: 169-173, 1982.

Holmes, J.E. and Adey, W.R. Electrical activity of the entorhinal cortex during conditioned behaviour. *Am. J. Physiol.* 199:741-744, 1960.

Holsheimer, J. Generation of theta activity (RSA) in the cingulate cortex of the rat. *Exp. Brain Res.* 47: 309-312, 1982.

Horikawa, K. and Armstrong, W.E. A versatile means of intracellular labeling: injection of biocytin and its detection with avidin conjugates. *J. Neurosci. Methods* 25: 1-11, 1988.

Hoston, J.R., Prince, D.A. and Schwartzkroin, P.A. Anomalous inward rectification in hippocampal neurons. *J. Neurophysiol.* 42: 889-895, 1979.

Insausti, R., Amaral, D.G. and Cowan, W.M. The entorhinal cortex of the monkey. II. Cortical afferents. *J. Comp. Neurol.* 264: 356-395, 1987a.

Insausti, R., Amaral, D.G. and Cowan, W.M. The entorhinal cortex of the monkey. III. Subcortical afferents. *J. Comp. Neurol.* 264: 396-408, 1987b.

Jahnsen, H. and Llinás, R. Electrophysiological properties of guinea-pig thalamic neurones: an *in vitro* study. *J. Physiol. (Lond.)* 349: 205-226, 1984.

Jones, E.G. and Powell, T.P.S. An anatomical study of convergin sensory pathways within the cerebral cortex of the monkey. *Brain* 93: 793-820, 1970.

Jones, R.S.G. and Heinemann, V. Synaptic and intrinsic responses of medial entorhinal cortical cells in normal and magnesium-free medium "in vitro". *J. Neurophysiol.* 59: 1476-1496, 1988.

Jones, R.S.G. and Lambert, J.D.C. The role of excitatory amino acid receptors in the propagation of epileptiform discharges from the entorhinal cortex to the dentate gyrus in vitro. *Exp Brain Res* 80: 310-322, 1990.

Kamondi, A. and Reiner, P.B. Hyperpolarization-activated inward current in histaminergic tuberomammillary neurons of the rat hypothalamus. *J. Neurophysiol.* 66: 1902-1911, 1991.

Khateb, A., Muhlethaler, M., Alonso, A., Serafin, M., Mainville, L. and Jones, B.E. Cholinergic nucleus basalis neurons display the capacity for rhythmic bursting activity mediated by low threshold calcium spikes. *Neuroscience* (in press) 1992.

Klink, R. and Alonso, A. Serotoninergic and cholinergic concert actions on entorhinal cortex layer II neurons: an in vitro study. *Soc. Neurosci. Abstr.* 18: 317.4, 1992a.

Klink, R. and Alonso, A. Ionic mechanisms for the subthreshold oscillations and differential electroresponsiveness of medial entorhinal cortex layer II neurons. *submitted* 1992b.

Komisaruk, B.R. Synchrony between limbic system theta activity and rhythmical behavior in rats. *J. Comp. Physiol. Psychol.* 70: 482-492, 1970.

Krettek, J.E. and Price, J.L. Projections from the amygdala to the perirhinal and entorhinal cortices and subiculum. *Brain Res.* 71: 150-154, 1974.

Lancaster, B. and Adams, P.R. Calcium-dependent current generating the after-hyperpolarization of hippocampal neurons. *J. Neurophysiol.* 55: 1286-1282, 1986.

Lancaster, B. and Nicoll, R.A. Properties of two calcium-activated hyperpolarizations in rat hippocampal neurones. *J. Physiol. (Lond.)* 389: 187-204, 1987.

Lanthorn, T., Storm, J. and Andersen, P. Current-to-frequency transduction in CA1 hippocampal pyramidal cells: slow prepotentials dominate the primary range firing. *Exp. Brain Res.* 53: 431-443, 1984.

Larson, J. and Lynch, G. Induction of synaptic potentiation in hippocampus by patterned stimulation involves two events. *Science* 232: 985-988, 1986.

Leung, L.-W.S. and Borst, J.G.G. Electrical activity of the cingulate cortex. I. Generating mechanisms and relations to behavior. *Brain Res.* 407: 68-80, 1987.

Levisohn, L.F. and Isacson, O. Excitotoxic lesions of the rat entorhinal cortex. Effects of selective neuronal damage on acquisition and retention of non-spatial reference memory task. *Brain Res.* 564: 230-244, 1991.

Lingenhöl, K. and Finch, D.M. Morphological characterization of rat entorhinal neurons in vivo: soma-dendritic structure and axonal domains. *Exp. Brain Res.* 84: 57-74.

Llinás, R.R. The Intrinsic electrophysiological properties of mammalian neurons: Insights into central nervous system function. *Science* 242: 1654-1664, 1988.

Llinás, R.R. and Alonso, A. Electrophysiology of the mammillary complex in vitro. I. Tuberomammillary and lateral mammillary neurons. *J. Neurophysiol.* 68: 1992.

Llinás, R.R., Grace, A.A. and Yarom, Y. *In vitro* neurons in mammalian cortical layer 4 exhibit intrinsic oscillatory activity in the 10- to 50-Hz frequency range. *Proc. Natl. Acad. Sci. USA* 88: 897-901, 1991.

Lorenzon, N.M. and Foehring, R.C. Relationship between repetitive firing and afterhyperpolarizations in human neocortical neurons. *J. Neurophysiol.* 67: 350-363, 1992.

MacVicar, B.A. Depolarizing prepotentials are Na^+ dependent in CA1 pyramidal neurons. *Brain Res.* 333: 378-381, 1985.

Madison, D.V. and Nicoll, R.A. Control of the repetitive discharge of rat CA1 pyramidal neurones *in vitro*. *J. Physiol. (Lond.)* 354: 319-331, 1984.

McCormick, D.A., Connors, B.W., Lighthall, J.W. and Prince, D.A. Comparative electrophysiology of pyramidal and sparsely spini stelletae neurons of the neocortex. *J. Neurophysiol.* 54: 782-806, 1985.

McCormick, D.A. and Pape, H.-C. Properties of a hyperpolarization-activated cation current and its role in rhythmic oscillation in thalamic relay neurones. *J. Physiol. (Lond).* 431: 291-318, 1990.

Mignard, M., Bentzinger, D., Bender, N. and Grabiel, M. Type I and type II theta-like unit activity in structures of the papez circuit during differential avoidance conditioning in rabbits. *Soc. Neurosci. Abstr.* 13: 305.15, 1987.

Milner, B. Memory and the medial temporal regions of the brain. In: *Biology of Memory*, New York/London: Academic Press, p. 29-50, 1970.

Mishkin, M. A memory system in the monkey. *Philos. Trans. R. Soc. Lond. [Biol.]* 298: 85-95, 1982.

Mitchell, S.J. and Ranck, J.B.J. Generation of theta rhythm in medial entorhinal cortex of freely moving rats. *Brain Res.* 189: 49-66, 1980.

Mitchell, S.J., Rawlins, J.N.P., Steward, O. and Olton, D.S. Medial septal area lesions disrupt θ rhythm and cholinergic staining in medial entorhinal cortex and produce impaired radial arm maze behavior in rats. *J. Neurosci.* 2: 292-302, 1982.

Mühlethaler, M., Khateb, A., Fort, P., Jones, B.E. and Alonso, A. Forty Hz membrane potential oscillations and theta-like activity in basal forebrain neurons. *Soc. Neurosci. Abstr.* 18: 92.11, 1992.

Murray, E.A. and Mishkin, M. Visual recognition in monkeys following rhinal cortical ablations combined with either amigdalectomy or hippocampectomy. *J. Neurosci.* 6: 1991-2003, 1986.

Osmanovic, S.S. and Shefner, S.A. Anomalous rectification in rat locus coeruleus neurons. *Brain Res.* 417: 161-166, 1987.

Paré, D., de Curtis, M. and Llinás, R. Role of the hippocampal-entorhinal loop in temporal lobe epilepsy: extra- and intracellular study in the isolated guinea pig brain *in vitro*. *J. Neurosci.* 12: 1867-1881, 1992.

Quirk, G.J., Muller, R.U., Kubie, J.L. and Ranck, J.B., Jr. The positional firing properties of medial entorhinal neurons: description and comparison with hippocampal place cells. *J. Neurosci.* 12: 1945-1963, 1992.

Ramon y Cajal, S. Sobre un ganglio especial de la corteza esfeno-occipital. *Trab. del Lab. de invest. Biol. Univ. Madrid* 1: 189-201, 1902.

Room, P. and Groenewegen, H.J. The connections of the parahippocampal cortex in the cat. I Cortical afferents. *J. Comp. Neurol.* 251: 415-450, 1986a.

Room, P. and Groenewegen, H.J. Connections of the parahippocampal cortex in the cat. II. Subcortical afferents. *J. Comp. Neurol.* 251: 451-473, 1986b.

Rutecki, P.A., Grossman, R.G., Armstrong, D. and Irish-Loewen, S. Electrophysiological connections between the hippocampus and entorhinal cortex in patients with complex partial seizures. *J. Neurosurg.* 70: 667-675, 1989.

Schwartz, S.P. and Coleman, P.D. Neurons of origin of the perforant path. *Expl. Neurol.* 74: 305-312, 1981.

Schwindt, P.C., Spain, W.J. and Crill, W.E. Calcium-dependent potassium currents in neurons from cat sensorimotor cortex. *J. Neurophysiol.* 67: 216-226, 1992.

Schwindt, P.C., Spain, W.J., Foehring, R.C., Chubb, M.C. and Crill, W.E. Slow conductances in neurons from cat sensorimotor cortex in vitro and their role in slow excitability changes. *J. Neurophysiol.* 59: 450-467, 1988a.

Schwindt, P.C., Spain, W.J., Foehring, R.C., Stafstrom, C.E., Chubb, M.C. and Crill, W.E. Multiple potassium conductances and their functions in neurons from cat sensorimotor cortex in vitro. *J. Neurophysiol.* 59: 424-449, 1988b.

Silva, L.R., Amital, Y. and Connors, B.W. Intrinsic oscillations of neocortex generated by layer 5 pyramidal neurons. *Science* 251: 432-434, 1991.

Spain, W.J., Schwindt, P.C. and Crill, W.E. Anomalous rectification in neurons from cat sensorimotor cortex in vitro. *J. Neurophysiol.* 57: 1555-1576, 1987.

Squire, L.R. and Zola-Morgan, S. The neurology of memory: the case for correspondence between the findings for human and nonhuman primate. In: *The Physiological Basis of Memory,* New York/London/Sydney/Toronto: Academic Press, p. 199-268, 1983.

Stafstrom, C.E., Schwindt, P.C. and Crill, W.E. Repetitive firing in layer V neurons from cat neocortex in vitro. *J. Neurophysiol.* 52: 264-277, 1984a.

Stafstrom, C.E., Schwindt, P.C., Flatman, J.A. and Crill, W.E. Properties of subthreshold response and action potential recorded in layer V neurons from cat sensorimotor cortex in vitro. *J. Neurophysiol.* 52: 244-263, 1984b.

Stanton, P.K., Jones, R.S.G., Mody, I. and Heinemann, U. Epileptiform activity induced by lowering extracellular magnesium in combined hippocamapl-entorhinal cortex slices: modification by receptors for norepinephrine and N-methyl-D-aspartate. *Epilepsy Res.* 1: 53-62, 1987.

Steriade, M., Curró Dossi, R., Paré, D. and Oakson, G. Fast oscillations (20-40 Hz) in thalamocortical systems and their potentiation by mesopontine cholinergic nuclei in the cat. *Proc. Natl. Acad. Sci. USA* 88: 4396-4400, 1991.

Steward, O. Topographic organization of the projections from the entorhinal area to the hippocampal formation of the rat. *J. Comp. Neurol.* 167: 285-314, 1976.

Steward, O. and Scoville, S.A. The cells of origin of entorhinal afferents to the hippocampus and fascia dentata of the rat. *J. comp. Neurol.* 169: 347-370, 1976.

Stewart, M. and Fox, S.E. Do septal neurons pace the hippocampal theta rhythm? *Trends Neurosci.* 13: 163-168, 1990.

Stumpf, C. The fast component in the electrical activity of rabbit's hippocampus. *Electroenceph. clin. Neurophysiol.* 18: 477-486, 1965.

Van Hoesen, G.W. The parahippocampal gyrus. New observations regarding its cortical connections in the monkey. *Trends Neurosci.* 5: 345-350, 1982.

Van Hoesen, G.W., Hyman, B.T. and Damasio, A.R. Entorhinal cortex pathology in Alzheimer's disease. *Hippocampus* 1: 1-8, 1991.

Van Hoesen, G.W. and Pandya, D.N. Some connections of the entorhinal (area 28) and perirhinal (area 35) cortices of the rhesus monkey. I. Temporal lobe afferents. *Brain Res.* 95: 1-24, 1975.

Wilcox, K.S., Gutnick, M.J. and Christoph, G.R. Electrophysiological properties of neurons in the lateral habenula nucleus: an *in vitro* study. *J. Neurophysiol.* 59: 212-225, 1988.

Wong, R.K.S. and Prince, D.A. Afterpotential generation in hippocampal pyramidal cells. *J. Neurophysiol.* 45: 86-97, 1981.

Yarom, Y. and Llinás, R. Long-term modifiability of anomalous and delayed rectification in guinea pig inferior olivary neurons. *J. Neurosci.* 7: 1166-1177, 1987.

Table 1. Electrophysiological parameters of stellate (SC) and non-stellate (non-SC) cells of medial entorhinal cortex layer II.

Values are mean ± SD for forty nine and twenty six representative SCs and non-SCs, respectively. Vr: resting membrane potential; Ri: apparent input resistance; Tau: apparent membrane time constant; Sp Thr: spike threshold; Sp Dur: spike duration; fAHP and mAHP: fast and medium AHP amplitude, respectively; DAP: depolarizing after potential; Vm Osc: membrane potential of most prominent oscillatory activity; Freq Osc: frequency of oscillations measured at Vm Osc; Amp Osc: mean amplitude of oscillations measured at Vm Osc; Hs% and DS%: hyperpolarization-induced and depolarization-induced sag percentage, respectively; MSL: maximum spike latency. See METHODS section for details on measurements.

	Vr mV	Ri MΩ	Tau ms	Sp Thr mV	Sp Dur ms	fAHP mV	mAHP mV	DAP mV	Vm Osc mV	Freq Osc Hz	Amp Osc mV	HS%	DS%	MSL ms
SC	-62.4±3.1	36±9	8.5±2.4	-50.9±2.4	1.27±0.22	10.4±2.6	10.7±3.1	1.1±1.0	-55.6±2.1	8.6±2.1	2.6±0.5	30±7	57±17	42±17
non-SC	-63.7±4.1	40±11	11.9±3.7	-48.7±2.5	1.77±0.43	9.1±2.3	10.0±2.1	0.4±0.6	-	-	-	17±8	10±9	180±68

Figure 1. Morphology of medial entorhinal cortex layer II neurons. *A* and *B*: camera lucida reconstructions of a stellate and a non-stellate (pyramidal-like) cell from medial entorhinal cortex layer II, respectively.

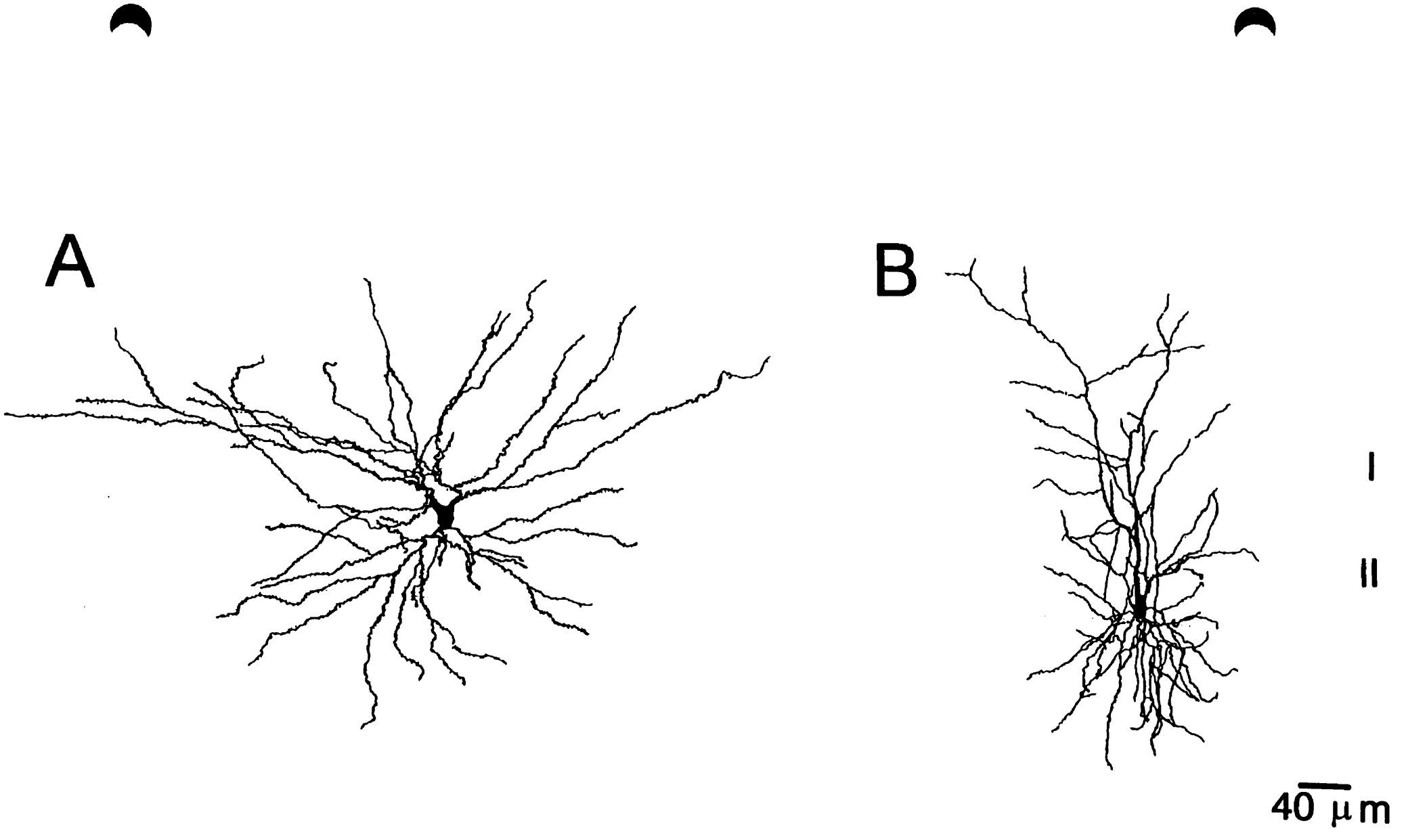
A
B
I
II
40 µm

Figure 2. Voltage-current relationship of stellate cells. *A*: responses to injection of depolarizing and hyperpolarizing current pulses applied from the resting membrane potential (-64mV). Vp signals the early peak of the voltage responses which then "sag" towards a steady state level (Vs). *B*: plots of membrane potential (Vm) vs. amplitude of current pulse from the cell in A. Filled circles plot levels of Vm at the peak of the voltage response. Filled triangles plot levels of Vm at steady state (measurements towards the end of the current pulse). Note that both plots are concave over the whole range, thus demonstrating inward rectification in both the hyperpolarizing and depolarizing direction. *C*: Voltage responses to low amplitude subthreshold depolarizing and hyperpolarizing current pulses taken from A and plotted at an expanded voltage scale. Note that minimal voltage changes evoke an active membrane response (sag). *D*: detail of the rebound responses to hyperpolarizing pulses of increasing amplitude from A plotted at an expanded voltage scale. Note that the largest hyperpolarization elicits burst firing (dots).

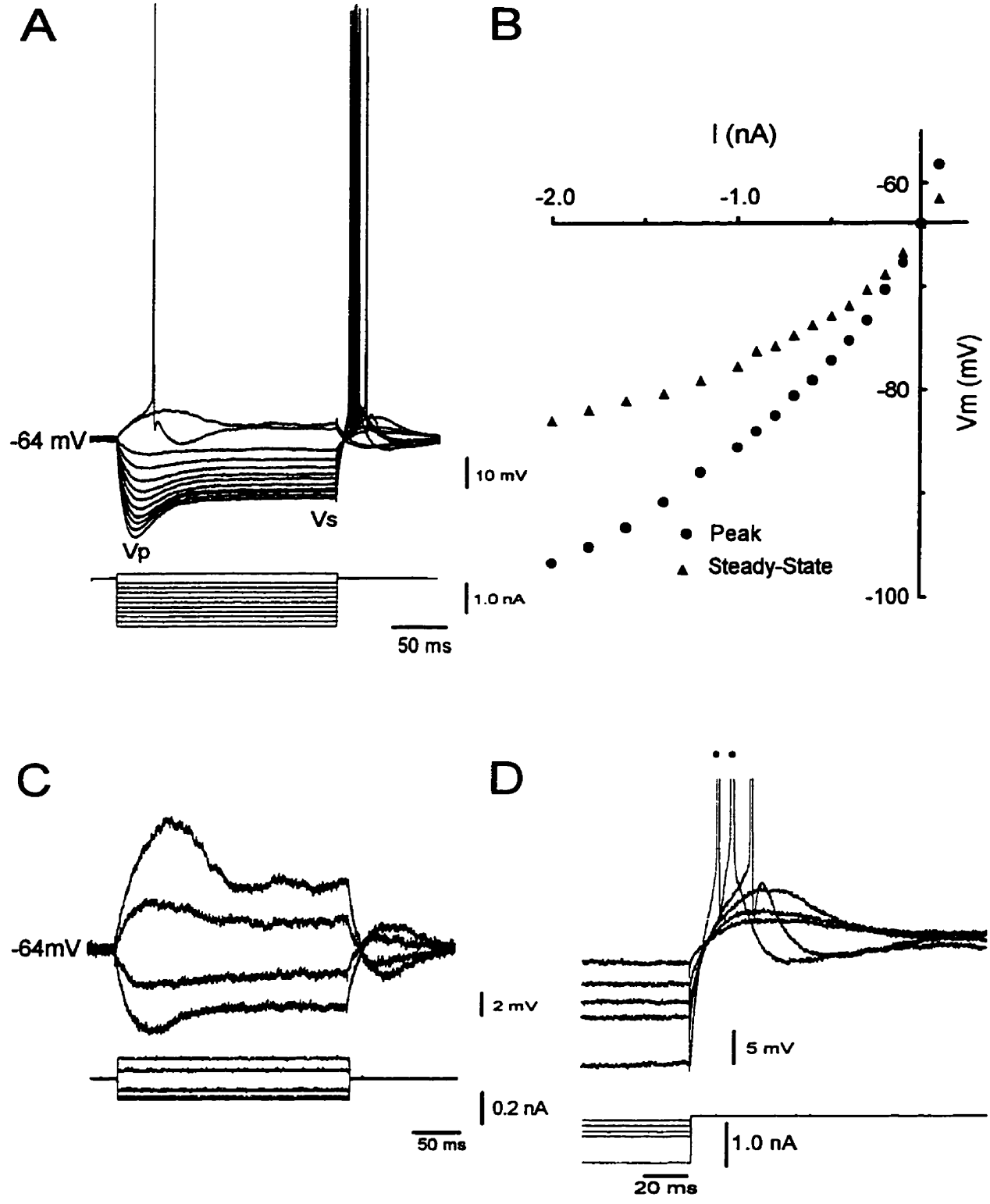
A
-64 mV
Vp
Vs
10 mV
1.0 nA
50 ms
B
I (nA)
-2.0
-1.0
-60
-80
-100
Vm (mV)
Peak
Steady-State
C
-64mV
2 mV
0.2 nA
50 ms
D
5 mV
1.0 nA
20 ms

Figure 3. Voltage-current relationship of non-stellate cells. *A*: responses to injection of depolarizing and hyperpolarizing current pulses applied from the resting membrane potential (-64 mV). *B*: plots of membrane potential (Vm) vs. amplitude of current pulse from the cell in A. Filled circles plot levels of Vm at the peak of the voltage response. Filled triangles plot levels of Vm at steady state (measurements towards the end of the current pulse). *C*: Voltage responses from a different cell to low amplitude depolarizing and hyperpolarizing current pulses. Note the absence of depolarization-induced sag and the slowly rising ramp potential evoked by the largest depolarizing pulse. *D*: rebound responses to hyperpolarizing pulses of increasing amplitude. Note that the largest rebound potentials can trigger a plateau depolarization and spiking (arrowhead).

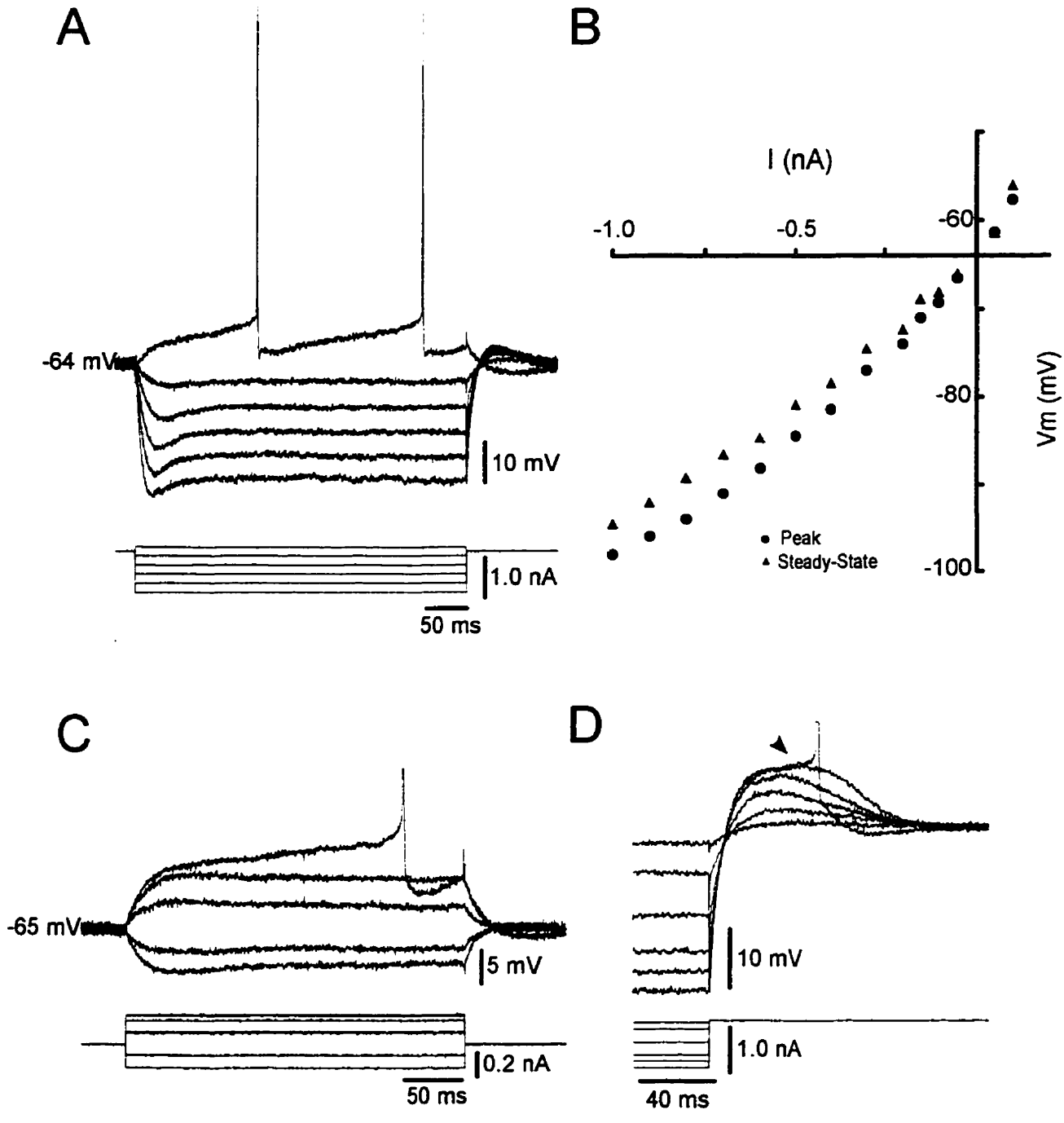
A
-64 mV
10 mV
1.0 nA
50 ms
B
I (nA)
-1.0
-0.5
-60
-80
-100
Vm (mV)
Peak
Steady-State
C
-65 mV
5 mV
0.2 nA
50 ms
D
10 mV
1.0 nA
40 ms

Figure 4. Stellate cell subthreshold rhythmic voltage oscillations. *A*: development of oscillations with increasing levels of depolarization. Note that at rest (0 nA, Vm=-64mV) no membrane potential oscillations are present but they clearly develop with current injection of 0.28 nA (Vm=-58mV). *B*: autocorrelogram for the 0.36 nA current injection level (Vm=-55 mV) demonstrating clear rhythmicity at a dominant frequency of 8.3 Hz. The dotted line on the autocorrelogram indicates 0 level. *C*: graphic representation of the average amplitude of the subthreshold oscillations plotted against membrane potential (Vm) from four different neurons.

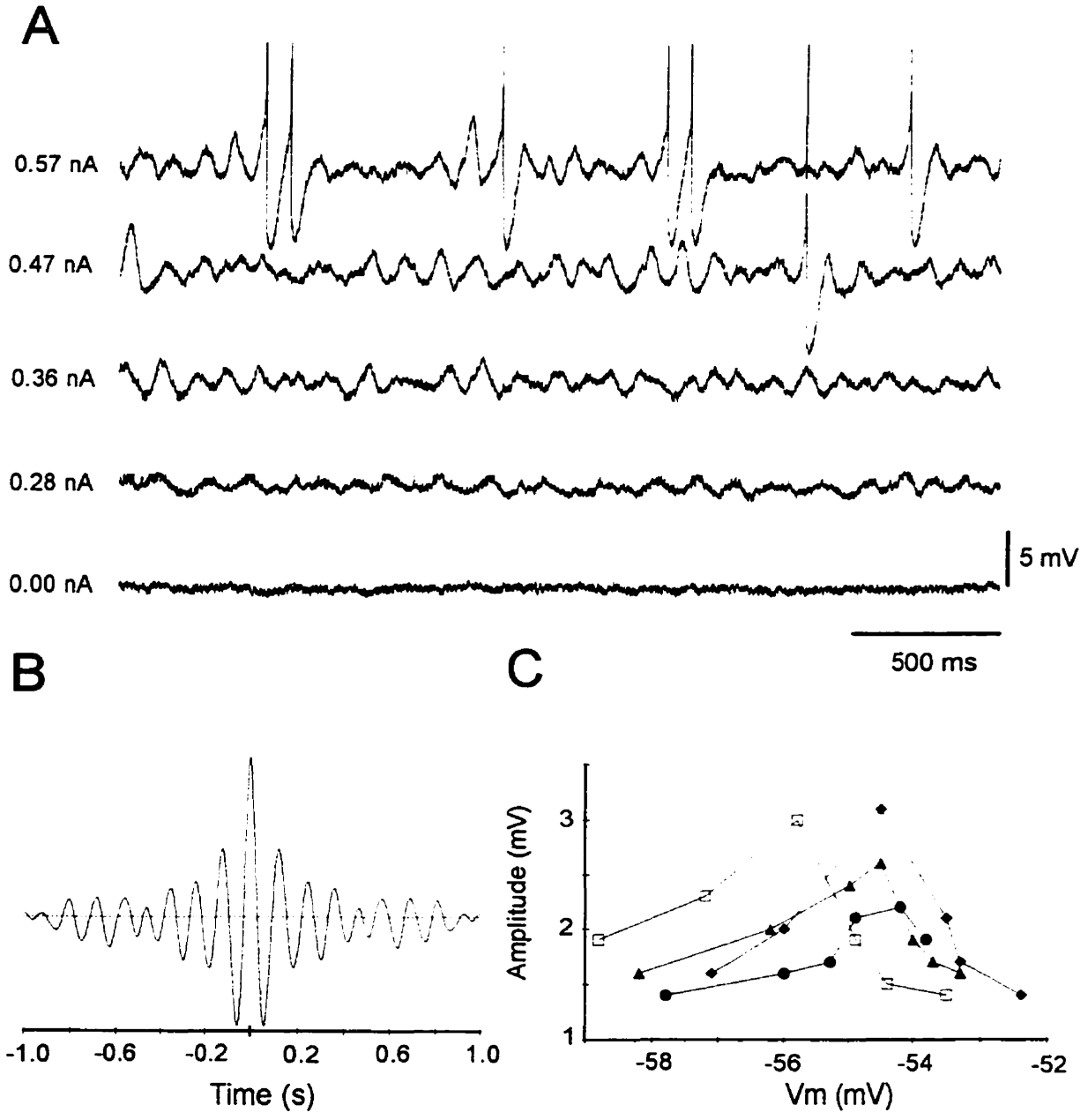
A
0.57 nA
0.47 nA
0.36 nA
0.28 nA
0.00 nA
5 mV
500 ms
B
-1.0
-0.6
-0.2
0.2
0.6
1.0
Time (s)
C
Amplitude (mV)
3
2
1
-58
-56
-54
-52
Vm (mV)

Figure 5. Spike "clusters" and subthreshold oscillations in the stellate cells. *A-C*: spiking and subthreshold oscillations at three different levels of depolarizing constant current injection. Note the emergence of spike clusters in B and the development of a repetitive bursting pattern in C. Note also that bursts are separated by subthreshold oscillations and are not followed by a slow AHP. *D*: short epochs from A and C (bottom dotted lines) at an expanded time and voltage scale. Note the higher frequency of the subthreshold oscillations during inter-burst intervals (upper trace) as compared to those interspersed with single spiking (lower trace). *E*: superimposition of the four action potentials from the labeled burst in C (upper thick line) aligned with respect to their peaks. Note the regularity of the spike (inset) and interspike trajectories. The filled circle in E and C signals the second spike of the burst. *F*: graphic representation of the frequency of the subthreshold oscillations plotted against membrane potential (Vm) in four different neurons. Note the non-linearity of this relationship with a rapid increase in frequency at potentials positive to about -55mV. *G*: graphic representation of the duration of the intra-burst inter-spike intervals as a function of the inter-spike interval number for ten consecutive bursts of 3-4 spikes form the same cell in A-E.

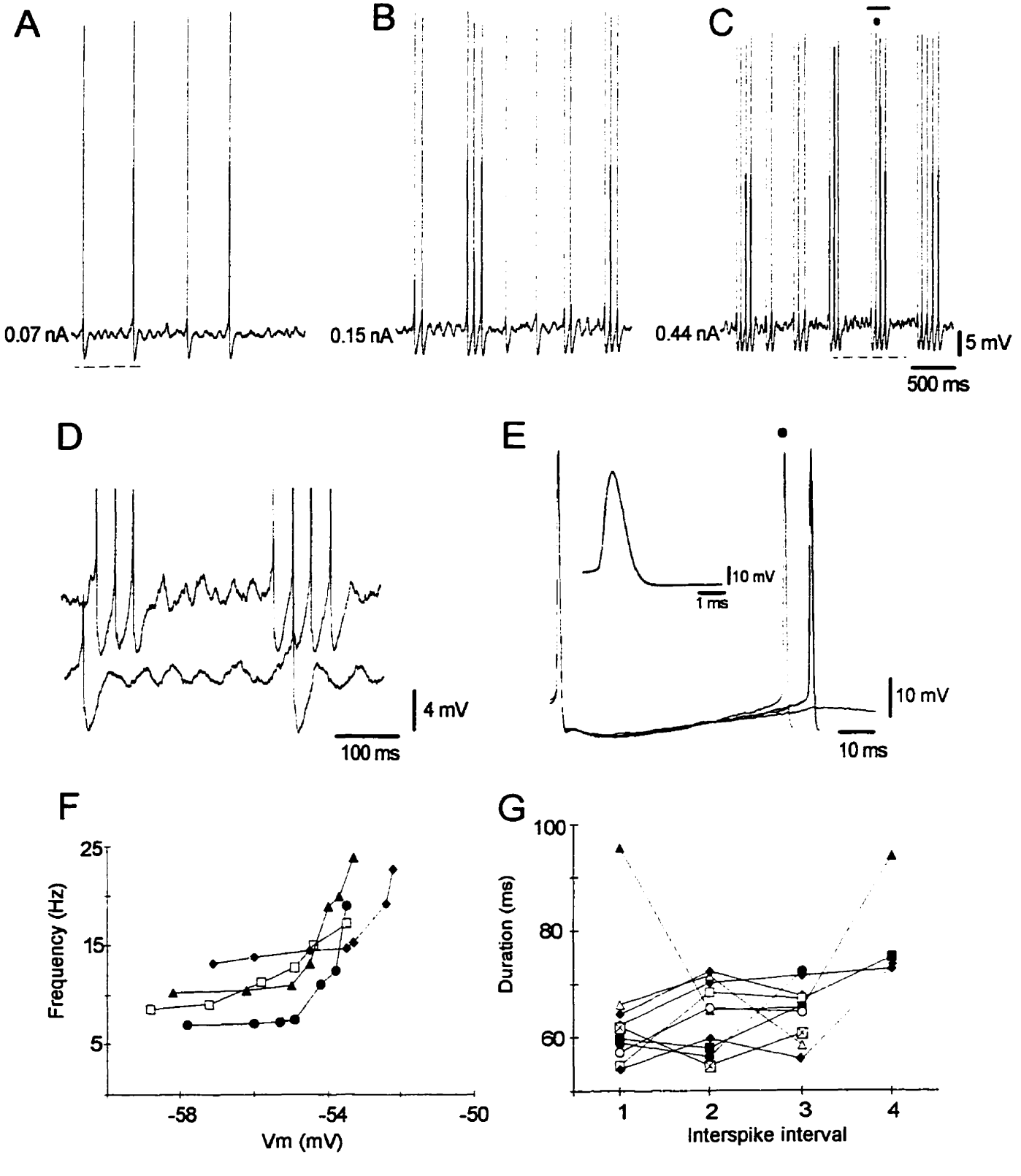
A
B
C
0.07 nA
0.15 nA
0.44 nA
5 mV
500 ms
D
4 mV
100 ms
E
10 mV
1 ms
10 mV
10 ms
F
Frequency (Hz)
25
15
5
-58
-54
-50
Vm (mV)
G
Duration (ms)
100
80
60
1
2
3
4
Interspike interval

Figure 6. Tonic firing in the stellate cells evoked by depolarizing constant current injection. *A*: subthreshold oscillations and occasional spikes at a membane potential of about -54 mV. *B*: tonic firing with a spike failure (arrow) with current injection of 0.64 nA.

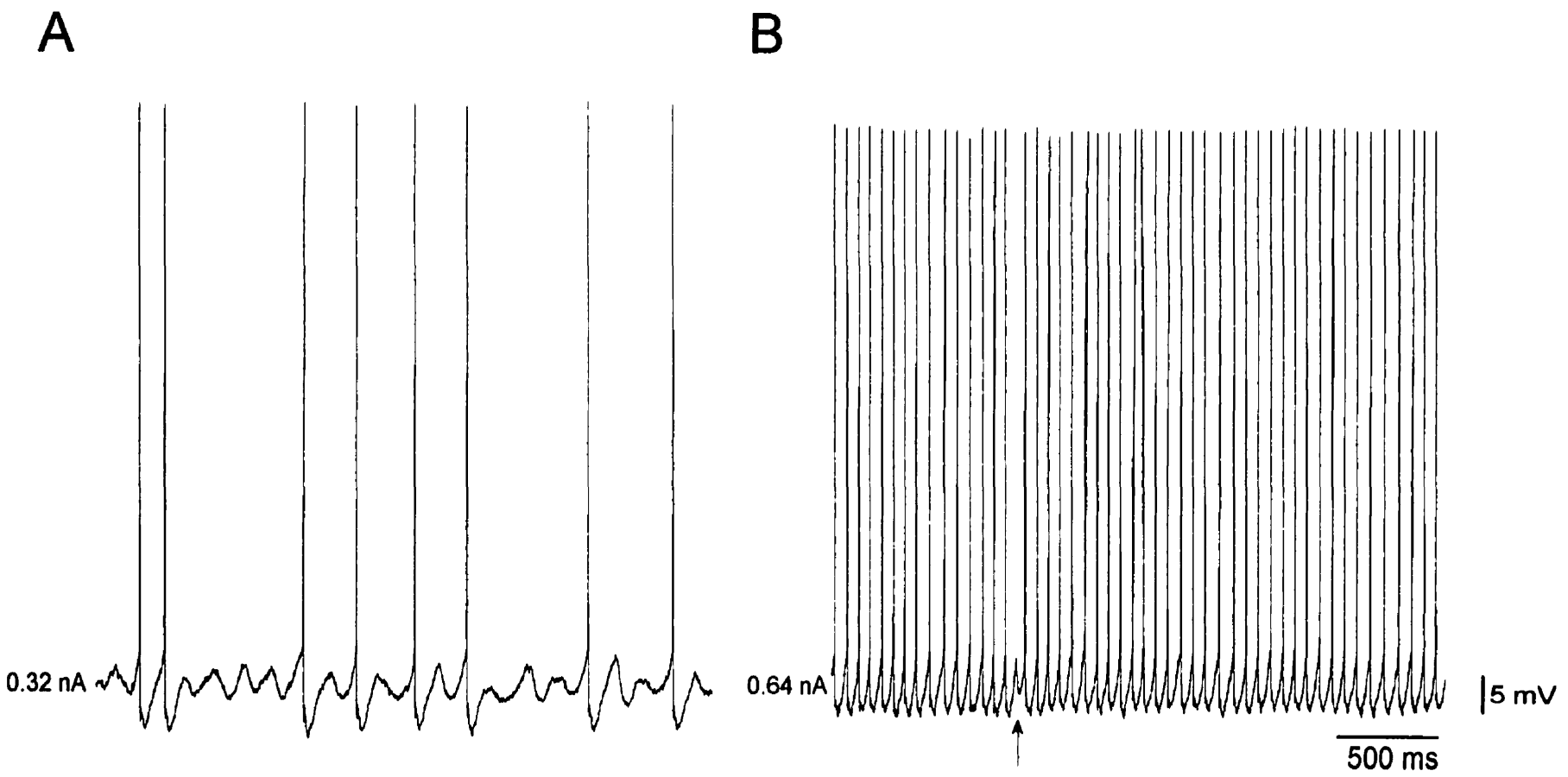
A
B
0.32 nA
0.64 nA
5 mV
500 ms

Figure 7. Subthreshold membrane voltage behavior of non-stellate cells upon d.c. depolarization. Note the absence of both the persistent rhythmic subthreshold oscillatory activity, as indicated by the non rhythmic autocorrelogram to the right, and the spike clusters typical of the stellate cells (Fig. 4).

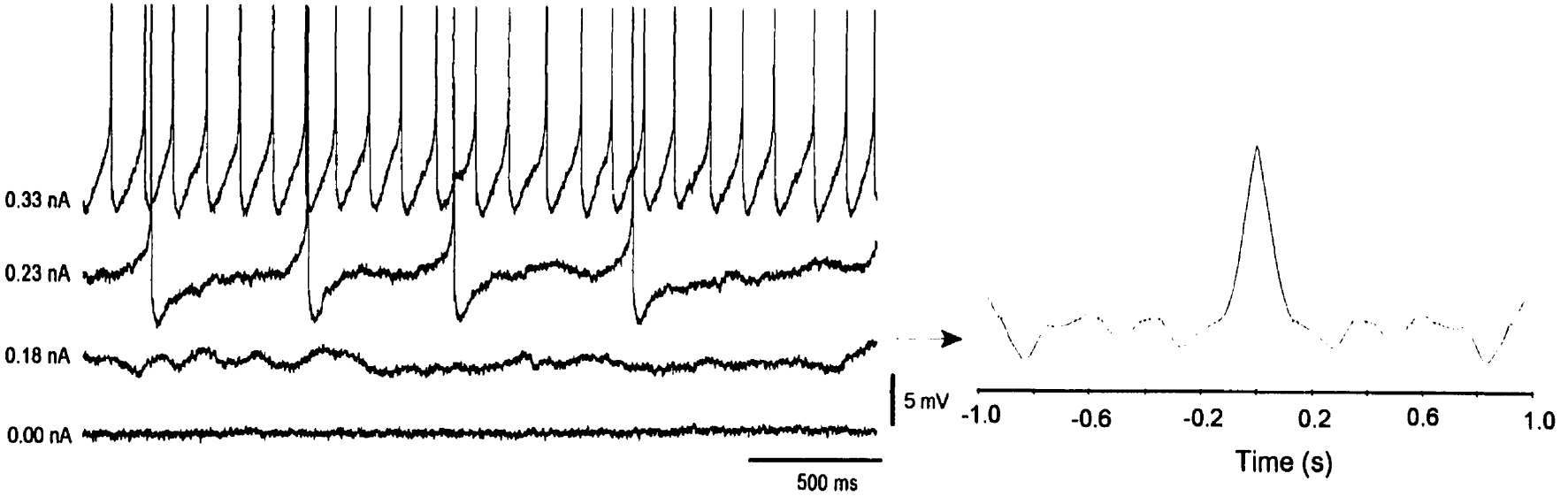
0.33 nA
0.23 nA
0.18 nA
0.00 nA
500 ms
5 mV
-1.0
-0.6
-0.2
0.2
0.6
1.0
Time (s)

Figure 8. Electrophysiological parameters that vary between stellate and non-stellate cells (SC and non-SC, respectively). Distributions: depolarization-induced sag percentages (*A*, DS%); hyperpolarization-induced sag percentages (*B*, HS%); spike duration (*C*, SpDur); spike threshold (*D*, SpThr); depolarizing after potential amplitude (*F*, DAP); apparent membrane time-constant (*G*, Tau). *E*: spike afterpotentials in stellate (upper trace) and non-stellate (lower trace) cells. Action potentials truncated. fAHP, fast afterhyperpolarization; DAP, depolarizing afterpotential; mAHP, medium afterhyperpolarization.

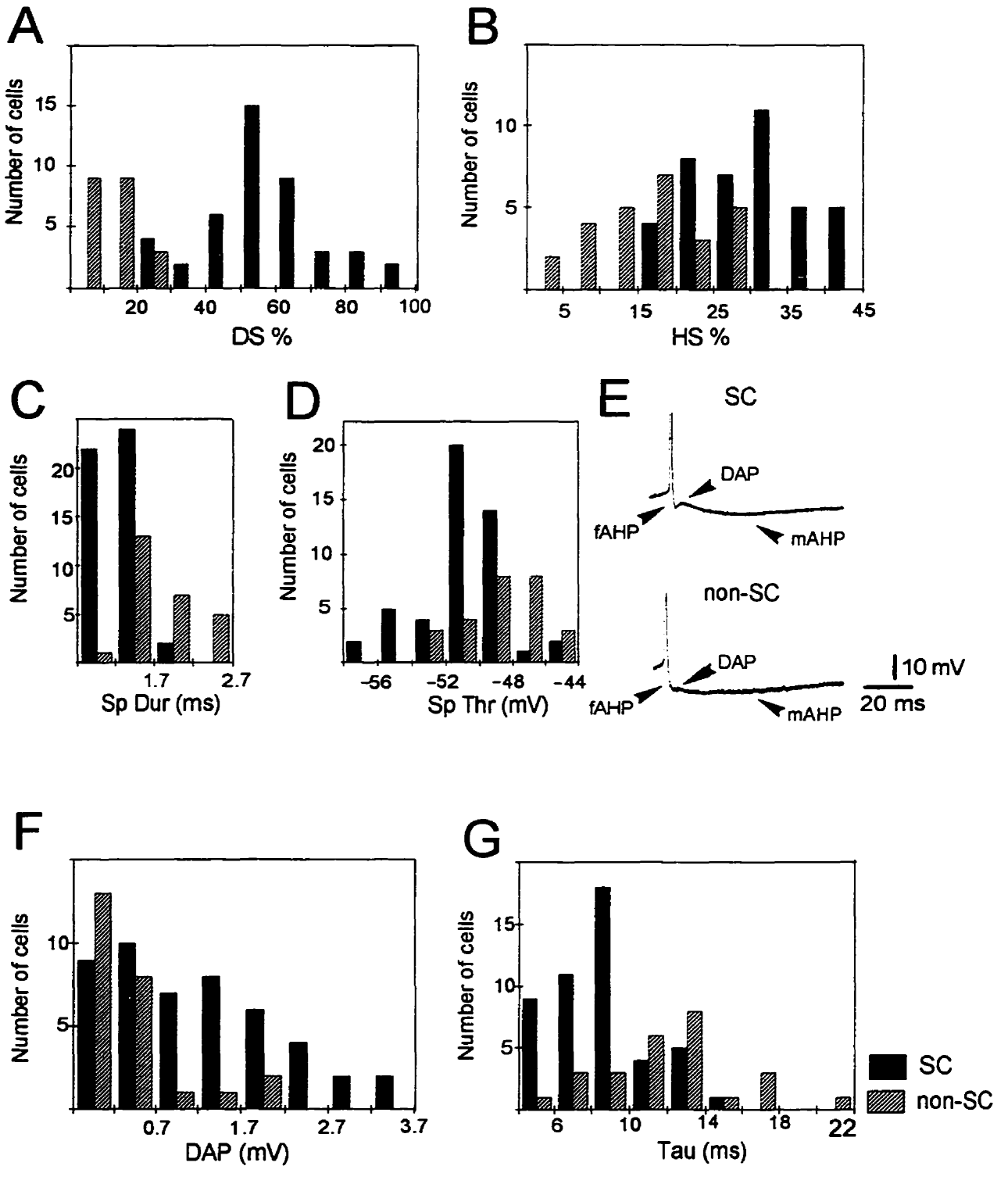
A
Number of cells
15
10
5
20
40
60
80
100
DS %
B
Number of cells
10
5
5
15
25
35
45
HS %
C
Number of cells
20
15
10
5
1.7
2.7
Sp Dur (ms)
D
Number of cells
20
15
10
5
-56
-52
-48
-44
Sp Thr (mV)
E
SC
DAP
fAHP
mAHP
non-SC
DAP
fAHP
mAHP
10 mV
20 ms
F
Number of cells
10
5
0.7
1.7
2.7
3.7
DAP (mV)
G
Number of cells
15
10
5
6
10
14
18
22
Tau (ms)
SC
non-SC

Figure 9. Firing frequency versus injected current in stellate cells. *A*: increased firing frequency response to injection of constant current pulses of increasing amplitude (left to right). *B*: plot of firing frequency versus injected current (f-I relation) for early (1,2, and 3) and late (6 and 8) inter-spike intervals (ISIs). *C*: plot of the number of spikes evoked by 220ms current pulses as a function of the amplitude of the pulses. *D*: plot of instantaneous firing rate versus time for two different steps of injected current. The lines represent the best-fits for the fast (logarithmic fit) and slow (exponential fit) phases of adaptation.

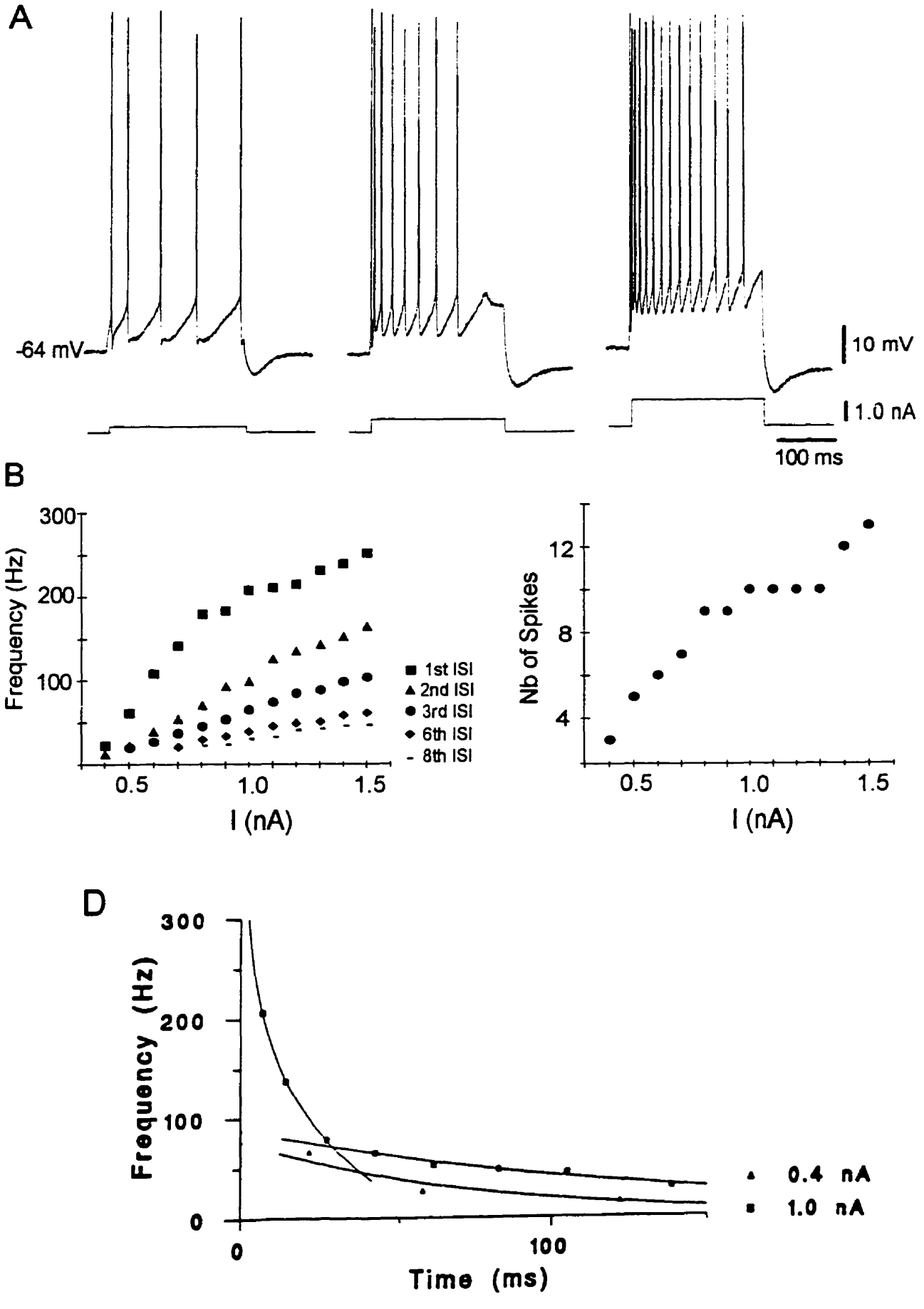
A
-64 mV
10 mV
1.0 nA
100 ms
B
Frequency (Hz)
300
200
100
0.5
1.0
1.5
I (nA)
1st ISI
2nd ISI
3rd ISI
6th ISI
8th ISI
Nb of Spikes
12
8
4
0.5
1.0
1.5
I (nA)
D
Frequency (Hz)
300
200
100
0
0
100
Time (ms)
0.4 nA
1.0 nA

Figure 10. Firing frequency versus injected current in non-stellate cells. *A*: increased firing frequency response to injection of constant current pulses of increasing amplitude (left to right). *B*: plot of firing frequency versus injected current (f-I relation) for early (1,2, and 3) and late (6 and 8) inter-spike intervals (ISIs). *C*: plot of the number of spikes evoked by a 240ms current pulse as a function of the amplitude of the pulse. *D*: plot of instantaneous firing rate versus time for two different steps of injected current. The lines represent the best-fits for the fast (logarithmic fit) and slow (exponential fit) phases of adaptation.

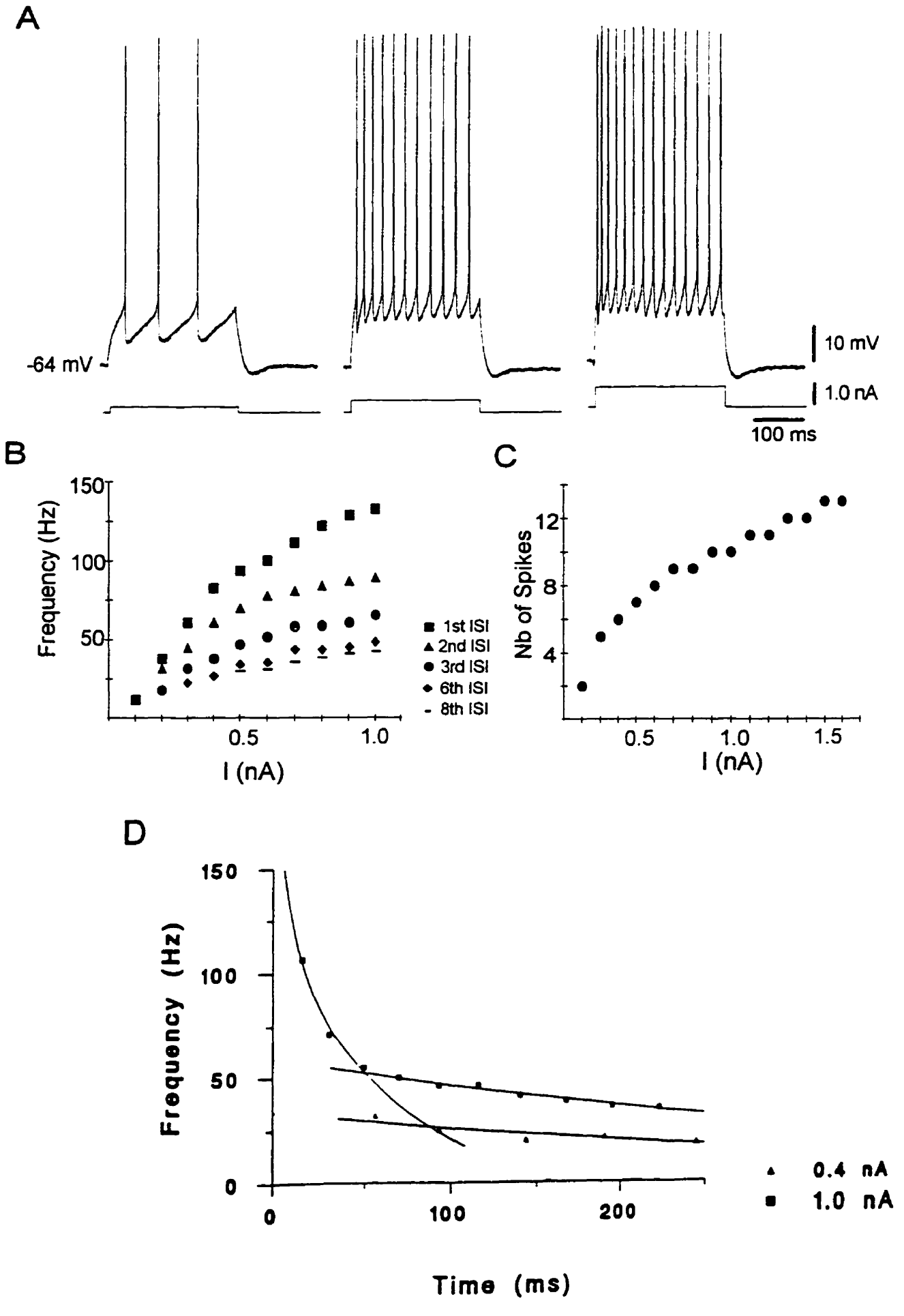
A
-64 mV
10 mV
1.0 nA
100 ms
B
Frequency (Hz)
150
100
50
0.5
1.0
I (nA)
1st ISI
2nd ISI
3rd ISI
6th ISI
8th ISI
C
Nb of Spikes
12
8
4
0.5
1.0
1.5
I (nA)
D
Frequency (Hz)
150
100
50
0
0
100
200
Time (ms)
0.4 nA
1.0 nA

Figure 11. Spike and interspike trajectories during current-pulse triggered spike-trains in stellate cells. *A*: spike train triggered by a 230ms current pulse of 0.6 nA. *B*: superimposition of the first, second, third and sixth spike of the train in A. The traces have been offset to match spike thresholds. *C*: plots of spike duration versus spike number during individual trains evoked by current pulses of increasing amplitude. Note the clear decrease in spike duration for the late spikes of the train at all current intensities.

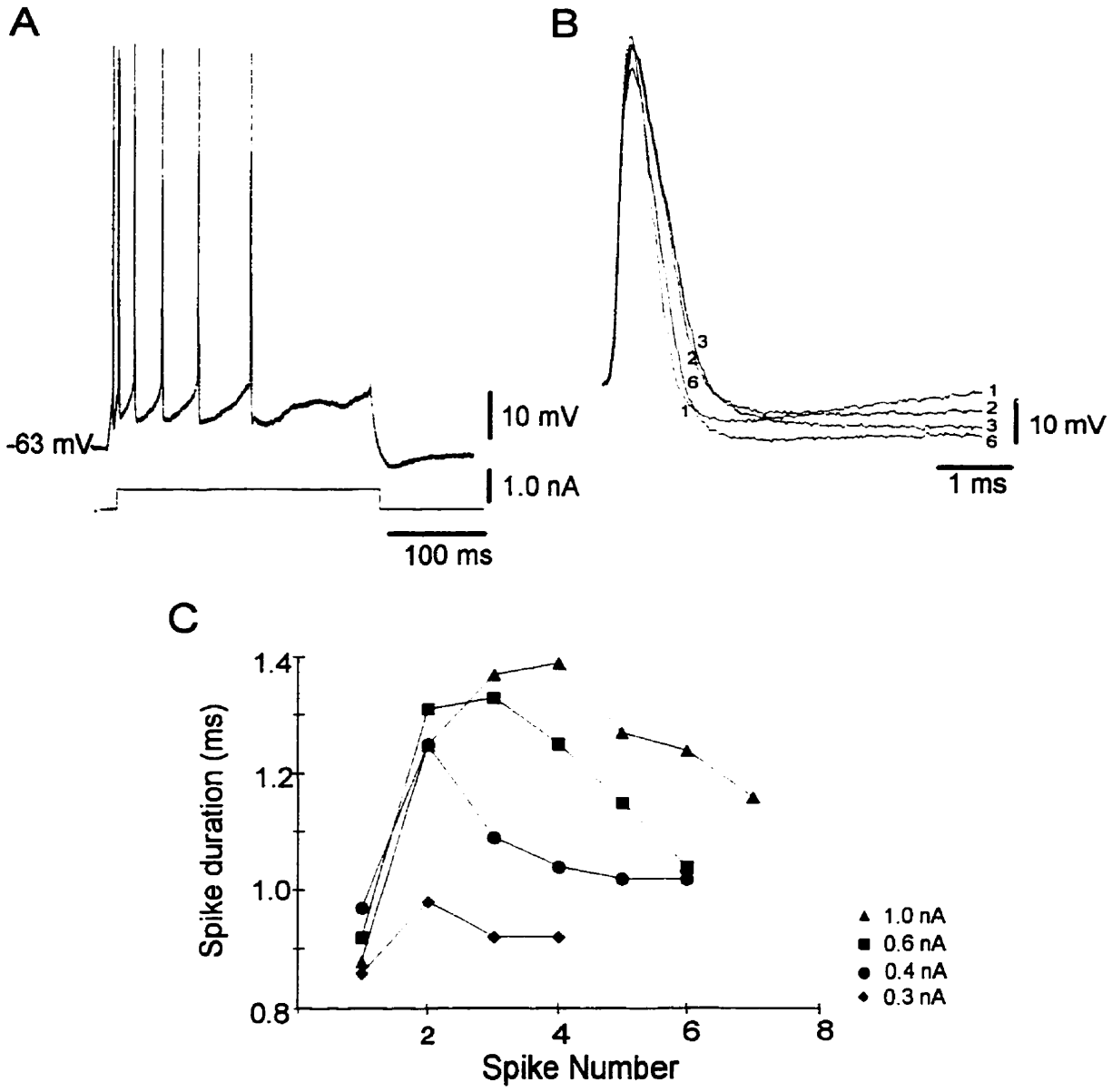
A
B
C
-63 mV
10 mV
1.0 nA
100 ms
1 ms
10 mV
1
2
3
6
Spike duration (ms)
Spike Number
1.4
1.2
1.0
0.8
2
4
6
8
1.0 nA
0.6 nA
0.4 nA
0.3 nA

Figure 12. Spike and interspike trajectories during current-pulse triggered spike-trains in non-stellate cells. *A*: spike train triggered by a 230ms current pulse of 0.6 nA. *B*: superimposition of the first, second, third and sixth spike of the train in A. The traces have been offset to match spike thresholds. *C*: plots of spike duration versus spike number during individual trains evoked by current pulses of increasing amplitude. Note that, as opposed to the stellate cells (Fig. 10), the spike duration never decreased during the train at any current intensity.

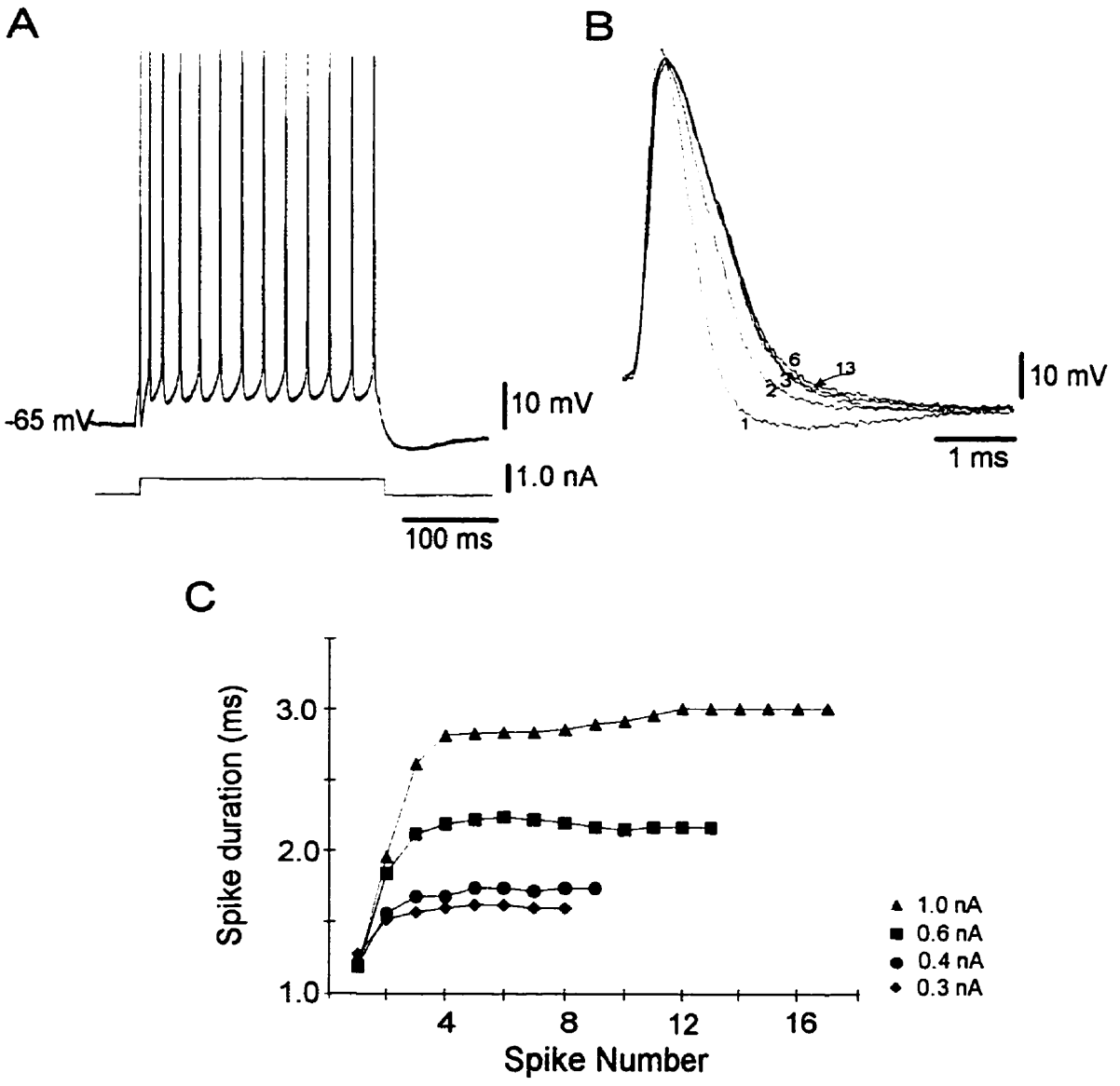
A
B
-65 mV
10 mV
1.0 nA
100 ms
10 mV
1 ms
1
2
3
6
13
C
Spike duration (ms)
3.0
2.0
1.0
4
8
12
16
Spike Number
1.0 nA
0.6 nA
0.4 nA
0.3 nA

Figure 13. Characteristics of the AHP following current-pulse triggered spike-trains in stellate and non-stellate cells. *A* and *B*: AHP following a 1nA current pulse in a stellate and a non-stellate cell, respectively. A medium duration (asterisk) and a slow AHP component are present in both types of neurons. Note that in spite of the shorter pulse applied to the stellate cell the AHP amplitude was larger than that of the non-stellate cell. Also the stellate cell slow AHP was distinctively biphasic (arrowhead). *C* and *D*: Plots of medium AHP peak amplitude (C) and slow AHP peak amplitude (D) for both stellate (filled diamonds) and non-stellate (filled squares) cells.

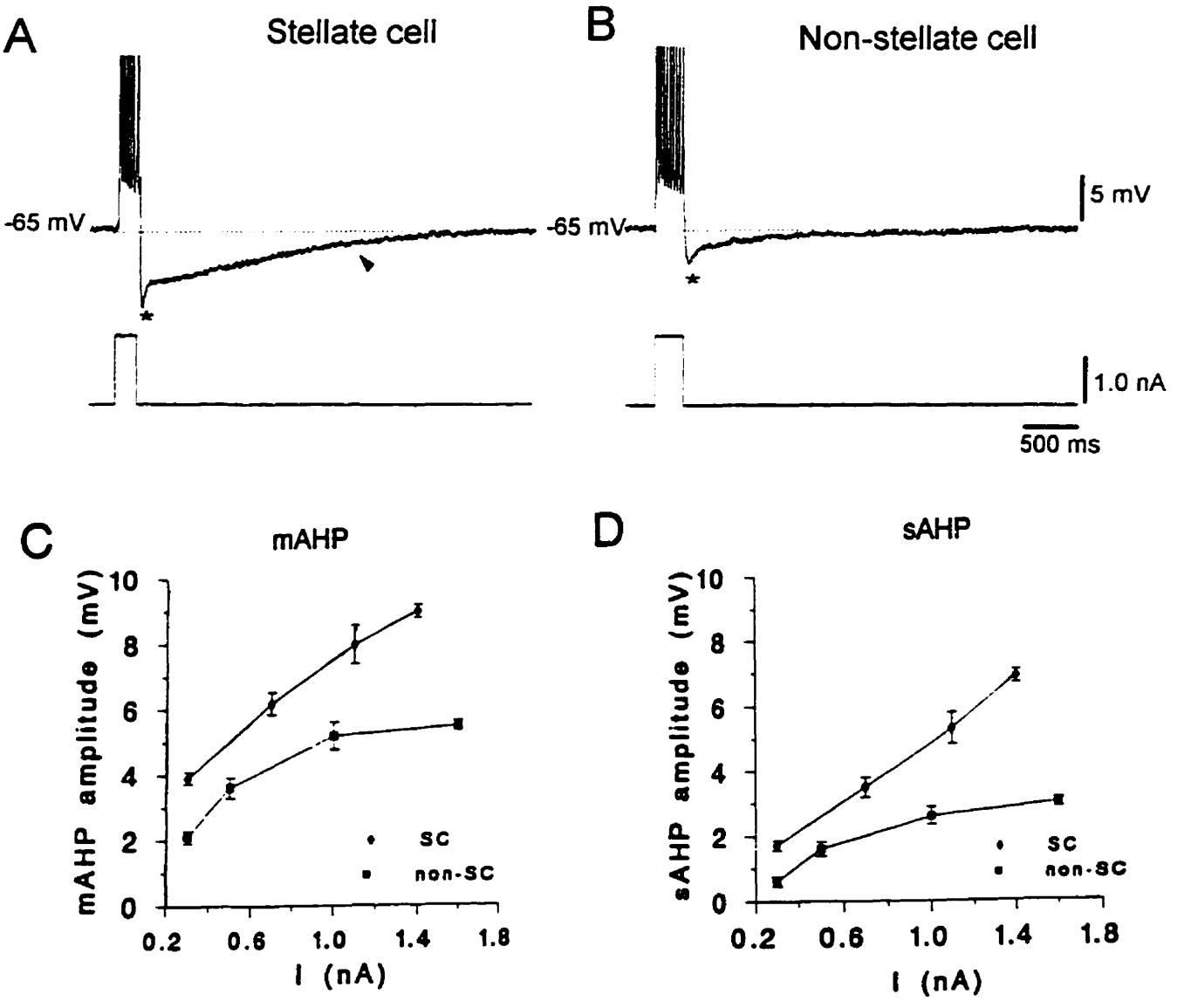
A
Stellate cell
B
Non-stellate cell
-65 mV
-65 mV
5 mV
1.0 nA
500 ms
C
mAHP
mAHP amplitude (mV)
I (nA)
SC
non-SC
D
sAHP
sAHP amplitude (mV)
I (nA)
SC
non-SC

CHAPTER IV

IONIC MECHANISMS FOR THE SUBTHRESHOLD OSCILLATIONS AND DIFFERENTIAL ELECTRORESPONSIVENESS OF MEDIAL ENTORHINAL CORTEX LAYER II NEURONS

Ruby Klink and Angel Alonso

ABBREVIATIONS

EC	Entorhinal cortex
MEC	Medial entorhinal cortex
TTX	Tetrodotoxin
g_{NaP}	Persistent low-threshold sodium conductance
TEA	Tetraethylammonium
SC	Stellate cell

SUMMARY AND CONCLUSIONS

1. Layer II of the medial entorhinal cortex is comprised of two electrophysiologically and morphologically distinct types of projection neurons: stellate cells (SCs) which are distinguished by rhythmic subthreshold oscillatory activity and non-stellate cells (non-SCs). The ionic mechanisms underlying their differential electroresponsiveness, particularly in the subthreshold range of membrane potentials, was investigated in an "*in vitro*" slice preparation.

2. In both, SCs and non-SCs, the apparent membrane input resistance was markedly voltage-dependent, respectively decreasing or increasing at hyperpolarized or subthreshold depolarized potential levels. Thus, the neurons displayed inward rectification in the hyperpolarizing and depolarizing range.

3. In the depolarizing range, inward rectification was blocked by tetrodotoxin (TTX, 1μM) in both types of neurons and thus shown to depend on the presence of a persistent low-threshold Na^+-conductance (g_{Nap}). However, in the presence of TTX, pronounced outward rectification became manifest in the subthreshold depolarizing range of membrane potentials (positive to -60mV) in the SCs but not in the non-SCs.

4. The rhythmic subthreshold membrane potential oscillations which were present only in the SCs were abolished by TTX and not by Ca^{2+}-conductance block with Cd^{2+} or Co^{2+}. Subthreshold oscillations thus rely on the activation of voltage-gated Na^+, and not Ca^{2+}, conductances. The Ca^{2+}-conductance block also had no effect on the subthreshold outward rectification.

5. Prominent time-dependent inward rectification in the hyperpolarizing range in the SCs persisted after Na^+- and Ca^{2+}-conductance block. This rectification was not affected by Ba^{2+} (1mM), but was blocked by Cs^+ (1-4mM). Therefore, it is most probably generated by a hyperpolarization activated cationic current (Q-like current). However, the

Q-like current appears to play no major role in the generation of subthreshold rhythmic membrane potential oscillations since these persisted in the presence of Cs^+.

6. On the other hand, in the SCs, the fast, sustained, outward rectification that strongly developed (after Na^+-conductance block) at the oscillatory voltage level was not affected by Cs^+ but was blocked by Ba^{2+} (1mM). Barium was also effective in blocking the subthreshold membrane potential oscillations.

7. In the non-SCs, which do not generate subthreshold rhythmic membrane potential oscillations nor manifest subthreshold outward rectification in TTX, Ca^{2+}-conductance block abolished spike repolarization and caused the development of long-lasting Na^+-dependent plateau potentials at a high suprathreshold voltage level. At this level, where prominent delayed rectification is present, the Na^+ plateaus sustained rhythmic membrane potential oscillations. In the SCs, Ca^{2+}-conductance block caused only a spike broadening at the base and blocked the fast afterhyperpolarization.

8. The results provide further evidence that the different electroresponsiveness of SCs vs non-SCs rests to a large extent in a different expression of ionic conductances in their respective neuronal membranes. With regard to the distinct rhythmic subthreshold oscillations present only in the SCs, the data suggest that their mechanism of generation relies on the interplay of g_{Nap} and a subthreshold outward rectifying K^+-conductance.

INTRODUCTION

A substantial amount of *in vitro* neurophysiological investigations over the last 15 years have demonstrated a previously unexpected, rich electrophysiological diversity of CNS neurons in both subcortical or cortical structures (Connors and Gutnick 1990; Llinás 1988). Mammalian brain neurons indeed possess a great variety of voltage-gated ionic conductances which depending upon relative prominence and somatodendritic location shape their individual electroresponsiveness and thus the way they process information. In certain brain areas, electrophysiological diversity even appears to exceed that of morphology (Alonso and Llinás 1992).

In line with the above, the study of the general electrophysiological characteristics of medial entorhinal cortex (MEC) layer II neurons reported in the accompanying paper (Alonso and Klink 1992) demonstrated the presence in this key cortical layer of two groups of projection neurons that were morphologically identified as stellate and non-stellate cells and which displayed clearly distinct intrinsic electroresponsiveness. Among multiple differences in their non-linear input-output relations, the most striking was the ability of the stellate cells (SCs) to generate rhythmic voltage oscillations in the subthreshold range of membrane potentials. In the present study, we have investigated with conventional current-clamp and pharmacological techniques some of the ionic mechanisms underlying the differential electroresponsiveness of SCs and non-SCs. In particular, we have placed special emphasis on those mechanisms responsible for the non-linearity of the membrane in the subthreshold range of membrane potentials and thus for subthreshold voltage oscillations. While in other brain neurons, these oscillations generally rely on the activation of voltage-dependent Ca^{2+}-conductances, our results demonstrate that subthreshold membrane potential oscillations in the SCs depend on the activation of a low-threshold persistent Na^{+}-conductance (g_{NaP}). Evidence is also presented that the

interplay of (g_{NaP}) and a delayed K^+ rectifier is necessary and sufficient for the generation of rhythmic subthreshold oscillatory activity.

METHODS

The materials and methods used for the preparation of EC slices and for recording the cells were similar to those described in the accompanying paper (Alonso and Klink 1992). The control Ringer solution contained (in mM) : 124 NaCl; 5 KCl; 1.2 KH_2PO_4; 2.4 $CaCl_2$; 2.6 $MgSO_4$; 26 $NaHCO_3$; and 10 glucose. pH was adjusted to 7.4 by saturating with 95% O_2 and 5% CO_2. In experiments where the effects of Cd^{2+}, Co^{2+} or Ba^{2+} were tested, phosphate and sulfate were omitted to avoid precipitation and divalent cations were maintained at a normal concentration by adjusting the Mg^+ concentration. In order to block Na^+-conductances, tetrodotoxin (TTX, 1μM) was routinely used, though in some experiments the lidocaine derivative QX314 (Strichartz 1973) was applied internally (25-100 nM in pipette) or the NaCl and $NaHCO_3$ were substituted with choline Cl and choline HCO_3 on an equimolar basis. In some experiments extracellular cesium was applied at a concentration of 1-4mM, tetraethylammonium (TEA) at 10-20 mM, carbachol at 15-30 μM and EGTA at 0.5 mM.

Extracellular stimulation was implemented by the use of a twisted Teflon-coated wire pair placed on the molecular layer of the EC 0.5 mm laterally to the recording electrode and connected to an isolation unit.

RESULTS

Na^+-DEPENDENT INWARD RECTIFICATION AND SUBTHRESHOLD OSCILLATIONS

As described in the accompanying paper (Alonso and Klink 1992), both stellate cells (SCs) and non-stellate cells (non-SCs) from medial entorhinal cortex (MEC) layer II display a non-linear voltage-current (V/I) relationship that exhibits inward rectification in both the hyperpolarizing and subthreshold depolarizing direction. Thus, in both groups of neurons, the apparent input resistance (Ri), which was estimated from the peak voltage response to the injection of small hyperpolarizing current pulses, was found to decrease or increase when the resting membrane potential was shifted with constant current injection in the hyperpolarizing or depolarizing direction, respectively (Fig. 1A1 and B1).

(Fig. 1 near here)

It has been shown in other cortical (Connors et al. 1982; Spain et al. 1987; Stafstrom et al. 1982) or subcortical neurons (Llinás and Alonso 1992) that an Ri increase in the subthreshold range may be due to the presence of a persistent low-threshold Na^+ conductance (g_{NaP}), similar to that found in cerebellar Purkinje cells (Llinás and Sugimori 1980), and blocked by TTX. In order to investigate the contribution of g_{NaP} to inward rectification in SCs and non-SCs, we constructed Ri versus voltage (Ri-V) plots before and after application of TTX (1μm) (Fig. 1A2 and B2). In both SCs and non-SCs, inward rectification in the depolarizing direction was totally and selectively abolished by TTX. As a consequence, depolarizing inward rectification that at first glance might be viewed as a conductance decrease (apparent membrane resistance increase), appears in fact to reflect the regenerative nature of an inward Na^+ current.

Analysis of the steady-state Ri-V relationship in TTX made it possible to further differentiate the electroresponsiveness of SCs versus non-SCs (Alonso and Klink 1992). While at potentials between -60 and -50 mV Ri progressively decreased in the SCs (thus depolarizing inward rectification in normal Ringer reversed to outward rectification in

TTX; see below), this was never the case in the non-SCs (Fig. 1A2 and B2). A linear fit to the Ri-V plot in TTX between -60 and -50 mV gave a negative slope of -0.57 ± 0.16 MΩ/mV (mean ± SD, n=6) for the SCs, significantly different (two-tailed Student-t-test; $P<0.001$) from the non-SCs positive slope of 0.71 ± 0.15 MΩ/mV (n=6).

As presented in the accompanying paper (Alonso and Klink 1992), perhaps the most striking electrophysiological characteristic of the SCs is their ability to generate a self-sustained rhythmic oscillatory activity that develops below firing threshold for the fast Na^+ spike. Non-SCs also display subthreshold oscillations of the membrane potential, but these are of lower frequency and non-rhythmic. Blockage of voltage-dependent Na^+ conductances with TTX (1μm) completely abolished the subthreshold oscillations in both populations of neurons (n=50; Fig. 1C), as did replacing the extracellular Na^+ by choline (n=2) or the intracellular injection of the lidocaine derivative QX314 (n=10) (Connors and Prince 1982; Stafstrom et al. 1985) (not shown).

Effects of Ca^{2+}-channel block on subthreshold oscillations and spike afterpotentials

(Fig. 2 near here)

That activation of a Na^+ conductance (not Ca^{2+}) is necessary for rhythmic subthreshold membrane potential oscillations in the SCs is shown for a typical neuron in Fig. 2. Panel A illustrates the characteristic subthreshold oscillatory activity and spike "clustering" phenomenon (Alonso and Klink 1992) that were elicited by membrane depolarization to about -54 mV. Note in B that during Ca^{2+}-conductance block, after 14 min superfusion with 2mM Co^{2+}-100μM Cd^{2+} in a low-Ca^{2+} medium, prominent rhythmic subthreshold oscillations and some spike "clustering" still persisted. The upper insets in Fig. 2A and B demonstrate that synaptic transmission was actually blocked within 7 min after switching to the modified solution. Panel C further illustrates that Ca^{2+}-conductance block was also accompanied by a broadening of the base of the spike and the

coincident abolition of the fast component of the afterhyperpolarization. No change was observed, however, in the initial repolarizing phase of the action potential (Fig. 2C, inset). In all SCs tested, rhythmic subthreshold oscillations persisted during superfusion with Cd^{2+} (100-200μM) and/or Co^{2+} (1mM) in a low-Ca^{2+} (0-0.6mM) medium (n=12) as well as with a Ca^{2+}-free medium with 0.5mM EGTA (n=2). The cells were maintained in such modified solutions for periods that ranged from 8 to 40 min. As in the cell shown in Fig. 2, the frequency of the subthreshold oscillations after Ca^{2+}-conductance block always decreased by 15-40%. It was also a consistent observation that after Ca^{2+} -conductance block rhythmic subthreshold oscillatory activity always emerged accompanied by low-frequency spiking. In addition, though the spike "clustering" phenomenon could still be observed (Fig. 2B), the cells were much more easily driven by d.c. depolarization into tonic firing than in normal Ringer. In some cells (n=2), the spike broadening and concomitant depolarizing afterpotential could cause firing in duplets. Ca^{2+}-independent subthreshold oscillations and spiking were always abolished (n=4) with TTX (1μM) and were thus dependent on the activation of voltage-gated Na^{+} conductances.

(Fig. 3 near here)

The effects of Ca^{2+}-conductance block with Cd^{2+}- and/or Co^{2+}-containing solutions on the rather irregular subthreshold oscillatory activity and spike afterpotentials of the non-SCs were also investigated (n=8) (Fig. 3). These experiments facilitated another clear-cut distinction between SCs and non-SCs. In Fig. 3A, a non-SC was held at about -52 mV where some low-threshold membrane potential oscillations (rather apparent for this type of EC layer II neuron) and spiking were generated. Following 10 min superfusion with 200μM Cd^{2+} in a Ca^{2+}-free solution the irregular subthreshold oscillations were largely, though not completely, abolished (Fig. 3B). However, as can be clearly noticed in Fig. 3B, the most striking and distinct effect of Ca^{2+}-conductance block on the non-SCs was the complete abolition of the spike afterhyperpolarization and coincident substitution of single spike firing with plateau depolarizations. The depolarizing

event present in Fig. 3B is illustrated in more detail at an expanded time scale in Fig. 3C. The event is initiated by rapidly inactivating action potentials that give way to low-amplitude rhythmic membrane potential oscillations riding on a slowly decaying plateau depolarization. The plateau terminates with an increase in the amplitude of the membrane potential oscillations and finally, with an abrupt repolarization followed by a slow afterhyperpolarization. In Fig. 3D, in a different neuron from Fig. 3A to C, a similar plateau potential is generated after Ca^{2+}-conductance block by current pulse injection from -60 mV. Note the protracted duration of the plateau that largely outlasts the current pulse. Note also that the plateau sustains high frequency (50Hz) rhythmic membrane potential oscillations. Similar results were observed in all non-SCs tested as in Fig. 3 (n=10). Ca^{2+}-independent plateau potentials and slow prepotentials were always abolished by TTX (1μM) (n=3). Na^{+}-dependent plateau potentials similar to those shown in Fig. 3 were also obtained in the SCs but only after reduction of K^{+} conductances with tetraethylammonium (TEA) (10-40mM) (n=3). As in other CNS neurons (French and Gage 1985; Huguenard et al. 1989; Stafstrom et al. 1985), the persistent Na^{+} current present in the SCs and non-SCs shows very little voltage dependant inactivation.

Na^{+}- AND Ca^{2+}-INDEPENDENT SUBTHRESHOLD RECTIFICATION

(Fig. 4 near here)

We reported in the accompanying paper (Alonso and Klink 1992) that EC layer II SCs display a very prominent hyperpolarization-activated time-dependent inward rectification. In addition, as advanced above (Fig. 1), subthreshold (non-transient) outward rectification also becomes manifest in the I-V relationship of SCs after Na^{+}-conductance block with TTX. That conspicuous outward rectification develops at the oscillatory voltage level in these neurons is illustrated in more detail in Fig. 4. Fig. 4A and B illustrate the voltage responses of a SC to inward/outward current pulse injection from a membrane potential of -63 mV in control Ringer (A) and after Na^{+}- and

Ca^{2+}-conductance block with TTX (0.5μM) and Co^{2+} (2mM) (B). Note that the prominent time-dependent rectifying responses typically evoked in the SCs by hyperpolarization persisted after Na^{+}-Ca^{2+}-conductance block, as did the associated sag responses at the break of the current pulses. However, the TTX-Co^{2+} solution completely abolished inward rectification in the depolarizing direction and demonstrated the presence of Na^{+}- and Ca^{2+}-independent subthreshold outward rectification. This result is better illustrated in Fig. 4C where the steady-state V/I relationships (measurement at the end of the current pulse) from Fig. 4A and B have been plotted superimposed. Note that the turn-up on the positive end of the control V/I plot (squares) has been selectively affected by the Na^{+}-Ca^{2+}-conductance block (triangles). In fact, as shown in detail in Fig. 4D (enlargement from Fig. 4C), the TTX-Co^{2+} V/I plot shows a turn-down that gradually develops at potentials positive to about -60 mV, thus demonstrating an increase in slope conductance and outward rectification in the subthreshold range of membrane potentials. The straight line in Fig. 4D represents a linear regression fit to TTX-Co^{2+} values between -60 and -70 mV. The above result was observed in all SCs tested as in Fig. 4 (n=12).

(Fig. 5 near here)

The effects of Na^{+}-Ca^{2+}-conductance block on the voltage responses to inward/outward current pulses of the non-SCs were also investigated (Fig. 5A and B) (n=6). As in the SCs, such block also selectively abolished inward rectification in the depolarizing direction (Fig. 5C and C). However, in contrast to the SCs, the steady-state V/I relationship of the non-SCs under these conditions did not display outward rectification at potentials negative to about -45 mV (Fig. 5D). Prominent outward rectification did, however, develop at more positive potentials (Fig. 5C).

Thus, the SCs which generate prominent rhythmic subthreshold oscillatory activity also display a prominent time-dependent inward rectification and a marked outward rectification (Na^{+}- and Ca^{2+}-conductance-independent) that strongly develops at the

oscillatory voltage level. On the other hand, non-SCs, with rather fragile and irregular subthreshold oscillations, display a much less prominent time-dependent inward rectification than the SCs (Fig. 5) (Alonso and Klink 1992) and no (non-transient) outward rectification in the subthreshold range of membrane potentials after Na^+-Ca^{2+}-conductance block.

EFFECTS OF Cs^+ AND Ba^{2+} ON STELLATE-CELL SUBTHRESHOLD RECTIFICATION AND OSCILLATIONS

In many electroresponsive cells, time-dependent inward rectification is generated by a cationic conductance to both Na^+ and K^+ that is blocked by extracellular Cs^+ and not affected by Ba^{2+} (DiFrancesco 1981, 1986; Halliwell and Adams 1982; Mayer and Westbrook 1983; McCormick and Pape 1990; Spain et al. 1987; Yanaghihara and Irisawa 1980). In the brain, a hyperpolarization-activated cationic current was first explored in hippocampal pyramids and termed I_Q (Halliwell and Adams 1982).

(Fig. 6 near here)

The effects of Cs^+ and Ba^{2+} on the V/I relationship of the SCs suggest that these neurons also have a Q-like current (Fig. 6 and 7). Fig. 6A and B illustrate the voltage responses of a SC to inward/outward current pulse injection before (A) and 10 min after addition of Cs^+ (1mM) to a TTX- (1μM) and Co^{2+}-containing perfusate (B). Cs^+ largely abolished the time-dependent sag responses to the current pulses as well as the transient resting potential overshoots that followed (Fig. 6B). As a consequence, in the presence of Cs^+ the V/I relationship demonstrated a linear membrane behavior at potentials negative to about -60 mV (Fig. 6C). On the other hand, Cs^+ had no effect on the subthreshold depolarizing outward rectification. Note in Fig. 6B that in the presence of Cs^+ the voltage responses (positive to -60 mV) to outward current pulses became clearly smaller than those evoked by equal inward current pulses. Subthreshold outward rectification after Q-like current block is more clearly illustrated in Fig. 6D (V/I enlargement from C) which

demonstrates that in the presence of Cs^+, the V/I relationship still displayed a clear turn-down at potentials positive to -60 mV.

(Fig. 7 near here)

Consistent with a Q-like current underlying time-dependent inward rectification in SCs were the results of bath application of Ba^{2+} (1mM). As illustrated in Fig. 7A and B, Ba^{2+} abolished neither the time-dependent sag responses to subthreshold current pulse injection nor the associated membrane potential overshoots at the break of the pulses. However, Ba^{2+}, in contrast to Cs^+, blocked subthreshold outward rectification (Fig. 7C to F). Note in Fig. 7C and D, that the typical turn-down at the positive end of the steady-state V/I plot in TTX-Co^{2+} (squares) reverses (turns up) after 7 min superfusion with Ba^{2+} (triangles). It is possible that such effect may have been caused by the block of an M-current which may be activated negative to -50 mV and which is sensitive to Ba^{2+} (Halliwell and Adams 1982). However, this seems unlikely since the blocking action of Ba^{2+} on outward rectification below -50 mV was also manifested on the "instantaneous" V/I relationship (Fig. 7E and F), an observation that appears inconsistent with the slow time course of an M-current. Similar results were observed in all cells tested as in Fig. 6 or in TTX-only-containing solutions (n=6). Arguing against a significant contribution of an M-current to outward rectification below -60 mV was the result of bath application of the muscarinic agonist carbachol (15-60μM) which produced no detectable effect on subthreshold outward rectification (Fig. 8A and B) (n=5). Carbachol did, however, have other multiple direct actions on the SCs' electroresponsiveness that will be reported in detail elsewhere (Alonso and Klink 1991; Klink and Alonso, in preparation).

(Fig. 8 near here)

A Q-like current active at the resting membrane potential may contribute to the generation of rhythmic membrane potential oscillations as demonstrated in thalamic neurons (McCormick and Pape 1990; Soltesz et al. 1991) and proposed for the SCs (Alonso and Llinás 1989). That a Q-like current is active at the resting membrane

potential of the SCs was indicated by the finding that extracellular Cs^+ always: a) caused a membrane hyperpolarization (1-5mV) and b) largely abolished the time-dependent hyperpolarizing sag responses observed upon subthreshold depolarizations from the resting potential as well as the associated afterpotentials (Fig. 6A and B; see also Fig. 9C). However, if a Q-like current is indeed essential for the generation of rhythmic subthreshold oscillations, Cs^+ should completely abolish the oscillations. The effects of Cs^+ in normal Ringer solution are illustrated in Fig. 9. Panels A and B illustrate the voltage responses to current pulses in normal Ringer and 10 min after changing to a 3mM Cs^+ containing solution. Cs^+ largely blocked the time-dependent sags to current pulse injection. Note, however, that in spite of the Q-like current block, a robust, transient, rebound potential followed the largest hyperpolarizing current pulse (Fig. 9B, arrow). This regenerative event was dependent upon the activation of a low-threshold Na^+ conductance since it was abolished with TTX (1μM) (Fig. 9C). Nonetheless, larger hyperpolarizations also revealed a distinct Ca^{2+}-dependent rebound event (not shown). Fig. 9F illustrates that Cs^+ also increased the spike duration (inset), blocked the fast afterhyperpolarization (arrow), and reduced the amplitude and increased the duration of the medium afterhyperpolarization. Finally, Fig. 9E illustrates that, in spite of all the above actions, subthreshold oscillatory activity persisted in the presence of Cs^+, though its rhythmic character was less pronounced. The frequency of the oscillation was also reduced from about 9 to 6 Hz. Similar results were observed in all cells tested as in Fig. 9 (n=10).

(Fig. 9 near here)

After Na^+-conductance block in SCs, the presence in the V/I relationship of sustained outward rectification that markedly develops at the oscillatory voltage level suggests that the oscillatory mechanism may, in fact, require the interplay of a g_{Nap} and an outward-rectifying K^+ conductance. Indeed, non-SCs which, like SCs, show g_{Nap} but, unlike SCs, do not display subthreshold outward rectification in TTX, are not capable of generating rhythmic subthreshold oscillatory activity (Alonso and Klink 1992). However,

after Ca^{2+}-conductance block non-SCs did generate low-amplitude Na^{+}-dependent rhythmic membrane potential oscillations at a high suprathreshold voltage (Fig. 3) where a "classical" delayed rectifier must be powerfully activated (Fig. 5).

(Fig. 10 near here)

That the mechanism underlying subthreshold outward rectification appears necessary for rhythmic subthreshold oscillations in the SCs is shown in Fig. 10. Panels A and B illustrate the subthreshold membrane potential behavior of a SC held at about -54 mV in normal Ringer solution (A) and 8 min after Ba^{2+} superfusion (B). Note that Ba^{2+}, which blocks subthreshold outward rectification (Fig. 7), completely abolished the rhythmic subthreshold oscillatory activity. Some slow prepotentials, similar to those displayed by the non-SCs in normal Ringer, could still be observed in Ba^{2+} (Fig. 10B, arrows). Fig. 10C (inset) shows that Ba^{2+} also caused the development of a pronounced shoulder on the repolarizing phase of the action potential which was, nevertheless, followed by a deep and relatively fast AHP. Similar results were observed in all cells tested as in Fig. 10 (n=7). In addition to Ba^{2+}, we also tested the effects of TEA (10-30mM), another classical delayed rectifier blocker (Castle et al. 1989). Similarly to Ba^{2+}, TEA also abolished the subthreshold oscillations and blocked subthreshold outward rectification (n=5). In addition, after Ca^{2+}-conductance block, it caused the development of Na^{+}-dependent plateau events similar to those of the non-SCs (which did not require Ca^{2+}-independent K^{+}-conductance reduction). On the other hand, rhythmic subthreshold oscillations persisted in the presence of carbachol (15-60μM), which did not block subthreshold outward rectification (Fig. 8).

DISCUSSION

In the accompanying paper two electrophysiologically and morphologically distinct classes of MEC layer II projection neurons were described using a brain slice preparation (Alonso and Klink 1992). SCs and non-SCs (mostly pyramidal-like) displayed a differential set of electroresponsive properties, the most striking distinction being the generation of rhythmic subthreshold oscillatory activity by the SCs. The present results suggest that the interplay between a low-threshold persistent Na^+ conductance and a subthreshold outward rectifying K^+ conductance is necessary and sufficient for the generation of rhythmic subthreshold oscillations by the SCs.

The analysis of the voltage-current relations of both SCs and non-SCs demonstrated a pronounced inward rectification in the depolarizing direction that, in both cell types, was found to be dependent on the activation of a subthreshold non-inactivating Na^+ conductance. A TTX-sensitive persistent Na^+ current has previously been described in many other mammalian brain neurons and plays a role as a pacemaker element in sustaining a repetitive tonic discharge (Llinás and Alonso 1992; Stafstrom et al. 1984). Such seems to be an important function for g_{Nap} in the non-SCs, which readily develop rhythmic firing upon small depolarizations from the resting potential (Alonso and Klink 1992). However, in the SCs, other currents, notably a subthreshold outward rectifier, come into play to restrict the maintenance of tonic firing by g_{NaP}. These currents determine the generation of g_{Nap}-driven low-amplitude subthreshold oscillations.

Our experiments in low-Ca^{2+}-, Cd^{2+}- and/or Co^{2+}-containing solutions demonstrate that the persistent rhythmic subthreshold oscillations of the SCs are independent of the activation of Ca^{2+} conductances. Also, the typical "spike-clustering" phenomenon of these neurons was not abolished, though it was significantly diminished by Ca^{2+}-conductance block. These observations are in sharp contrast to those in many other neurons of the brain where subthreshold oscillations rely on the activation of low-threshold

voltage-gated Ca^{2+}-conductances and, most frequently, the Ca^{2+}-dependent K^+ conductance that usually follows (Alonso and Llinás 1992; Avanzini et al. 1989; Llinás and Yarom 1981; Wong and Prince 1981). The frequency decrease that Ca^{2+}-conductance block had on the SCs subthreshold oscillations may have been caused by a differential effect of divalent cations on the gating properties of the Na^+-channel involved in the oscillations (Armstrong and Cota 1990; Hille 1992). Na^+-dependent, Ca^{2+}-independent subthreshold oscillations which are rather irregular and resemble those of SCs and non-SCs have also been described in hippocampal pyramidal cells (MacVicar 1985), where they have also been referred to as slow prepotentials (Lanthorn et al. 1984; MacVicar 1985). SCs also displayed similar slow prepotentials following abolition of the persistent rhythmic subthreshold oscillations by Ba^{2+} or TEA . In principle, the presence of a slowly inactivating component in g_{NaP} (Alonso and Llinás 1989; Huguenard et al. 1988) may explain these events.

A second characteristic of the SC V/I relationship is the presence of a very robust time-dependent inward rectification that becomes evident in the voltage recordings as large depolarizing sags back toward rest during hyperpolarizing current pulses (Alonso and Klink 1992). Such a phenomenon has been described in many other electroresponsive cells and shown to be generated by a mixed cationic current carried by both Na^+ and K^+ (Angstadt and Calabrese 1989; Bader and Bertrand 1984; Bobker and Williams 1989; DiFrancesco 1981, 1986; Halliwell and Adams 1982; Kamondi and Reiner 1991; Mayer and Westbrook 1983; McCormick and Pape 1990; Spain et al. 1987; Yanaghihara and Irisawa 1980). This current (variable referred to as I_Q, I_H, I_f and I_{AR}) activates slowly with hyperpolarization and also deactivates slowly. Several of its properties including threshold, time course and reversal potential, appear to differ between different cell types, however. As in all those cells exhibiting a Q-like current, we found in the SCs that time-dependent inward rectification persisted during Na^+- and Ca^{2+}-conductance block, was not affected by Ba^{2+} and could be blocked by Cs^+.

It has previously been proposed that the deactivation/activation of a Q-like current may, in conjunction with g_{Nap}, be fundamental to the generation of rhythmic subthreshold oscillatory activity by the SCs (Alonso and Llinás 1989). Consistent with a Q-like current contribution to the development of rhythmic subthreshold oscillations was the finding that Cs^+ substantially reduced the frequency of the oscillations and also decreased their rhythmicity. However, persistent rhythmic subthreshold oscillatory activity continued in the presence of Cs^+, thus indicating that a Q-like current is not essential for the generation of rhythmic subthreshold oscillations by the SCs.

Another salient non-linear membrane property in the subthreshold range of membrane potentials was evident in the SCs, but not in the non-SCs, after Na^+-conductance block. The study of the V/I relationship in this condition revealed a pronounced, fast, sustained outward rectification that strongly developed at the oscillatory voltage level (about -55mV). This rectification was not Ca^{2+}-dependent, was not affected by Cs^+ (2mM) and carbachol (15-60μM), but was blocked by Ba^{2+} (1mM). The above results suggest that subthreshold outward rectification may be generated in the SCs by a "low-threshold" type of delayed rectifier (Dubois 1983) sensitive to Ba^{2+} like the slow M-current (Constanti et al. 1981; Halliwell and Adams 1982) but of faster activation than the M-current. Given the extraordinary diversity and ubiquity of K^+ channels recently reviewed by Rudy (1988) and Adams and Nonner (1989), it seems reasonable to hypothesize that SCs express a specific subtype of K^+ current that is optimal for the individual cell's activity profile and which may or may not be expressed in other brain neurons. In this respect, a transient, rapidly activating but very slowly inactivating K^+ current has recently been described by Spain et al (1991a) in large neocortical pyramidal cells and proposed to result from the opening of two channel types, an inactivating type and a non-inactivating type (Spain et al. 1991b). Interestingly these pyramidal cells, also possess a prominent g_{Nap} (Stafstrom et al. 1985) and in Fig. 1D of Spain et al (1991a) clear rhythmic low-amplitude membrane potential oscillations can be seen during the slow

rise of the membrane potential toward threshold which is caused by the prominent activation of the transient outward current. The same phenomenon occurs in tuberomammillary neurons (Fig. 1; Llinás and Alonso 1992) which also possess prominent g_{Nap} and slowly inactivating outward current (Kamondi and Reiner 1991; Llinás and Alonso 1992). We propose that an important function for the conductance underlying subthreshold outward rectification in the SCs is that of generating, in reciprocity with g_{Nap}, rhythmic subthreshold oscillations. Indeed, those agents (Ba^{2+}, TEA) that blocked subthreshold outward rectification also abolished the oscillations. The development of sustained, low-amplitude, membrane potential oscillations may depend on a fine-tuning of specific biophysical properties of I_{Nap} and outward rectifying K^+ current compounded by the electrotonic characteristics of the cells.

A recent whole-cell patch-clamp study of acutely dissociated cells from superficial layers of the EC has provided evidence for prominent sustained outward K^+ currents in neurons potentially identified as stellate cells (Eder et al. 1991). It is difficult to comparatively discuss this report, however, since a time-dependent inward rectifier (typical of the SCs) was not present in the dissociated cells investigated, nor was mention made of a persistent Na^+ current.

The present results have also allowed an insight into the mechanisms responsible for action potential repolarization in MEC layer II neurons and permitted a further clear-cut distinction between SCs and non-SCs on this basis. In the SCs, a delayed rectifier, rather than a Ca^{2+}-dependent K^+ conductance, dominated the initial (1/3 to 1/2) repolarizing phase of the action potential. Nonetheless, Ca^{2+} entry during the spike's falling phase (Llinás et al. 1981) could activate a fast Ca^{2+}-dependent K^+ conductance since Ca^{2+}-conductance block caused a broadening of the base of the spike and abolished the fast-AHP (Lancaster and Nicoll 1987; Spain et al. 1991a; Storm 1987). On the other hand, in the non-SCs Ca^{2+}-conductance block abolished single spiking leading to the development of long-lasting g_{Nap}-dependent plateau potentials at a high suprathreshold

voltage level. Thus, in the non-SCs action potential repolarization seems entirely dependent on the activation of a fast Ca^{2+}-dependent K^+ conductance. Indeed, in comparison to other cells in the CNS (Llinás and Alonso, 1992; Bourque et al. 1985; Dekin and Getting 1987; Spain et al. 1991a; Storm 1987; Yarom et al. 1985) non-SCs appear to be the most dependent on Ca^{2+} influx for spike repolarization. Na^+-dependent plateau potentials, similar to those observed in the non-SCs after Ca^{2+}-conductance block, have also been reported in other cortical (Stafstrom et al. 1985) or subcortical neurons (Llinás and Alonso 1992) possessing g_{Nap}. However, in these cells, as well as in the EC SCs, the generation of high-voltage Na^+ plateau required reduction of voltage-gated K^+ conductances with TEA.

With regard to the SCs' fast AHP, the results also demonstrate that extracellular Cs^+ abolished the fast AHP suggesting a Cs^+ block of the Ca^{2+}-dependent K conductance underlying the fast AHP. On the other hand, Ba^{2+} caused the development of a pronounced shoulder on the falling phase of the SCs' spike. This shoulder was probably due to the conjoint action of several factors including a better permeation of Ba^{2+} through the Ca^{2+} channels opened by the spike depolarization, the inability of Ba^{2+} to activate Ca^{2+}-dependent conductances and the Ba^{2+} block of outward rectifying K^+ currents (at least the subthreshold outward rectifier). Nevertheless, the Ba^{2+} shoulder was followed by a deep and fast AHP which may have been primarily produced by the same Ca^{2+}-dependent conductance that produced the fast AHP in normal Ringer.

FUNCTIONAL IMPLICATIONS

The results have provided further evidence that the differences in the electroresponsive behavior between SCs and non-SCs rely to a large extent on a differential set of ionic conductances in each of the two neuronal types. Modulation of such conductances by neurotransmitters as a function of behavioral state may additionally differentiate the processing capabilities of the two groups of neurons that we hypothesize

constitute two parallel channels of information for the hippocampal formation (Alonso and Klink 1992). Indeed, preliminary results suggest that under cholinergic modulation by basal forebrain inputs (Alonso and Köhler 1984) the differences in the firing behavior between SCs and non-SCs may be enhanced (Alonso and Klink 1991).

The study of EC electrophysiology is a subject of great interest because of the role of this structure in temporal lobe epilepsy (Alonso et al. 1990; Jones and Heinemann 1988; Jones and Lambert 1990; Paré et al. 1992). The fact that action potential repolarization in the non-SCs appears to rely entirely on the activation of a Ca^{2+}-dependent K^+ current (and not a delayed rectifier), and taking into account that this type of current is a frequent target for neuromodulation (Rudy 1988), suggests that the non-SCs may be primed for bursting epileptogenic behavior (facilitated by g_{NaP}). On the other hand, prominent outward currents appear to set a rigid control upon the SCs' electroresponsiveness to avoid hyperexcitability. In this respect, a robust delayed K^+ current appears to counteract the persistent Na^+ current and prominent slow outward currents generate large amplitude and long-lasting hyperpolarizations after high-frequency spike trains in the SCs but not in the non-SCs (Alonso and Klink 1992). Since the SCs are the most abundant cell group in layer II, they integrate a large convergence of excitatory inputs from multiple cortical and subcortical structures that are directed towards the hippocampus (see Lopes da Silva et al. 1990 and Witter et al. 1989 for review) and play a critical role in both Hebbian and non-Hebbian enhancement of synaptic strength (Alonso et al. 1990), it is not surprising that a rigid control is imposed upon their electroresponsiviness in order to prevent an excessive tendency towards epileptogenesis in such a nodal point of the temporal lobe.

We have discussed in the accompanying paper the functional implications of intrinsic voltage oscillations in the SCs and their possible contribution to the generation of limbic theta rhythm. Interestingly, multiple subsets of neurons that occupy key anatomical positions in the limbic network display a striking pacemaker autorhythmicity. This is the case for the EC SCs, for medial mammillary body neurons (Alonso and Llinás 1992) and

for basal forebrain cholinergic (Khateb et al. 1992) and non-cholinergic (Mühlethaler et al. 1992) cells. However, the biophysical mechanisms underlying such rhythmicities are different in each of the neuronal populations. Obviously, each group of neurons possesses a particular biophysical identity, largely determined by a differential expression of ionic conductances, to comply with the functions of the local network. On the other hand, however, such identity is remarkably well "molded" to allow for the development of an overall limbic rhythmicity that requires the synaptic interaction of multiple, otherwise independent, oscillators.

ACKNOWLEDGMENTS

We would like to thank Dr. R. Llinás for many helpful suggestions and support, and Drs. B. Jones, A. Kay and Ch. Bourque for comments on the manuscript. This work was supported by the Canadian Medical Research Council.

REFERENCES

Adams, D.J. and Nonner, W. Voltage-dependent potassium channels: gating, ion permeation and block (Ch.2). In: *Potassium channels: structure, classification, function and therapeutic potential,* Chichester, U.K.: Ellis Horwood Ltd., 1989, p. 42-69.

Alonso, A., de Curtis, M. and Llinas, R. Postsynaptic Hebbian and non-Hebbian long-term potentiation of synaptic efficacy in the entorhinal cortex in slices and in the isolated adult guinea pig brain. *Proc. Natl. Acad. Sci. USA* 87: 9280-9284, 1990.

Alonso, A. and Klink, R. Cholinergic modulation of entorhinal cortex layer II neurons' intrinsic excitability. *Soc. Neurosci. Abstr.* 17: 535.10, 1991.

Alonso, A. and Klink, R. Differential electroresponsiveness of stellate and pyramical-like cells of medial entorhinal cortex layer II. *(submitted)* 1992.

Alonso, A. and Köhler, C. A study of the reciprocal connections between the septum and the entorhinal area using anterograde and retrograde axonal transport methods in the rat brain. *J. Comp. Neurol.* 225: 327-343, 1984.

Alonso, A. and Llinás, R.. Subthreshold Na^+-dependent theta-like rhythmicity in stellate cells of entorhinal cortex layer II. *Nature* 342: 175-177, 1989.

Alonso, A. and Llinás, R. Electrophysiology of the mammillary complex in vitro. II. Medial mammillary neurons. *J. Neurophysiol.* 64: 1992.

Angstadt, J.D. and Calabrese, R.L. A Hyperpolarization-activated inward current in heart interneurons of the medical leech. *J. Neurosci.* 9: 2846-2857, 1989.

Armstrong C.M and Cota, G. Modification of sodium channel gating by lanthanum. Some effects that can not be explained by surface charge theory. *J. Gen Physiol.* 96: 1129-1140, 1990.

Avanzini, G., de Curtis, M., Panzica, F. and Sprefacio, R. Intrinsic properties of nucleus reticularis thalami neurones of the rat studied *in vitro*. *J. Physiol. (Lond.)* 416: 111-122, 1989.

Bader, C.R. and Bertrand, D. Effects of changes in intra- and extracellular sodium on the inward (anomalous) rectification in salamander photoreceptors. *J. Physiol. (Lond.)* 347: 611-631, 1984.

Bobker, D.H. and Williams, J.T. Serotonin augments the cationic current IH in central neurons. *Neuron* 2: 1535-1540, 1989.

Bourque, Ch.W., Randle, J.C.R and Renaud, L.P. Calcium-dependent potassium conductance in rat supraoptic nucleus neurosecretory neurons. *J. Neurophysiol.* 54: 1375-1382.

Castle, N.A., Haylett, D.G. and Jenkinso, D.H. Toxins in the characterization of potassium channels. *Trends Neurosci.* 12: 59-65, 1989.

Connors, B.W. and Gutnick, M.J. Intrinsic firing patterns of diverse neocortical neurons. *Trends Neurosci.* 13: 99-104, 1990.

Connors, B.W., Gutnick, M.J. and Prince, D.A. Electrophysiological properties of neocortical neurons *in vitro*. *J. Neurophysiol.* 48: 1302-1320, 1982

Connors, B.W. and Prince, D.A. Effects of local anesthetic QX-314 on the membrane properties of hippocampal pyramidal neurons. *J. Pharmachol. Exp. Ther.* 220: 476-481, 1982.

Constanti, A., Adams, P.R. and Brown, D.A. Why do barium ions imitate acetylcholine? *Brain Res.* 206: 244-250, 1981.

Dekin, M.S. and Getting, P.A. In vitro characterization of neurons in the ventral part of the nucleus tractus solitarius. II. Ionic basis for repetitive firing patterns. *J. Neurophysiol.* 58: 215-229.

DiFrancesco, D. A study of the ionic nature of the pace-making current in calf Purkinje fibers. *J. Physiol. (Lond.)* 314: 377-393, 1981.

DiFrancesco, D.A., Ferroni, A., Mazzanti, M. and Tromba, C. Properties of the hyperpolariizing-activated current (i_f) in cells isolated from the rabbit sino-atrial node. *J. Physiol. (Lond.)* 377: 61-88, 1986.

Dubois, J.M. Potassium currents in the frog node of Ranvier. *Prog. Biophys. molec. Biol.* 42: 1-20, 1983.

Eder, C., Ficker, E., Gündel, J. and Heinemann, U. Outward currents in rat entorhinal cortex stellate cells studied with conventional and perforated patch recordings. *Eur. J. Neurosci.* 3: 1271-1280, 1991.

French, C.R. and Gage, P.W. A threshold sodium current in pyramidal cells in rat hippocampus. *Neurosci. Lett.* 56: 289-293, 1985.

Halliwell, J.V. and Adams, P.R. Voltage-clamp analysis of muscarinic excitation in hippocampal neurons. *Brain Res.* 250: 71-92, 1982.

Hille, B. Ionic channels of excitable membranes. Sinauer Associates, Sunderland, MA. 607 pp. 1992.

Huguenard, J.R., Hamill, O.P. and Prince, D.A. Developmental changes in Na conductances in rat neocortical neurons: appearence of a slowly inactivating component. *J. Neurophysiol.* 59: 778-795, 1988.

Huguenard, J.R., Hamill, O.P. and Prince, D.A. Sodium channels in dendrites of rat cortical pyramidal neurons. *Proc. natl. Acad. Sci. U.S.A.* 86: 2473-2477, 1989.

Jones, R.S.G. and Heinemann, V. Synaptic and intrinsic responses of medial entorhinal cortical cells in normal and magnesium-free medium "in vitro". *J. Neurophysiol.* 59: 1476-1496, 1988.

Jones, R.S.G. and Lambert, J.D.C. Synchronous discharges in the rat entorhinal cortex *in vitro*: site of initiation and the role of excitatory amino acid receptors. *Neuroscience* 34: 657-670, 1990.

Kamondi, A. and Reiner, P.B. Hyperpolarization-activated inward current in histaminergic tuberomammillary neurons of the rat hypothalamus. *J. Neurophysiol.* 66: 1902-1911, 1991.

Khateb, A., Muhlethaler, M., Alonso, A., Serafin, M., Mainville, L. and Jones, B.E. Cholinergic nucleus basalis neurons display the capacity for rhythmic bursting activity mediated by low threshold calcium spikes. *Neuroscience* (in press) 1992.

Lancaster, B. and Nicoll, R.A. Properties of two calcium-activated hyperpolarizations in rat hippocampal neurones. *J. Physiol. (Lond.)* 389: 187-204, 1987.

Lanthorn, T., Storm, J. and Andersen, P. Current-to-frequency transduction in CA1 hippocampal pyramidal cells: slow prepotentials dominate the primary range firing. *Exp. Brain Res.* 53: 431-443, 1984.

Llinás, R.. The Intrinsic electrophysiological properties of mammalian neurons: Insights into central nervous system function. *Science* 242: 1654-1664, 1988.

Llinás, R.. and Alonso, A. Electrophysiology of the mammillary complex in vitro. I. Tuberomammillary and lateral mammillary neurons. *J. Neurophysiol.* 68: 1992.

Llinás, R., Steimberg, I.Z. and Walton, K. Relationship between presynaptic calcium current and postsynaptic potential in squid giant synapse. *Biophys. J.* 33: 323-352, 1981.

Llinás, R. and Sugimori, M. Electrophysiological properties of in vitro Purkinje cell somata in mammalian cerebellar slices. *J. Physiol. (Lond.)* 305: 197-213, 1980.

Llinás, R. and Yarom, Y. Properties and distribution of ionic conductances generating electroresponsiveness of mammalian inferior olivary neurones "in vitro". *J. Physiol. (Lond.)* 315: 519-584, 1981.

Lopes da Silva, F.H., Witter, M.P., Boeijinga, P.H. and Lohman, H.M. Anatomic organization and physiology of the limbic cortex. *Physiol. Rev.* 76: 453-511, 1990.

MacVicar, B.A. Depolarizing prepotentials are Na^+ dependent in CA1 pyramidal neurons. *Brain Res.* 333: 378-381, 1985.

Mayer, M.L. and Westbrook, G.L. A voltage-clamp analysis of inward (anomalous) rectification in mouse spinal sensory ganglion neurones. *J. Physiol. (Lond.)* 340: 19-45, 1983.

McCormick, D.A. and Pape, H.-C. Properties of a hyperpolarization-activated cation current and its role in rhythmic oscillation in thalamic relay neurones. *J. Physiol. (Lond.)* 431: 291-318, 1990.

Muhlethaler, M., Khateb, A., Fort, P., Jones, B.E. and Alonso, A. Forty Hz membrane potential oscillations and theta-like activity in basal forebrain neurons. *Soc. Neurosci. Abstr.* 18: 92.11, 1992.

Paré, D., de Curtis, M. and Llinás, R. Role of the hippocampal-entorhinal loop in temporal lobe epilepsy: extra- and intracellular study in the isolated guinea pig brain *in vitro*. *J. Neurosci.* 12: 1867-1881, 1992.

Rudy, B. Diversity and ubiquity of K channels. *Neuroscience* 25: 729-749, 1988.

Soltesz, I., Lightowler, S., Leresche, N., Jassik-Gerschenfeld, D., Pollard, C.E. and Crunelli, V. Two inward currents and the transformation of low-frequency oscillations of rat and cat thalamocortical cells. *J. Physiol. (Lond.)* 441: 175-197, 1991.

Spain, W.J., Schwindt, P.C. and Crill, W.E. Anomalous rectification in neurons from cat sensorimotor cortex in vitro. *J. Neurophysiol.* 57: 1555-1576, 1987.

Spain, W.J., Schwindt, P.C. and Crill, W.E. Two transient potassium currents in layer V pyramidal neurones from cat sensorimotor cortex. *J. Physiol. (Lond.)* 434: 591-607, 1991a.

Spain, W.J., Schwindt, P.C. and Crill, W.E. Post-inhibitory excitation and inhibition in layer V pyramidal neurones from cat sensorimotor cortex. *J. Physiol. (Lond.)* 434: 609-626, 1991b.

Stafstrom, C.E., Schwindt, P.C., Chubb, M.C. and Crill, W.E. Properties of persistant sodium conductance and calcium conductance of layer V neurons from cat sensorimotor cortex in vitro. *J. Neurophysiol.* 53: 153-170, 1985.

Stafstrom, C.E., Schwindt, P.C. and Crill, W.E. Negative slope conductance due to a persistent subthreshold sodium current in cat neocortical neurons *in vitro*. *Brain Res.*236: 221-226, 1982.

Stafstrom, C.E., Schwindt, P.C. and Crill, W.E. Repetitive firing in layer V neurons from cat neocortex in vitro. *J. Neurophysiol.* 52: 264-277, 1984.

Storm, J.F. Action potential repolarization and a fast-hyperpolarization in rat hippocampal pyramidal cells. *J. Physiol. (Lond.)* 385: 733-759, 1987.

Strichartz, G.R. The inhibition of sodium currents in myelinated nerve by quaternary derivatives of lidocaine. *J. Gen. Physiol.* 62: 37-57, 1973.

Witter, M.P., Groenewegen, H.J., Lopes da Silva, F.H. and Lohman, A.H.M. Functional organization of the extrinsic and intrinsic circuitry of the parahippocamapal region. *Progr. Neurobiol.* 33: 161-253, 1989.

Wong, R.K.S. and Prince, D.A. Afterpotential generation in hippocampal pyramidal cells. *J. Neurophysiol.* 45: 86-97, 1981.

Yanaghihara, K. and Irisawa, H. Inward current activated during hyperpolarization in the rabbit sino atrial node cell. *Pfügers Arch.* 385: 11-19, 1980.

Yarom, Y, Sugimori, M. and Llinás R. Ionic currents and firing patterns of mammalian vagal motoneurons *in vitro*. *Neuroscience* 16: 719-737, 1985.

Figure 1. Apparent input resistance versus voltage relationship in stellate (*A1* and *A2*) and non-stellate (*B1* and *B2*) cells. *A1* and *B1*: voltage responses to a hyperpolarizing constant current pulse (-0.15 and -0.1 nA, respectively) applied at a depolarized (top) and hyperpolarized (bottom) membrane potential level. *A2* and *B2*: from the same neurons, plot of the apparent input resistance (Ri) as a function of membrane potential in control Ringer solution (filled circles) and in the presence of 1μM TTX (open circles). Note that Na^+-conductance block abolished depolarizing inward rectification in both type of neurons and revealed subthreshold outward rectification in the stellate cell exclusively. *C1* and *C2*: block of subthreshold membrane oscillations with TTX in SCs. The subthreshold membrane oscillations in control (*C1*) are totally abolished in TTX 1 μM (*C2*). Spikes have been truncated. .

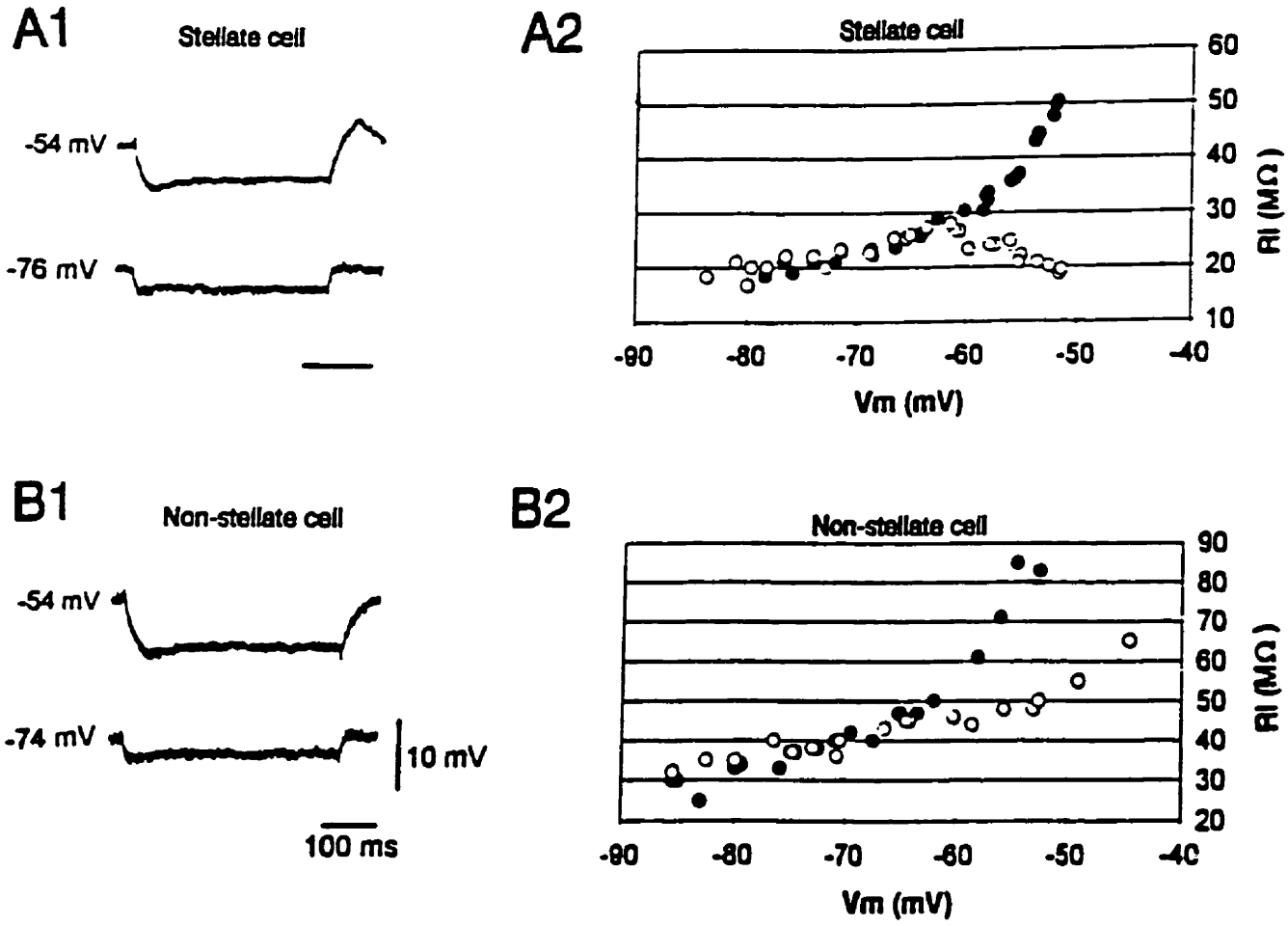
A1
Stellate cell
-54 mV
-76 mV
A2
Stellate cell
60
50
40
30
20
10
RI (MΩ)
-90
-80
-70
-60
-50
-40
Vm (mV)
B1
Non-stellate cell
-54 mV
-74 mV
10 mV
100 ms
B2
Non-stellate cell
90
80
70
60
50
40
30
20
RI (MΩ)
-90
-80
-70
-60
-50
-40
Vm (mV)
C1
Control
-53 mV
C2
TTX
-53 mV
5 mV
500 ms

Figure 2. Effects of Ca^{2+}-conductance block on the stellate cell subthreshold oscillations and spike afterpotentials. *A* and *B*: subthreshold oscillatory properties of a stellate cell held at ~ –54mV before and after Ca^{2+}-conductance block with a Co^{2+}-Cd^{2+} containing solution (14min). The top traces in A and B demonstrate synaptic transmission block by the manipulation (Vm=-68 mV). Note that subthreshold oscillations persist after Ca^{2+}-conductance block. *C*: superimposed spikes from the same neuron before and after Ca^{2+}-conductance block. Note the broadening of the spike at the base (inset) and the block of the fast component of the afterhyperpolarization.

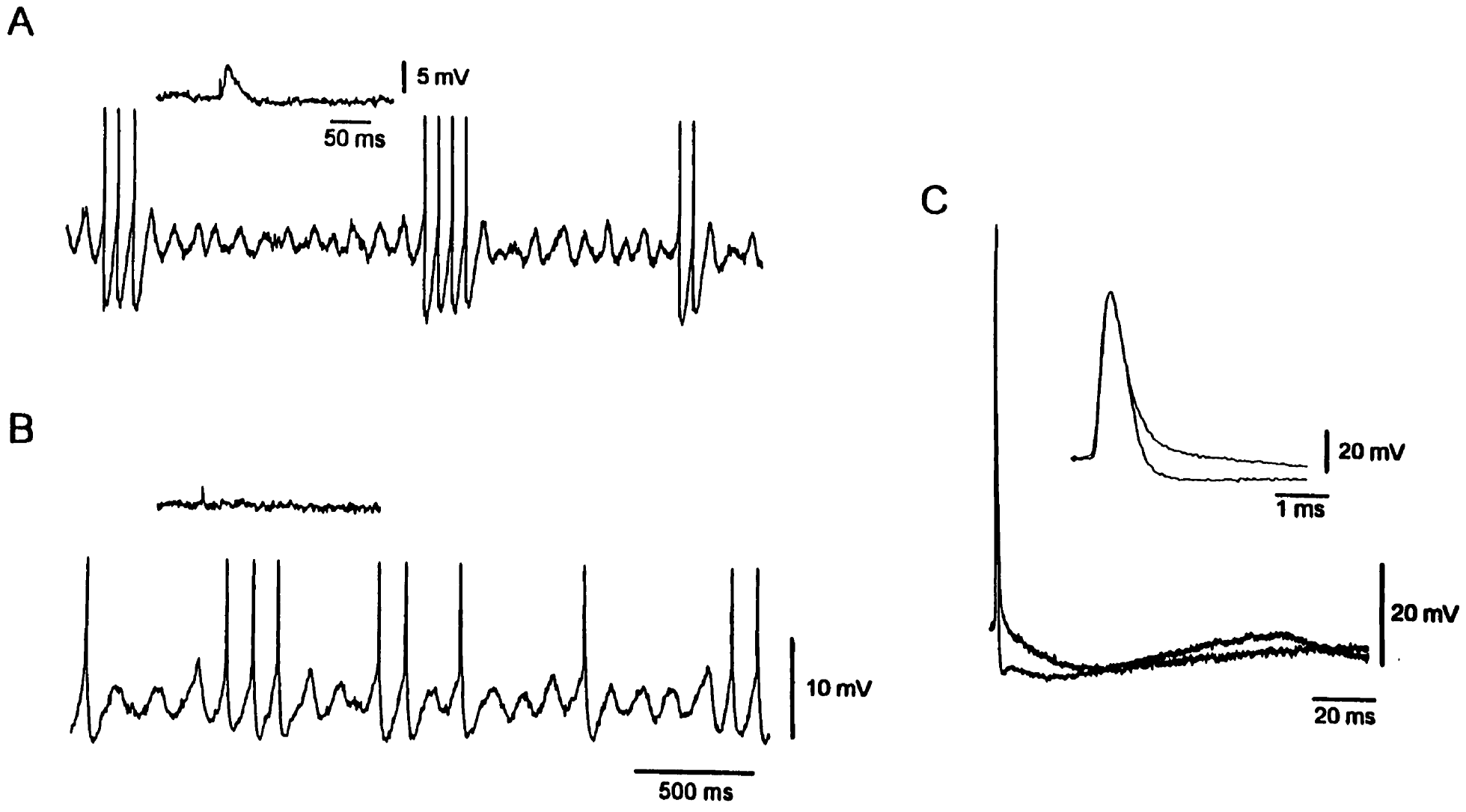
A
5 mV
50 ms
B
10 mV
500 ms
C
20 mV
1 ms
20 mV
20 ms

Figure 3. Effects of Ca^{2+}-conductance block on the non-SCs subthreshold voltage behavior and spike afterpotentials. *A* and *B:* membrane-voltage behavior of a non-stellate cell held at ~ −52 mV in control Ringer (A) and after Ca^{2+}-conductance block with a Ca^{2+}-free 200μM Cd^{2+} solution (B). Note that the irregular subthreshold oscillatory activity is largely eliminated by the Cd^{2+} solution. Spike repolarization is, however, completely abolished. *C*: plateau potential from B at an expanded time scale. *D*. in a different cell, after Ca^{2+}-conductance block a short duration depolarizing current pulse triggers a protracted plateau that outlasts the current pulse and sustains rhythmic membrane potential oscillations (as that in C).

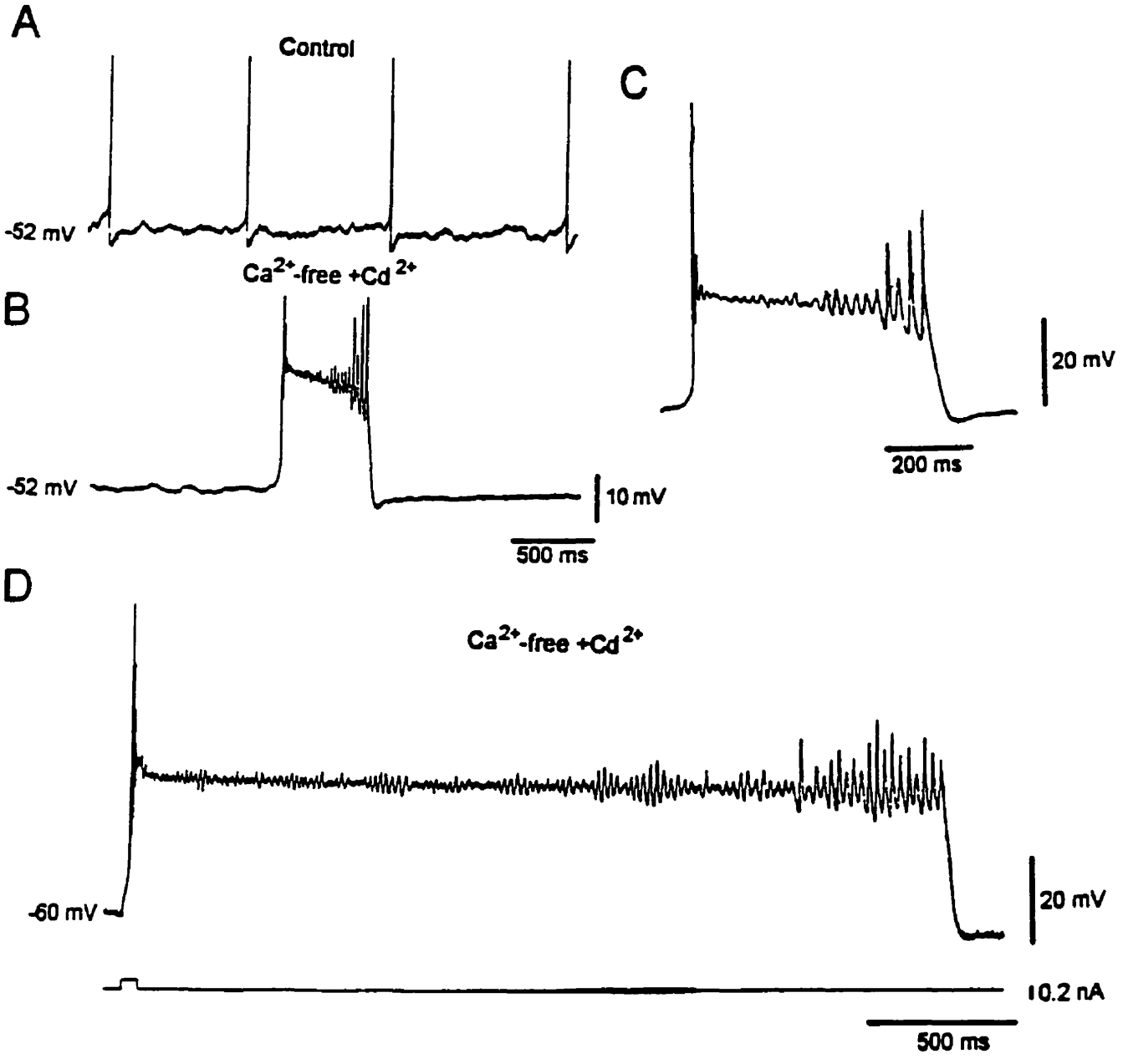
A
Control
-52 mV
B
Ca2+-free +Cd 2+
-52 mV
10 mV
500 ms
C
20 mV
200 ms
D
Ca2+-free +Cd2+
-60 mV
20 mV
10.2 nA
500 ms

Figure 4. Stellate-cell subthreshold outward rectification persisted after Ca^{2+}-conductance block. *A* and *B*: voltage responses to the injection of depolarizing and hyperolarizing current pulses in control Ringer (A) and after Na^{+}-and Ca^{2+}-conductance block with TTX (1μM) and Co^{2+} (2mM). *C*: from the same cell, plot of membrane potential (Vm) vs. amplitude of current pulse before (filled squares) and after Na^{+}-Ca^{2+}-conductance block. *D*: enlargement of boxed area in C. In this and the following figures, unless otherwise specified, voltage measurements were taken towards the end of the current pulse and the straight line represents a linear regression fit to test solution values between -60 and -70mV. Note the progressive increase in slope conductance at potentials positive to -60mV (subthreshold outward rectification) in the TTX-Co^{2+} solution.

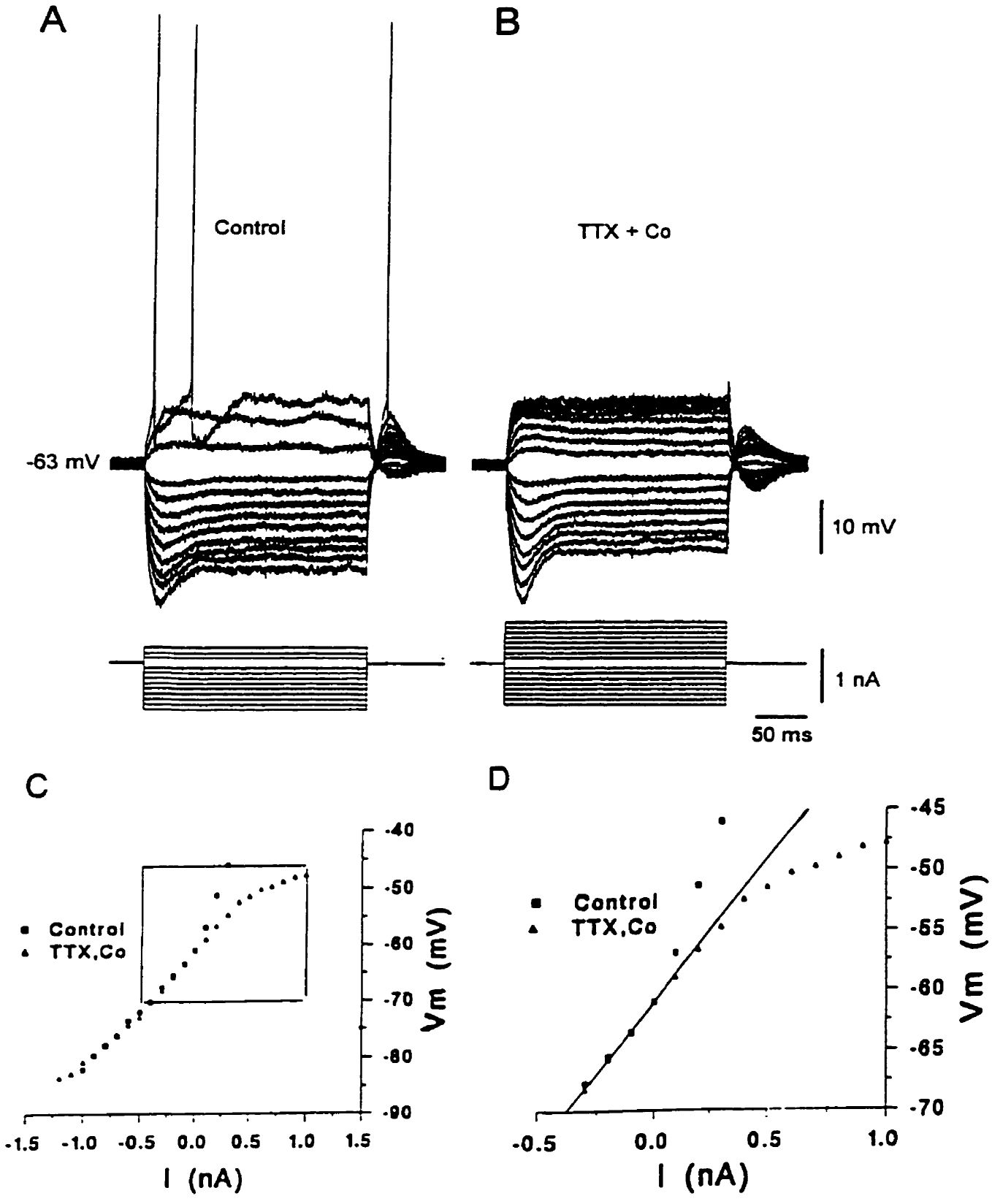
A
B
Control
TTX + Co
-63 mV
10 mV
1 nA
50 ms
C
D
Control
TTX,Co
-40
-50
-60
-70
-80
-90
Vm (mV)
-1.5
-1.0
-0.5
0.0
0.5
1.0
1.5
I (nA)
-45
-50
-55
-60
-65
-70
-0.5
0.0
0.5
1.0

Figure 5. Effect of Na^{+}-Ca^{2+}-conductance block on the non-stellate cell voltage-current relationship. *A* and *B*: voltage responses to the injection of depolarizing and hyperolarizing current pulses in control Ringer (A) and after Na^{+}-and Ca^{2+}-conductance block with TTX (1μM) and Co^{2+} (2mM). *C*: from the same cell, plot of membrane potential (Vm) vs. amplitude of current pulse before (filled squares) and after Na^{+}-Ca^{2+}-conductance block. *D*: enlargement of boxed area in C. Note that, similarly to stellate cells, Na^{+}-Ca^{2+}-conductance block abolished depolarizing inward rectification. On the other hand, as opposed to stellate cells, subthreshold outward rectification was not manifested in the voltage-current relationship after Na^{+}-Ca^{2+}-conductance block.

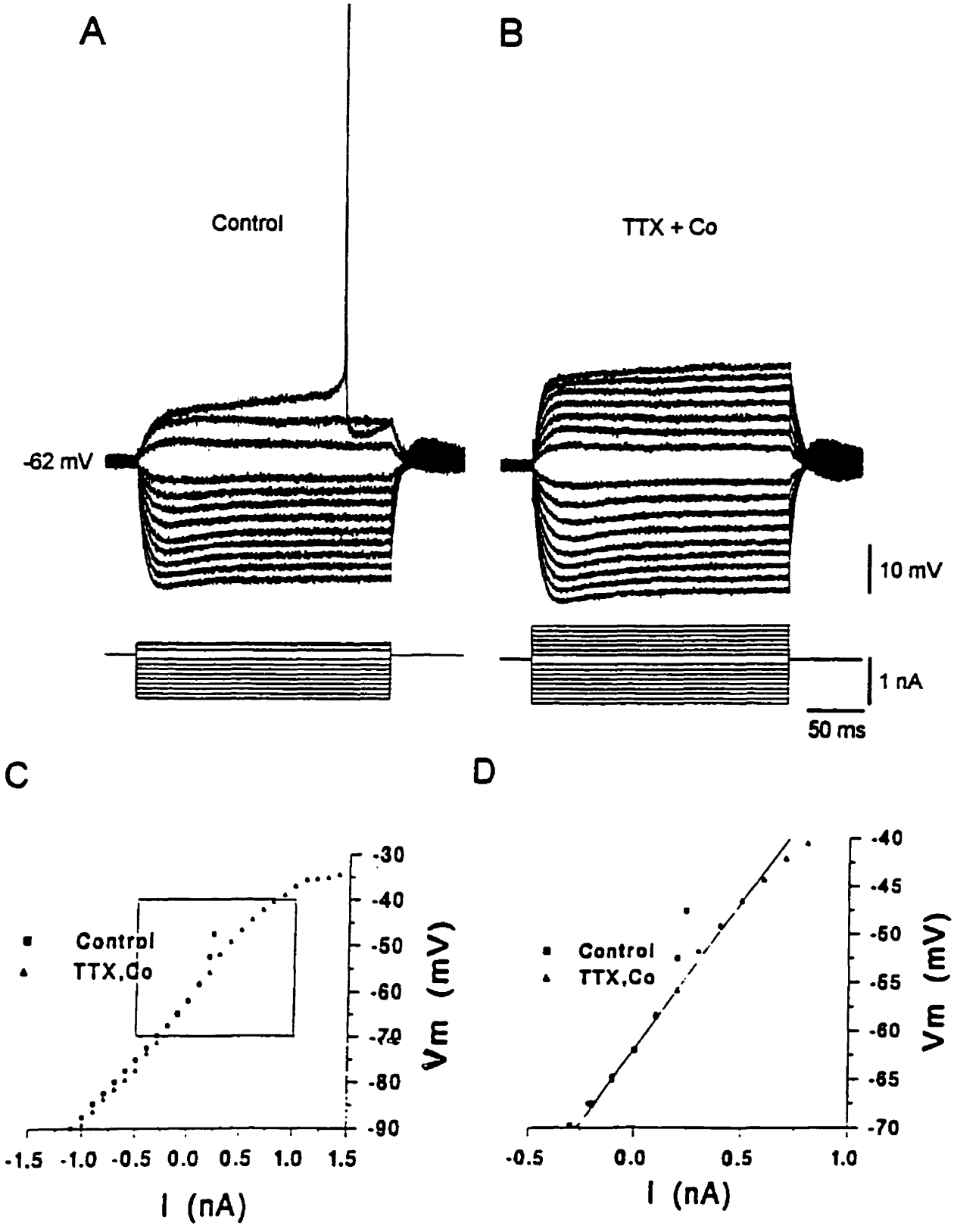
A
B
Control
TTX + Co
-62 mV
10 mV
1 nA
50 ms
C
D
Control
TTX,Co
-30
-40
-50
-60
-70
-80
-90
Vm (mV)
-1.5 -1.0 -0.5 0.0 0.5 1.0 1.5
I (nA)
-40
-45
-50
-55
-60
-65
-70
-0.5 0.0 0.5 1.0

Figure 6. Cs^+ blocks time dependent inward rectification. *A* and *B*: voltage responses to the injection of depolarizing and hyperolarizing current pulses before (A) and 10 min after the addition of Cs^+ (1mM) (B) to a TTX + Co^{2+} solution. *C*: from the same cell, plot of Vm vs. amplitude of current pulse before (filled squares) and during Cs^+ (filled triangles). *D*: enlargement of boxed area in C. Note that Cs^+ selectively abolished time-dependent inward rectification.

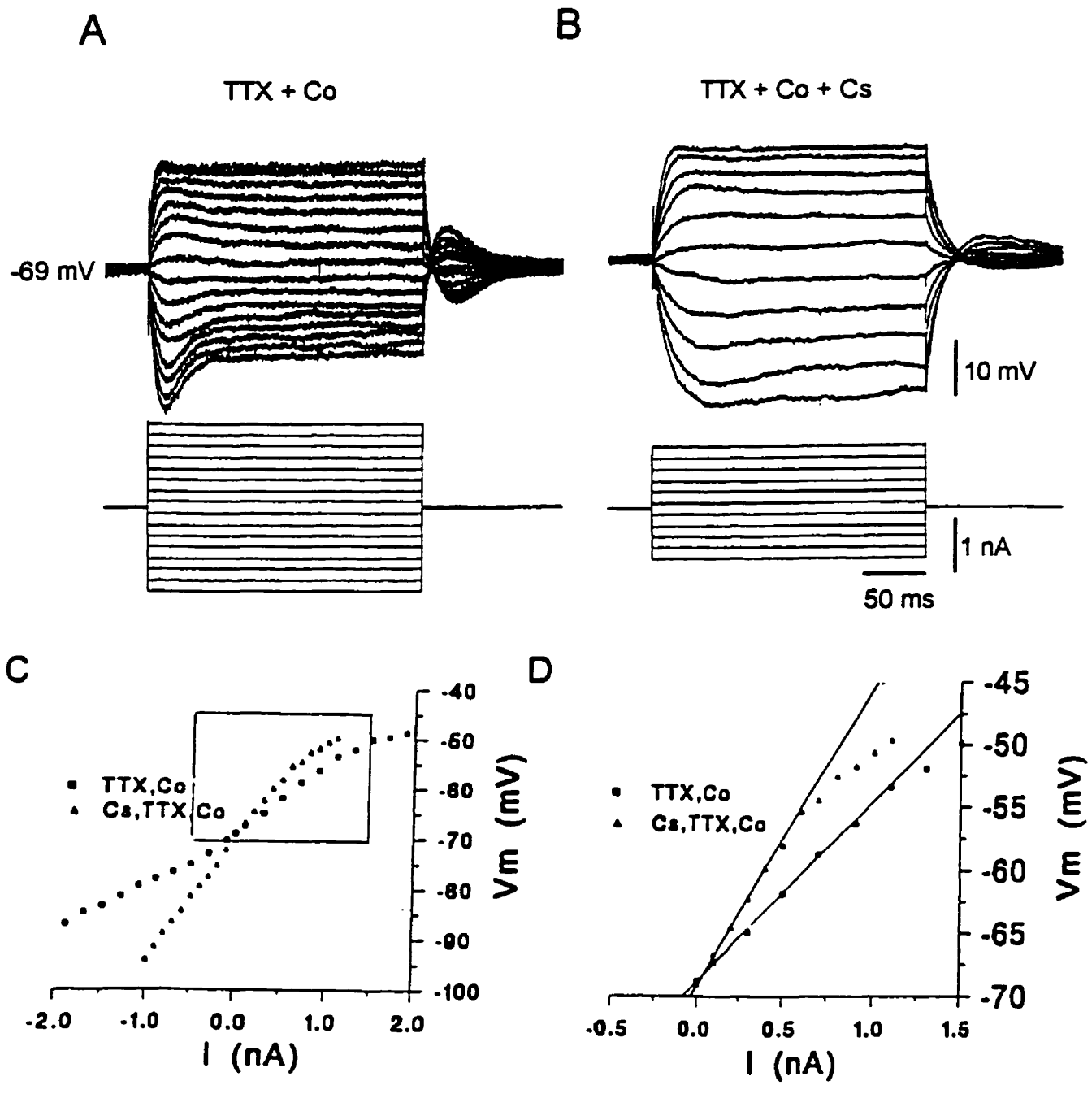
A
TTX + Co
-69 mV
B
TTX + Co + Cs
10 mV
1 nA
50 ms
C
TTX,Co
Cs,TTX,Co
-40
-50
-60
-70
-80
-90
-100
Vm (mV)
-2.0
-1.0
0.0
1.0
2.0
I (nA)
D
TTX,Co
Cs,TTX,Co
-45
-50
-55
-60
-65
-70
Vm (mV)
-0.5
0.0
0.5
1.0
1.5
I (nA)

Figure 7. Ba^{2+} blocks subthreshold outward rectification. *A* and *B*: voltage responses to the injection of depolarizing and hyperolarizing current pulses before (A) and 7 min after the addition of Ba^{2+} (1mM) (B) to a TTX + Co^{2+} solution. *C* and *E*: from the same cell, plot of steady state (C) and peak (E) Vm vs. amplitude of current pulse before (filled squares) and during Ba^{2+} (filled triangles). *D* and *F* : enlargements of boxed areas in C and D, respectively. Note that Ba^{2+} had no effect on time-dependent inward rectification but blocked the outward rectification that is manifested below -50mV in both the steady state (C and D) and peak (E and F) voltage-current relations.

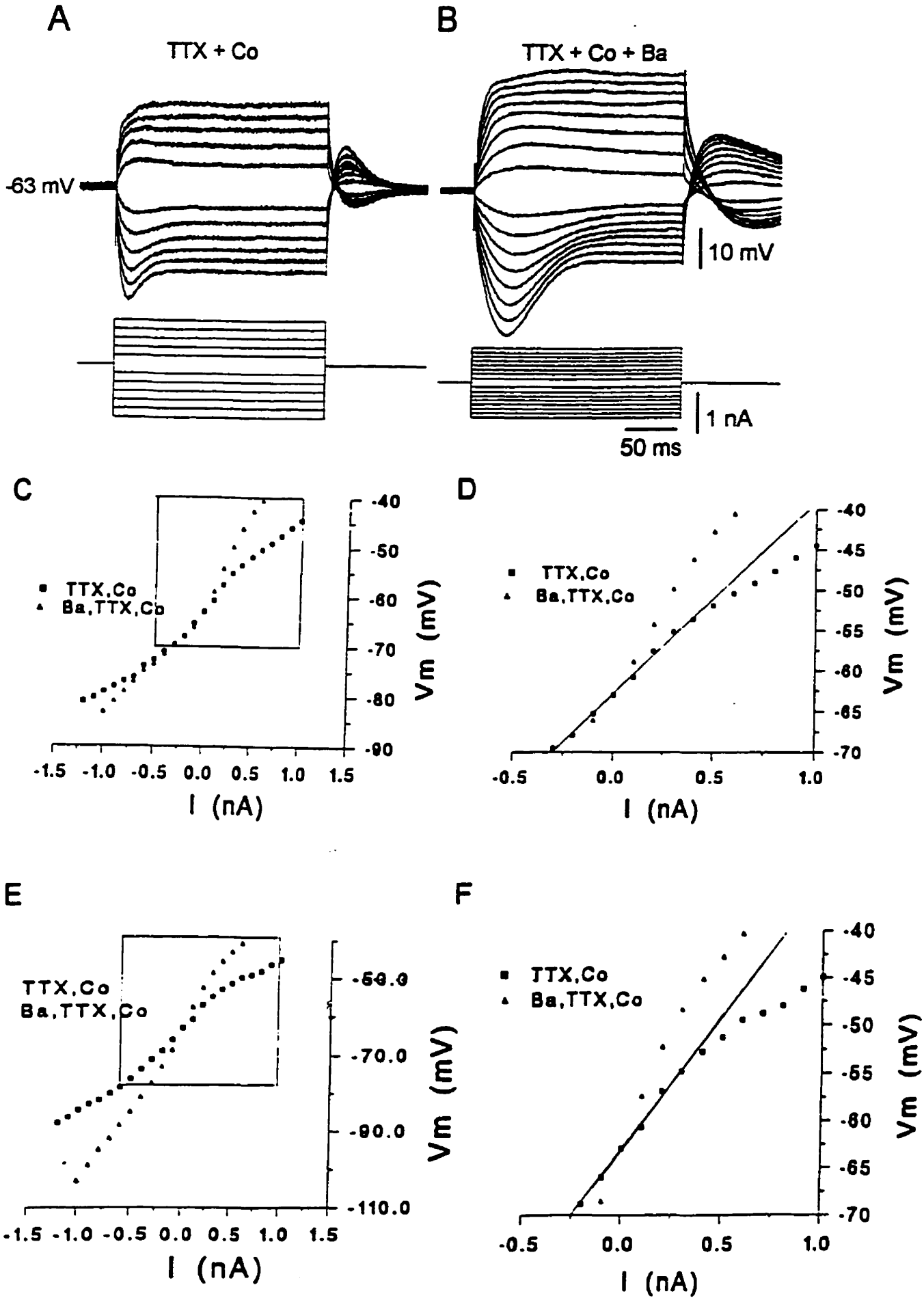
A
TTX + Co
-63 mV
B
TTX + Co + Ba
10 mV
1 nA
50 ms
C
TTX,Co
Ba,TTX,Co
-40
-50
-60
-70
-80
-90
Vm (mV)
-1.5 -1.0 -0.5 0.0 0.5 1.0 1.5
I (nA)
D
TTX,Co
Ba,TTX,Co
-40
-45
-50
-55
-60
-65
-70
Vm (mV)
-0.5 0.0 0.5 1.0
I (nA)
E
TTX,Co
Ba,TTX,Co
-50.0
-70.0
-90.0
-110.0
Vm (mV)
-1.5 -1.0 -0.5 0.0 0.5 1.0 1.5
I (nA)
F
TTX,Co
Ba,TTX,Co
-40
-45
-50
-55
-60
-65
-70
Vm (mV)
-0.5 0.0 0.5 1.0
I (nA)

Figure 8. Subthreshold outward rectification persists in the presence of carbachol (CCh). *A* and *B*: voltage responses to the injection of depolarizing and hyperolarizing current pulses before (A) and 11 min after the addition of CCh (30μM) to a TTX containing solution. *C*: from the same cell, plot of Vm vs. amplitude of current pulse before (filled squares) and during CCh (filled triangles). *D*: enlargement of boxed area in C. Note that subthreshold outward rectification was unaffected by CCh.

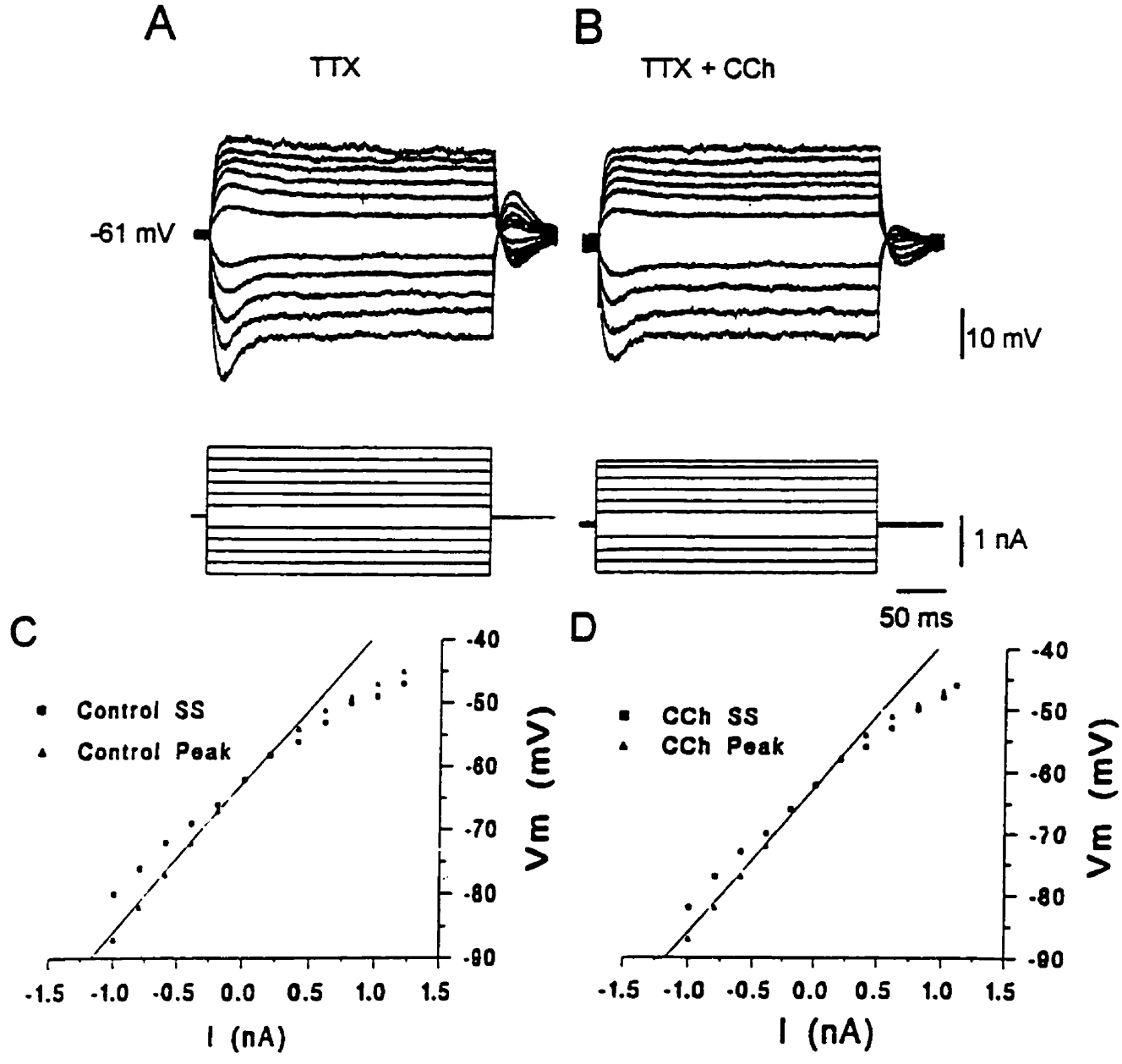
A
TTX
B
TTX + CCh
-61 mV
10 mV
1 nA
50 ms
C
Control SS
Control Peak
-40
-50
-60
-70
-80
-90
Vm (mV)
-1.5
-1.0
-0.5
0.0
0.5
1.0
1.5
I (nA)
D
CCh SS
CCh Peak
-40
-50
-60
-70
-80
-90
Vm (mV)
-1.5
-1.0
-0.5
0.0
0.5
1.0
1.5
I (nA)

Figure 9. Stellate cells rhythmic membrane potential oscillations persist after Q-like current block by Cs^+. *A*, *B* and *C*: voltage responses to the injection of depolarizing and hyperolarizing current pulses in normal Ringer (A), 10 min after changing to a 3mM Cs^+ containing solution (B) and 4 min after further addition of TTX (1μM) to block Na^+ conductances (C). Note that a very pronounced Na^+-dependent depolarizing rebound potential (B, arrow) persisted after Q-like current block by Cs^+. *D* and *E*: from the same cell, subthreshold oscillatory properties at ~ −53mV before (D) and after Q-like current block by Cs^+ (E). *F*: superimposed spikes from the same neuron before and after Q-like current block. Note the broadening of the spike (inset) and the block of the fast component of the afterhyperpolarization.

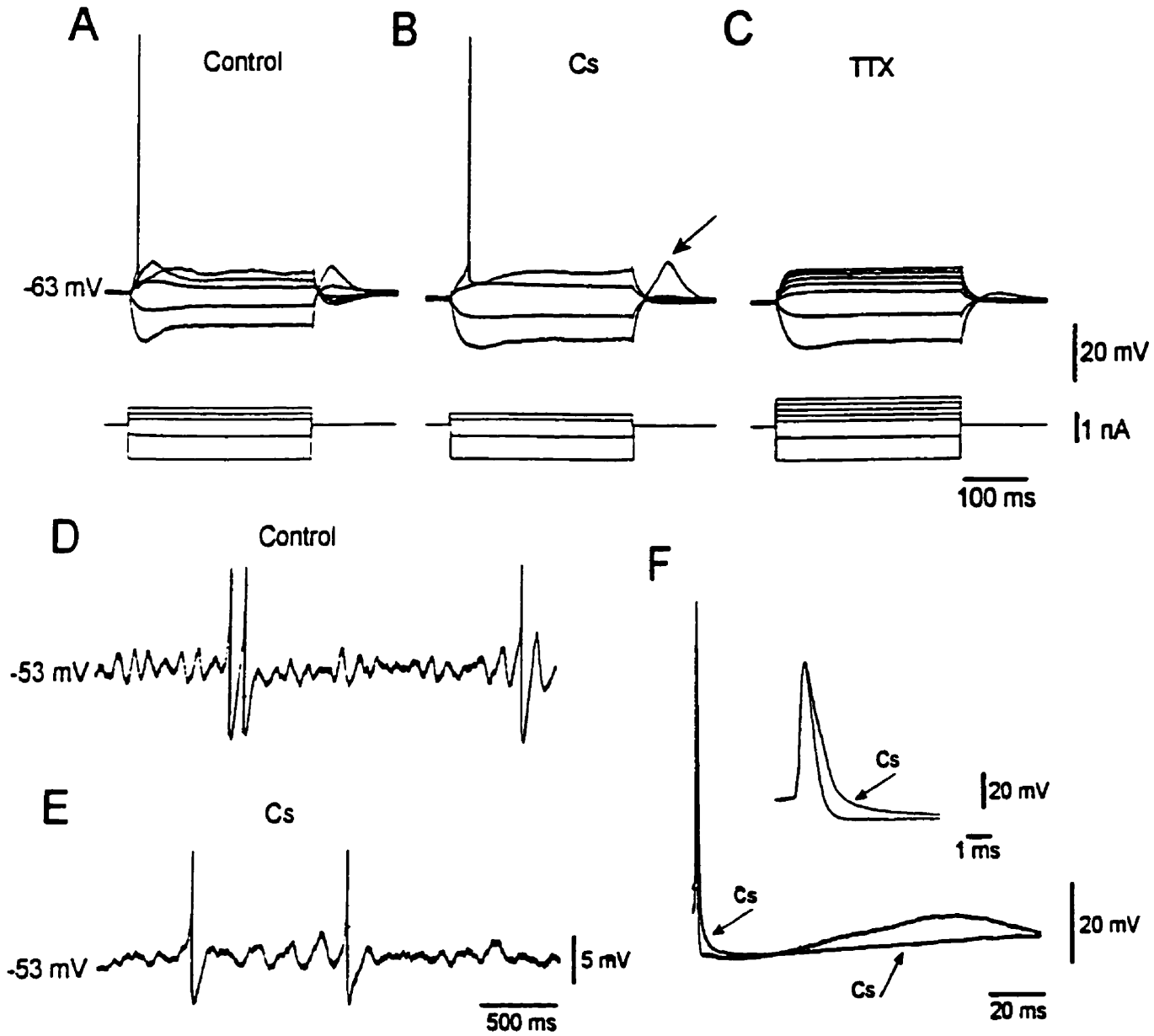
A
Control
B
Cs
C
TTX
-63 mV
20 mV
1 nA
100 ms
D
Control
-53 mV
E
Cs
-53 mV
5 mV
500 ms
F
Cs
20 mV
1 ms
Cs
20 mV
Cs
20 ms

Figure 10. Ba^{2+} blocks the stellate cells subthreshold rhythmic membrane potential oscillations. *A* and *B*: subthreshold voltage behavior of a stellate cell held at ~ –54mV before (A) and during Ba^{2+} (1mM) superfusion (B). Note the complete block of the rhythmic membrane potential oscillations by Ba^{2+} though some slow prepotentials can still be observed (arrows).*C*: superimposed spikes from the same neuron before and during Ba^{2+} superfusion. Note the development of a pronounced shoulder on the falling phase of the spike.

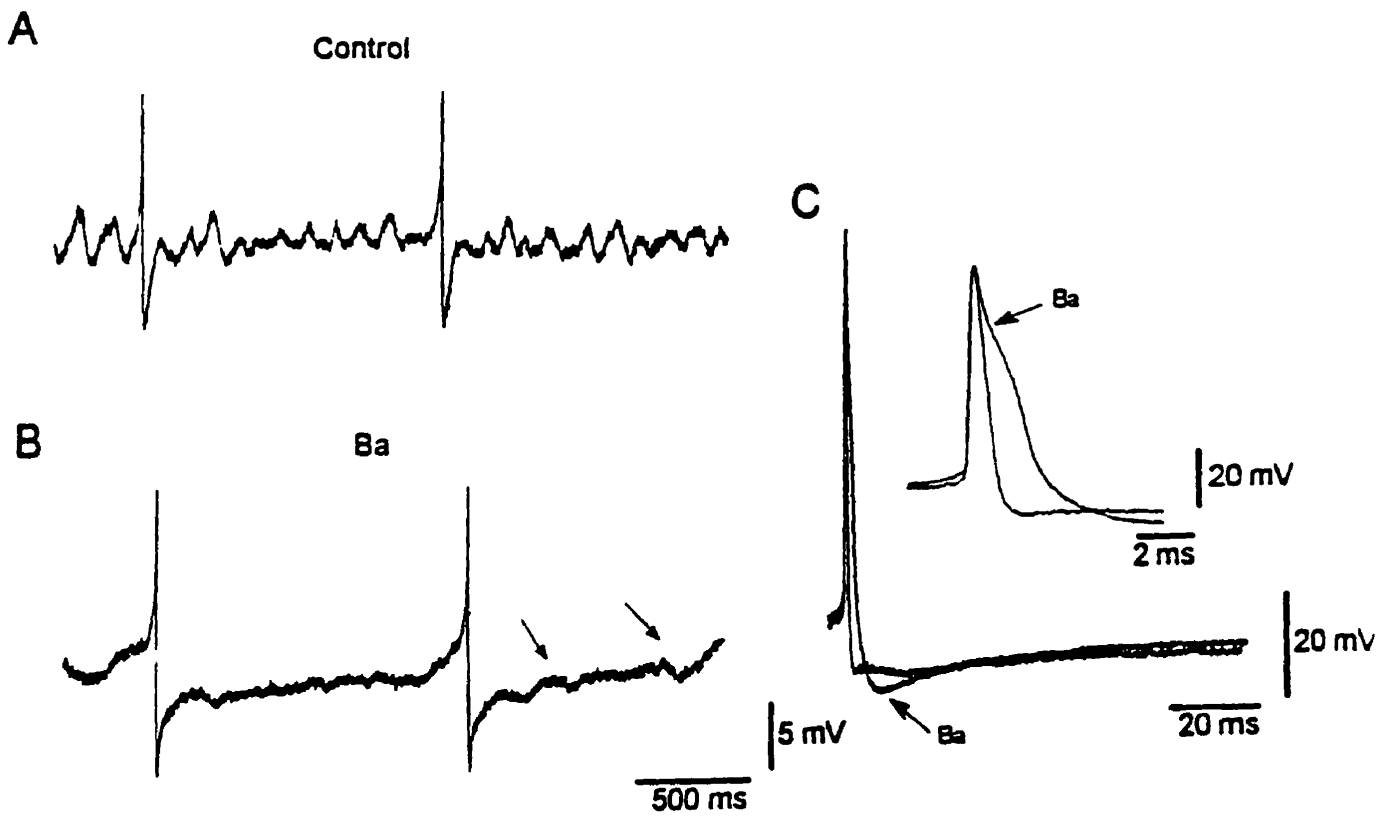
A
Control
B
Ba
500 ms
C
Ba
20 mV
2 ms
20 mV
5 mV
Ba
20 ms

CHAPTER V

MUSCARINIC MODULATION OF THE OSCILLATORY AND REPETITIVE FIRING PROPERTIES OF ENTORHINAL CORTEX LAYER II NEURONS

Ruby Klink and Angel Alonso

ABBREVIATIONS

ADP	after depolararizing potential
AHP	after hyperpolarizing potential
CCh	carbachol
EC	entorhinal cortex
f-I	firing frequency *vs* injected current
f-t	firing frequency *vs* time
MEC	middle entorhinal cortex
non-SC	non-stellate
sAHP	slow after hyperpolarizing potential
S_n-I	spike number *vs* injected current
SC	stellate

SUMMARY AND CONCLUSIONS

1. Cholinergic modulation of the electroresponsive properties of the two electrophysiologically and morphologically distinct classes of projection neurons in layer II of the rat medial entorhinal cortex (MEC), the stellate cells (SCs) and non-stellate cells (non-SCs), were studied by intracellular recording under current clamp in an *in vitro* brain slice preparation.
2. In both SCs (n=34) and non-SCs (n=26), muscarinic receptor activation with CCh (10-50 μM) caused membrane depolarization which in most cases (83%) was not associated with a measurable change in apparent input resistance at the resting potential. CCh-induced depolarization as well as all other modulatory actions were fully blocked by atropine (300 nM).
3. In SCs, the CCh-induced membrane depolarization was associated with subthreshold membrane potential oscillations and "spike-cluster" discharge which are typically expressed by these cells upon depolarization (Alonso and Klink 1993). CCh, however, caused a decrease of the dominant frequency of the subthreshold membrane potential oscillations from 9.2±1.1 Hz to 6.3±1.1 Hz, as well as a decrease of the intra-cluster firing frequency from 18.1±1.7 Hz to 13.6±1.3 Hz (clusters of 3-5 spikes). In addition, the spike-cluster discharge was less robust and the cells tended to shift into tonic firing during CCh. CCh also strongly reduced the robust spike-frequency adaptation exhibited by the SCs in response to depolarizing current pulses and the slow afterhyperpolarizing potential (sAHP) that follows the spike train.
4. In SCs, CCh selectively reduced a tetrodotoxin-sensitive slow potential that developed in response to subthreshold depolarizing current pulses and at the break of hyperpolarizing current pulses.

5. In both SCs and non-SCs, CCh produced conspicuous changes on the single spike afterpotentials and the action potential waveform itself. First, in all neurons, the fast AHP was largely reduced (by 37±12% in SCs and 26±15% in non-SCs) without any measurable effect on the medium duration AHP. Second, in most SCs (88%) and in all non-SCs, CCh decreased spike amplitude (by 8.9±2.8% in SCs and 18.6±9.5% in non-SCs) and rate of rise (by 24.4±7.7% in SCs and 40.0±12.6% in non-SCs). These CCh-induced changes in the action potential upstroke in SCs and non-SCs and reduction of the Na^+-dependent subthreshold potential in SCs, may be due to modulation of a voltage-dependent Na^+ conductance by CCh.
6. In contrast to SCs, in non-SCs, CCh drastically affected firing behavior by promoting the development of voltage-dependent, long duration (1-5 sec) slow bursts of action potentials which, in most cases (62%), could repeat rhythmically at slow frequencies (0.2-0.5 Hz). Also, the slow AHP that typically follows current-pulse triggered trains of spikes was substituted by long-lasting plateau post-depolarizations that sustained firing.
7. Whereas CCh abolished the sAHP in both SCs and non-SCs, the membrane permeant anologs of cAMP, 8-CPT-cAMP and 8-bromo-cAMP abolished the sAHP in SCs, but not in non-SCs. Similarly, the monoamine serotonin was effective in blocking the sAHP in SCs but not in non-SCs.
8. The data demonstrate that cholinergic modulation further differentiates the intrinsic electroresponsiveness of SCs and non-SCs. This differentiation gives further support to the presence of two parallel processing systems in EC layer II (Alonso and Klink 1993) with distinct synaptic modulation that could thereby differentially influence their hippocampal targets. The results also point to an important role for the cholinergic system in tuning oscillatory dynamics in the entorhinal network.

INTRODUCTION

The entorhinal cortex (EC) is crucially located within the parahippocampal region, providing bi-directional connections between the neocortex and the hippocampal formation (Witter et al. 1989). Studies of cortical connectivity have shown that the superficial layers (II and III) of the EC receive convergent inputs from a variety of associational cortices and that this convergent information is then funneled to the hippocampal formation via the perforant path (Insausti et al. 1987; Ramon y Cajal 1902). In turn, the hippocampal formation feeds back onto the deep layers of the EC which give rise to projections that remarkably reciprocate the input channels. Neuropsychological studies in rats, monkeys and humans (Alvarez and Squire 1994; Squire 1992) have demonstrated a role of the neocortical-hippocampal-neocortical circuitry in high order cognitive processes, particularly in learning and memory. The parahippocampal region and hippocampal formation together form the medial temporal lobe memory system that is primarily involved in the early stages of declarative memory formation. The central involvement of the EC in human cognition is underscored by the pathological changes targeting the superficial EC layers in conditions such as Alzheimer's disease (Braak and Braak 1991; Van Hoesen et al. 1991) and schizophrenia (Arnold et al. 1991).

Acetylcholine is critically involved in promoting cortical activation and plasticity (Dunnett and Fibiger 1993; Winkler et al. 1995). Cholinergic innervation of the cerebral cortex originates almost exclusively from a continuum of cells located in the basal forebrain (Amaral and Kurz 1985; Rye et al. 1984; Shute and Lewis 1967), and the discovery that these cholinergic neurons degenerate in Alzheimer's disease (Geula and Mesulam 1994; Price 1986) has suggested that they play an important role in mechanisms of learning and memory (Dunnett and Fibiger 1993). In the EC, basal forebrain cholinergic afferent fibers densely innervate layer II in the rat (Alonso and Köhler 1984), primate

(Alonso and Amaral 1995) and human (De Lacalle et al. 1994). It is the layer II EC cells which give rise to the most prominent component of the perforant path which activates the intrinsic hippocampal circuitry (Steward 1976; Witter and Groenewegen 1984). In the EC layer II and several hippocampal subfields, the activation of the cholinergic system during various wake states and REM sleep promotes the development of a very prominent rhythmic population activity known as the "theta rhythm" (Alonso and García-Austt 1987; Bland 1986; Dickson et al. 1994; Mitchell and Ranck 1980; Mitchell et al. 1982). The theta rhythm has been suggested to be instrumental in implementing synaptic plasticity (Huerta and Lisman 1993; Huerta and Lisman 1996; Larson and Lynch 1986), a basic mechanism for learning.

It has been proposed that the EC might achieve its memory functions through synchronizing mechanisms (Damasio 1990) by which the activity patterns of the multiple cortical inputs that converge upon EC neurons may be temporally coordinated for the production of a memory representation (Alonso and Klink 1993). Synchronization and temporal coordination of neuronal population activity can best be produced via intrinsic oscillatory mechanisms in some of the network elements (König et al. 1995; Lampl and Yarom 1993; Llinàs et al. 1991). Interestingly, the electrophysiological study of medial EC (MEC) layer II neurons (Alonso and Klink 1993; Alonso and Llinàs 1989; Klink and Alonso 1993) demonstrated that the most abundant MEC layer II cell type, the stellate cells, display robust intrinsic rhythmicity.

The present study focuses on the analysis of cholinergic actions on oscillatory and repetitive firing properties in MEC layer II neurons, as a step in understanding the cellular basis of cholinergic involvement in rhythmic population activities and learning and memory in the EC. It has been shown, in many cortical regions, that muscarinic receptor activation produces a long lasting depolarization and enhancement of the intrinsic excitability of principal neurons (Krnjevic 1993) and also regulates synaptic transmission (Cox et al. 1994; Hasselmo and Bower 1992). The present study demonstrates profound and

differential neuromodulatory actions of muscarinic receptor activation on stellate and pyramidal-like cells of EC layer II that collectively may facilitate network oscillations and bursts of activity. The results also support the view that two parallel channels of information processing with different integrative properties exist in layer II of the MEC (Alonso and Klink 1993). Part of this work has already been published in abstract form (Klink and Alonso 1992).

METHODS

Brain slices (350 μM) were derived from male Long-Evans rats (150-250 g) following standard procedures. Dissection methods, recording procedures and intracellular staining methods have been described in detail elsewhere (Alonso and Klink 1993). Briefly, after Nembutal (30mg/Kg) anesthesia animals were decapitated, the brain was rapidly removed and a block of tissue containing the retrohippocampal region was placed in a cold (6-10°C) oxygenated Ringer solution (see below). Horizontal slices (350μm) were cut using a vibratome and then allowed to recover at room temperature for at least 2 hours in oxygenated incubation chambers. For recording, a single slice was transferred to a recording chamber, submerged at 35 ± 1°C and superfused with a solution containing (in mM) 124 NaCl; 5 KCl; 1.2 KH_2PO_4; 2.4 $CaCl_2$; 2.6 $MgSO_4$; 26 $NaHCO_3$; and 10 glucose. pH was adjusted to 7.4 by saturating with 95% O_2 and 5% CO_2. Intracellular glass electrodes were filled with 2-3 M potassium acetate (tip resistance 40-120 MΩ), 2-3M potassium chloride (40-80 MΩ) or 1-2% biocytin in 2-3 M potassium acetate (100-200 MΩ). Histochemical procedures followed for biocytin revealing were as described elsewhere (Alonso and Klink 1993). In order to block Na^+ conductances tetrodotoxin (TTX, 1μM) was used. Carbachol (CCh, 10-50 μM) was added to control or TTX Ringer and bath applied for variable periods of time ranging from 30 seconds to the entire duration of the experiment. In some experiments, 5-Hydroxytryptamine (5-HT; 30

μM), 8-(4-Chlorophenylthio)-adenosine-cyclic monophosphate (8-CPT-cAMP, 100-300 μM) or 8-Bromo-adenosine-cyclic-monophosphate (8-Bromo-cAMP; 1 mM) were bath applied to compare with CCh actions. Atropine (300 nM; to block muscarinic responses) was superfused for 20 minutes before test applications of CCh. All drugs were purchased from Sigma except for TTX (Calbiochem).

Electrophysiological parameters were measured as follows: action potential waveform was quantified in normal Ringer and during CCh by eliciting a single spike from the control resting membrane potential in response to a threshold current pulse; spike amplitude and fast AHP were measured relative to threshold; spike rate of rise was taken as spike amplitude divided by duration from threshold to peak. The dominant frequency of subthreshold membrane potential oscillations was estimated by computing power spectra of 3 s long traces digitized at 3 kHz. The area under input-output relation plots was calculated by integrating the corresponding curves using the graphics and data analysis package Origin™. Data are given as mean ± standard deviation. Statistical significance was tested according to the one or two-tailed Student t test.

RESULTS

The present study is based on a database of 60 neurons from layer II of the MEC, recorded for at least 30 minutes in stable conditions and tested with bath applications of the cholinergic agonist carbachol (CCh). 10 of these neurons were also intracellularly injected with biocytin for morphologic characterization. In control Ringer, all neurons had a resting membrane potential negative to -55mV, an input resistance larger than 15 MΩ, and a spike amplitude larger than 60 mV. As previously found (Alonso and Klink 1993), neurons fell into two distinct electrophysiological and morphological categories, the stellate (SCs; n=34) and the non-stellate cells (non-SCs; n=26), whose main characteristics are summarized in Fig. 1. In brief, SCs have multiple primary dendrites and a widely

branching upper dendritic tree (Fig. 1A, top). Their subthreshold voltage responses to current pulses are markedly non-linear, exhibiting pronounced time-dependent rectification in both the depolarizing and hyperpolarizing direction (Fig. 1B, top). The most remarkable electrophysiological characteristic of SCs is their ability to generate subthreshold, sinusoidal-like, membrane potential oscillations which reach their maximal amplitude and have a frequency of about 8 Hz at ~ -54mV (Fig. 1C, top and Fig. 3A). Upon d.c. depolarization, tonic firing is not readily induced in SCs. Instead, a 1-3 Hz repetitive bursting pattern, constituted by non-adapting spike clusters, emerges (Fig. 4A). Non-SCs have, in their majority, a pyramidal-like morphology, with one or two major apical dendrites and a profuse basal dendritic tree (Fig. 1A, bottom). Their responses to current pulses are easily distinguished from those of SCs by a less pronounced time-dependent rectification and delayed firing upon threshold depolarization (Fig. 1B, bottom). Moreover, non-SCs never exhibit persistent rhythmic subthreshold oscillations nor spike clusters and, when d.c.depolarized, readily go into tonic firing (Fig. 1C, bottom).

Fig. 1 near here

CCh (10-50 μM) applied at rest (SCs:-61.6 ± 2.2 mV; non-SCs:-63.2 ± 3.6 mV) in normal Ringer (n=52) caused membrane depolarization in most SCs (27/29) and in all non-SCs (23). This depolarization was large enough to reach firing threshold in 7/29 SCs and in 5/23 non-SCs. CCh applied during Na^+-conductance block with TTX (1μM) depolarized all SCs and non-SCs (n=46). No statistically significant difference ($p > 0.1$) was found in the magnitude of a 30 μM CCh induced depolarization between SCs (4.3 ± 2.7 mV; n=24) and non-SCs (3.7 ± 1.8 mV; n=18). In a large majority of neurons (50/60), the CCh-induced depolarization was not accompanied by a measurable change in apparent input resistance at the control resting membrane potential (e. g. Fig. 2). In the remaining neurons, the apparent input resistance increased by 19.7 ± 6.4%. Again, there was no significant difference between SCs and non-SCs with regard to the magnitude of the input

resistance increase (SCs:18.5 ± 5.3%, n=6; non-SCs:21.2 ± 9.2%, n=4). The CCh induced depolarization as well as all other CCh neuromodulatory actions on EC layer II neurons did not develop in the presence of atropine (300 nM; n=5, not shown), therefore indicating their mediation through muscarinic receptors.

Fig. 2 near here

STELLATE CELLS: OSCILLATORY PROPERTIES

As illustrated in Figs. 2 and 3, the depolarizing action of CCh brought the membrane potential of the SCs to within the voltage range where subthreshold oscillations develop. It was a consistent observation that during CCh the voltage threshold for the ocurrence of subthreshold oscillations was shifted by about 1-3 mV in the negative direction (Fig. 3A). More notably, in all SCs, CCh substantially decreased the frequency of the subthreshold oscillations by ~ 30%. Similarly to the case illustrated in Fig. 3A and B, the mean frequency of the subthreshold oscillations in control Ringer was 9.2 ± 1.0 Hz (measured at -53.5 ± 0.8 mV; n=26) and it decreased to 6.3 ± 1.1 Hz (measured at -55.2 ± 1.3 mV) during CCh application.

Fig.3 near here

The discharge in repetitive spike-clusters typical of the SCs was also affected by CCh. Essentially, as in the typical case illustrated in Fig. 4A and B, the phenomenon of spike-clusters was less robust during CCh in the sense that the cells switched more readily from cluster discharge into tonic firing upon membrane depolarization. Concomitant with the CCh-induced decrease in the frequency of the subthreshold oscillations described above, there was a parallel decrease in the instantaneous intra-cluster firing frequency (Fig. 4C). While the instantaneous intra-cluster firing frequency for clusters of 3-5 spikes averaged 18.1 ± 1.7 Hz in control, it decreased to 13.6 ± 1.3 Hz in CCh (n=6).

Fig. 4 near here

STELLATE CELLS: SPIKE-TRAIN AND ACTION POTENTIAL PROPERTIES

In SCs, the trains of spikes evoked by depolarizing current steps exhibit pronounced adaptation which, for large current pulses (> 0.5 nA), leads to cessation of firing 100-200 ms after pulse onset (Alonso and Klink 1993). This adaptation is primarily caused by the build up of a Ca^{2+}-dependent slow AHP (Klink and Alonso 1993). We consistently observed that CCh application markedly reduced the spike-train adaptation evoked by 250-350 ms depolarizing current pulses, which caused repetitive firing to be present for the entire duration of the pulse (Fig. 5A). Concomitant with the adaptation block, CCh also abolished the slow AHP (sAHP) following the current-pulse triggered spike-trains (Fig. 5B) without affecting a medium duration AHP (★).

Fig. 5 near here

The actions of CCh on the SCs input-output relationships were investigated in detail by analyzing plots of instantaneous firing frequency versus injected current (*f-I*; Fig. 6A), instantaneous firing frequency as a function of time after onset of the current pulse (*f-t*; Fig. 6B) and number of spikes as a function of injected current (S_n-*I*; Fig. 6C), in control and CCh containing Ringer (n=8). In control, all SCs displayed a bilinear *f-I* relationship for the first interspike interval (ISI), and simply linear for subsequent ISIs (Fig. 6A). During CCh, in most SCs (7/8), the first ISI *f-I* relationship became linear, but its average slope (340.3 ± 202.7 Hz/nA) was not significantly different from that of the primary segment of the control *f-I* relationship (362.4 ± 97.1 Hz/nA). This means that CCh did not significantly increase firing frequency at the begining of the current pulse. In fact, on average, the slope of the *f-I* relationship for the 2^{nd}-4^{th} ISIs was not significantly affected by CCh; it could slightly decrease in some cells (Fig. 6A) or increase in others. CCh-induced increases in firing frequency (reflecting block of adaptation) were, however, always present after the 4^{th} ISI and were particularly manifest for large current amplitudes. This CCh action was especially apparent when comparing the *f-t* plots in control and CCh.

Fig. 6B depicts a typical *f-t* plot for a 1.0 nA current pulse in control (■) and CCh (▲) demonstrating that CCh only had an obvious effect on adaptation after the 4th ISI. Note in fact that during CCh (▲) the cell fired at a constant rate for the second half of the current pulse, while in control (■), firing frequency monotonically decreased and the cell ceased firing after about 125 ms of pulse onset.

It has been shown that changes in the area under the S_n-I curve represent a good quantitative estimate of changes in adaptation (Barkai and Hasselmo 1994). Fig. 6C illustrates the S_n-I plot for the same cell as in Fig. 6A and B and demonstrates that, for each current step, the cell fired more spikes in CCh (▲) than in control (■), especially at high stimulus intensities. The same was observed in all neurons tested (n=8). Integration of the S_n-I curves gave corresponding S_n-I areas for control and CCh. On average, CCh largely increased the S_n-I value by 88.8%, from 5.4 ± 1.9 to 9.7 ± 2.8 spikes per pulsexnA.

Fig. 6 near here

CCh also produced clear modulatory effects on the single spike afterpotentials and the action potential waveform itself (Fig. 7). In SCs, the action potential is followed by both a fast AHP (Fig. 7A, ▲) and a medium AHP (Fig. 7A, ✱) separated by a depolarizing after-potential (Alonso and Klink 1993). As in the case shown in Fig. 7A, in all SCs, CCh reduced the fast AHP (by 37 ± 12%; n=22) without affecting the medium AHP, and in 56% of SCs, the depolarizing after potential was no longer manifest in CCh. Fig. 7B shows in detail the alteration in action potential waveform that was typically produced by CCh. It can be observed that CCh produced a small positive shift in spike threshold, and decreased spike amplitude, rate of rise and rate of repolarization. While reduction in fast AHP and rate of repolarization may be explained by CCh block of repolarizing potassium conductances (Hille 1992), the other changes cannot be ascribed to this mechanism. We have thus quantified these changes. In 88% of neurons (n=22), CCh increased the spike

threshold by about 1mV, decreased spike amplitude by 8.9 ± 2.8% and decreased spike rate of rise by 24.4 ± 7.7%. In the remaining 12% of neurons only the above mentioned decrease in fast AHP and a concomittant decrease in rate of repolarization were observed.

Fig. 7 near here

STELLATE CELLS: SUBTHRESHOLD Na^+-DEPENDENT POTENTIALS

SCs exhibit pronouced "sags" in membrane potential in response to low amplitude hyperpolarizing and, particularly, depolarizing current pulses applied from rest ((Alonso and Klink 1993); this paper Fig. 8). We demonstrated in a previous study that while the hyperpolarization-induced sag response is primarily generated by an I_h-like current, the depolarization-induced sag and anodal-break potentials are largely due to Na^+-conductance activation (Klink and Alonso 1993). Given the above described modulatory actions of CCh on the Na^+-dependent action potential and subthreshold oscillations, we also investigated whether CCh modulated the subthreshold time-dependent voltage responses to current pulses. Fig. 8A ("Control") illustrates a prominent slow depolarizing potential followed by a sag to a lower level in response to a 0.1 nA current pulse (top), and a hyperpolarization-induced sag and associated rebound potential in response to a -0.4 nA current pulse (bottom). Remarkably, during perfusion with CCh (30 μM) the slow depolarization-induced potential was largely reduced while the hyperpolarization-induced sag was not significantly affected (Fig. 8A, "CCh 30 μM" and "Control + CCh"). The CCh block of the slow depolarizing potential completely recovered following washout (Fig. 8A, "Washout"). This result, which was observed in all neurons tested (n=18), may be explained by a CCh block of a voltage-dependent Na^+-current. Consistent with this idea, CCh produced no detectable action on the subthreshold time-dependent responses to depolarizing (Fig. 8B) or small hyperpolarizing (not shown) current pulses during Na^+-conductance block with TTX (n=6). Interestingly, in most cases we observed that the CCh

reduction of the Na^+-dependent subthreshold responses developed before any measurable steady membrane potential depolarization took place.

Fig. 8 near here

NON-STELLATE CELLS: OSCILLATORY PROPERTIES

In contrast to SCs, non-SCs do not display rhythmic subthreshold membrane potential oscillations and when d.c. depolarized, readily go into tonic firing (Figs. 1C and 10). This typical regular spiking was drastically affected by CCh. Remarkably, in most non-SCs (16/26), bath application of CCh induced a voltage-dependent repetitive bursting discharge which could emerge either spontaneously, by the direct depolarizing action of CCh, or upon additional current injection. The bursts typically consisted of long-duration clusters of spikes with an accelerando-decelerando pattern separated by a silent interval with little hyperpolarization. We considered that a cell displayed a repetitive bursting discharge when, every time that it was depolarized to about -55 mV, a sequence of at least three slow bursts emerged. The CCh concentrations required to evoke this bursting response were relatively low, usually in the range of 10-30 μM. A typical example is illustrated in Fig. 9. In this neuron, bath application of CCh caused a small (~ 4mV) membrane depolarization to about -60 mV (panel A). From this initial CCh resting level, application of a 0.1 nA short current pulse fired the cell and triggered a regenerative slow bursting pattern sustained by a very long-lasting (~ 1min) depolarizing after-potential (panel A, traces within the rectangle expanded in panel B). Individual bursts lasted for 2 to 5 s and repeated every ~ 6 s. Once the membrane potential returned to the resting CCh level further minimal d.c. depolarization (panel A, horizontal arrows) resumed the slow bursting activity which then became self-sustained. Panel C illustrates the initial burst from B (rectangle) at an expanded time base and demonstrates that the burst considerably outlasted the duration of the pulse with firing frequency peaking towards the end of the pulse (at ~114 Hz). Subsequent spontaneous bursts, though not stereotyped, were rather

consistent in pattern in terms of firing frequency and burst duration. As in this case, in all other non-SCs, CCh spontaneous bursts were always initiated by a ramp-like depolarization that triggered spiking at a gradually accelarating frequency which peaked towards the end of the burst, to then decrease rapidly with an abrupt membrane repolarization. For any given cell and membrane potential, individual burst durations and inter-burst intervals could vary considerably (up to ~100%), however. In those non-SCs that did not display a repetitive bursting sequence during CCh (10/26), low amplitude current pulses that reached threshold nonetheless triggered a long lasting burst riding on a plateau depolarization. CCh-triggered post depolarizations and plateau potentials were also observed in all non-SCs tested in the presence of TTX (1μM; n=18) (Fig. 9D), thus indicating that this phenomenon does not depend on the activation of the persistent Na^+ current that theses neurons possess (Klink and Alonso 1993)

Fig. 9 near here

The ability of CCh to switch the firing pattern of the non-SCs from regular spiking to rhythmic bursting, and the voltage-dependence of the bursting mode is further demonstrated in Fig. 10. Panel A illustrates the typical regular discharge of a non-SC in control Ringer at different levels of membrane potential depolarization and panel B illustrates the actions of d.c. membrane depolarization upon the CCh induced bursting discharge in the same neuron. Note that membrane depolarization first decreased the bursting frequency and increased the duration of the bursts (level 0.09), and then gradually switched the firing pattern into rhythmic single spiking (0.10 and 0.11 levels). For comparison note that level 0.30 nA in panel A (control) and level 0.11 in panel B (CCh) correspond to approximately the same mean firing frequency (~ 15Hz; note different time scale).

Fig. 10 near here

NON-STELLATE CELLS: ACTION POTENTIAL PROPERTIES

As in the SCs, the action potential in non-SCs is followed by a fast AHP and a medium AHP (Alonso and Klink 1993). Similarly to the SCs, in all non-SCs examined (n=15), CCh reduced the fast AHP by 26±15% without affecting the medium AHP. Also, as in the SCs, in non-SCs CCh-induced changes in action potential waveform were manifest. CCh increased threshold by about 1 mV, and decreased amplitude by 18.6±9.5% and rate of rise by 40.0±12.6%. The CCh induced reduction in action potential amplitude and rate of rise was larger than that observed in SCs but the difference did not reach statistical significance ($p>0.001$).

IN NON-STELLATE CELLS THE sAHP IS NOT MODULATED VIA cAMP

The finding that CCh promotes long lasting post-depolarizations raises the question whether muscarinic activation unmasks an after depolarizing potential (ADP) or whether it induces it. If in addition to a slow Ca^{2+}-dependent K^+ current ($I_{k(AHP)}$), a slow inward current is also significantly activated during the sAHP, the reversal potential for the sAHP (E_{AHP}) should be different from the K^+ equilibrium potential (E_k). We estimated E_{AHP} in both SCs and non-SCs by evoking trains of spikes at different membrane potentials. The estimated E_{AHP} was approximately the same in SCs and nonSCs (-95 mV, n=2 and -94 mV, n=3, respectively) and this approximates the expected E_K for the extracellular K^+ concentration used in our experiments. This observation suggest that an inward curent does not significantly overlap with the sAHP.

We also considered that if CCh unmasks a ADP by blocking the sAHP, then other agents that block the sAHP should, in principle, also promote post-depolarization and bursting activity in non-SCs. In addition to acetylcholine, monoamines are also known to efficiently block the sAHP in hippocampal pyramidal cells and other brain neurons (McCormick and Williamson 1989; Nicoll 1988). However, while in hippocampal pyramidal cells, modulation of the sAHP by acetylcholine involves the Ca^{2+}-Calmodulin

Kinase II pathway (Müller et al. 1992), modulation of the sAHP by monoamines (including serotonin, norepinephrine, histamine and dopamine) is mediated via cAMP-dependent protein kinase (Pedarzani and Storm 1993; Pedarzani and Storm 1995). For this reason, we examined whether membrane permeant anologs of cAMP could block the sAHP without unmasking any ADP. To our surprise, bath application of 8-CPT-cAMP (n=4; Fig 11A, left two panels) and 8-Bromo-cAMP (n=2; not shown) did not affect the sAHP or spike-train adaptation (insets) in non-SCs. Consistent with this observation, we also found that serotonin had no effect on the non-SCs sAHP (Fig. 11A, right two panels; n=6), while still causing membrane hyperpolarization via a direct action (not shown). On the other hand, similarly to what was observed in other neurons, 8-CPT-cAMP (n=4; Fig. 11B, left two panels), 5-HT (n=4; Fig 11B, right two panels) and 8-Bromo-cAMP (n=1; not shown), always greatly reduced spike adaptation (insets) and totally abolished the sAHP in SCs. This result demonstrates that SCs and non-SCs are not only different with regard to their basic electrophysiology and morphology (Alonso and Klink 1993), but also with respect to their pharmacology and metabolism.

Fig. 11 near here

DISCUSSION

The intent of the present study was to evaluate the possible cholinergic modulation of the intrinsic excitable properties of neurons from layer II of the MEC. Our findings demonstrate that the firing characteristics of the two types of projection neurons present in this crucial cortical layer, the SCs and the non-SCs, are prominently yet differentially influenced by CCh. Whereas muscarinic receptor activation modulated in a rather subtle manner the subthreshold membrane voltage oscillations and spike clusters typical of the SCs, muscarinic actions were very robust on the non-SCs and could transform their regular tonic firing into a slow repetitive bursting discharge. In addition, our data also

demonstrate that SCs and non-SCs differ not only with regard to their electrophysiology and morphology, as previously reported (Alonso and Klink 1993; Klink and Alonso 1993), but also with respect to their metabolism since, for example, the sAHP can be modulated by cAMP-dependent protein kinase in SCs, but not in non-SCs.

In spite of the differential effects on firing pattern, CCh application (30 μM) produced, via direct muscarinic receptor activation, a modest membrane depolarization of similar amplitude (~ 4 mV) in both SCs and non-SCs. This issue is discussed in detail in an accompanying manuscript (Klink and Alonso 1996) where we provide evidence that the mechanism underlying the CCh induced depolarization largely relies on the activation of a voltage and Ca^{2+}-dependent non-specific cationic conductance in both SCs and non-SCs.

MUSCARINIC ACTIONS ON SCS

Muscarinic receptor activation facilitated the development of oscillatory activity in SCs by depolarizing the membrane potential to within the voltage range where the characteristic Na^{+}-dependent subthreshold membrane potential oscillations of these neurons develop. That subthreshold oscillations persisted during relatively high concentrations of CCh (30-50 μM) clearly indicates that a classical M-current is not essential for their generation (Gutfreund et al. 1995; Klink and Alonso 1993). Membrane potential depolarization and development of subthreshold 5-10 Hz (theta-like; (Alonso and Llinàs 1989)) oscillations in the SCs by muscarinic receptor activation is consistent with the well established role of the basal forebrain cholinergic system in promoting theta rhythmicity in hippocampal and entorhinal cortices (Alonso and García-Austt 1987; Green and Arduini 1954). We observed that while the subthreshold oscillatory frequency of the SCs is about 9 Hz when d.c.depolarized in control conditions, the frequency of the spontaneous subthreshold oscillations decreased to about 6 Hz during CCh. This frequency decrease agrees with the low frequency range of the cholinergic-dependent theta rhythm (Bland 1986). In neocortical neurons, however, muscarinic receptor activation

appears to facilitate the frequency of Na^+-dependent intrinsic subthrehold oscillations (Metherate et al. 1992). It may be that in the neocortex the cholinergic system is biased to promote high frequency (gamma range) oscillatory activity that constitutes the so called low-voltage fast activity typical of cortical activation (Alonso et al. 1996; Buzsàki et al. 1988; Vanderwolf 1988). In a similar manner as different ionic conductances in different neurons may determine the same pattern of activity (Alonso and Llinàs 1992; Alonso and Llinàs 1989), the same modulatory system (in this case cholinergic) in different neurons and networks (archi- and periallocortex v.s. neocortex) may well produce distinct patterns of activity.

The phenomenon of spike clustering in SCs persisted, although diminished, during CCh superfusion. This result is somewhat paradoxical since we observed that, as described in many other cortical neurons (Constanti and Sim 1987; Cox et al. 1994; Hasselmo and Bower 1992; Lancaster and Nicoll 1987; Madison and Nicoll 1984; McCormick and Prince 1986; Schwindt et al. 1988; Tseng and Haberly 1989), muscarinic receptor activation blocked adaptation and the Ca^{2+}-dependent sAHP following current-pulse triggered spike trains. The observation is consistent, however, with our previous finding that spike-clusters also remain during Ca^{2+}-conductance block (Klink and Alonso 1993) and suggests that while the sAHP contributes to cluster generation, it is not an essential factor.

Our analysis of the SCs input/output relationship as assessed by 250-350 ms current pulse injection produced similar results to those previously reported in other cortical neurons (Barkai and Hasselmo 1994). CCh had no, or a small effect, on the initial firing rates (upt to ~4th ISI) but the block of adaptation at later times resulted in a substantial increase in the total number of spikes per current pulse. In no case did we observe, however, an aceleration in firing frequency or the production of an after-depolarization, as occurred in the non-SCs (discussed below). In a recent biophysical model of rat piriform cortex, simulated cholinergic block of adaptation has been shown to

implement an appropriate dynamic for learning within the network (Barkai et al. 1994; Liljenström and Hasselmo 1995). In the case of the EC, this mechanism may also work and operate in conjunction with the cholinergic facilitation of oscillations.

Muscarinic receptor activation produced manifest modulatory actions on the action potential waveform of the SCs, and also equivalent effects on the action potential of the non-SCs. The most obvious effect of CCh was the block of the fast AHP with a concomitant broadening of the spike at the base and decrease in the action potential rate of repolarization. In addition, CCh also decreased the rate of rise and amplitude of the action potential. Such conspicuous cholinergic modulatory actions on the action potential do not appear to occur in neocortical neurons (Cox et al. 1994; McCormick and Prince 1986). In hippocampal pyramidal cells, one early study (Segal 1982) reported a decrease in a fast AHP by CCh, but this observation was not repeated (Benardo and Prince 1982; Lancaster and Nicoll 1987). However, in a recent study reevaluating cholinergic modulation of the action potential in hippocampal neurons (Figenschou et al. 1996), results identical to ours have been reported, namely positive shift in threshold, increase in spike duration, and reduction in spike amplitude and rate of rise.

We have previously demonstrated that the fast AHP in EC layer II neurons is generated by a Ca^{2+}-dependent K^+ conductance ($g_{k(Ca)}$ (Klink and Alonso 1993)). Since it is well known that in many neurons muscarinic agonists can depress Ca^{2+} currents (Allen and Brown 1993; Berhein et al. 1991; Gähwiler and Brown 1987; Howe and Surmeier 1995), it seems likely that the fast AHP block may be an indirect result of Ca^{2+}-current reduction by CCh. Alternatively, it may also be that muscarinic receptor activation can directly modulate a fast $g_{k(Ca)}$ (Figenschou et al. 1996).

Of particular interest was the observed consistent decrease in the spike's amplitude and rate of rise by CCh. This result may be explained by a reduction in the Na^+-conductance(s) underlying action potential generation since the slope of the rising phase of the action potential is directly related to the instantaneous depolarizing current density.

Consistent with this interpretation was also the observed decrease by CCh of the slow Na^+-dependent subthreshold potentials to current pulses (slow depolaring potential and anodal break potential; Fig. 8). It has been shown that, like voltage gated Ca^{2+} and K^+ channels, Na^+ channels can be targets for neuromodulation (Cohen-Armon et al. 1989; Gershon et al. 1992; Li et al. 1992; Li et al. 1993). In fact, recent studies described a decrease in peak Na^+ current by CCh in acutely isolated neostriatal neurons (Howe and Surmeier 1994) and hippocampal neurons (Cantrell et al. 1996). Regarding the possible mechanism of action of CCh on the Na^+ current, it is well known that in many cells muscarinic receptor stimulation can increase intracellular [Ca^{2+}] via inositol triphosphate mediated mobilization of Ca^{2+} from intracellular stores (Berridge 1993), and it has recently been shown that an increase in intracellular [Ca^{2+}] can decrease total Na^+ current by reducing the fraction of Na^+ channels available for activation (Bulatko and Greeff 1995). Muscarinic modulation of the voltage-gated Na^+-conductances in SCs may also be related to the observed changes in the frequency of the Na^+-dependent subthreshold oscillations by CCh.

INDUCTION OF REPETITIVE BURSTING IN NON-SCS

Muscarinic receptor activation had a profound action on the firing pattern of the non-SCs. While in control conditions current-pulse triggered spike trains displayed moderate adaptation and were followed by a sAHP, during muscarinic activation, firing frequency accelerated during the train and the sAHP was substituted by a prolonged post-depolarization that could sustain robust burst firing. In addition, during muscarinic activation, d.c depolarization could induce a repetitive bursting sequence in most cases. Since the slow bursting oscillations produced by CCh were voltage-dependent, being blocked by hyperpolarization and changing in frequency to become inactivated with depolarization, the underlying mechanism must be intrinsic to the cells and not synaptically mediated. We did not test whether muscarinic activation could trigger slow afterpotentials

and bursting activity during Ca^{2+}-conductance block, since in non-SCs spike repolarization is for the most Ca^{2+}-dependent and these neurons possess a robust non-inactivating Na^{+}-conductance. In consequence, in non-SCs, Ca^{2+}-conductance block results by itself in the production of robust Na^{+}-dependent post-depolarizations (Klink and Alonso 1993). However, we observed that during TTX-sensitive Na^{+} conductance block, CCh always produced the development of prolonged post-depolarizations that could sustain Ca^{2+}-spiking. In an accompanying paper (Klink and Alonso 1996), we provide further evidence that the CCh induced depolarization and slow post-depolarizations are, in fact, largely mediated by a Ca^{2+}-dependent non-specific cationic current. We thus propose that CCh induces bursting by blocking $I_{k(AHP)}$ and activating a Ca^{2+}-dependent non-specific cationic current which sustains a regenerative process once the intracellular Ca^{2+} concentration rises over a certain threshold. Consistent with this interpretation is the fact that slow bursts during CCh could be triggered by the firing of one or a few Na^{+}-spikes which allow Ca^{2+} entry (Klink and Alonso 1993). Cholinergic induction of a slow post-depolarization has also been described in other cortical neurons and similarly attributed, in most cases, to the cholinergic activation of an inward non-specific cationic current (Andrade 1991; Caeser et al. 1993; Hasuo and Gallagher 1990; Schwindt et al. 1988). In EC layer II non-SCs, however, the phenomenon appears to be more robust than in other brain neurons, giving rise to a very prominent slow repetitive bursting activity.

In hippocampal pyramidal cells in slices, CCh application ($\geq$ 50μM) can induce synchronized oscillatory bursting at 4-10 Hz (MacVicar and Tse 1989) or, during block of ionotropic glutamatergic and GABAergic transmission, very slow (0.002-0.05 Hz) long lasting (8-30 s) repetitive bursts (Bianchi and Wong 1994). In contrast to the results presented in the present study, CCh induced hippocampal bursts are synaptically mediated. In a few experiments (<10%), however, we did observe a transient synaptically mediated rhythmic population activity of EC neurons at the begining of the CCh perfusion. We have recently found that this epileptic-like activity develops with nearly every CCh application

and has a persistent character when using an interface slice-chamber. The properties and basis of this network oscillation are currently under investigation (Dickson and Alonso 1995).

THE CAMP PATHWAY MODULATES THE SAHP IN SCS BUT NOT IN NON-SCS

We found that in the SCs the sAHP could efficiently be blocked by bath application of the cAMP membrane permeant analogs 8-CPT-cAMP and 8-Bromo-cAMP or by the classical monoamine serotonin, as typically observed in other neurons ((Pedarzani and Storm 1993) and references therein). However, interestingly and to our surprise, in the non-SCs none of these agents had any effect on the spike-frequency adaptation or the sAHP. It thus appears that in the non-SCs the signaling cAMP pathway is not operative for sAHP ion channel modulation. To our knowledge, this apparent inefficiency of the cAMP pathway has not been reported in any other neuronal type. For the moment, we can only speculate that the EC layer II network appears to be specifically designed so that activation of the cholinergic and not of any monoaminergic system can induce bursting activity. Considering the nodal location of EC layer II within the temporal lobe, and given that non-SCs posses robust voltage-gated slow inward currents and lack, in contrast to SCs, pronounced Ca^{2+}-independent repolarizing K^+ currents (Klink and Alonso 1993), it does make sense that few neurotransmitters may block the Ca^{2+}-dependent sAHP in non-SCs in order to prevent the production of paroxysmal-like depolarizations and epileptogenic activity. The ascending cholinergic system appears thus specifically suited to switch the EC network into an oscillatory bursting mode, and at the cost of risking the production of epileptic activity (Dickson and Alonso 1995).

FUNCTIONAL IMPLICATIONS

The present study has demonstrated that muscarinic receptor activation exerts a profound and differential modulatory action on the two morphologically and

electrophysiologically distinct projection cell types in EC layer II, the SCs and the non-SCs. We have further demonstrated that the non-SCs, unlike any other CNS neuron studied so far to our knowledge, do not have their sAHP modulated via the cAMP messanger pathway. These data add further support to the existence of two parallel output systems of information in EC layer II that could act very differently upon their hippocampal targets.

The function of the EC has to be understood from its position as an interface between the hippocampus and the neocortex and considering the established role of the neocortical-hippocampal-neocortical circuit in memory function. Neurons in EC layer II are particularly important in this (declarative) memory system since polysensory information from multiple cortical association areas converges upon them and their output represents the almost exclusive source of sensory information to the hippocampus (Insausti et al. 1987; Ramon y Cajal 1902). The basal forebrain cholinergic system, which plays a role in memory (Dunnett and Fibiger 1993; Winkler et al. 1995), densely innervates EC layer II neurons. Electrophysiologically, at the macroscopic level, activation of the cholinergic system produces theta rhythm in the EC and hippocampus, and rhythmic theta related events appear to influence memory mechanisms and function (Huerta and Lisman 1993; Huerta and Lisman 1996; Winson 1978). In the EC layer II, the genesis of the theta rhythm appears also to be directly related to the rhythmic subthreshold oscillations of the SCs (Alonso and García-Austt 1987; Alonso and Llinàs 1989).

Lampl and Yarom (1993) recently showed that subthreshold membrane potential oscillations can operate as powerful synchronizing devices in a frequency dependent manner. Hopfield has also recently shown (Hopfield 1995) that a network of neurons having subthreshold membrane potential oscillations can exquisitely encode information by using action potential timing with respect to an ongoing collective oscillatory pattern. The muscarinic induction of intrinsic oscillations and modulation of oscillatory frequency in the EC SCs might thus be of crucial importance in setting the proper temporal dynamics for

the coordination of the multiple cortical inputs that converge upon these neurons and for the ultimate generation of sensory representations within the hippocampal region.

ACKNOWLEDGMENTS

We would like to thank Drs. C. Dickson and B. Jones for comments on the manuscript. This work was supported by the canadian Medical Research Council.

REFERENCES

Allen, T. G. and Brown, D. A. M_2 muscarinic receptor-mediated inhibition of the Ca^{2+} current in rat magnocellular cholinergic basal forebrain neurones. *J. Physiol. (Lond.).* 466: 173-189, 1993.

Alonso, A. and García-Austt, E. Neuronal sources of theta rhythm in the entorhinal cortex of the rat. II. Phase relations between unit discharges and theta field potentials. *Exp. Brain Res.* 67: 502-509, 1987.

Alonso, A., Khateb, A., Fort, P., Jones, B. E., and Muhlethaler, M. Differential oscillatory properties of cholinergic and non-cholinergic neurons in the nucleus basalis. *Eur. J. Neurosci.* 8: 169-182, 1996.

Alonso, A. and Klink, R. Differential electroresponsiveness of stellate and pyramidal-like cells of medial entorhinal cortex layer II. *J. Neurophysiol.* 70: 128-143, 1993.

Alonso, A. and Köhler, C. A study of the reciprocal connections between the septum and the entorhinal area using anterograde and retrograde axonal transport methods in the rat brain. *J. Comp. Neurol.* 225: 327-343, 1984.

Alonso, A. and Llinàs, R. Electrophysiology of the mammillary complex in vitro. II. Medial mammillary neurons. *J. Neurophysiol.* 64: 1992.

Alonso, A. and Llinàs, R. R. Subthreshold Na^+-dependent theta-like rhythmicity in stellate cells of entorhinal cortex layer II. *Nature.* 342: 175-177, 1989.

Alonso, J. R. and Amaral, D. G. Cholinergic innervation of the primate hippocampal formation. I. Distribution of choline acetyltransferase immunoreactivity in the *Macaca fascicularis* and *Macaca mulatta* monkeys. *J. Comp. Neurol.* 355: 135-170, 1995.

Alvarez, P. and Squire, L. R. Memory consolidation and the medial temporal lobe: a simple network model. *Proc. Natl. Acad. Sci. USA.* 91: 7041-7045, 1994.

Amaral, D. G. and Kurz, J. An analysis of the origins of the cholinergic and noncholinergic septal projections to the hippocampal formation of the rat. *J. Comp. Neurol.* 240: 37-59, 1985.

Andrade, R. Cell excitation enhances muscarinic cholinergic responses in rat association cortex. *Brain Res.* 548: 81-93, 1991.

Arnold, E. S., Hyman, B. T., Van Hoesen, G. W., and Damasio, A. Some cytoarchitectural abnormalities of the entorhinal cortex in schizophrenia. *Arch. Gen. Psychiatry.* 48: 625-632, 1991.

Barkai, E., Bergman, R. E., Horwitz, G., and Hasselmo, M. E. Modulation of associative memory function in a biophysical simulation of rat piriform cortex. *J. Neurophysiol.* 72: 659-677, 1994.

Barkai, E. and Hasselmo, M. E. Modulation of the input/output function of the rat pyriform cortex pyramidal cells. *J. Neurophysiol.* 72: 644-658, 1994.

Benardo, L. S. and Prince, D. A. Cholinergic excitation of mammalian hippocampal pyramidal cells. *Brain Res.* 249: 315-331, 1982.

Berhein, L., Beech, D. J., and Hille, B. A diffusible second messenger mediates one of the pathways coupling receptors to calcium channels in rat sympathetic neurons. *Neuron.* 6: 859-867, 1991.

Berridge, M. J. Inositol triphosphate and calcium signalling. *Nature.* 361: 315-325, 1993.

Bianchi, R. and Wong, R. K. S. Carbachol-induced synchronized rhythmic bursts in CA3 neurons of guinea-pig hippocampus in vitro. *J. Neurophysiol.* 72: 131-138, 1994.

Bland, B. H. The physiology and pharmachology of hippocampal formation theta rhythms. *Prog. Neurobiol.* 26: 1-54, 1986.

Braak, H. and Braak, E. Neuropathological stageing of Alzheimer-related changes. *Acta Neuropathol.* 82: 239-259, 1991.

Bulatko, A. K. and Greeff, N. G. Functional availability of sodium channels modulated by cytosolic free Ca^{2+} in cultured mammalian neurons (N1E-115). *J. Physiol. (Lond.).* 484: 307-312, 1995.

Buzsàki, G., Bickford, R. G., Ponomareff, G., Thal, L. J., Mandel, R., and Gage, F. H. Nucleus basalis and thalamic control of neocortical activity in the freely moving rat. *J. Neurosci.* 8: 4007-4026, 1988.

Caeser, M., Brown, D. A., Gähwiler, B. H., and Knöpfel, T. Characterization of a calcium-dependent current generating a slow afterdepolarization of CA3 pyramidal cells in rat hippocampal slice cultures. *Eur. J. Neurosci.* 5: 560-569, 1993.

Cantrell, A. R., Ma, J. Y., Scheuer, T., and Caterall, W. A. Muscarinic modulation of sodium current by activation of protein kinase C in rat hippocampal neurons. *Neuron.* 16: 1019-1026, 1996.

Cohen-Armon, M., Sokolovsky, M., and Dascal, N. Modulation of the voltage-dependent sodium channel by agents affecting G-proteins: a study in *Xenopus* oocytes injected with brain RNA. *Brain Res.* 496: 197-203, 1989.

Cole, A. E. and Nicoll, R. A. Characterization of a slow cholinergic post-synaptic potential recorded "in vitro" from rat hippocampal pyramidal cells. *J. Physiol. (Lond.).* 352: 173-188, 1984.

Constanti, A., Bagetta, G., and Libri, V. Persistent muscarinic excitation in guinea-pig olfactory cortex neurons: involvement of a slow post-stimulus afterdepolarizing current. *Neuroscience.* 56: 887-904, 1993.

Constanti, A. and Sim, J. A. Calcium-dependent potassium conductance in guinea-pig olfactory cortex neurones *in vitro*. *J. Physiol. (Lond.).* 387: 173-194, 1987.

Cox, C. L., Metherate, R., and Ashe, J. H. Modulation of cellular excitability in neocortex: muscarinic receptor and second messenger-mediated actions of acetylcholine. *Synapse.* 16: 123-136, 1994.

Damasio, A. R. Synchronous activation in multiple cortical regions: a mechanism for recall. *Semin. Neurosci.* 2: 287-296, 1990.

De Lacalle, S., Lim, C., Sobreviella, T., Mufson, E. J., Hersh, L. B., and Saper, C. B. Cholinergic innervation in the human hippocampal formation including the entorhinal cortex. *J. Comp. Neurol.* 345: 321-344, 1994.

Dickson, C. T. and Alonso, A. The entorhinal cortex contains two intrinsic pacemakers of epileptiform activity: an in vitro study. *Epilepsia.* 36, suppl 4: 87, 1995.

Dickson, C. T., Trepel, C., and Bland, B. H. Extrinsic modulation of theta field activity in the entorhinal cortex of the anesthetized rat. *Hippocampus.* 4: 37-52, 1994.

Dunnett, S. B. and Fibiger, H. C. Role of forebrain cholinergic systems in learning and memory: relevance to the cognitive deficits of aging and Alzheimer's dementia. *Prog. Brain Res.* 98: 413-420, 1993.

Figenschou, A., Hu, G.-Y., and Storm, J. F. Cholinergic modulation of the action potential in rat hippocampal neurons. *Eur. J. Neurosci.* 8: 211-219, 1996.

Gähwiler, B. H. and Brown, D. A. Muscarine affects calcium currents in rat hippocampal pyramidal cells in vitro. *Neurosci. Lett.* 76: 301-306, 1987.

Gershon, E., Weigl, L., Lotan, I., Schreibmayer, W., and Dascal, N. Protein kinase A reduces voltage-dependent Na^+ current in *Xenopus* oocytes. *J. Neurosci.* 12: 3743-3752, 1992.

Geula, C. and Mesulam, M. M. Cholinergic systems and related neuropathological predilection pattern's in Alzheimer's disease. In: *Alzheimer's disease*, edited by R. D. Terry, R. Katzman, and K. L. Bick. New York: Raven, 1994, 263-291

Green, J. D. and Arduini, A. Hippocampal electrical activity in arousal. *J. Neurophysiol.* 17: 533-557, 1954.

Gutfreund, Y., Yarom, Y., and Segev, I. Subthreshold oscillations and resonant frequency in guinea-pig cortical neurons: physiology and modelling. *J. Physiol. (Lond.).* 483: 621-640, 1995.

Hasselmo, M. E. and Bower, J. M. Cholinergic suppression specific to intrinsic not afferent fiber synapses in rat piriform (olfactory) cortex. *J. Neurophysiol.* 67: 1222-1229, 1992.

Hasuo, H. and Gallagher, J. P. Facilitatory action of muscarine on the slow afterdepolarization of rat dosolateral septal nucleus neurons in vitro. *Neurosci. Lett.* 112: 1990.

Hille, B. *Ionic Channels of Excitable Membranes.* Sunderland, Mass: Sinauer Associates Inc, 1992, 607p.

Hopfield, J. J. Pattern recognition computation using action potential timing for stimulus representation. *Nature.* 376: 33-36, 1995.

Howe, A. R. and Surmeier, D. J. Muscarinic modulation of sodium current in acutely isolated neostriatal neurons from the adult rat. *Soc. Neurosc. Abstr.* 20: 238.9, 1994.

Howe, A. R. and Surmeier, J. Muscarinic receptors modulate N-, P-, and L-type Ca^{2+} currents in rat striatal neurons trough parallel pathways. *J. Neurosci.* 15: 458-469, 1995.

Huerta, P. T. and Lisman, J. E. Heightened synaptic plasticity of hippocampal CA1 neurones during a cholinergically induced rhythmic state. *Nature.* 19: 723-725, 1993.

Huerta, P. T. and Lisman, J. E. Low-frequency stimulation at the troughs of θ-oscillation induces long-term depression of previously potentiated CA1 synapses. *J. Neurophysiol.* 75: 877-884, 1996.

Insausti, R., Amaral, D. G., and Cowan, W. M. The entorhinal cortex of the monkey: II. Cortical afferents. *J. Comp. Neurol.* 264: 356-395, 1987.

Klink, R. and Alonso, A. Ionic mechanisms for the subthreshold oscillations and differential electroresponsiveness of medial entorhinal cortex layer II neurons. *J. Neurophysiol.* 70: 144-157, 1993.

Klink, R. and Alonso, A. Ionic mechanisms of muscarinic depolarization in entorhinal cortex layer II neurons. *J. Neurophysiol.* submitted: 1996.

König, P., Engel, A. K., and Singer, W. Relation between oscillatory activity and long-range synchronization in cat visual cortex. *Proc. Natl. Acad. Sci. USA.* 92: 290-294, 1995.

Krnjevic, K. Central cholinergic mechanisms and function. *Prog. Brain Res.* 1993: 285-292, 1993.

Lampl, I. and Yarom, Y. Subthreshold oscillations of the membrane potential: a functional synchronizing and timing device. *J. Neurophysiol.* 70: 2181-2186, 1993.

Lancaster, B. and Nicoll, R. A. Properties of two calcium-activated hyperpolarizations in rat hippocampal neurones. *J. Physiol. (Lond.).* 389: 187-204, 1987.

Larson, J. and Lynch, G. Induction of synaptic potentiation in hippocampus by patterned stimulation involves two events. *Science.* 232: 985-988, 1986.

Li, M., West, J. W., Lai, Y., Scheuer, T., and Catterall, W. A. Functional modulation of brain sodium channels by cAMP-dependent phosphorylation. *Neuron.* 8: 1151-1159, 1992.

Li, M., West, J. W., Numann, R., Murphy, B. J., Scheuer, T., and Catterall, W. A. Convergent regulation of sodium channels by protein kinase C and cAMP-dependent protein kinase. *Science.* 261: 1439-1442, 1993.

Liljenström, H. and Hasselmo, M. E. Cholinergic modulation of cortical oscillatory dynamics. *J. Neurophysiol.* 74: 288-297, 1995.

Llinàs, R. R., Grace, A. A., and Yarom, Y. *In vitro* neurons in mammalian cortical layer 4 exhibit intrinsic oscillatory activity in the 10- to 50-Hz frequency range. *Proc. Natl. Acad. Sci. USA.* 88: 897-901, 1991.

MacVicar, B. A. and Tse, F. W. Y. Local neuronal circuitry underlying cholinergic rhythmical slow activity in CA3 area of rat hippocampal slices. *J. Physiol. (London).* 417: 197-212, 1989.

Madison, D. V. and Nicoll, R. A. Control of the repetitive discharge of rat CA1 pyramidal neurones *in vitro*. *J. Physiol. (Lond.).* 354: 319-331, 1984.

McCormick, D. A. and Prince, D. A. Mechanisms of action of acetylcholine in the guinea-pig cerebral cortex in vitro. *J. Physiol. (Lond.).* 375: 169-194, 1986.

McCormick, D. A. and Williamson, A. Convergence and divergence of neurotransmitter action in human cerebral cortex. *Proc. Natl. Acad. Sci. USA.* 86: 8098-8102, 1989.

Metherate, R., Cox, C. L., and Ashe, J. H. Cellular bases of neocortical activation: modulation of neural oscillations by the nucleus basalis and endogenous acetylcholine. *J. Neurosci.* 12: 4701-4711, 1992.

Mitchell, S. J. and Ranck, J. B. J. Generation of theta rhythm in medial entorhinal cortex of freely moving rats. *Brain Res.* 189: 49-66, 1980.

Mitchell, S. J., Rawlins, J. N. P., Steward, O., and Olton, D. S. Medial septal area lesions disrupt theta rhythm and cholinergic staining in medial entorhinal cortex and produce impaired radial arm maze behavior in rats. *J. Neurosci.* 2: 292-302, 1982.

Müller, W., Petrozzino, J. J., Griffith, L. C., Danho, W., and Connor, J. A. Specific involvement of Ca^{2+}-calmodulin kinase II in cholinergic modulation of neuronal responsiveness. *J. Neurophysiol.* 68: 2264-2269, 1992.

Nicoll, R. A. The coupling of neurotransmitter receptors to ion channels in the brain. *Science.* 241: 545-551, 1988.

Pedarzani, P. and Storm, J. F. PKA mediates the effects of monoamine transmitters on the K^+ current underlying the slow spike frequency adaptation in hippocampal neurons. *Neuron.* 11: 1023-1035, 1993.

Pedarzani, P. and Storm, J. F. Dopamine modulates the slow Ca^{2+}-activated K^+ current I_{AHP} via cyclic AMP-dependent protein kinase in hippocampal neurons. *J. Neurophysiol.* 74: 2749-2753, 1995.

Price, D. New perspectives on Alzheimer's disease. *Annu. Rev. Neurosci.* 9: 489-512, 1986.

Ramon y Cajal, S. Sobre un ganglio especial de la corteza esfeno-occipital. *Trab. del Lab. de invest. Biol. Univ. Madrid.* 1: 189-201, 1902.

Rye, D. B., Wainer, B. H., Mesulam, M.-M., Mufson, E. J., and Saper, C. B. Cortical projections arising from the basal forebrain: a study of cholinergic and noncholinergic components employing combined retrograde tracing and immunohistochemical localization of choline acetyltransferase. *Neuroscience.* 13: 627-643, 1984.

Schwindt, P. C., Spain, W. J., Foehring, R. C., Chubb, M. C., and Crill, W. E. Slow conductances in neurons from cat sensorimotor cortex in vitro and their role in slow excitability changes. *J. Neurophysiol.* 59: 450-467, 1988.

Segal, M. Multiple actions of acetylcholine at a muscarinic receptor studied in the rat hippocampal slice. *Brain Res.* 246: 77-87, 1982.

Shute, C. C. D. and Lewis, P. R. The ascending cholinergic reticular systems: neocortical, olfactory and subcortical projections. *Brain.* 90: 497-520, 1967.

Squire, L. R. Memory and the hippocampus: a synthesis from findings with rats, monkeys, and humans. *Psychol. Rev.* 99: 195-231, 1992.

Steward, O. Topographic organization of the projections from the entorhinal area to the hippocampal formation of the rat. *J. Comp. Neurol.* 167: 285-314, 1976.

Tseng, G.-F. and Haberly, L. B. Deep neurons in piriform cortex. II. Membrane properties that underlie unusual synaptic responses. *J. Neurophysiol.* 62: 386-400, 1989.

Van Hoesen, G. W., Hyman, B. T., and Damasio, A. R. Entorhinal cortex pathology in Alzheimer's disease. *Hippocampus.* 1: 1-8, 1991.

Vanderwolf, C. H. Cerebral activity and behavior: control by central cholinergic and serotoninergic systems. *Int. Rev. Neurobiol.* 30: 225-340, 1988.

Winkler, J., Suhr, S. T., Gage, F. H., Thal, L. J., and Fisher, L. J. Essential role of neocortical acetylcholine in spatial memory. *Nature.* 375: 484-487, 1995.

Winson, J. Loss of hippocampal theta rhythm results in spatial memory deficit in the rat. *Science.* 201: 160-163, 1978.

Witter, M. P. and Groenewegen, H. J. Laminar origin and septotemporal distribution of entorhinal and perirhinal projections to the hippocampus in the cat. *J. Comp. Neurol.* 224: 371-385, 1984.

Witter, M. P., Groenewegen, H. J., Lopes da Silva, F. H., and Lohman, A. H. M. Functional organization of the extrinsic and intrinsic circuitry of the parahippocampal region. *Progr. Neurobiol.* 33: 161-253, 1989.

Figure 1. Basic morphological and electroresponsive properties of MEC layer II neurons. *A*: camera lucida reconstruction of a stellate cell (SC; top) and a non-stellate cell (non-SC; bottom). *B*: Voltage-current relationships in SCs (top) and non-SCs (bottom). Note the pronounced time-dependent rectification in response to inward and outward current pulses in the SC and delayed firing in the non-SC. *C*: Membrane voltage behavior upon close to rheobase d.c. depolarization in a SC (top) and non-SC (bottom). Note the robust subthreshold sinusoidal-like membrane potential oscillations in the SC.

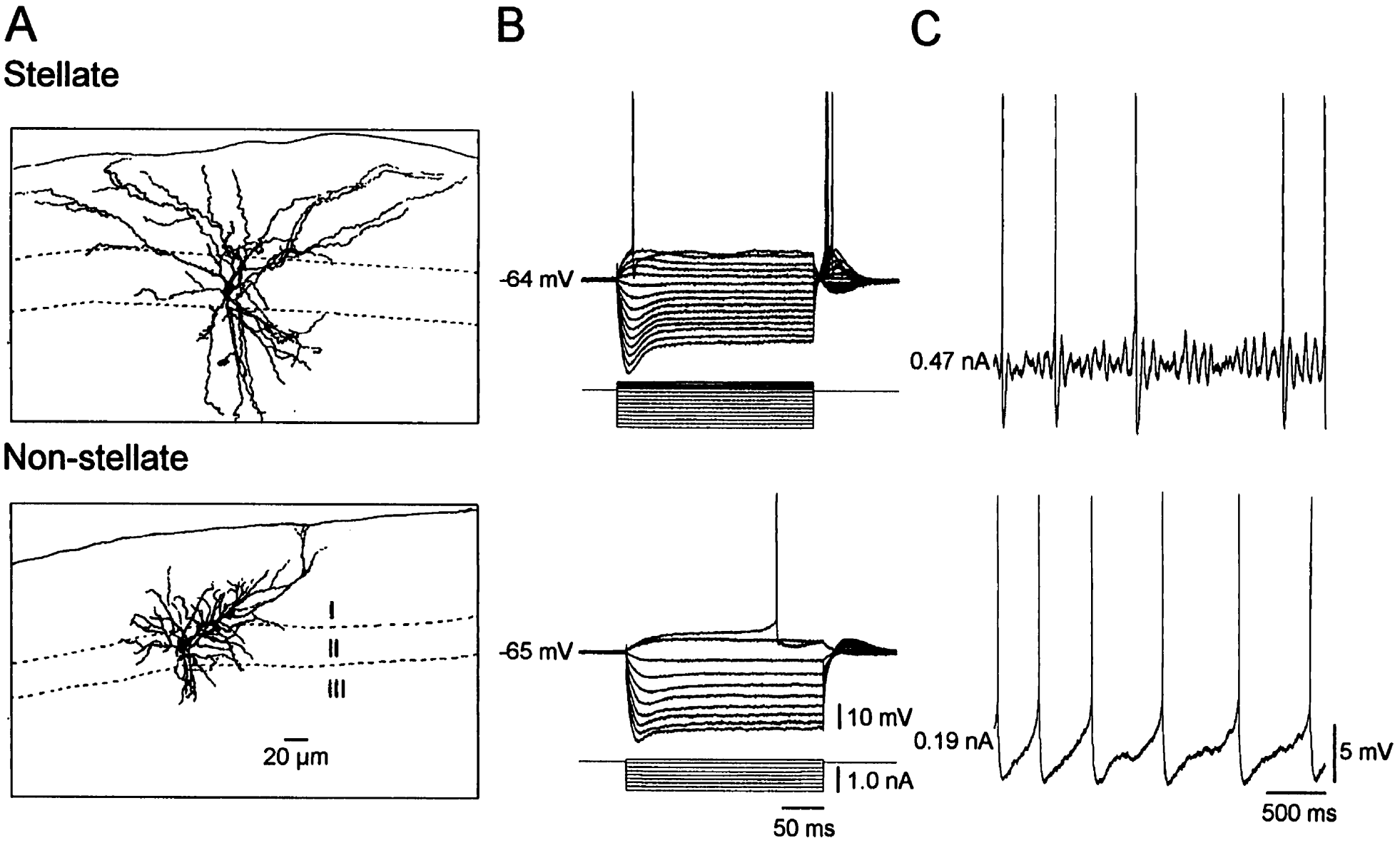
A
Stellate
Non-stellate
I
II
III
20 µm
B
-64 mV
-65 mV
10 mV
1.0 nA
50 ms
C
0.47 nA
0.19 nA
5 mV
500 ms

Figure 2. Depolarizing response of SCs to cholinergic receptor activation. *A*: CCh 30 μM, applied at rest for the duration indicated by bar, depolarized the membrane potential to the subthreshold oscillatory voltage level, without measurable change in apparent input resistance at the control resting level. *B*: Traces at an expanded time scale taken at the time points indicated by small arrows in *A*. Before CCh application (left), the cell fired at the anodal break from a resting membrane potential of -59 mV.

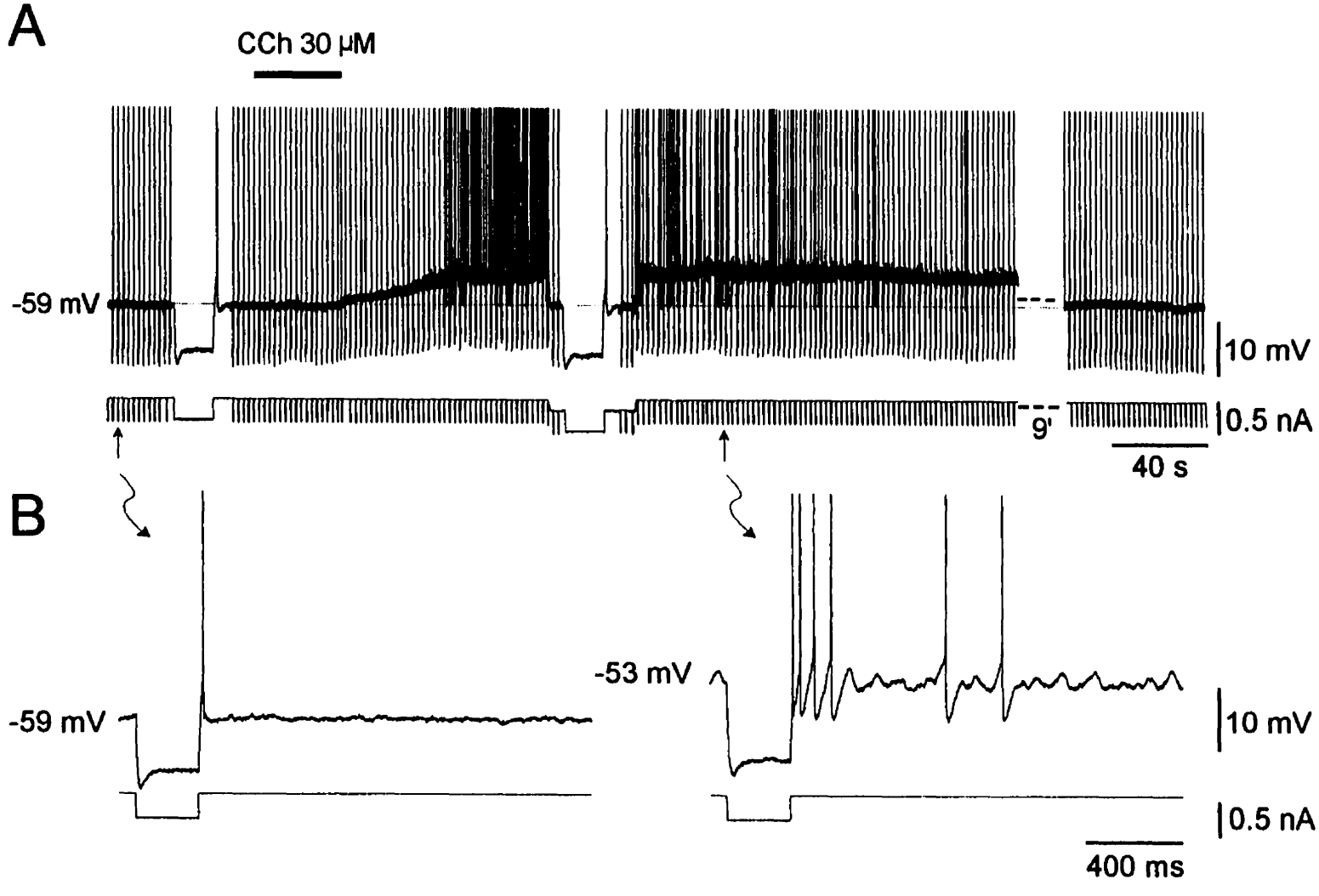
A
CCh 30 µM
-59 mV
10 mV
0.5 nA
40 s
B
-59 mV
-53 mV
10 mV
0.5 nA
400 ms

Figure 3. CCh decreases the frequency of the SCs subtreshold oscillations. *A*: subthreshold membrane oscillations at different levels of d.c. polarization in control Ringer (left) and during CCh (right). *B*. Power spectral plots of topmost traces in *A*; CCh reduced the dominant frequency of subthreshold membrane potential oscillations from 10 Hz to 6 Hz.

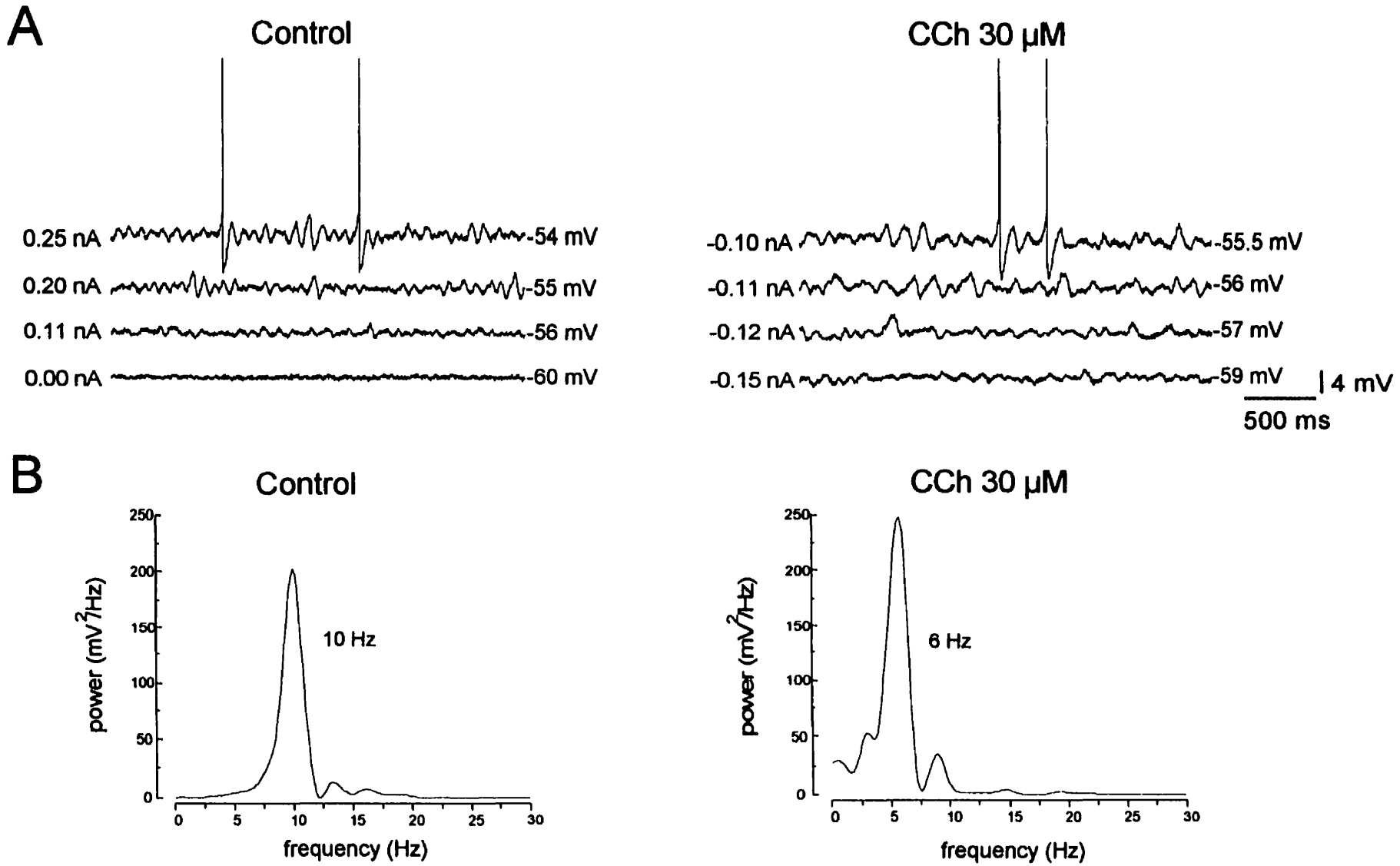
A
Control
CCh 30 µM
0.25 nA
-54 mV
0.20 nA
-55 mV
0.11 nA
-56 mV
0.00 nA
-60 mV
-0.10 nA
-55.5 mV
-0.11 nA
-56 mV
-0.12 nA
-57 mV
-0.15 nA
-59 mV
4 mV
500 ms
B
Control
CCh 30 µM
power (mV²/Hz)
10 Hz
6 Hz
frequency (Hz)
0
50
100
150
200
250
0
5
10
15
20
25
30

Figure 4. CCh modulates spike-clusters. *A*: in control Ringer, a SC exhibits the typical spike clustering phenomenon upon d.c. depolarization. Note that even with injection of 0.54 nA (top) tonic firing was not induced and clustering was still prominent. *B*: CCh, 30 μM, depolarized the cell to a level where spike-clusters develop (0.00 nA, middle), and further minor manual d.c. depolarization induces tonic discharge (0.07 nA, top). *C*: Plots of instantaneous intra-cluster firing frequency *vs* interspike interval number, for a series of clusters of 3-5 spikes in control (left) and CCh (right). Control plot corresponds to the topmost trace in *A* (0.54 nA); CCh plot corresponds to the middle trace in *B* (0.00 nA).

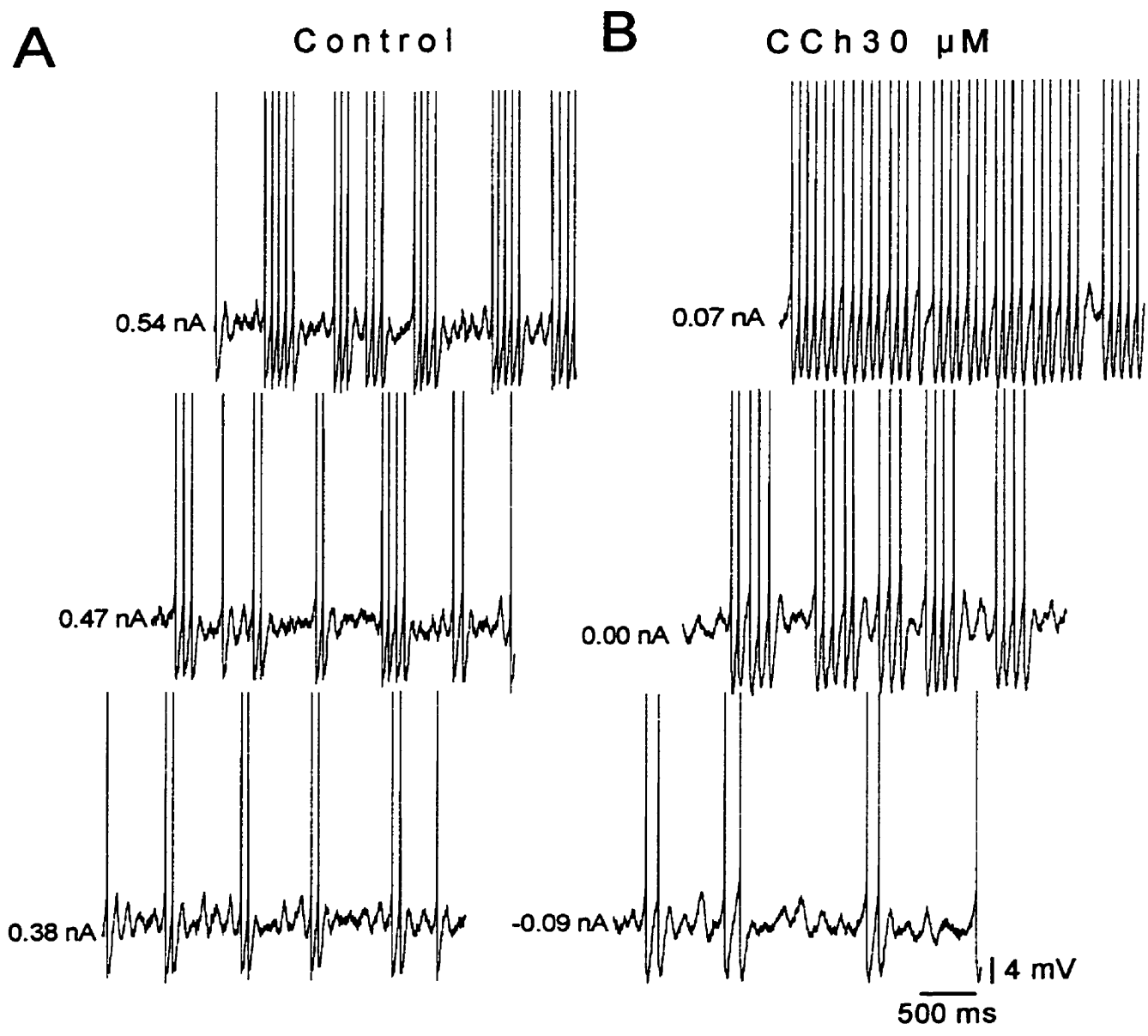
A
Control
B
CCh30 µM
0.54 nA
0.47 nA
0.38 nA
0.07 nA
0.00 nA
-0.09 nA
4 mV
500 ms

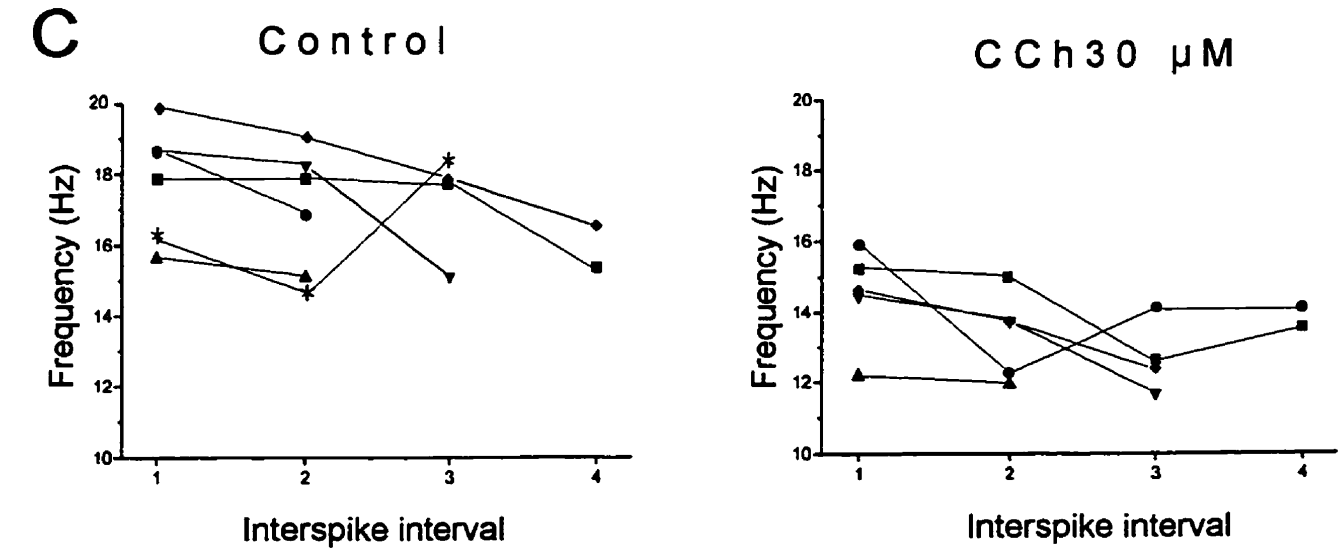
C
Control
CCh30 µM
Frequency (Hz)
Interspike interval
20
18
16
14
12
10
1
2
3
4

Figure 5. CCh action on SCs spike train adaptation and sAHP. *A*: Spike trains evoked by a 1.0 nA current pulse in control (left) and during CCh (right). Note the cessation of firing towards the end of the pulse in control as compared to the regular dischargue during CCh. *B*: control (left) and CCh (middle) traces from A at a condensed time scale, and superimposition (right) ; CCh block selectively the sAHP without affecting the medium AHP (✱).

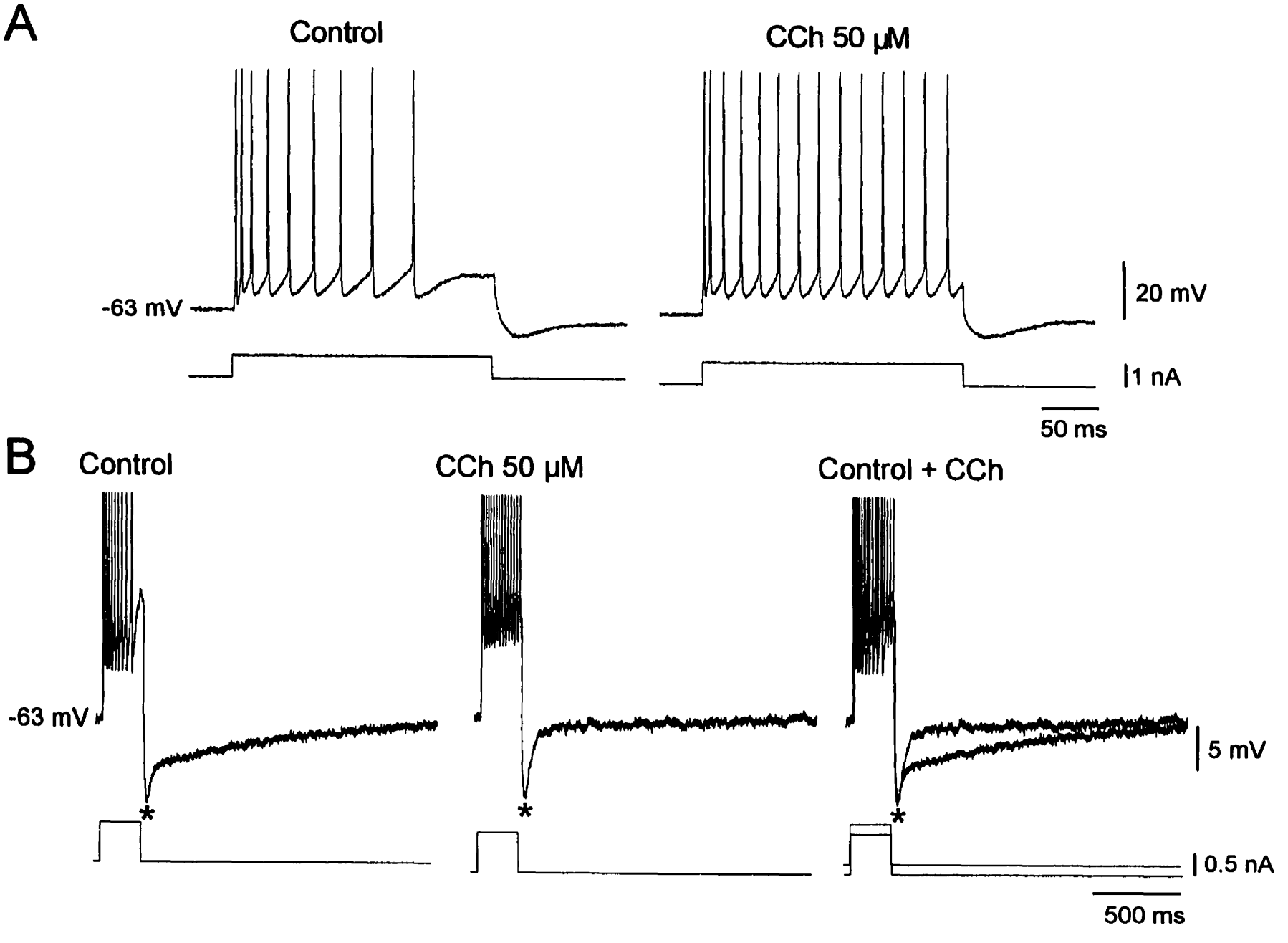
A
Control
CCh 50 µM
-63 mV
20 mV
1 nA
50 ms
B
Control
CCh 50 µM
Control + CCh
-63 mV
5 mV
0.5 nA
500 ms

Figure 6. CCh actions on SCs input-output relations. *A*: instantaneous firing frequency *vs* injected current (*f-I*) in control (left) and CCh (right). For the first ISI, the bilinear *f-I* relation in control became simply linear in CCh without a significant change in mean slope; for second and third ISIs, *f-I* slopes were slightly smaller in CCh and were increased for latter ISIs. *B*: Instantaneous firing rate *vs* time (*f-t*) for a 240 ms pulse of 1.0 nA in control (■) and during CCh (▲). CCh had only a clear effect on adaptation after 50ms of pulse onset. Dotted lines are double exponential fits to data points. *C*: Spike number *vs* injected current (S_n-*I*). CCh (▲) increased spike numbers at all injected current intensities with a more pronounced effect at higher amplitudes. All plots taken from the same cell.

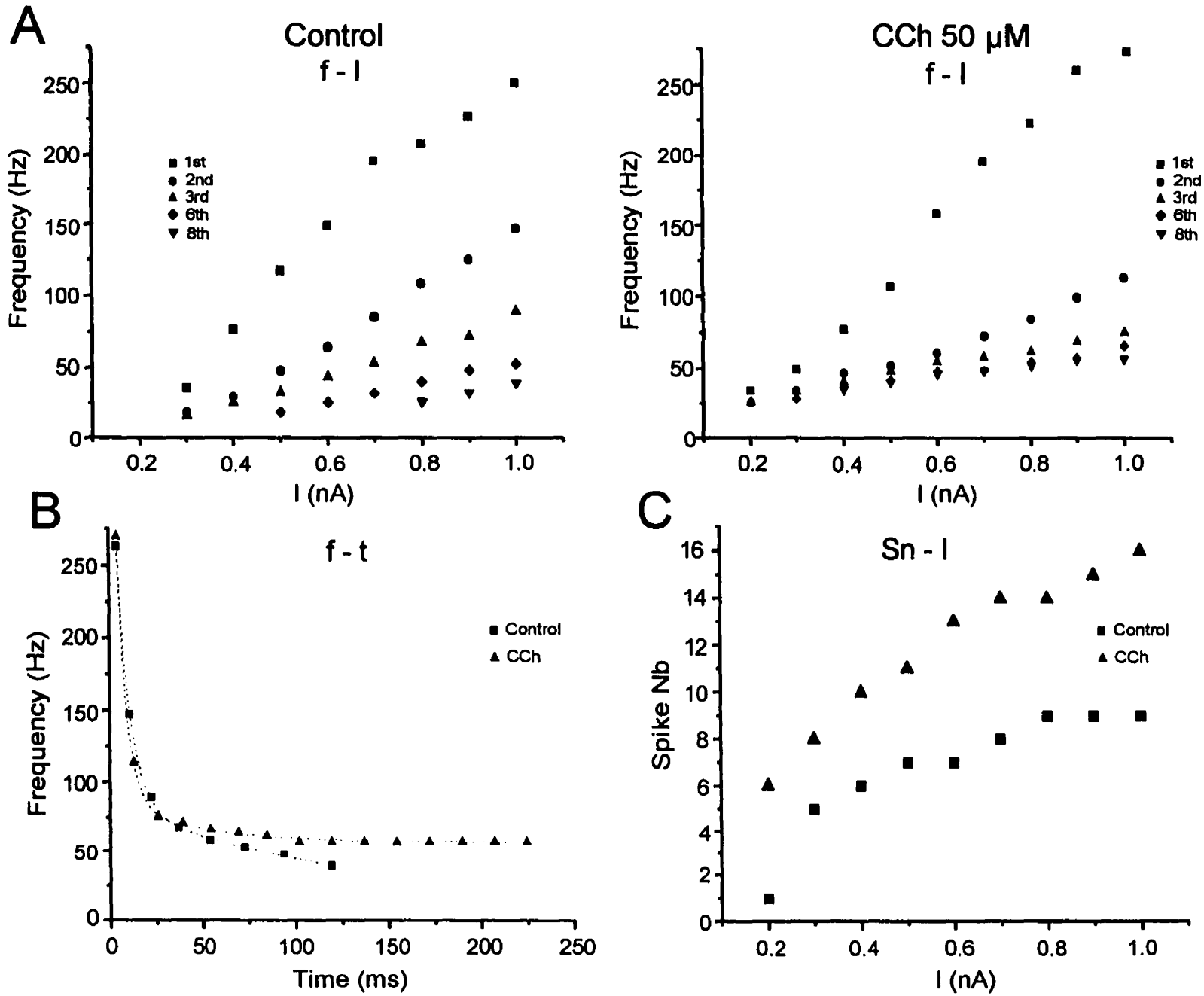
A
Control
f - I
Frequency (Hz)
I (nA)
1st
2nd
3rd
6th
8th
CCh 50 µM
f - I
B
f - t
Time (ms)
Control
CCh
C
Sn - I
Spike Nb

Figure 7. CCh actions on SCs action potential and afterpotentials. *A*: CCh reduced the fast AHP (▲) without affecting the medium AHP (✱). Insets show action potential at an expanded time scale. *B*: In another SC, details on action potential waveform. CCh raised firing threshold by ~1 mV, reduced amplitude by ~ 10% and reduced spike rate of rise by ~ 30%. Superimposition "control + CCh" shows CCh trace delimited by arrows.

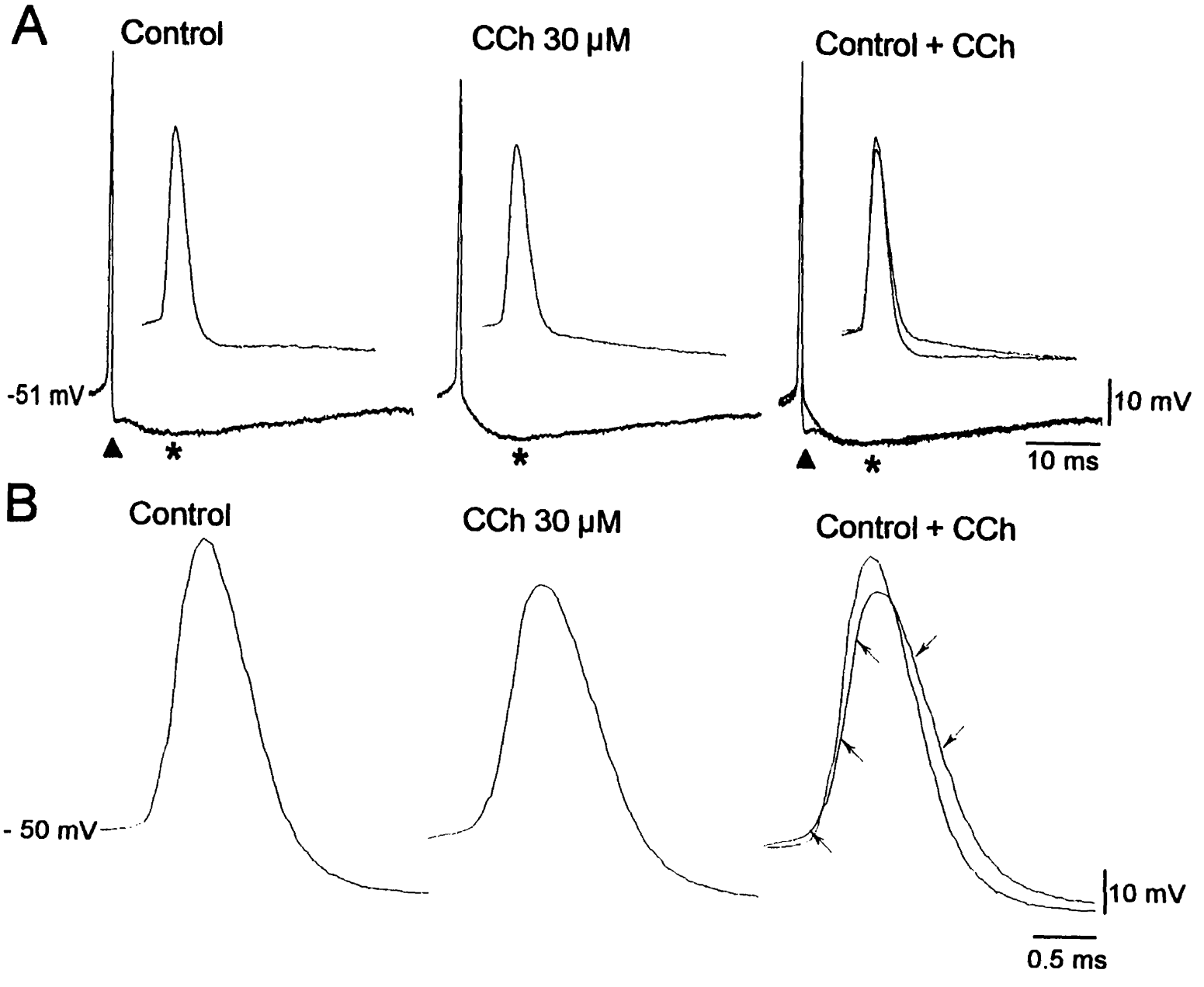
A
Control
CCh 30 µM
Control + CCh
-51 mV
10 mV
10 ms
B
Control
CCh 30 µM
Control + CCh
- 50 mV
10 mV
0.5 ms

Figure 8. CCh blocks a TTX-sensitive subthreshold potential in SCs. *A*: Voltage responses to low amplitude subthreshold depolarizing (upper row) and hyperpolarizing (lower row) current pulses in control, during CCh (30 μM) and washout. Note (control + CCh superimposition, rightmost panels) that CCh selectively blocked a voltage "sag" response triggered by depolarization and the rebound potential at the break of the hyperpolarizing current pulse. *B*: in another SC, the depolarization-induced sag response suppressed by CCh (top 3 panels) is also fully blocked by TTX (bottom panel, left); addition of CCh to TTX (bottom panel, middle) did not affect the voltage responses to the current pulses.

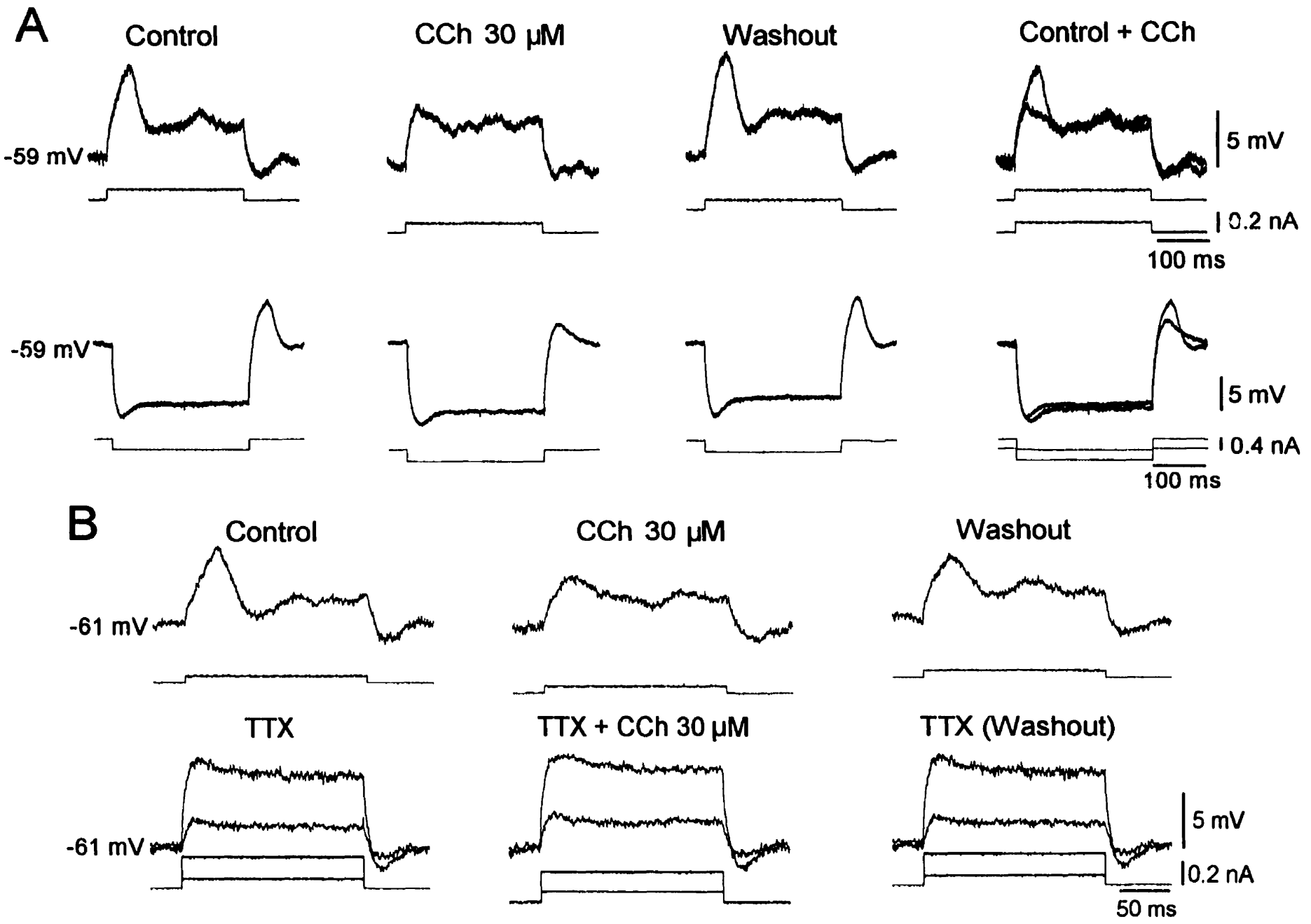
A
Control
CCh 30 µM
Washout
Control + CCh
-59 mV
5 mV
0.2 nA
100 ms
-59 mV
5 mV
0.4 nA
100 ms
B
Control
CCh 30 µM
Washout
-61 mV
TTX
TTX + CCh 30 µM
TTX (Washout)
-61 mV
5 mV
0.2 nA
50 ms

Figure 9. CCh promotes bursting in non-SCs. *A*: CCh (30 μM) depolarized the cell by ~4 mV without measurable change in apparent input resistance at the control resting level. Application of a 230 ms, 0.1 nA depolarizing pulse (vertical arrow under current trace) triggered a transient slow repetitive bursting behavior which could be switched on permanently by further d.c. depolarization. *B*: enlarged boxed area in *A*; triggered bursts were sustained by a long lasting (50 s) plateau potential; individual bursts lasted for 2-5 s and occurred ~ every 6 s. *C*: enlarged boxed area in *B*; the initial burst considerably outlasted the duration of the current pulse. *D*: Afterpotentials to current pulse depolarization in normal Ringer (left panel), in the presence of CCh only (30 μM, middle panel) and in the presence of CCh (30 μM) and TTX (1 μM) to block Na^+-conductances (right panel).

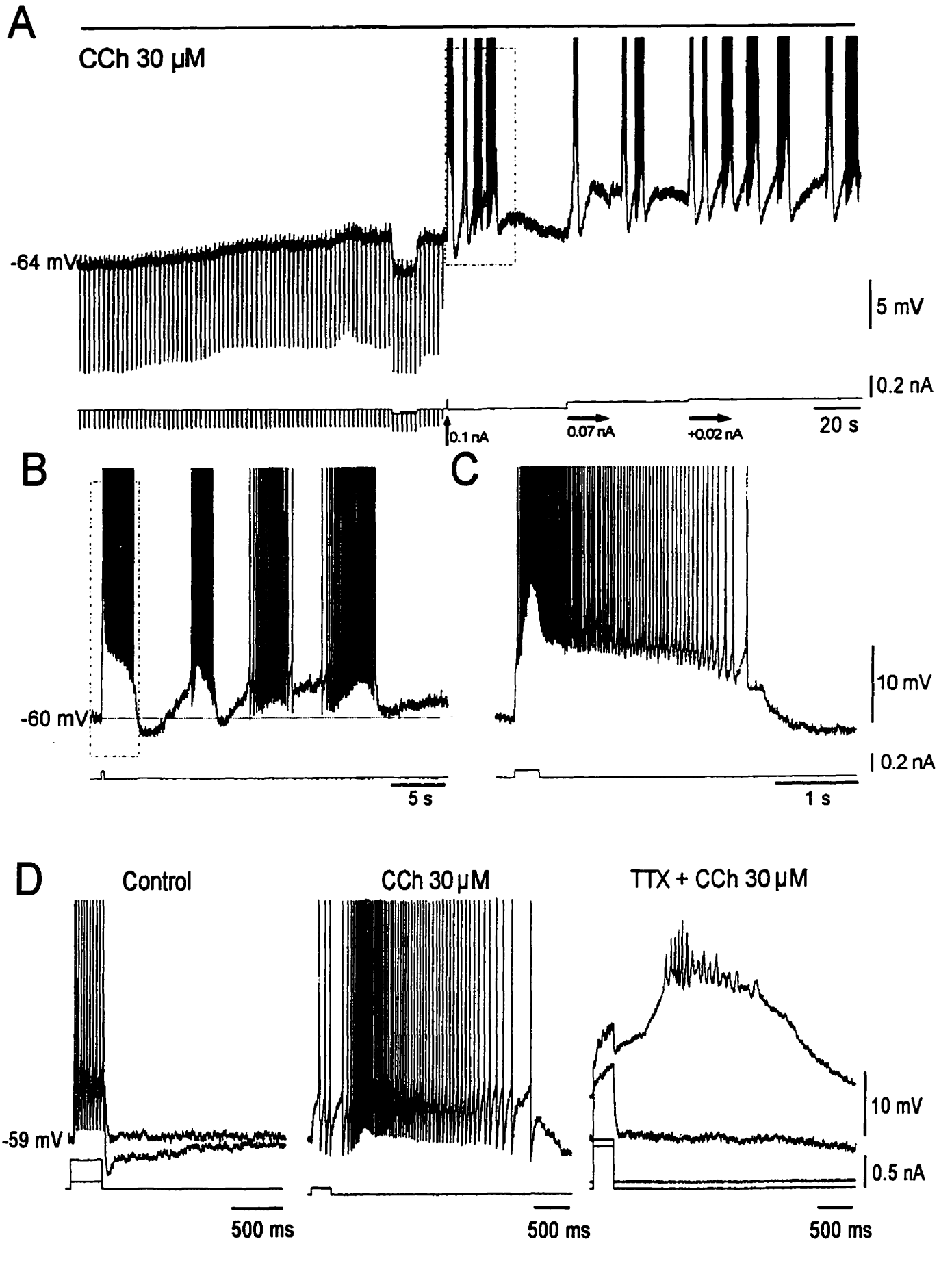
A
CCh 30 µM
-64 mV
5 mV
0.2 nA
0.1 nA
0.07 nA
+0.02 nA
20 s
B
-60 mV
5 s
C
10 mV
0.2 nA
1 s
D
Control
CCh 30 µM
TTX + CCh 30 µM
-59 mV
10 mV
0.5 nA
500 ms
500 ms
500 ms

Figure 10. Voltage-dependence of CCh-induced bursting pattern. *A*: in a non-SC, in normal Ringer, increasing levels of d.c. depolarization (bottom to top) elicited tonic firing at corresponding increasing frequencies. *B*: in the same neuron, CCh (30 μM) caused bursting discharge in a voltage-dependent manner. Bursting can be turned off by d.c hyperpolarization (not shown) or by substantial d.c. depolarization (upper panel, 0.11 nA).

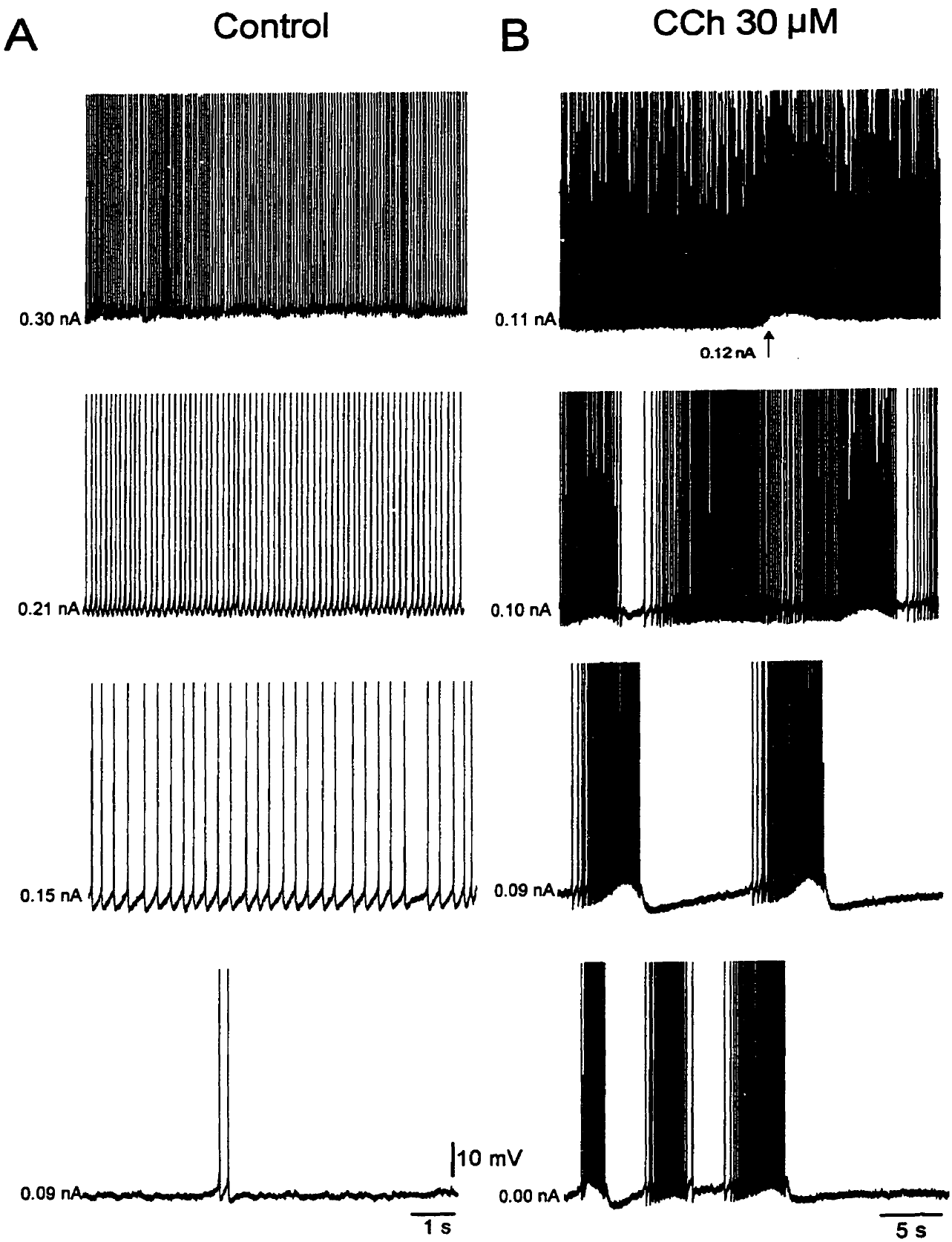
A
Control
B
CCh 30 µM
0.30 nA
0.11 nA
0.12 nA
0.21 nA
0.10 nA
0.15 nA
0.09 nA
10 mV
0.09 nA
0.00 nA
1 s
5 s

Figure 11. The slow AHP can be modulated via the cAMP second messenger pathway in SCs, but not in non-SCs. *A*: in non-SCs neither 8CPT-cAMP, 300 μM (leftmost two panels), nor the monoamine 5-HT, 30 μM (rightmost two panels), affect the sAHP or spike train adaptation (insets). *B*: in SCs, 8CPT-cAMP, 200 μM (leftmost two panels) and 5-HT (rightmost two panels) block the sAHP and adaptation (insets). In all cases, the sAHP was evoked by generating a train of 27 spikes at 70 Hz with 2 ms suprathreshold current pulses. The spike-trains in the insets were generated by depolarizing constant current pulses. In both SCs and non-SCs, 5HT caused a ~2 mV hyperpolarization (not shown).

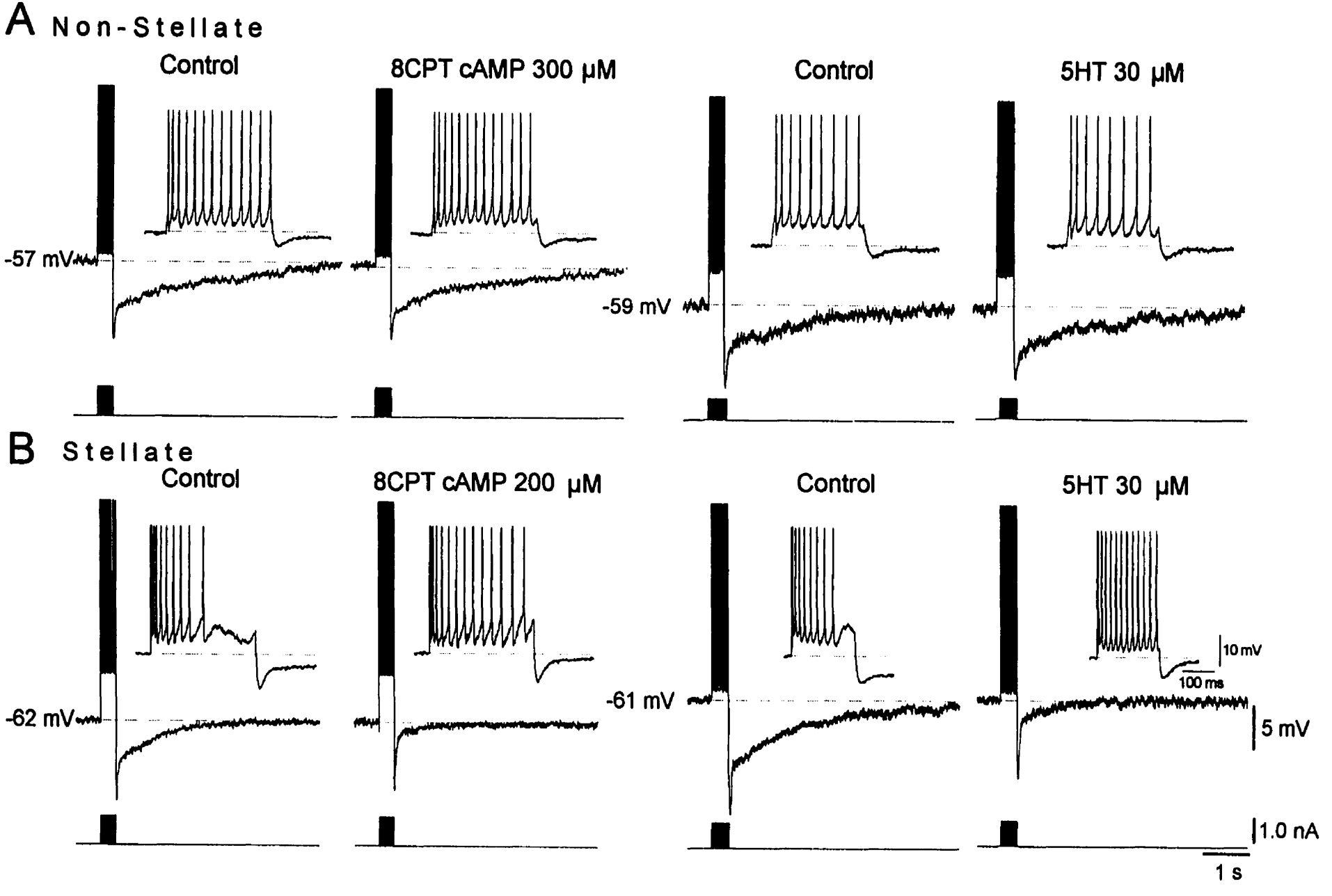
A Non-Stellate
Control
8CPT cAMP 300 µM
Control
5HT 30 µM
-57 mV
-59 mV
B Stellate
Control
8CPT cAMP 200 µM
Control
5HT 30 µM
-62 mV
-61 mV
10 mV
100 ms
5 mV
1.0 nA
1 s

CHAPTER VI

IONIC MECHANISMS OF MUSCARINIC DEPOLARIZATION IN ENTORHINAL CORTEX LAYER II NEURONS

Ruby Klink and Angel Alonso

ABBREVIATIONS

ADP	after-depolarizing potential
AHP	after-hyperpolarizing potential
CCh	carbachol
$InsP_3$	inositol triphosphate
MEC	middle entorhinal cortex
Rin-Vm	slope input resistance-membrane potential
SC	stellate cell
V-I	voltage-current

SUMMARY AND CONCLUSIONS

1. Cholinergic muscarinic depolarizing mechanisms in medial entorhinal cortex (MEC) layer II principal neurons were investigated in tissue slices *in vitro* by means of intracellular recording under current clamp and pressure-pulse applications of carbachol (CCh).
2. In normal Ringer solution, CCh triggered membrane voltage depolarizations that, for any given dose, were of similar magnitude in both the stellate cells (SCs) and non-SCs. However, during voltage-gated Na^+ conductance block with tetrodotoxin (TTX, 1μM), CCh depolarizations were much larger (2-5 fold) in non-SCs than in SCs. Also, in non-SCs, in these conditions, CCh depolarizations could be accompanied by spike-like large amplitude membrane voltage oscillations at a slow frequency (0.02-0.2 Hz).
3. Subthreshold CCh depolarizing responses were greatly potentiated in amplitude and duration when paired to a short (5-10 s) manual d.c. depolarization that triggered cell firing. In TTX-containing Ringer, CCh depolarizations were also potentiated by brief d.c. depolarizations positive to -50 mV to allow Ca^{2+} influx and the magnitude of the potentiation was ~3.5 times larger in non-SCs than in SCs.
4. In both SCs and non-SCs, the voltage-current relations (V-Is) were similarly affected by CCh which caused a shift to the left of the steady state V-Is over the entire voltage range explored (-40 to -95 mV). A plot of slope input resistance *vs* membrane potential (Rin-Vm) revealed, however, a CCh-induced increase in apparent slope input resistance at potentials positive to ~ - 70 mV, and a decrease, or occasionally no change, in slope input resistance below ~ -70 mV. Potentiated CCh responses by Ca^{2+} influx demonstrated a selective increase in slope input resistance at potentials positive to ~ -75 mV in relation to the non-potentiated responses.
5. K^+ conductance block with Ba^{2+} (1 mM), TEA^+ (5-20 mM), or intracellular injection of Cs^+ (3M), neither abolished CCh depolarizing responses nor resulted in any

qualitatively distinct effect of CCh on the V-I relations. CCh depolarizations were also undiminished by block of the time-dependent inward rectifier I_h with extracellular Cs^+ (2 mM) alone or in combination with K^+ conductance block.

6. CCh depolarizing responses were abolished during Ca^{2+} conductance block by superfusion with low Ca^+ (0.5 mM) solutions containing Cd^{2+} (200 μM), Co^{2+} (2 mM) or Mn^{2+} (4 mM), as well as by intracellular Ca^{2+} chelation with BAPTA (200 mM). The depolarization was not affected by pharmacological block of ionotropic and metabotropic glutaminergic transmission.
7. During superfusion with strophanthidin (20-60 μM), a reversible Na^+-K^+-ATPase inhibitor, CCh triggered larger depolarizing responses. On the other hand, when NaCl was replaced by an equimolar amount of N-methyl-D-glucamine, CCh depolarizing responses were largely diminished.
8. CCh depolarizing responses were fully antagonized by pirenzepine at concentrations of 0.8 μM, whereas p-F-HHSiD (5 μM) and himbacine (13 μM) were only effective antagonists at 5-10 fold larger concentrations.
9. It is concluded that despite the differential modulatory effect of CCh on the SCs and non-SCs firing behavior (Klink and Alonso 1996), the same mechanism underlies the CCh triggered depolarization in both types of cells. Our data are consistent with the CCh-triggered depolarization being mediated primarily by m1 receptor activation of a Ca^{2+}-dependent cationic conductance largely permeable to Na^+. Activation of this conductance is greatly potentiated in a voltage dependent manner by activity triggering Ca^{2+} influx. This property implements a Hebbian-like mechanism whereby muscarinic receptor activation may only be translated into substantial membrane depolarization if coupled to post-synaptic cell activity. Such a mechanism could be highly significant in light of the key role of EC layer II in learning and memory as well as in pathologies such as temporal lobe epilepsy and Alzheimer's dementia.

INTRODUCTION

Acetylcholine, via muscarinic receptors, is known to exert profound control over the excitability of many CNS neurons by modulating multiple ionic channels. In cortical neurons, excitatory actions of muscarinic agonists have been attributed to suppression of several K^+ currents (see Krnjevic 1993 for recent review). These include the voltage and time dependent M-current (I_M), the slow Ca^{2+}-activated K^+ current (I_{AHP}), the fast transient outward current (I_A), and a resting "leak" conductance. However, it has been frequently recognized that block of K^+ conductances can not account for all depolarizing actions of muscarinic receptor activation in CNS neurons. Membrane conductance changes observed in hippocampal pyramidal cells during muscarinic depolarization led to the postulate of cholinergic activation of a cationic conductance (Benson et al. 1988; Segal 1982). Also, the muscarinic induction of a slow after-depolarizing potential (ADP) in hippocampal (Benardo and Prince 1982; Caeser et al. 1993; Gähwiler and Dreifuss 1982; Fraser and MacVicar 1996) and neocortical (Andrade 1991; Schwindt et al. 1988) pyramidal cells has been attributed to the cholinergic potentiation of a Ca^{2+}-activated nonspecific cationic conductance. Moreover, it is well known that in mammalian smooth muscle cells, muscarinic receptor activation causes membrane depolarization by acting primarily on a non-selective cationic conductance which is potentiated by a rise in intracellular Ca^{2+} concentration (Benham et al. 1985; Inoue and Isenberg 1990b; Pacaud and Bolton 1991)

In an accompanying paper (Klink and Alonso 1996), we described the modulatory action of muscarinic receptor activation on the intrinsic excitability of the two electrophysiologically and morphologically distinct types of projection neurons in layer II of the medial entorhinal cortex (MEC), the stellate cells (SCs) and the non-stellate cells (non-SCs) (Alonso and Klink 1993). Bath application of the cholinergic agonist carbachol (CCh), acting via atropine sensitive receptors, was found to depolarize both SCs and non-

SCs while differentially modulating their oscillatory and firing behavior. In non-SCs, in particular, firing was drastically modified with induction of a slow rhythmic bursting pattern ostensibly driven by a TTX-insensitive plateau potential.

The present work aims at elucidating the principal ionic mechanism generating the CCh-induced depolarization in EC layer II neurons. In particular, the induction of slow TTX-insensitive plateau potentials in non-SCs led us to examine whether activation of a Ca^{2+}-dependent cationic conductance plays a role in cholinergic depolarization, and if so, through which pharmacological subtype of muscarinic receptor.

METHODS

The materials and methods used for the preparation of EC slices and recording are as those described in the accompanying and previous papers (Alonso and Klink 1993; Klink and Alonso 1996) with the exception that in the present experiments an interface recording chamber was used. The normal Ringer solution contained (in mM): NaCl 124; KCl 5; KH_2PO_4 1.2; $CaCl_2$ 2.4; $MgSO_4$ 2.6; $NaHCO_3$ 26; glucose 10. pH was adjusted to 7.4 by saturating with 95% O_2- 5% CO_2. In experiments where the effects of Cd^{2+}, Co^{2+}, Mn^{2+} or Ba^{2+} were tested, phosphate and sulfate were omitted to avoid precipitation and divalent cations were maintained at a normal concentration by adjusting the Mg^{2+} concentration. In order to block Na^{+}-conductances, tetrodotoxin (TTX, 1μm) was routinely used. N-methyl-D-Glucamine (NMDG) Ringer consisted of normal Ringer or TTX Ringer in which NaCl (124 mM) was substituted with NMDG (124 mM). Carbachol (CCh; 10 mM dissolved in bath solution) was delivered by pressure pulse (15-20 psi) applications of variable duration (5-1000 ms) through a patch pipette (tip diameter 2 μM) positioned in close proximitiy to the entry point of the recording electrode. The muscarinic antagonists atropine, pirenzepine, himbacine and p-F-HHSiD were bath applied at the specified concentrations for exactly 20 minutes at a rate of 2 ml/min prior to CCh test

applications. Antagonists were tested at the following concentations (μM), in the given order: atropine, 0.2, 0.3; pirenzepine, 0.3, 1.3, 0.6, 1.0, 0.8; himbacine, 1.5, 13.0, 10.0; p-F-HHSiD, 2.5, 7.5, 5.0, 4.0. We estimated the "minimal" antagonist concentration necessary to inhibit the CCh response as that concentration that reduced the response to less than 10% of control. 2-amino-5-phosphonovaleric acid (AP-5; 100 μM), 6-cyano-7-nitroquinoxaline-2,3-dione (CNQX; 10 μM), α-methyl-4-carboxyphenylglycine (MCPG; 500 μM), strophanthidin (20-60 μM), were bath applied for at least 20 minutes before test applications of CCh. The apparent slope input resistance of the cells was estimated from the first derivative (using Origin™ analysis package) of voltage-current relationship (V-I) plots constructed from the membrane voltage responses to square current pulses.

Strophanthidin, atropine, and AP-5 were purchased from Sigma, pirenzepine and p-F-HHSiD from RBI, CNQX and MCPG from Tocris Cookson and himbacine was a generous gift from W.C. Taylor, Australia.

Data are given as mean ± standard deviation. Significance was tested according to the one or two-tailed Student t test.

RESULTS

The present study is based on intracellular recordings from 79 neurons in layer II of the MEC to which pressure pulse applications of the cholinergic agonist CCh were delivered. At the CCh application intervals used in this study (≥5 min), multiple test pulses could be delivered to the same neuron without any observable desensitization of the CCh response. Recording selection criteria were as described in the preceeding paper (Klink and Alonso 1996). Neurons fell into the two previously described morphological and electrophysiological classes (Alonso and Klink 1993), the SCs (Vrest=-62.8±2.2 mV; n=37, 3 of which were morphologically identified) and non-SCs (Vrest=-63.6±2.0 mV; n=42, 4 of which were morphologically identified).

CHARACTERISTICS OF THE DEPOLARIZATION

In control Ringer, pulse applications of CCh (5-600 ms; n=48) resulted in membrane potential depolarizing responses of similar characteristics in SCs and non-SCs (Fig. 1A). For any given neuron, the amplitude and duration of the depolarization increased with increasing CCh pulse durations and typically consisted of a fast rising and a slow decaying phase (Fig. 1B).

(Fig. 1 near here)

In TTX containing Ringer, however, CCh applications (5-1000 ms; n=49) resulted in membrane potential depolarizations of apparent larger amplitude and duration in non-SCs than in SCs (Fig. 2A). Also, in non-SCs exclusively, CCh frequently triggered (n=11/30) an initial spike-like response followed by a plateau potential (Fig. 2A, right). In addition, in some non-SCs (n=6/30) the initial spike-like response repeated for a few cycles (2-5) at a slow frequency (0.02-0.2 Hz) (Fig. 2B). This oscillatory phenomenon appeared to be cell specific and relatively dose independent. For any given non-SC that displayed the oscillatory response to CCh, increased doses of CCh increased the frequency

of the oscillation but not the number of cycles (Fig. 2C). With regard to the amplitude of the CCh depolarizations, in those non-SCs that did not display an initial spike-like response CCh, depolarizations averaged 10.5±11.3 mV (n=13; pulse duration of 372±309 ms), and in those non-SCs that displayed spike-like potentials the plateau phase averaged 10.2±4.2 mV (n=11; pulse duration of 194±184 ms). In SCs, CCh depolarizations were smaller, averaging 4.3±2.1 mV (pulse duration of 222±216 ms; n=19).

(Fig. 2 near here)

In an accompanying paper, we have shown that bath applications of CCh block, in both SCs and non-SCs, the sAHP that follows a train of spikes and, in non-SCs particularly, promote the development of robust depolarizing afterpotentials. Similarly, when CCh pulse-triggered subthreshold depolarizations were coupled to an additional brief (1-10 s) manual d.c. depolarization that elicited spiking, the magnitude of the CCh depolarizing response was largely enhanced in non-SCs and also, though to a lesser degree (see below), in SCs. This potentiation phenomenon was observed in all neurons tested (n=16; 9 SCs and 5 non SCs) and is illustrated for a typical non-SC in Fig. 3. Panel A shows a 4 mV depolarization that lasted for ~ 4 min in response to a 500 ms CCh pulse. Panel B shows, in a subsequent CCh application of equal duration, that a manual d.c. depolarization that triggered cell firing applied at the peak of the initial response induced a bi-stable state in which the cell continued to fire for a very prolonged period of time. This additional plateau depolarization could not be cut short by hyperpolarizing the membrane potential to the initial resting potential (Fig. 3B *). Also, note that neither during the initial subthreshold (A) nor the potentiated suprathreshold (B) depolarization, did the apparent input resistance significantly change (see below).

(Fig. 3 near here)

During Na^+ conductance block with TTX, the magnitude of CCh pulse depolarizations was also greatly potentiated by superimposing a brief manual d.c. depolarization to about -40mV (n=17) (Fig. 4). It became apparent that during TTX the

phenomenon was far more prominent in non-SCs than in SCs, and this was related to the ease by which Ca^{2+} spiking (Fig. 4B, *) was triggered in non-SCs *vs* SCs. In SCs, initial CCh depolarizations of 2.6±1.2 mV increased by 2.2±1.8 mV (~ 100%; n=8) after ~10 s manual d.c. depolarizations positive to -50 mV. In non-SCs, initial CCh depolarizations of 2.1±1.4 mV increased by 7.0±3.9 mV (~ 350%; n=9) after similar manual d.c. depolarizations.

(Fig. 4 near here)

VOLTAGE-CURRENT RELATIONSHIPS

As in the case illustrated in Fig. 3, in most neurons tested (17/22) the CCh-triggered depolarization was not associated with a measurable change in apparent input resistance (Ri) at resting membrane potential , and in the other cells only a minor increase in R_i (8.4±3.6%) was observed. To assess conductance changes more fully, voltage-current (V-I) relationships estimated before and during CCh depolarizations were compared. Since layer II neurons possess the time-dependent hyperpolarization-activated inward rectifier I_h (Klink and Alonso 1993), both peak and steady state V-I plots were constructed from the voltage responses to inward and outward current steps (Fig. 4).

Fig. 5 depicts for a SC (A) and a non-SC (B) typical peak (left column) and steady-state (right column) V-I plots constructed before (filled symbols) and during CCh triggered depolarization (open symbols). The V-I relations of SCs and non-SCs, while differing with regard to the range and magnitude of inward and outward rectification (Klink and Alonso 1993), were similarly affected by CCh . In all neurons tested (n=12), CCh induced a shift to the left of the steady-state V-Is over the entire voltage range explored (-40 to -95 mV) (Fig. 5, right). This shift was, however, larger at potentials positive to ~ -70 mV. With respect to the peak V-Is (Fig.5, left), CCh induced an overall increase in their slope with convergence of the V-Is at -80 to -90 mV. To rule out that these observations were caused by spurious effects due to the mode of application of CCh,

we constructed V-Is following bath applications of CCh (n=5), and exactly the same pattern was observed.

To better detect the changes in the slope of the V-Is induced by CCh, which reflect CCh's actions on the membrane apparent input resistance, we estimated the first derivative of the control and CCh V-I plots (see methods) and constructed plots of slope input resistance *vs* membrane potential (Rin-Vm; n=12; Fig. 5 A and B, insets). In all cases, comparison of control and CCh peak Rin-Vm plots demonstrated an overall increase in the slope input resistance at potentials positive to ~ -75 mV and no significant change at more negative voltages. With respect to the steady-state Rin-Vm plots, in all cases, these also demonstrated an increase in the slope input resistance at potentials positive to ~ -70 mV, but, in most cases (8/12 neurons), a decrease at more negative voltages.

(Fig. 5 near here)

Given the potentiation of the CCh responses by membrane depolarization (and thus Ca^{2+} influx; Fig. 4), it appeared of interest to look for possible differences in the V-I relationships of non-potentiated (e.g. Fig. 4A) vs potentiated (e.g. Fig. 4B) CCh depolarizations. As in the case illustrated in Fig. 6 A and B (same neuron as in Fig. 4), in all neurons tested (n=4), the potentiated steady state V-Is (crossed circles) demonstrated a selective increase in slope with respect to the CCh non-potentiated V-Is (open circles) at potentials positive to ~ -75mV (Fig. 6, left). This voltage-dependent enhancement was more clearly manifested when comparing the CCh non-potentiated and potentiated Rin-Vm plots (Fig. 6B).

(Fig. 6 near here)

Several mechanisms could be responsible for the leftward shifts in the V-I relationships induced by CCh such as: a) stimulation of an electrogenic pump or ion exchanger; b) changes in a distant dendritic conductance; c) compound actions of opposite direction in different conductances; or d) changes in a conductance with a positive reversal

potential well out of the range explored. In the following sections we describe experiments aimed to distinguish between these various possibilities.

EFFECT OF VARIOUS ION CHANNEL BLOCKERS

In hippocampal pyramidal cells, inhibition of a "leak" K^+ conductance seems to be the main mechanism underlying the cholinergic depolarization observed at rest (Krnjevic 1993), and the K^+-channel blockers TEA^+ and Ba^{2+} have been shown to abolish the CCh-induced depolarization (Benson et al. 1988). Neither TEA^+ (5-20 mM; n=7) nor Ba^{2+} (1 mM; n=3) (not shown) diminished the CCh responses in MEC layer II neurons thus suggesting that a mechanism other than K^+-conductance block may be primarily responsible for muscarinic dependent depolarization in EC layer II neurons.

To give stronger support to the above hypothesis, we also tested whether a more powerful block of K^+ conductances by intracellular injection of Cs^+ ions would block or affect the V-I characteristics of the CCh depolarizing response. In an initial set of experiments we performed intracellular injections of Cs^+ alone (3M; n=4), or in combination with extracellular Ba^{2+} perfusion (1mM; n=3) to maximize "leak" K^+ conductance block. As in the case illustrated in Fig 7A, under either of the above experimental conditions, short CCh pulse applications (100 ms top; 40 ms bottom) always resulted in very robust membrane depolarizations in all SCs and non-SCs tested (n=7). Moreover, the changes in the V-I relations induced by CCh in Cs^+ injected neurons (Fig. 7B) were qualitatively the same as those observed in neurons recorded with K^+ containing electrodes and described in detail above. It thus appears that in MEC layer II neurons (SCs and non-SCs) K^+ conductances do not play an important role in the CCh depolarizing response.

(Fig. 7 near here)

As mentioned above, CCh frequently, though not always, induced a small decrease in the steady-state slope resistance at potentials negative to ~ -70mV (Fig. 5 and Fig. 8A

and B, left panels). This could be caused by a CCh enhancement of the time-dependent inward rectifier (I_h) that EC layer II neurons posses (Klink and Alonso 1993). Indeed, CCh application during exclusive I_h block with extracellular Cs^+ (2mM; n=3) did not cause any decrease in slope resistance at negative voltages (Fig. 8B, right panel), though CCh still produced membrane depolarizations (6.3±2.4 mV) undiminished from those in control (6.0±2.8 mV), and a parallel shift in the V-I relation (Fig. 8A, right panel; n=3). CCh was also effective in causing robust membrane depolarization and a parallel shift in the V-I relation during combined K^+-channel block with intracellular Cs^+ (3M) and extracellular Ba^{2+} (1mM), and Ih block with extracellular Cs^+ (3mM; n=6) (Fig. 8C and D). Under these pharmacological conditions the CCh-induced membrane depolarization can not be ascribed to a combined I_h enhancement and K^+-conductance block by CCh

(Fig. 8 near here)

CA^{2+} DEPENDENCE

The data presented above indicate that in MEC layer II SCs and non-SCs, CCh-induced depolarizations and associated changes on V-I relations do not result from major CCh actions on K^+ conductances. We then tested for the possible Ca^{2+} dependence of the CCh depolarizations by pulse applying the drug during Ca^{2+} conductance block with inorganic Ca^{2+} channel blockers. As in the case illustrated in Fig. 9A, superfusion with low Ca^{2+} solutions (0.5mM) containing either Cd^{2+} (n=4) , Co^{2+} (n=2) or Mn^{2+} (n=3) largely abolished (from 8.0±4.5 mV to 1.1±1.2 mV) the depolarizing response to CCh in both SCs (n=4) and non-SCs (n=5). This was true for both the direct depolarizing effect as well as the post-depolarization (potentiated response) following d.c. membrane depolarization (note the current trace in Fig. 9A). This result suggests that Ca^{2+}-entry and a possible rise in intracellular Ca^{2+} concentration ($[Ca^{2+}]_{in}$) may be responsible for the CCh induced depolarization. To test this possibility we performed CCh applications in neurons recorded with electrodes containing the Ca^{2+} chelator BAPTA (200 mM). As illustrated in Fig. 9B,

40-50 min following impalement, the depolarizing responses to CCh were abolished in all cells (Fig. 9B, 42') (n=2 SC and 3 non-SCs) with the exception of minimal effects triggered when the CCh dose was highly increased (Fig. 9B, 48'). However, this residual CCh action could not be potentiated by d.c. depolarization. These data suggests that muscarinic receptor activation in MEC layer II neurons causes membrane depolarization by activating a depolarizing conductance and that this activation is dependent upon $[Ca^{2+}]_{in}$. To further eliminate the unlikely possibility that blockade of the CCh responses by Ca^{2+}-channel blockers results from block of TTX-insensitive presynaptic cholinergic receptor-mediated release of a depolarizing neurotransmitter, we applied CCh during block of ionotropic and metabotropic glutamate receptors. A mixture of AP-5 (100 μM), CNQX (10 μM) and MCPG (500 μM) had no effect on the CCh induced depolarizing responses (n=3; not shown).

(Fig. 9 near here)

INVESTIGATION OF THE ELECTROGENIC Na^+-K^+-ATPASE PUMP MECHANISM

The parallel shift in V-I relationships caused by CCh could be due to an activated ionic flux through an electrogenic pump or exchange mechanism, thereby affecting membrane battery without producing changes in membrane resistance. Depolarization induced by cholinergic depression of the sodium pump was investigated, since receptor-mediated, Ca^{2+}-dependent modulation of this ATPase by neurotransmitters has been described in central neurons (Phillis and Wu 1981). As in the case illustrated in Fig. 10, in all neurons tested (n=2 SCs and 2 non-SCs), CCh pulse-application during superfusion with TTX and strophanthidin (20-60 μM), a reversible inhibitor of the Na^+-K^+-ATPase (Thompson and Prince 1986), resulted in an enhanced membrane potential depolarization that persisted until strophanthidin washout. This result indicates that the CCh-induced depolarization is not due to Na^+-K^+-ATPase block.

(Fig 10 near here)

THE CCH DEPOLARIZATION CONSISTS MOSTLY OF A Na^+ SENSITIVE COMPONENT

Since in mammalian smooth muscle cells, activation of muscarinic receptors induces a cationic current which is largely facilitated by a rise in intracellular Ca^{2+} concentration (Benham et al. 1985; Inoue and Isenberg 1990a; Inoue and Isenberg 1990b; Sims 1992), we next considered the possibility that the CCh depolarization results from activation of a non-specific cation channel with a high permeability to Na^+. Na^+ dependence was tested for by replacing extracellular Na^+ with equimolar concentrations of N-methyl-D-glucamine ($NMDG^+$), which does not permeate non-specific cation channels (n=3 SCs; n=5 non-SCs). As illustrated in Fig. 11, in control Ringer (panel A) or TTX Ringer (panel C) CCh applications that evoked robust depolarizations in control were largely reduced but still potentiated by manual depolarization during Na^+ substitution ($NMDG^+$ 124 mM; Na^+ 26 mM). The blockage was entirely reversible following washout of $NMDG^+$ (Fig. 11C, bottom). It is to be noted that perfusion with $NMDG^+$ did not compromise cell integrity (Fig. 11B).

(Fig. 11 near here)

PHARMACOLOGY OF THE CCH DEPOLARIZATION

As described in an accompanying manuscript (Klink and Alonso 1996), CCh effects on EC layer II neurons were entirely blocked by atropine (300 nM) (also shown here in Fig 12A) and thus dependent on the activation of muscarinic receptors. To further clarify the muscarinic receptor subtype responsible for the depolarizing action of CCh, we made use of pirenzepine, himbacine, and p-F-HHSiD, reported "selective" antagonists for the pharmacologically defined M1, M2 and M3 receptor subtypes, respectively (Hulme et al. 1990). Although binding studies have shown that each of the above antagonists has similar affinities for more than one molecularly defined receptor subtype (m1-m5), each of these subtypes shows a unique binding profile, as shown by Dörje et al. (1991). Thus, by

exploring the CCh-depolarization blocking profile for the three selected antagonists, one may narrow down pharmacologically the identification of the receptor subtype involved in the CCh depolarization. To address this issue, we estimated the "minimal" bath concentration of antagonist (see methods) necessary to inhibit the CCh depolarization. For pirenzepine, tested at concentrations from 0.3 to 1.3 μM (n=6) the minimal effective blocking concentration was found to be 0.8 μM (Fig 12B); for himbacine (1.5-13 μM; n=3), 13 μM (Fig 12C illustrates a residual CCh depolarization for a 10 μM antagonist concentration); and for p-F-HHSiD (1-5 μM; n=4), 5 μM. We then used these concentrations to estimate the p-F-HHSiD/pirenzepine, himbacine/pirenzepine and p-F-HHSiD/himbacine selectivity ratios which were 6.25, 16.25 and 0.38, repectively. Comparison of these ratios with those of the same antagonists estimated from their published affinities at the five cloned muscarinic receptors (Dörje et al. 1991) indicated a close match with the m1 receptor subtype (p-F-HHSiD/pirenzepine =3.55; himbacine/pirenzepine=16.99; p-F-HHSiD/himbacine=0.21) thus suggesting that the CCh depolarization is largely mediated by the m1 receptor subtype.

(Fig. 12 near here)

DISCUSSION

The results of the present study indicate that the slow membrane depolarization caused by CCh in EC layer II neurons is primarily generated by the activation of a Ca^{2+}-dependent non-specific cationic conductance. This observation is in contrast to what is found in hippocampal (Benson et al. 1988; Madison et al. 1987) or neocortical principal cells (McCormick and Prince 1986), where muscarinic receptor activation causes membrane depolarization primarily via block of K^+ conductance, though other depolarizing mechanisms, including the one reported here, probably also participate (Blitzer et al. 1991; Colino and Halliwell 1993; Guérineau et al. 1995). The robust Ca^{2+}-dependence of the cholinergic actions in EC neurons may have important functional implications given the

role of this structure in learning and memory (Alvarez and Squire 1994; Squire 1992) and the role of Ca^{2+} in neural plasticity (Gosh and Greenberg 1995; Henzi and MacDermott 1992).

Despite the differential modulatory actions of CCh on the oscillatory and firing pattern of stellate and non-stellate cells from EC layer II (Klink and Alonso 1996), the ionic mechanism underlying the basic CCh depolarizing response appeared to be the same in both cell types. In essence, in both stellate and non-stellate cells, CCh produced qualitatively equivalent changes on the V-I relations and the response displayed an equivalent ionic dependence and pharmacological profile. However, the CCh depolarizations were of larger amplitude and duration and were more strongly potentiated by Ca^{2+} entry in non-SCs than in SCs. This must be related to differences in the intrinsic membrane properties between both types of neurons such as, for example, the presence of a very robust subthreshold outward rectifier in SCs but not in non-SCs (Klink and Alonso 1993). This K^+ conductance is not blocked by CCh (Klink and Alonso 1993) and may effectively counteract the CCh-triggered inward current.

After cloning of the five muscarinic receptors (m1-m5), it was recognized that while the antagonist binding properties of the m2 and m3 receptors correlated well with those of the pharmacologically defined M2 and M3 subtypes, the antagonist binding properties of both m1 and m4 receptors were similar to those of the M1 receptors (Dörje et al. 1991). The fact that in EC layer II neurons CCh induced depolarizations were blocked by low concentrations (<1μM) of pirenzepine (M1-"selective") and only by ~10-fold higher concentrations of himbazine (m2- "specific", but with an affinity for m4 similar to that of pirenzipine for m1 (Dörje et al. 1991)) is a clear indication that the depolarizing responses were primarily (if not exclusively) mediated via the m1 receptor subtype. In fact, m1 receptors are known to have a preferential post-synaptic localization in cortical tissue (Levey et al. 1995) and it has been recently described that EC layer II projection neurons do express this receptor subtype (Rouse and Levey 1995). This data is consistent

with a direct postsynaptic action of CCh on layer II neurons as further indicated by our results demonstrating the persistence of the CCh response during synaptic transmission block with TTX, as well as during block of both ionotropic and metabotropic glutaminergic transmission.

CNS neurons possess several K^+ conductances that may be subject to modulation by acetylcholine and other neurotransmitters (see Storm 1990 for review). Decrease of several K^+ conductances has been shown to be the mechanism mainly responsible for the depolarization caused by muscarinic receptor activation in hippocampal and other cortical pyramidal cells (Benson et al. 1988; Halliwell and Adams 1982; Madison et al. 1987; McCormick and Prince 1986; Wang and McCormick 1993). However, in MEC layer II principal cells, K^+ conductance block does not seem to play a significant role in the CCh-triggered depolarization, as suggested by the absence of membrane conductance decrease with CCh and the enhanced depolarizing responses during K^+ conductance block with extracellular Ba^{2+} and TEA^+, and/or intracellular application of Cs^+.

EC layer II neurons display time-dependent inward rectification mediated by a hyperpolarization activated cation conductance (I_h) and this conductance has been shown to be subject to neuromodulation by neurotransmitters in other neurons (Bobker and Williams 1989; Colino and Halliwell 1993; Pape and McCormick 1989; Schwindt et al. 1992). Indeed, the small decrease in the steady state slope resistance below -70 mV that we observed with CCh suggests a minor enhancement of I_h by muscarinic receptor activation. This enhancement could have some contribution to the CCh depolarization. However, we found undiminished CCh responses during I_h block with extracellular Cs^+ indicating that the potential I_h contribution to the CCh depolarization, if present, must be minimal. In addition, during K^+ conductance block, CCh depolarizations were not accompanied by a membrane conductance increase at the resting level. This result is not compatible with I_h having a significant contribution to the CCh depolarization in EC layer II neurons.

On the other hand, CCh depolarizations were blocked by: 1) lowering extracellular Ca^{2+} concentration and bath applying the Ca^{2+} channel blockers Cd^{2+}, Co^{2+} or Mn^{2+}; 2) intracellular Ca^{2+} -chelation with BAPTA; and 3) substitution of extracellular Na^{+} by NMDG. Taken together these results suggest that in EC layer II neurons, CCh induces membrane depolarization by activating a cationic conductance, other than I_h, largely permeable to Na^{+} ions and that a rise in intracellular Ca^{2+} concentration largely due to Ca^{2+} influx is required for activating or controlling muscarinic receptor stimulation effects. It may be argued that simultaneous Na^{+} and Ca^{2+} dependence could denote activation of an electrogenic Na^{+}-Ca^{2+} exchange mechanism (Eisner and Lederer 1989). However, since the effectiveness of the Na^{+}-Ca^{2+} exchange process decreases with increased intracellular Na^{+} concentration (Fontana et al. 1995; Harrison and Boyett 1995), the robust CCh-triggered depolarization during inhibition of the Na^{+} pump with strophanditin is not compatible with a significant contribution of a Na^{+}-Ca^{2+} exchanger to the depolarization.

A recent study in insect motoneurons has also described the muscarinic induction of a Na^{+} current that requires external Ca^{2+} (Trimmer 1994) and it is also well known that in mammalian smooth muscle cells, activation of muscarinic receptors induces a cationic current which is largely facilitated by a rise in intracellular Ca^{2+} concentration (Benham et al. 1985; Inoue and Isenberg 1990a; Inoue and Isenberg 1990b; Sims 1992). With respect to the mammalian CNS, early studies by Segal (1982) and Benson et al. (1988) on CCh actions on hippocampal pyramidal cells already suggested that in addition to block of K^{+} conductances, muscarinic receptor activation could promote activation of a cationic current. More recently Caesar et al (1993) and Fraser and MacVicar (1996) have provided more direct evidence that in hippocampal pyramidal cells, muscarinic agonists activate a Ca^{2+}-dependent cation current mainly carried by Na^{+} and which gives rise to an afterdepolarizing potential and long lasting plateau potentials. Also, the activation of muscarinic receptors in prefrontal cortex neurons elicits a slow, maybe Ca^{2+}-dependent, cationic current (Andrade 1991; Haj-Dahmane and Andrade 1995) which appears to be the

primary drive underlying muscarinic depolarization (Haj-Dahmane and Andrade 1996). In locus coeruleus neurons muscarine also causes membrane depolarization, in part, by activating a cation conductance which is not Ca^{2+}-dependent (Shen and North 1992). A similar voltage and Ca^{2+}-insensitive cationic current activated by muscarinic agonists has also been recently described in the hippocampus (Guérineau et al. 1995).

It is known that in several cell types the m1 receptor subtype couples efficiently to the activation of phospholipase C (McKinney 1993), which leads to the production of inositol triphosphate ($InsP_3$) and subsequent mobilization of Ca^{2+} from intracellular stores (Berridge and Irvine 1989). This intracellular Ca^{2+} signal is likely to play an important role in mediating the CCh depolarization. The fact that the CCh responses were largely abolished by Ca^{2+}-conductance block suggests that a cooperativity between calcium influx and calcium store release may be required in order to produce a substantial depolarizing response ((Lo and Thayer 1995; Shmigol et al. 1995); further discussed below). It may also be that Co^{2+}, Cd^{2+} and Mn^{2+} directly diminished the activated cationic conductance (Inoue 1991).

Depending on the cell type, the reversal potential for muscarinic activated Ca^{2+}-dependent cationic currents have been estimated in the range of -25 to 20 mV (Colino and Halliwell 1993; Guérineau et al. 1995; Shen and North 1992) which is well positive to the maximum voltage reached in our V-Is (-40mV). A positive reversal potential could explain a V-I parallel shift induced by CCh, provided that the current activated in EC neurons is voltage independent. However, CCh did not induce an "strictly" V-I parallel shift in EC neurons since it also caused an increase in slope resistance at potentials positive to -70mV. This non-linearity suggests the presence of an additional voltage dependent component in the muscarinic activated current. It appeared that this component was selectively enhanced when potentiating the CCh response by depolarization (Ca^{2+} entry; Fig. 6).

THE CCH RESPONSE IN NON-SCS MAY REFLECT COMPLEX Ca^{2+} DYNAMICS

In non-SCs, the CCh-triggered depolarization often displayed an oscillatory phenomenon (Fig. 2 B and C). Agonists like acetylcholine that lead to Ca^{2+} mobilization are known to induce repetitive patterns of $[Ca^{2+}]_{in}$ spikes with a distinct spatial organization (reviewed in Berridge 1993). Also, in several preparations, periodic increases in $[Ca^{2+}]_{in}$ closely coupled to oscillatory Ca^{2+} dependent currents have been imaged in response to muscarinic receptor activation (Komori et al. 1993; Lechleiter et al. 1991). We suggest that the slow membrane voltage oscillations triggered by CCh in non-SCs may thus reflect complex interactions between spatially and temporally organized Ca^{2+} release of intracellular stores, the Ca^{2+}-dependent cationic current, and influx of extracellular Ca^{2+}, resulting from activation of a muscarinic receptor subtype coupled to $InsP_3$ production. In fact, the pattern of the CCh-triggered membrane oscillations that we observed followed closely described patterns of $[Ca^{2+}]_{in}$ oscillations in many tissues (reviewed in Berridge and Irvine 1989). The dynamic and spatial properties of these oscillations vary in form and frequency from cell to cell, however, they are so remarkably constant for individual cells that they have been referred to as "fingerprints" (Berridge and Irvin e 1989). In non-SCs, we have observed a similar "fingerprinting" phenomenon since repeated applications of CCh in a given cell always produced an identical oscillatory response but this response could be different in different cells.

$[Ca^{2+}]_{in}$ oscillations have been modeled in several cell types (Friel 1995 and references therein). In neurons, the general scheme involves extracellular Ca^{2+} entry to replenish the oscillator (the actual stores) and a positive feedback mechanism whereby Ca^{2+} amplifies its own release. The importance of a threshold level of voltage gated Ca^{2+} entry for reestablishing Ca^{2+} mobilization has been demonstrated experimentally (Jaffe and Brown 1994; Komori et al. 1993). The preceeding explains the dependence of the CCh depolarization on operative Ca^{2+} channels that we have observed in layer II neurons, even in the absence of oscillatory responses.

FUNCTIONAL IMPLICATIONS

We have provided evidence that the major excitatory effect of muscarinic receptor activation on MEC layer II neurons is by induction of a Ca^{2+} activated cationic conductance mediated through the m1 receptor subtype. The activation of this conductance is largely potentiated by activity that causes Ca^{2+} influx. This property introduces a Hebbian-like mechanism whereby muscarinic receptor activation may only be translated into substantial membrane depolarization and repetitive firing if coupled to post-synaptic cell activity. As cells of origin of the perforant path (Ramon y Cajal 1902), EC layer II neurons occupy a pivotal position in the hippocampal system known to play a crucial role in the making of long term memories (Alvarez and Squire 1994; Squire 1992). Since the cholinergic system is also known to participate in learning and memory, the presently described cholinergic mechanism may be most instrumental in these tasks (Lisman and Idiart 1995). On the other hand, activity dependent potentiation of the muscarinic depolarization introduces a positive feedback mechanism both at the cellular and at the network level that may lead to hyperexcitability and epileptogenesis (Dickson and Alonso 1995). Also, the apparent Ca^{2+} mobilizing properties of the m1 transduction process and the Ca^{2+} dependent properties of the activated conductance may cooperate to sustain an elevated $[Ca^{2+}]_{in}$ signal. This signal might be important in mediating plastic changes but may also lead to metabolic compromises and neurodegeneration in the long term such as that observed in Alzheimer's disease where EC layer II is most affected (Dunnett 1991).

ACKNOWLEDGMENTS

We would like to thank Drs. C. Dickson, B. Jones, and E. Hamel for comments on the manuscript. This work was supported by the canadian Medical Research Council.

REFERENCES

Alonso, A. and Klink, R. Differential electroresponsiveness of stellate and pyramidal-like cells of medial entorhinal cortex layer II. *J. Neurophysiol.* 70: 128-143, 1993.

Alvarez, P. and Squire, L. R. Memory consolidation and the medial temporal lobe: a simple network model. *Proc. Natl. Acad. Sci. USA.* 91: 7041-7045, 1994.

Andrade, R. Cell excitation enhances muscarinic cholinergic responses in rat association cortex. *Brain Res.* 548: 81-93, 1991.

Benardo, L. S. and Prince, D. A. Cholinergic excitation of mammalian hippocampal pyramidal cells. *Brain Res.* 249: 315-331, 1982.

Benham, C. D., Bolton, T. B., and Lang, R. J. Acetylcholine activates an inward current in single mammalian smooth muscle cells. *Nature.* 316: 345-346, 1985.

Benson, D. M., Blitzer, R. D., and Landau, E. M. An analysis of the depolarization produced in guinea-pig hippocampus by cholinergic receptor stimulation. *J. Physiol. (Lond.).* 404: 479-496, 1988.

Berridge, M. J. Inositol triphosphate and calcium signalling. *Nature.* 361: 315-325, 1993.

Berridge, M. J. and Irvine, R. F. Inositol phosphates and cell signalling. *Nature.* 341: 197-205, 1989.

Blitzer, R. D., Gil, O., Omri, G., and Landau, E. M. Nifedipine blocks calcium-dependent cholinergic depolarization in the guinea pig hippocampus. *Brain Res.* 542: 293-299, 1991.

Bobker, D. H. and Williams, J. T. Serotonin augments the cationic current I_h in central neurons. *Neuron.* 2: 1535-1540, 1989.

Caeser, M., Brown, D. A., Gähwiler, B. H., and Knöpfel, T. Characterization of a calcium-dependent current generating a slow afterdepolarization of CA3 pyramidal cells in rat hippocampal slice cultures. *Eur. J. Neurosci.* 5: 560-569, 1993.

Colino, A. and Halliwell, J. V. Carbachol potentiates Q current and activates a calcium-dependent non-specific conductance in rat hippocampus *in vitro*. *Eur. J. Neurosci.* 5: 1198-1209, 1993.

Dickson, C. T. and Alonso, A. The entorhinal cortex contains two intrinsic pacemakers of epileptiform activity: an in vitro study. *Epilepsia.* 36, suppl 4: 87, 1995.

Dörje, F., Wess, J., Lambrecht, G., Tacke, R., Mutschler, E., and Brann, M. R. Antagonist binding profiles of five cloned human muscarinic receptor subtypes. *J. Pharmacol. Exp. Ther.* 256: 727-733, 1991.

Dunnett, S. Cholinergic grafts, memory and ageing. *Trends Neurosci.* 14: 371-375, 1991.

Eisner, D. A. and Lederer, W. J. The electrogenic sodium-calcium exchange. In: *Sodium-Calcium Exchange*, edited by T. J. A. Allen, D. Noble, and H. Reuter. Oxford: Oxford University Press, 1989, 178-207

Fontana, G., Rogowski, R. S., and Blaustein, M. P. Kinetic properties of the sodium-calcium exchanger in rat brain synaptosomes. *J. Physiol. (Lond.).* 485: 349-364, 1995.

Fraser, D. D. and MacVicar, B. A. Cholinergic-dependent plateau potential in hippocampal CA1 Pyramidal Neurons. *J. Neurosci.* in press, 1996.

Friel, D. D. $[Ca^{2+}]_i$ oscillations in sympathetic neurons: an experimental test of a theoretical model. *Biophys. J.* 68: 1752-1766, 1995.

Gähwiler, B. H. and Dreifuss, J. J. Multiple actions of acetylcholine on hippocampal pyramidal cells in organotypic explant cultures. *Neurosci.* 7: 1243-1256, 1982.

Gosh, A. and Greenberg, M. E. Calcium signalling in neurons: molecular mechanisms and cellular consequences. *Science.* 268: 239-247, 1995.

Guérineau, N. C., Bossu, J.-L., Gähwiler, B. H., and Gerberg, U. Activation of a non-selective cationic conductance by metabotropic glutamatergic and muscarinic agonists in CA3 pyramidal neurons of the rat hippocampus. *J. Neurosci.* 15: 4435-4407, 1995.

Haj-Dahmane, S. and Andrade, R. A voltage and calcium-dependent cation current underlies the depolarization and depolarizing after-potential elicited by muscarinic activation in rat cortex. *Soc. Neurosci. Abstr.* 21: 800.17, 1995.

Haj-Dahmane, S. and Andrade, R. Muscarinic activation of a voltage-dependent cation nonselective current in association cortex. *J. Neurosci.* 16: 3848-3861, 1996.

Halliwell, J. V. and Adams, P. R. Voltage-clamp analysis of muscarinic excitation in hippocampal neurons. *Brain Res.* 250: 71-92, 1982.

Harrison, S. M. and Boyett, M. R. The role of the Na^+-Ca^{2+} exchanger in the rate-dependent increase in contraction in guinea-pig ventricular myocytes. *J. Physiol. (Lond.).* 482: 555-566, 1995.

Henzi, V. and MacDermott, A. B. Characteristics and function of Ca^{2+}- and inositol 1,4,5-trisphosphate-releasable stores of Ca^{2+} in neurons. *Neuroscience.* 46: 251-273, 1992.

Hulme, E. C., Birdsall, N. J. M., and Buckley, N. J. Muscarinic receptor subtypes. *Annu. Rev. Pharmacol. Toxicol.* 30: 633-673, 1990.

Inoue, R. Effect of external Cd^{2+} and other divalent cations on carbachol-activated non-selective cation channels in guinea-pig ileum. *J. Physiol. (Lond.).* 442: 447-463, 1991.

Inoue, R. and Isenberg, G. Effect of membrane potential on acethylcholine-induced inward current in guinea-pig ileum. *J. Physiol. (Lond).* 424: 57-71, 1990a.

Inoue, R. and Isenberg, G. Intracellular calcium ions modulate acetylcholine-induced inward current in guinea-pig ileum. *J. Physiol. (Lond.).* 424: 73-92, 1990b.

Jaffe, D. B. and Brown, T. H. Metabotropic glutamate receptor activation induces calcium waves within hippocampal dendrites. *J. Neurophysiol.* 72: 471-474, 1994.

Kimura, J., Miyamae, S., and Noma, A. Identification of sodium-calcium exchange current in single ventricular cells of guinea-pig. *J. Physiol. (Lond.).* 384: 199-222, 1987.

Klink, R. and Alonso, A. Ionic mechanisms for the subthreshold oscillations and differential electroresponsiveness of medial entorhinal cortex layer II neurons. *J. Neurophysiol.* 70: 144-157, 1993.

Klink, R. and Alonso, A. Muscarinic modulation of the oscillatory and repetitive firing properties of entorhinal cortex layer II neurons. *J. Neurophysiol.* submitted: 1996.

Komori, S., Kawai, M., Pacaud, P., Ohashi, H., and Bolton, T. B. Oscillations of receptor-operated cationic current and internal calcium in single guinea-pig ileal smooth muscle cells. *Pflügers Arch.* 424: 431-438, 1993.

Krnjevic, K. Central cholinergic mechanisms and function. *Prog. Brain Res.* 1993: 285-292, 1993.

Lechleiter, J., Girard, S., Clapham, D., and Peralta, E. Subcellular patterns of calcium release determined by G protein-specific residues of muscarinic receptors. *Nature.* 350: 505-508, 1991.

Levey, A. I., Edmunds, S. M., Koliatsos, V., Wiley, R. G., and Heilman, C. J. Expression of m1-m4 muscarinic acetylcholine receptor proteins in rat hippocampus and regulation by cholinergic innervation. *J. Neurosci.* 15: 4077-4092, 1995.

Lisman, J. E. and Idiart, M. A. P. Storage of 7 + 2 short term memories in oscillatory subcycles. *Science.* 267: 1512-1515, 1995.

Lo, T.-M. and Thayer, S. A. Pharmacologic characterization of refilling inositol 1,4,5-triphosphate-sensitive Ca^{2+} stores in NG108-15 cells. *Brain Res.* 704: 10-18, 1995.

Madison, D. V., Lancaster, B., and Nicoll, R. A. Voltage clamp analysis of cholinergic action in the hippocampus. *J. Neurosci.* 7: 733-741, 1987.

McCormick, D. A. and Prince, D. A. Mechanisms of action of acetylcholine in the guinea-pig cerebral cortex in vitro. *J. Physiol. (Lond.).* 375: 169-194, 1986.

McKinney, M. Muscarinic receptor subtype-specific coupling to second messengers in neuronal systems. *Prog. Brain Res.* 98: 333-340, 1993.

Pacaud, P. and Bolton, T. B. Relation between muscarinic receptor cationic current and internal calcium in guinea-pig jejunal smooth muscle cells. *J. Physiol. (Lond.).* 441: 477-499, 1991.

Pape, H.-C. and McCormick, D. A. Noradrenaline and serotonin selectively modulate thalamic burst firing by enhancing a hyperpolarization-activated cation current. *Nature.* 340: 715-718, 1989.

Phillis, J. W. and Wu, P. H. Catecholamines and the sodium pump in excitable cells. *Prog. Neurobiol.* 17: 141-184, 1981.

Ramon y Cajal, S. Sobre un ganglio especial de la corteza esfeno-occipital. *Trab. del Lab. de invest. Biol. Univ. Madrid.* 1: 189-201, 1902.

Rouse, S. T. and Levey, A. I. m1-m4 muscarinic receptor proteins in rat dentate gyrus and afferent projection neurons. *Soc. Neurosci. Abstr.* 21: 800.13, 1995.

Schwindt, P. C., Spain, W. J., and Crill, W. E. Effects of intracellular calcium chelation on voltage-dependent and calcium-dependent currents in cat neocortical neurons. *Neuroscience.* 47: 571-578, 1992.

Schwindt, P. C., Spain, W. J., Foehring, R. C., Chubb, M. C., and Crill, W. E. Slow conductances in neurons from cat sensorimotor cortex in vitro and their role in slow excitability changes. *J. Neurophysiol.* 59: 450-467, 1988.

Segal, M. Multiple actions of acetylcholine at a muscarinic receptor studied in the rat hippocampal slice. *Brain Res.* 246: 77-87, 1982.

Shen, K.-Z. and North, R. A. Muscarine increases cation conductance and decreases potassium conductance in rat Locus Coeruleus neurones. *J. Physiol. (Lond.).* 455: 471-485, 1992.

Shmigol, A., Verkhratsky, A., and Isenberg, G. Calcium-induced calcium release in rat sensory neurons. *J. Physiol. (Lond.).* 489: 627-636, 1995.

Sims, S. Cholinergic activation of a non-selective cation current in canine gastric smooth muscle is associated with contraction. *J. Physiol (Lond.).* 449: 377-398, 1992.

Squire, L. R. Memory and the hippocampus: a synthesis from findings with rats, monkeys, and humans. *Psychol. Rev.* 99: 195-231, 1992.

Storm, J. F. Potassium currents in hippocampal pyramidal cells. *Prog. Brain Res.* 83: 161-187, 1990.

Thompson, S. M. and Prince, D. A. Activation of electrogenic sodium pump in hippocampal CA1 neurons following glutamate-induced depolarization. *J. Neurophysiol.* 56: 507-522, 1986.

Trimmer, B. A. Characterization of a muscarinic current that reguiates excitability of an identified insect motoneuron. *J. Neurophysiol.* 72: 1862-1873, 1994.

Wang, Z. and McCormick, D. A. Control of firing mode of corticotectal and corticopontine layer V burst-generating neurons by norepinephrine, acetylcholine, and 1 S,3**R**-ACPD. *J. Neurosci.* 13: 2199-2216, 1993.

Figure 1. Depolarizing responses of EC layer II neurons to pressure-pulse applications of CCh in normal Ringer. *A*: At the arrow, CCh was pressure-ejected for the specified duration (in milliseconds). In a SC (top) and a non-SC (bottom) CCh depolarized the membrane potential to firing level. *B*: pressure-pulse CCh applications of increasing duration produced responses of larger amplitude and longer duration. Depolarizations consisted of a fast rising and a slow decaying phase.

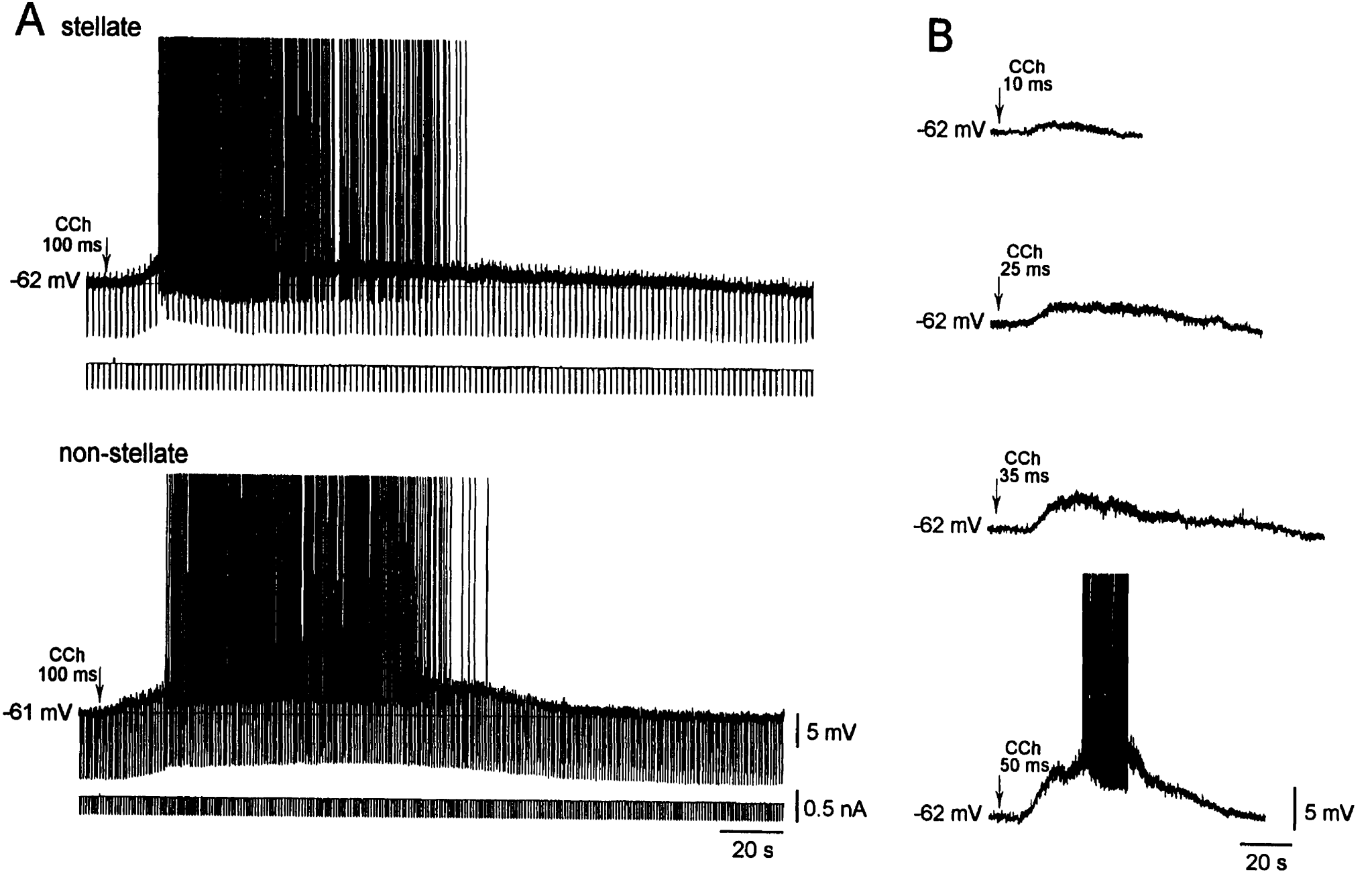
A
stellate
CCh
100 ms
-62 mV
non-stellate
CCh
100 ms
-61 mV
5 mV
0.5 nA
20 s
B
CCh
10 ms
-62 mV
CCh
25 ms
-62 mV
CCh
35 ms
-62 mV
CCh
50 ms
-62 mV
5 mV
20 s

Figure 2. In TTX Ringer, depolarizing responses to CCh are more robust in non-SCs than in SCs. *A*: Left panel, typical depolarizing response of a SC to 300 ms pulse application of CCh. Note that the membrane depolarized fast by about 6 mV and then repolarized exponentially. Right panel, typical depolarizing response in a non-SC. Note the initial spike-like response followed by a plateau phase. *B*: In another non-SC, CCh triggered large amplitude spike-like membrane potential oscillations at a slow frequency (0.06-0.02 Hz). *C*: In another non-SC exhibiting an oscillatory response, increasing CCh doses gradually increase the frequency of the oscillation (from 0.07 Hz for CCh 5 ms to 0.22 Hz for CCh 100 ms), without affecting the number of cycles.

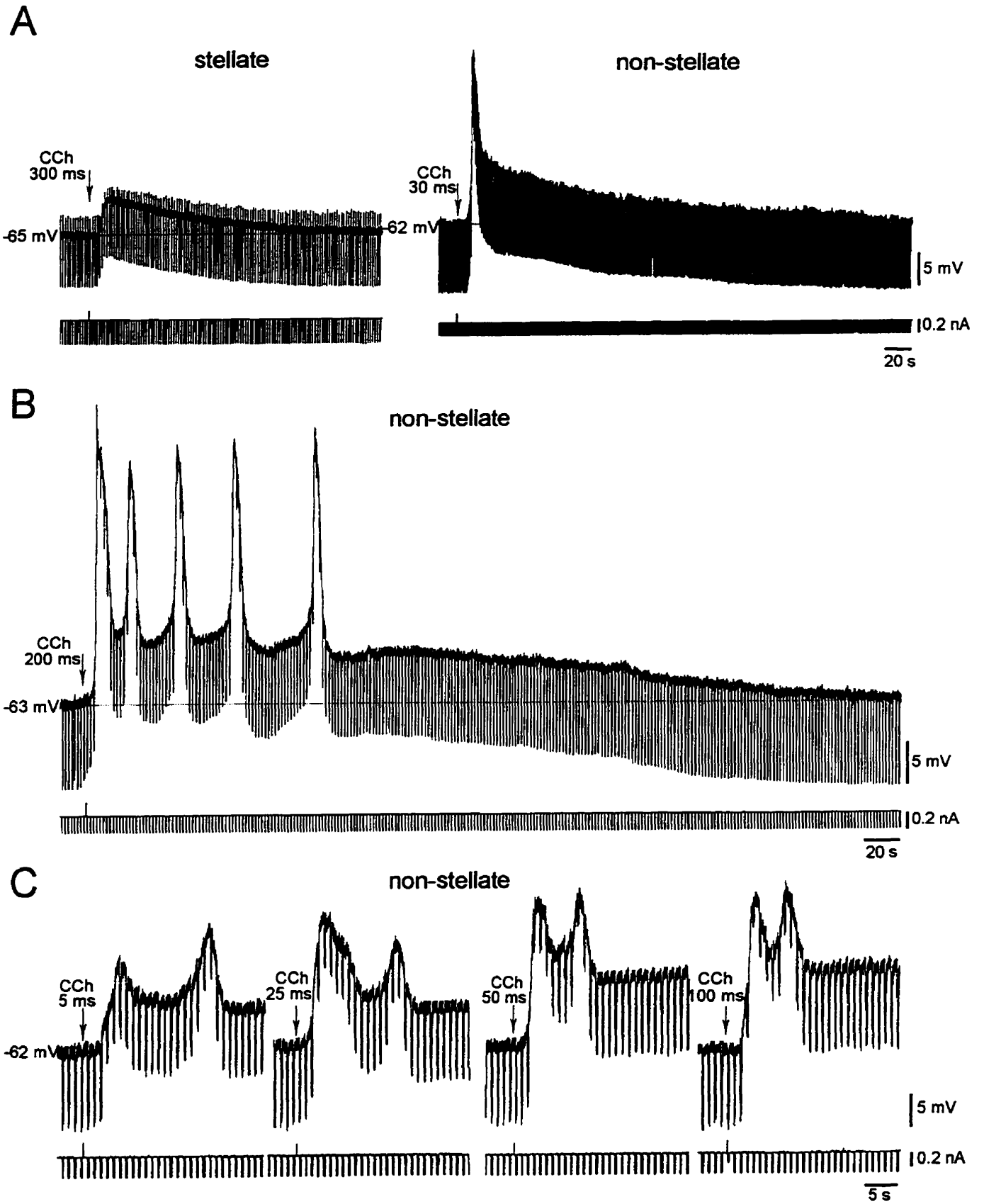
A
stellate
non-stellate
CCh
300 ms
CCh
30 ms
-65 mV
-62 mV
5 mV
0.2 nA
20 s
B
non-stellate
CCh
200 ms
-63 mV
5 mV
0.2 nA
20 s
C
non-stellate
CCh
5 ms
CCh
25 ms
CCh
50 ms
CCh
100 ms
-62 mV
5 mV
0.2 nA
5 s

Figure 3. Cell firing potentiates CCh triggered depolarization. *A*: in a non-SC, a pressure-pulse CCh application resulted in a subthreshold, 4 mV depolarization. *B*: traces at an expanded time scale taken at arrows marked 1 and 2 in *A* showing no significant change in apparent input resistance at the resting membrane potential. *C*: in the same cell, in a subsequent CCh application of equal magnitude, a manual d.c. depolarization (horizontal bar) that triggers cell firing is applied at the peak of the intial depolarizing response. This manipulation caused a post-depolarization plateau that sutained firing and this activity could not be turned off by a short (~ 10s) d.c. hyperpolarization (*). Note that as in *A*, membrane depolarization was not associated to a significant change in apparent input resistance at the resting membrane potential.

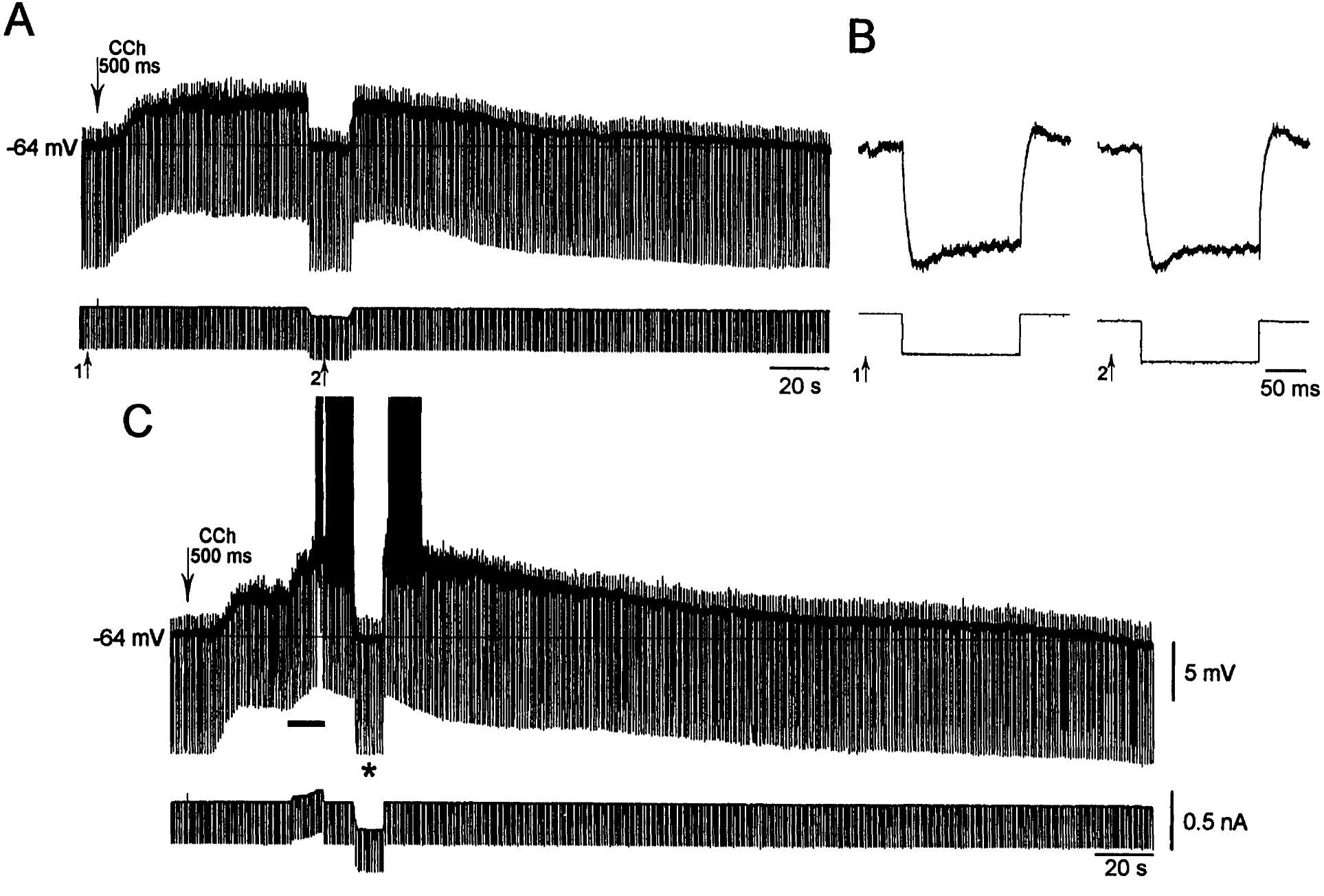
A
CCh
500 ms
-64 mV
1
2
20 s
B
1
2
50 ms
C
CCh
500 ms
-64 mV
5 mV
*
0.5 nA
20 s

Figure 4. In TTX Ringer, the CCh depolarizing response is potentiated in amplitude and duration by d.c. depolarization that elicits Ca^{2+} spiking. *A*: in a non-SC, a pressure-pulse CCh application resulted in a 4 mV depolarization. *B*: in the same cell, a subsequent application elicited the same depolarization that was potentiated by 250 % (additional 10 mV) following a 10 s manual d.c depolarization (thick bar) that triggered multiple Ca^{2+} spikes (*). A series of depolarizing and hyperpolarizing current-pulses were also applied in order to estimate voltage-current relationsships during the CCh depolarization (see Figs. 5 and 6).

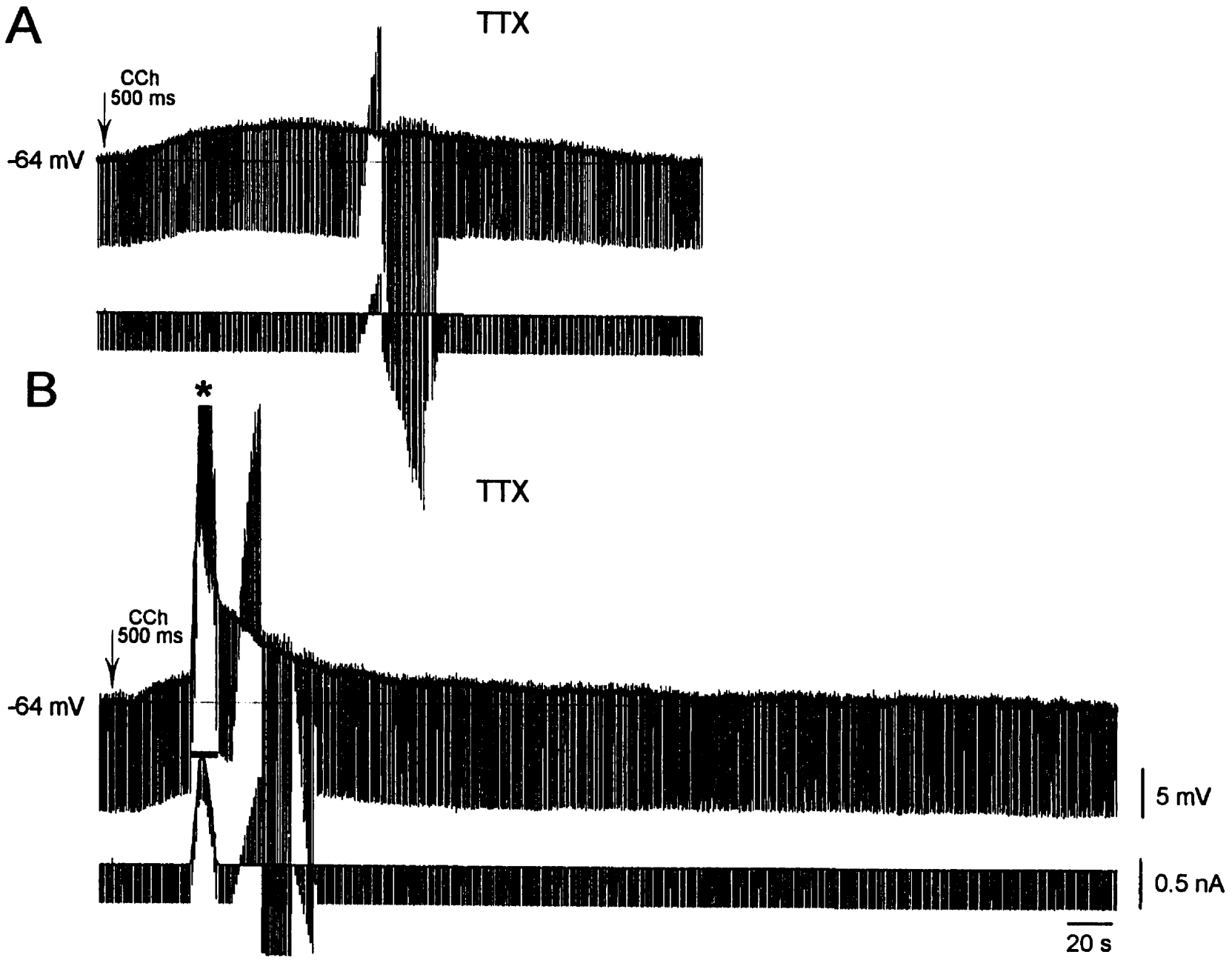
A
TTX
CCh
500 ms
-64 mV
B
*
TTX
CCh
500 ms
-64 mV
5 mV
0.5 nA
20 s

Figure 5. The voltage-current relationship of both SCs and non-SCs were similarly affected by CCh. *A* and *B*: In a SC (upper row) and a non-SC (lower row) peak (left) and steady-state (right) V-Is in control (filled symbols) and towards the maximum of CCh-triggered depolarizations (open symbols). In all panels, insets are slope resistance *vs* membrane potential plots estimated (as described in detail in the methods) from the corresponding V-I plots. Note that the most striking CCh action is a parallel shift in the negative direction of the steady-state V-I relation and that the slope-resistance was increased by CCh only at potentials positive to about -70mV. V-I plots were constructed from the initial peak and steady-state voltage responses to ~300ms current pulses applied from the resting level. CCh was applied under continuous superfusion with TTX.

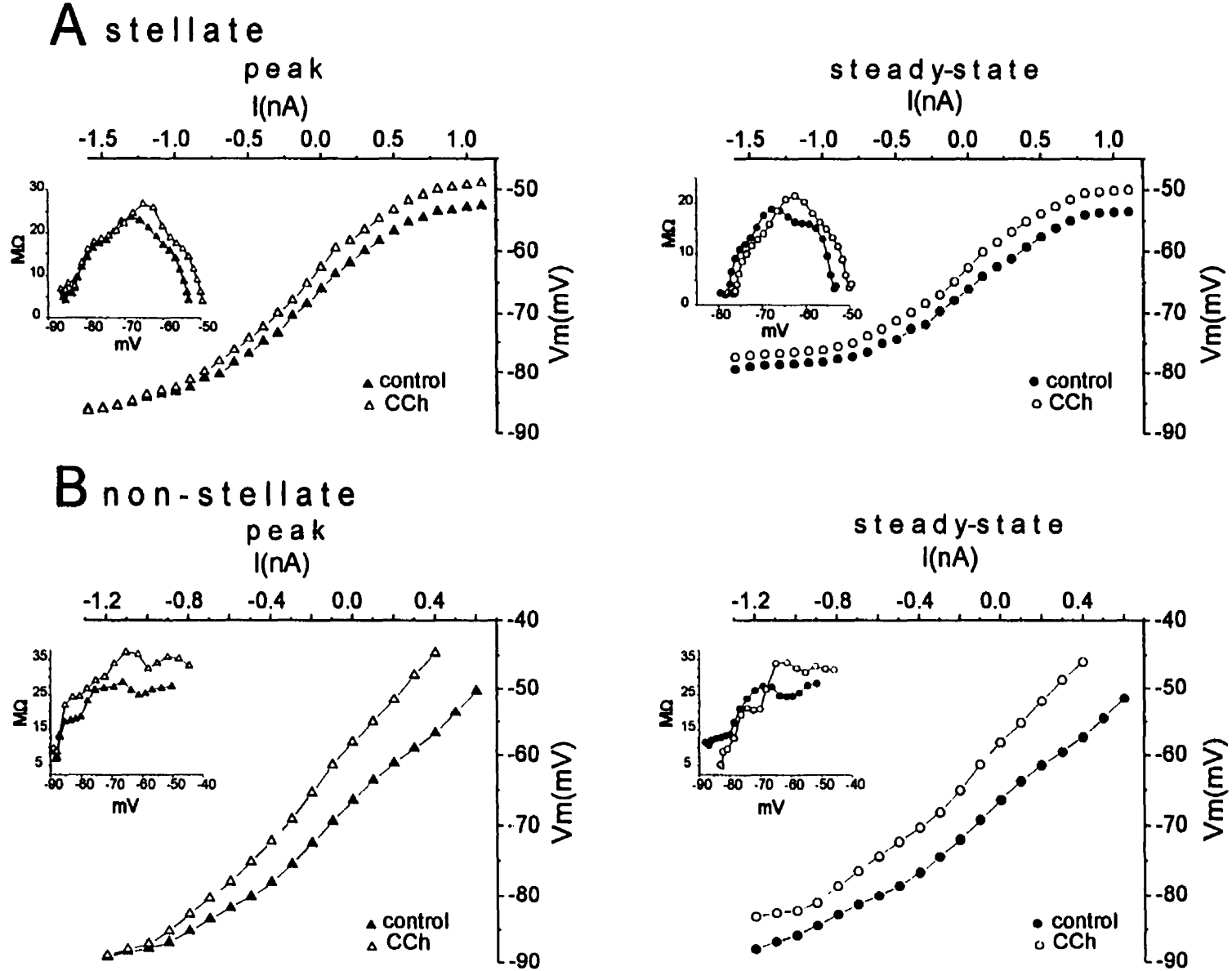
A stellate
peak
I(nA)
-1.5 -1.0 -0.5 0.0 0.5 1.0
MΩ
mV
Vm(mV)
control
CCh
steady-state
I(nA)
B non-stellate
peak
I(nA)
-1.2 -0.8 -0.4 0.0 0.4
steady-state
I(nA)

Figure 6. Potentiation of the CCh response by d.c. depolarization produced voltage-dependent changes in the CCh V-I. *A*: Steady state V-Is for the cell and protocols shown in Fig 4. The CCh V-I (○) exhibited the typical leftward shift relative to the TTX V-I (●). Following potentiation of the response by d.c. depolarization, the CCh V-I (⊕) exhibited a voltage-dependent increase in slope relative to the non-potentiated V-I. *B*: Steady state Rin-Vm plots show that the increase in slope input resistance in the potentiated V-I is above ~ -75 mV.

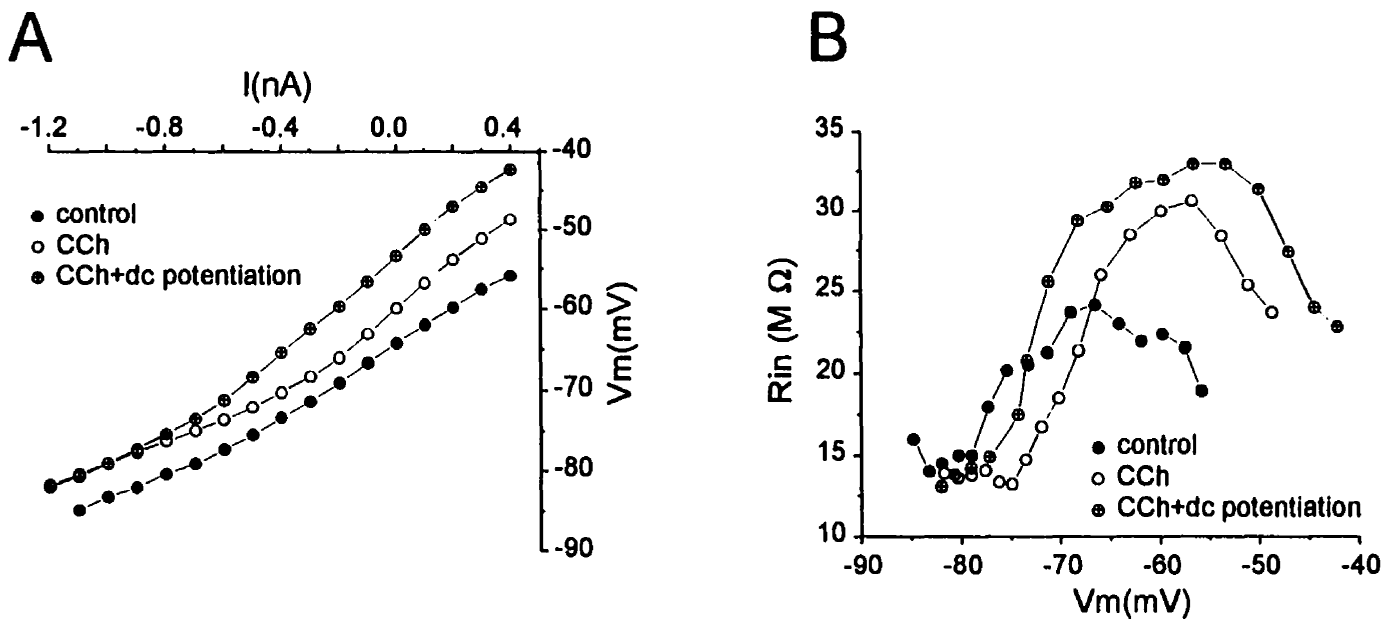
A
I(nA)
-1.2
-0.8
-0.4
0.0
0.4
-40
-50
-60
-70
-80
-90
Vm(mV)
control
CCh
CCh+dc potentiation
B
35
30
25
20
15
10
Rin (M Ω)
-90
-80
-70
-60
-50
-40
Vm(mV)
control
CCh
CCh+dc potentiation

Figure 7. CCh applications during K^+ channel block with intracellular Cs^+ resulted in robust depolarizations and actions on theV-I relations equivalent to those obtained in normal recording conditions. *A*: in a non-SC injected with Cs^+ (3 M), a 100 ms (top) pressure-pulse CCh application resulted in a robust, long lasting depolarization; the trace has been interrupted for 4 minutes and 42 seconds . Another shorter application (40 ms, bottom) resulted in a slower depolarizing potential of much shorter duration. In both cases no change in apparent input resistance was observed at the control membrane potential. Holding current was -0.15 nA; Ringer contained TTX and Ba^+ 1 mM. Inset shows that, before CCh application, removal of holding current results in a resting potential of -8 mV. *B*: in the same non-SC, peak and steady-state V-Is were constructed for hyperpolarizing pulses from a membrane potential of -62 mV. The peak (top, Δ) and steady-state (bottom, ○) CCh V-Is exhibited a leftward shift relative to the control TTX V-Is (▲ ,●)..

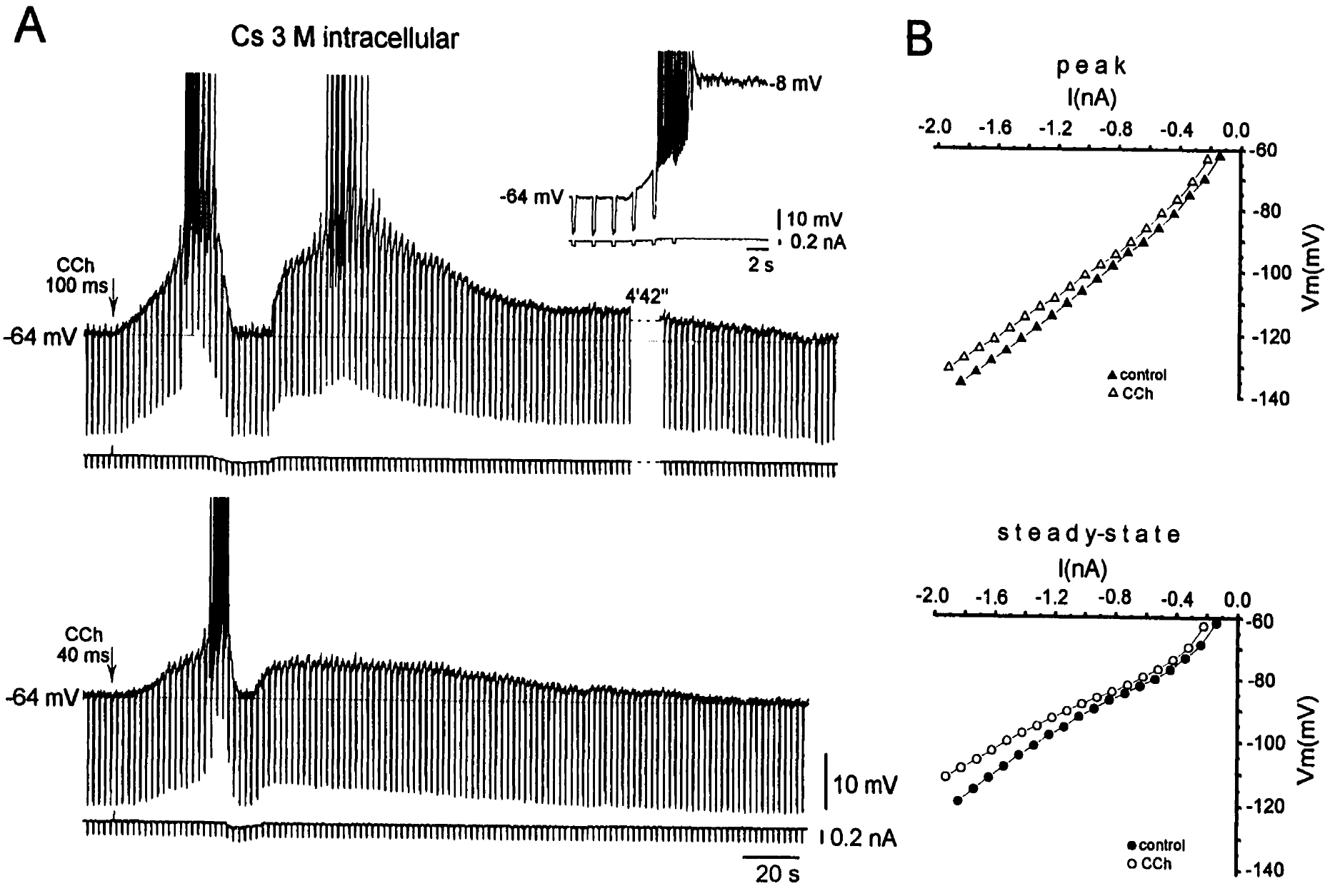
A
Cs 3 M intracellular
-8 mV
-64 mV
10 mV
0.2 nA
2 s
CCh
100 ms
4'42"
-64 mV
CCh
40 ms
-64 mV
10 mV
0.2 nA
20 s
B
peak
I(nA)
-2.0 -1.6 -1.2 -0.8 -0.4 0.0
-60
-80
-100
-120
-140
Vm(mV)
▲control
△ CCh
steady-state
I(nA)
-2.0 -1.6 -1.2 -0.8 -0.4 0.0
-60
-80
-100
-120
-140
Vm(mV)
●control
○ CCh

Figure 8. Extracellular Cs^+ blocks inward rectification and the CCh-induced decrease in slope resistance below -70 mV. *A*: left panel, the steady-state V-I (control TTX; ●) exhibits the usual leftward shift with CCh (○); Right panel, during perfusion with Cs^+ (2mM) inward rectification is blocked, and CCh still causes the typical parallel shift on the V-I relation. *B*: Rin-Vm plots show that the CCh-induced decrease in slope input resistance seen below - 70 mV in control Ringer (left panel) is not produced during Cs^+ superfusion (right panel). All plots taken from the same SC. *C*: in a non-SC, combined K conductance and Ih block was evidenced by a 168% increase in Rin and a disappearance of the time dependent Ih sag (right panel; holding current -0.13 nA). *D*: under the same conditions, the steady-state V-I (control; ●) exhibits the usual leftward shift with CCh (○) (right panel; same cell as as in *C*).

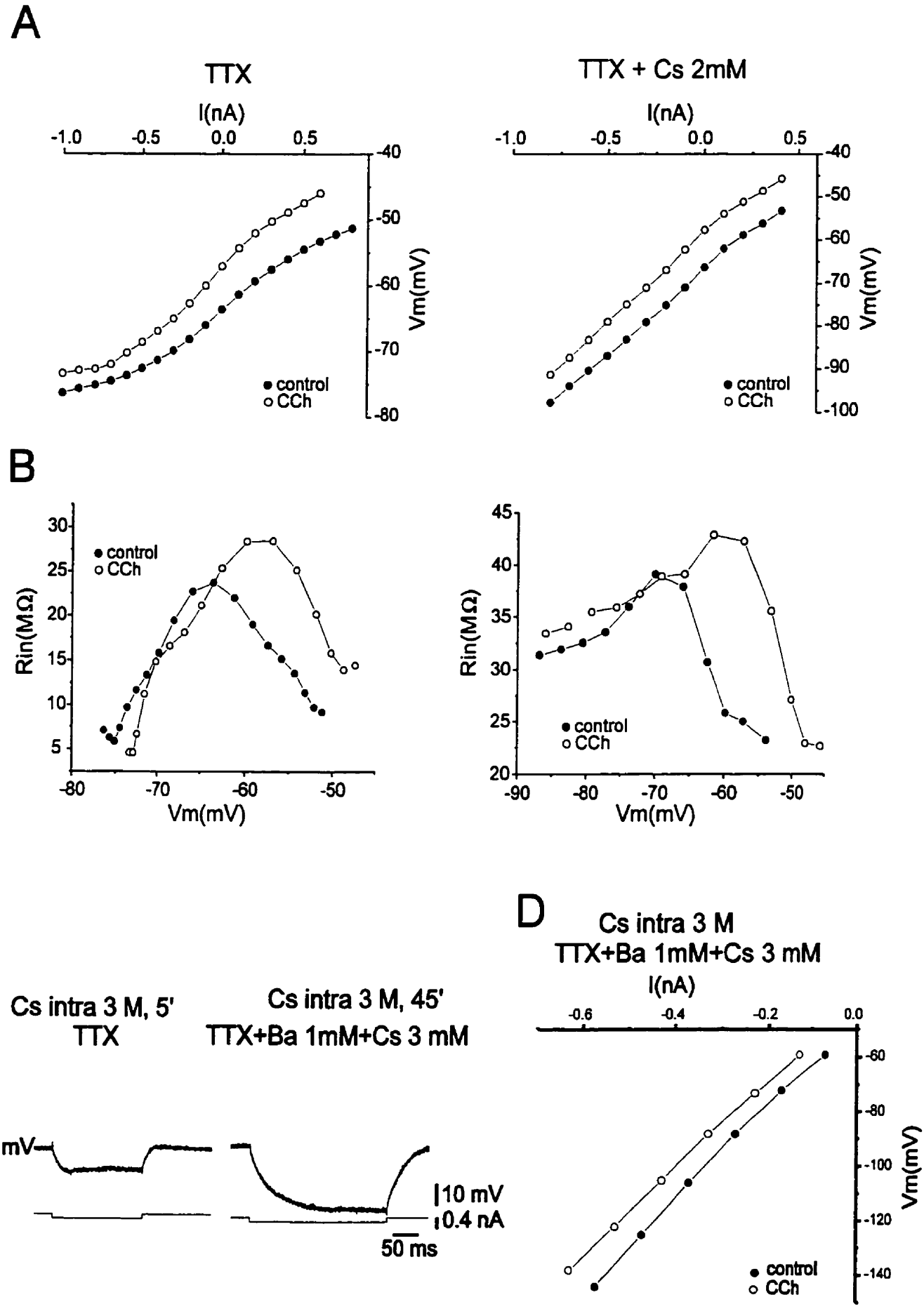
A
TTX
I(nA)
-1.0
-0.5
0.0
0.5
-40
-50
-60
-70
-80
Vm(mV)
control
CCh
TTX + Cs 2mM
I(nA)
-1.0
-0.5
0.0
0.5
-40
-50
-60
-70
-80
-90
-100
Vm(mV)
control
CCh
B
Rin(MΩ)
30
25
20
15
10
5
control
CCh
-80
-70
-60
-50
Vm(mV)
Rin(MΩ)
45
40
35
30
25
20
control
CCh
-90
-80
-70
-60
-50
Vm(mV)
C
Cs intra 3 M, 5'
TTX
Cs intra 3 M, 45'
TTX+Ba 1mM+Cs 3 mM
-60 mV
10 mV
0.4 nA
50 ms
D
Cs intra 3 M
TTX+Ba 1mM+Cs 3 mM
I(nA)
-0.6
-0.4
-0.2
0.0
-60
-80
-100
-120
-140
Vm(mV)
control
CCh

Figure 9. The CCh-induced depolarization and potentiated plateau potentials are dependent on Ca^{2+} entry and a rise in intracellular Ca^{2+}. *A*: in a non-SC, a pressure-pulse CCh application produced a 2 mV depolarization which was potentiated to 16 mV after d.c depolarization (left). Following perfusion with a low Ca^{2+} (0.5 mM) + Cd^{2+} solution the initial and post-depolarization response to CCh were totally blocked (middle). The CCh response recovered following washout of the low Ca^{2+}+Co^{2+} solution (right). *B*: in a non-SC injected with BAPTA (200 mM), a pressure-pulse CCh application 10 min after impalement produced a robust depolarization of 26 mV (left). 42 min after impalement, the same pressure-pulse CCh application did not cause any direct response (middle). 48 min after impalement, a pressure-pulse CCh application of double duration was required in order to observe a minimal CCh response wich could not be potentiated by d.c. depolarization (right).

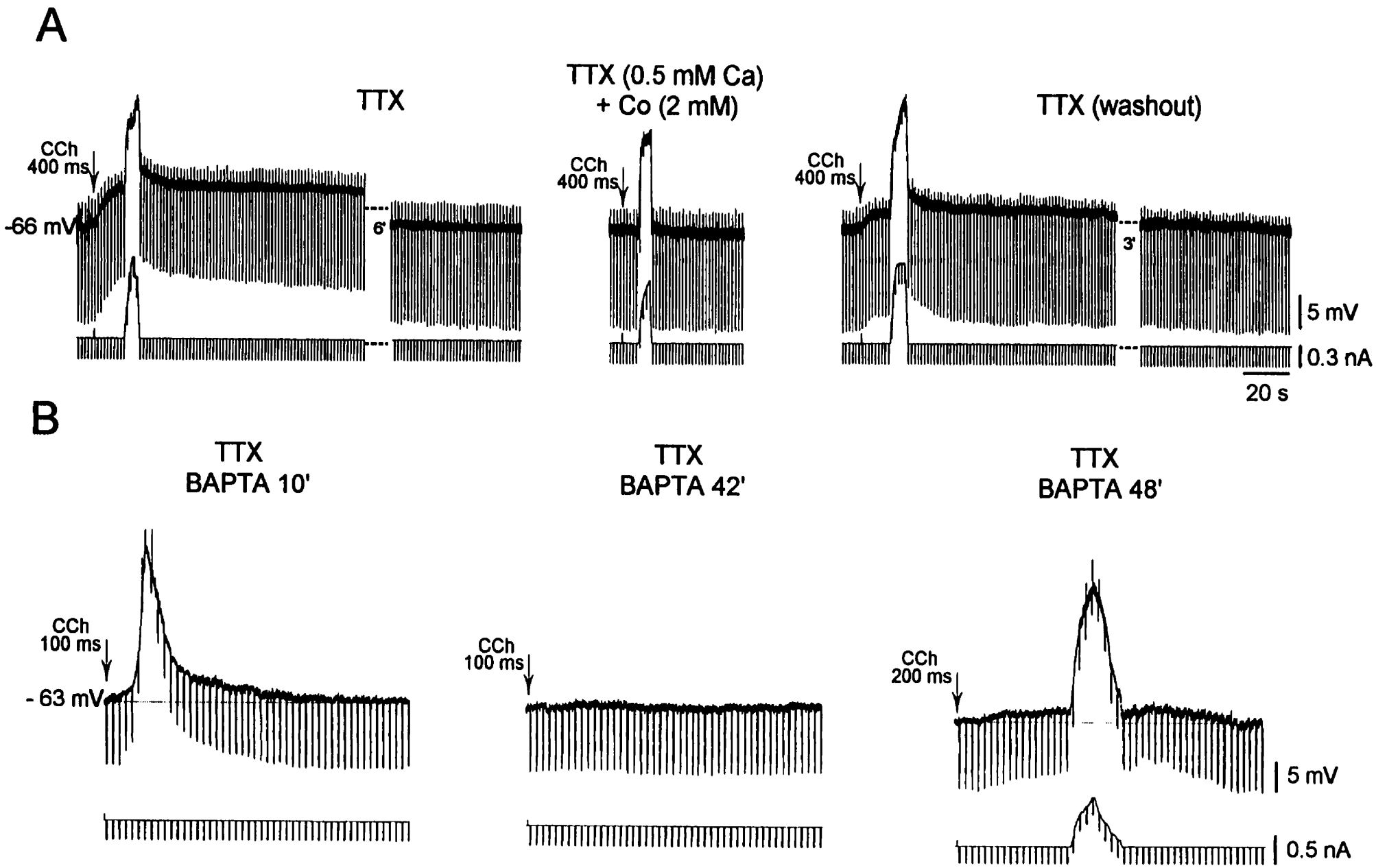
A
TTX
TTX (0.5 mM Ca)
+ Co (2 mM)
TTX (washout)
CCh
400 ms
-66 mV
6'
3'
5 mV
0.3 nA
20 s
B
TTX
BAPTA 10'
TTX
BAPTA 42'
TTX
BAPTA 48'
CCh
100 ms
- 63 mV
CCh
200 ms
5 mV
0.5 nA

Figure 10. The CCh-induced depolarization is enhanced following Na^+-K^+-ATPase inhibition. *A*: in a non-SC, a pressure-pulse CCh application resulted in a spike-like depolarization folowed by a slowly decaying plateau potential. *B*: during superfusion with strophanthidin (35 μM), the same pressure-pulse application resulted in in an enhanced plateau that sustained a second spike-like depolarization. Membrane potential depolarization persisted at a steady level until washout of strophanthidin was completed.

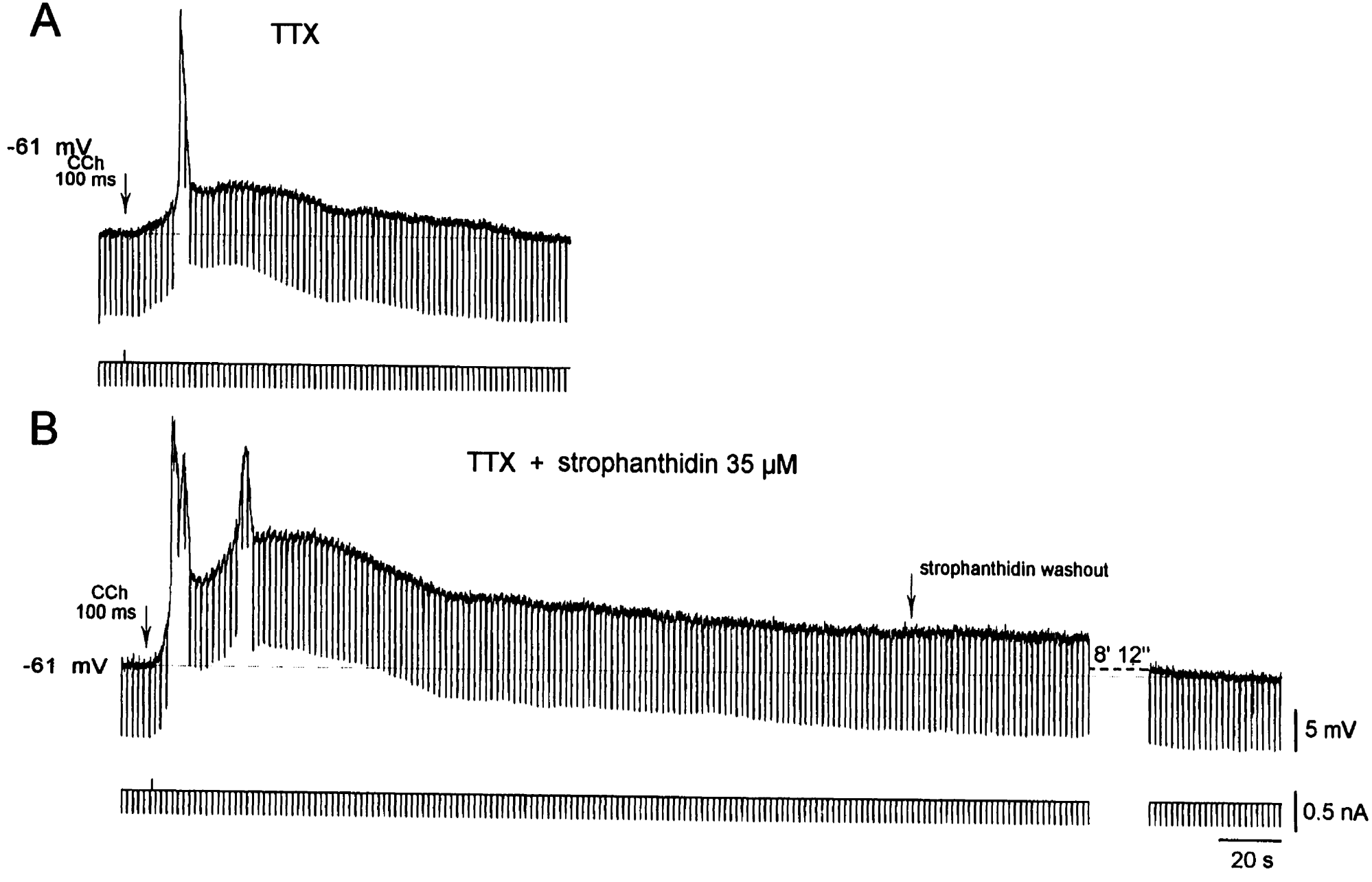
A
TTX
-61 mV
CCh
100 ms
B
TTX + strophanthidin 35 µM
CCh
100 ms
strophanthidin washout
-61 mV
8' 12"
5 mV
0.5 nA
20 s

Figure 11. The CCh-induced depolarization is largely Na^+ dependent. *A*: in control Ringer, a pressure-pulse CCh application in a non-SC resulted in a large suprathreshold depolarization (top). During equimolar Na^+ (124 mM) substitution with $NMDG^+$, the CCh response was reduced to an initial 1 mV depolarization and a 4 mV plateau potential following d.c. depolarization (bottom). *B*: Perfusion with $NMDG^+$ *per se* largely abolished Na^+ spiking and caused a 2 mV hyperpolarization, but did not significantly affect other membrane properties. *C*: in TTX Ringer, a pressure-pulse CCh application in the same cell as in *A* caused a 20 mV depolarization (top). After perfusion with $NMDG^+$ the same pressure-pulse application produced no initial depolarization and a 4 mV plateau potential following d.c depolarization (middle). The response to CCh totally recovered following washout of $NMDG^+$ (bottom).

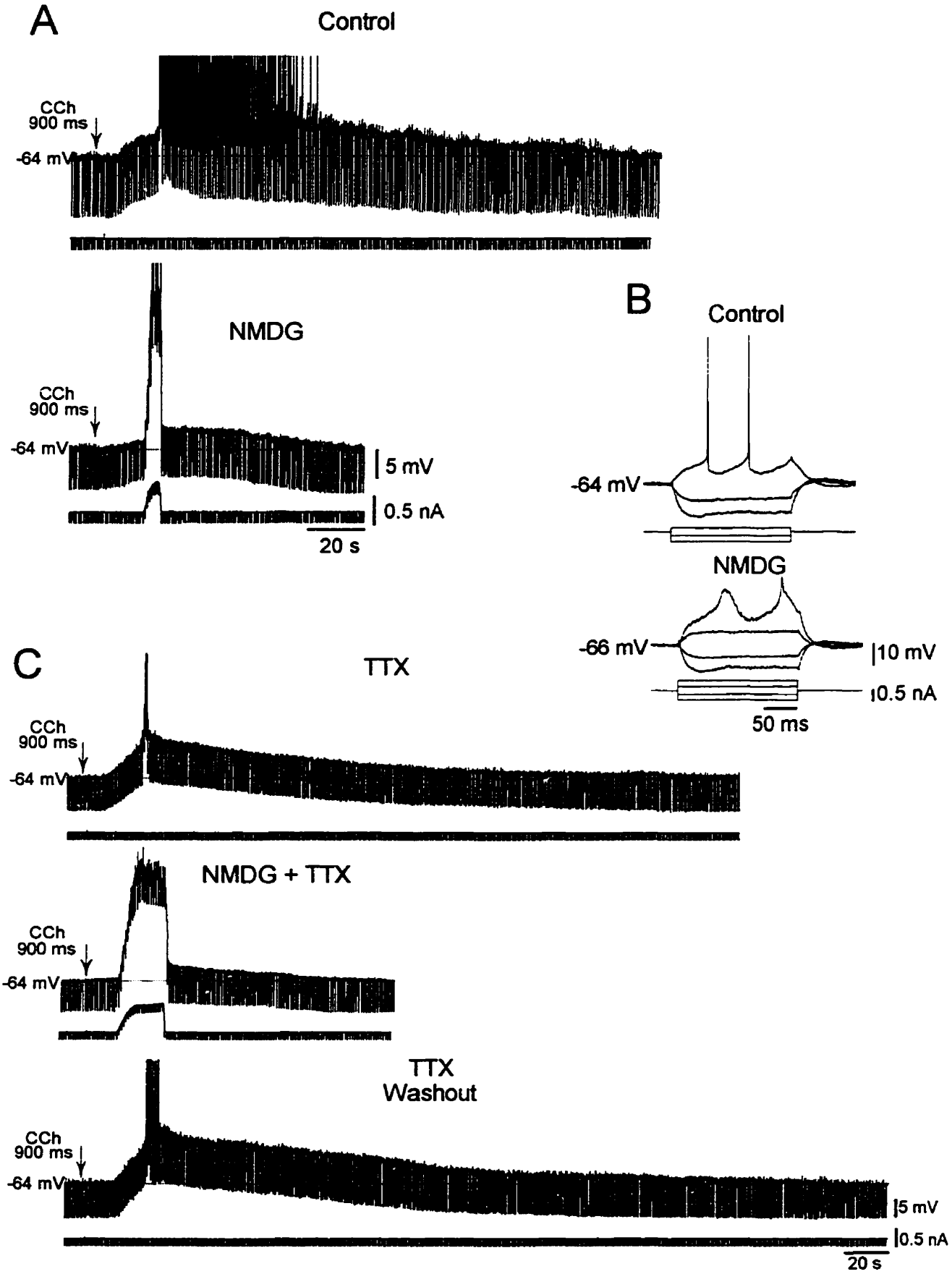
A
Control
CCh
900 ms
-64 mV
NMDG
CCh
900 ms
-64 mV
5 mV
0.5 nA
20 s
B
Control
-64 mV
NMDG
-66 mV
10 mV
0.5 nA
50 ms
C
TTX
CCh
900 ms
-64 mV
NMDG + TTX
CCh
900 ms
-64 mV
TTX
Washout
CCh
900 ms
-64 mV
5 mV
0.5 nA
20 s

Figure 12. Pharmacolgy of the CCh-induced response. A, B and C: in three different cells, pressure pulse applications of CCh that elicit large suprathreshold depolarizations in normal ringer (left panels), and pharmacological block of the responses (right panels) by 300nM atropine, 800nM pirenzipine and 10 μM himbacine, respectively. Note that the depolarizing response was not fully blocked by a dose of himbacine ~ 10 larger than that required for a complete block with pirenzipine.

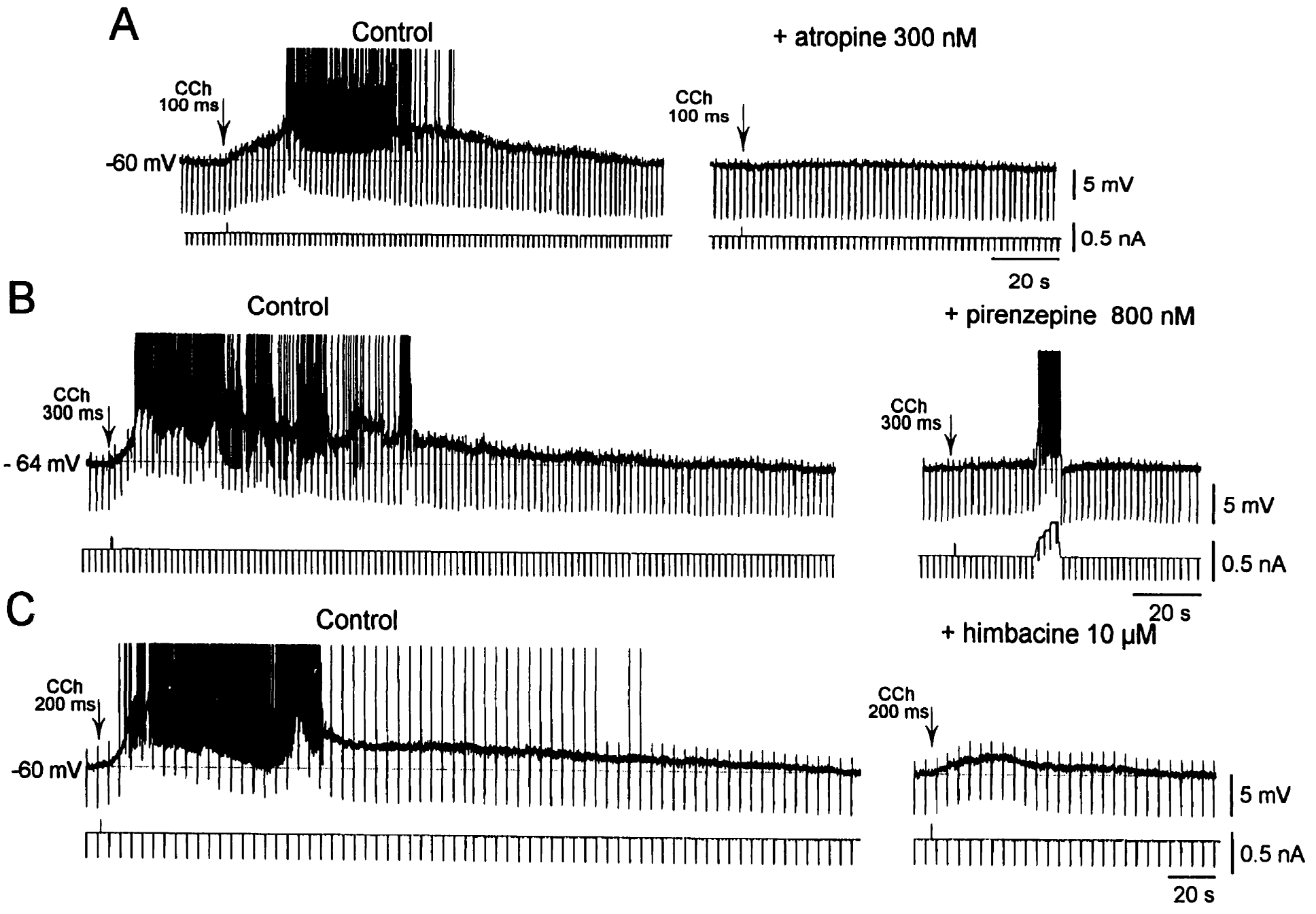
A
Control
+ atropine 300 nM
CCh
100 ms
-60 mV
CCh
100 ms
5 mV
0.5 nA
20 s
B
Control
+ pirenzepine 800 nM
CCh
300 ms
- 64 mV
CCh
300 ms
5 mV
0.5 nA
20 s
C
Control
+ himbacine 10 µM
CCh
200 ms
-60 mV
CCh
200 ms
5 mV
0.5 nA
20 s

CHAPTER VII

SEROTONERGIC MODULATION OF INTRINSIC ELECTRORESPONSIVENESS OF ENTORHINAL CORTEX LAYER II NEURONS

ABBREVIATIONS

5-HT	5-hydroxytryptamine (serotonin)
cAMP	cyclic adenosine monophosphate
EC	entorhinal cortex
fAHP	fast afterhyperpolarization
MEC	medial entorhinal cortex
non-SC	non-stellate cell
Rin	apparent input resistance
SC	stellate cell
sAHP	slow afterhyperpolarization
Vm	membrane potential

INTRODUCTION

Serotonin (5-hydroxytryptamine, 5-HT) has been implicated in a vast array of physiological and behavioral processes, such as thermoregulation, sexual and agressive drives, mood, sleep, arousal, and learning (Meltzer 1991). Cortical and subcortical areas of the forebrain are innervated by ascending projections from the superior groups of 5-HT cell bodies in the brainstem, mainly the median and dorsal raphe nuclei (Törk 1990). These serotonergic neurons exert a tonic modulatory influence on their widespread forebrain targets, in such a manner that they seem to regulate the expression of neuronal circuits without being a necessary component of them (Jacobs and Azmitia 1992).

A direct, almost linear positive relationship exists between the level of behavioral activation of the organism that is seen across the sleep-wake-arousal cycle, and the discharge rate of dorsal raphe nucleus neurons (Trulson and Jacobs 1979). The primary role of 5-HT neurons may thus be to coordinate the activity of target structures in conjuction with the organism's level of behavioral arousal (Jacobs and Azmitia 1992). Viewed in this perspective, early studies on the role of the 5-HT system in cognitive functions can better be apprehended. Such studies, although suggesting that altered serotonergic function affects an organism's ablility to acquire or express novel behaviors, were inconsistent in terms of both predictability and generalizability (Altman and Normile 1988). The current view is that the serotonergic system interacts with other systems, mainly the cholinergic, to regulate electrical activity in the forebrain (Khateb et al. 1993; Vanderwolf 1988; Vanderwolf and Baker 1986; Jacobs and Jones 1978) and learning behavior (Richter-Levin and Segal 1989; Richter-Levin and Segal 1991; Riekkinen Jr et al. 1990; Wenk et al. 1987).

Despite the recognized importance of serotonergic neurotransmission, relatively little is known about 5-HT actions on central mammalian neurons. Early literature on the postsynaptic effects of 5-HT in the CNS reports inhibition as the predominant mechanism

(Assaf and Miller 1978; Haigler and Aghajanian 1974; Segal 1980), however, it has become evident that hyperpolarizing/depolarizing (Andrade and Nicoll 1987) or only depolarizing (Araneda and Andrade 1991; Yakel et al. 1988) responses could be observed, suggesting an excitatory action for 5-HT in addition to its inhibitory action. Another effect of 5-HT has been referred to as a reduction in the signal to noise ratio, or synaptic modulation, whereby afferent induced excitation (Sizer et al. 1992) or inhibition (Waterhouse et al. 1986) is preferentially suppressed by 5-HT.

An important dimension of the postsynaptic effect of 5-HT is the temporal characteristics of its actions, i.e. latency and duration. 5-HT generally seems to exert a long latency and very long duration action on its postsynaptic target neurons. Fast actions of 5-HT, mediated through rapid and transient depolarization following activation of a ligand gated ion channel have, however, been recently described in the CNS (Bobker and Williams 1990; Hoyer et al. 1994). Diversity in the nature (excitatory, inhibitory or modulatory) and temporal characteristics of 5-HT actions are probably mediated by the specific types of 5-HT receptor subtypes affected and the membrane and intracellular biochemical mechanisms that are coupled to them. Physiological, pharmacological, and molecular cloning have revealed an unexpected heterogeneity within 5-HT receptors. To date, 14 different mammalian receptor subtypes have been identified, and classified into 7 groups of receptors (Hoyer et al. 1994; Hoyer and Martin 1996; Saudou and Hen 1994), three of which, the 5-ht_5, 5-ht_6, and 5-ht_7 groups have yet to be fully characterized operationally and transductionally in intact tissues.

The present work was undertaken to complement the investigation of neurotransmitter modulation of the intrinsic electroresponsiveness of medial entorhinal cortex (MEC) layer II neurons, to further our understanding of the possible cellular basis of learning and memory in the entorhinal cortex (EC). As with the cholinergic system (Chap. V), particular attention was payed to serotonergic modulation of the oscillatory and repetitive firing properties of layer II neurons, the stellate (SC) and non-stellate (non-SC)

cells. The observed actions of 5-HT again demonstrate differential modulatory actions of neurotransmitter receptor activation on SCs and non-SCs and further support the view of two parallel information processing channels in layer II of the EC.

METHODS

Brain slices (350 μM) were derived from male Wistar rats (150-250 g) following standard procedures. Dissection methods and recording procedures have been described in detail elsewhere (Chap. III and V). Briefly, after Nembutal (30mg/Kg) anesthesia animals were decapitated, the brain was rapidly removed and a block of tissue containing the retrohippocampal region was placed in a cold (6-10°C) oxygenated Ringer solution (see below). Horizontal slices (350μm) were cut using a vibratome and then allowed to recover at room temperature for at least 2 hours in oxygenated incubation chambers. For recording, a single slice was transferred to a recording chamber, submerged at 35 ± 1°C and superfused with normal Ringer containing (in mM): 124 NaCl; 5 KCl; 1.2 KH_2PO_4; 2.4 $CaCl_2$; 2.6 $MgSO_4$; 26 $NaHCO_3$; and 10 glucose. pH was adjusted to 7.4 by saturating with 95% O2 and 5% CO2. Intracellular glass electrodes were filled with 2-3 M potassium acetate (tip resistance 40-120 MΩ). In order to block Na^+ conductances tetrodotoxin (TTX, 1μM; Calbiochem) was used. 5-Hydroxytryptamine (5-HT, 15-60 μM; Sigma) was added to normal or TTX Ringer and bath applied for variable periods of time ranging from 30 seconds to the entire duration of the experiment.

Electrophysiological parameters were measured as follows: single spike amplitude and fast afterhyperpolarization were measured relative to threshold, in response to the minimum current pulse amplitude eliciting a single spike; the slow afterhyperpolarization following a train of spikes was measured at the termination of the medium afterhyperpolarization, relative to a baseline potential of -62 mV, in response to a current pulse amplitude of 0.7 nA. The dominant frequency of subthreshold membrane potential

oscillations was estimated by computing power spectra of 3 s long traces digitized at 3 kHz. Data are given as mean±standard deviation. Statistical significance was tested according to the two-tailed Student t test.

RESULTS

The present study is based on a a database of 55 neurons from layer II of the MEC, recorded for at least 30 minutes in stable conditions and tested with bath applications of 5-HT. As previously determined (Chaps II, III, and V), neurons fell into the two electrophysiological classes already described, the SCs (n=34) and non-SCs (n=21). 5-HT (15-60 μM) caused modest membrane potential (Vm) changes in SCs and non SCs, always accompanied by decreases in apparent input resistance (Rin). Differences, however, were observed between SCs and non SCs with respect to the variability and sign of the membrane potential changes.

CHARACTERISTICS OF 5-HT ACTION

In non-SCs, 5-HT applied at rest in normal Ringer (-63.5 mV±1.6 mV; n=16) produced a hyperpolarization and a decrease in Rin in 15/16 cells (Fig. 1A), and no change in Vm or Rin in the remaining cell. In TTX Ringer, for a 30 μM concentration of 5-HT (n=18), a hyperpolarization averaging 2.1±0.5 mV, associated with a reduction in Rin of 21±8% was observed (measured at the control Vm; n=14), while no significant response was detected in 4 cells.

In SCs, 5-HT applied at rest in normal Ringer (-62.1±1.8 mV; n=33) produced a variable response wich consisted of a hyperpolarization only (n=13; Fig 2A), a depolarization only (n=8), a depolarization followed by a hyperpolarization to about the control Vm (n=2; Fig. 1B), a hyperpolarization followed by a depolarization to about the control Vm (n=3), no change in Vm but only a change in Rin (n=5; Fig. 1C), and no

significant response (n=2). In all cells responsive to 5-HT a reduction in Rin was observed (Figs 1B, 1C and 2A). In a few cells (n=8) multiple 5-HT applications were performed. These resulted in consistent responses across subsequent applications, except for 3 of the cells in which no change in Vm was initially observed; 2 of those subsequently hyperpolarized and one depolarized in response to 5-HT. In TTX Ringer, for a 30 μM concentration of 5-HT (n=19), hyperpolarizations and concomitant reductions in Rin averaged respectively 2.3±0.9 mV and 27±12% (n=7; not significantly different from those in non-SCs), depolarizations and concomitant reductions in Rin averaged respectively 2.1±1.1 mV and 24±8% (n=6). Biphasic responses (n=3) were not quantified, while in 3 cells no response was exhibited.

A characteristic of the 5-HT response in both SCs and non-SCs was its long duration of action. Even for brief drug perfusions (30 s), 5-HT effects persisted for several minutes, and it generally took more than 10 minutes to totally recover the control membrane properties.

RHYTHMIC PROPERTIES IN STELLATE CELLS

Of particular interest were the effects of 5-HT on the subthreshold membrane potential oscillations and spike clustering phenomenon exhibited by the SCs. As illustrated in Figs. 2, 3, and 4, 5-HT did not abolish the rhythmic membrane and firing properties of SCs, but modulated them by increasing their frequency. In the SC shown in fig. 2A, the Vm was depolarized by d.c current injection to the level where subthreshold oscillations and spike clusters are prominent (shown expanded in 2B, left panel). Perfusion with 5-HT hyperpolarized the Vm by 3 mV, out of the voltage range where oscillatory behavior is exhibited. Restoring the Vm to the control level by d.c. current injection showed that the subthresold oscillations were still present (Fig. 2B, middle panel); their frequency, however, was increased (almost doubled) from 11.5 Hz to 21.0 Hz. In another SC, shown in normal Ringer at the level of the most prominent oscillatory level (Fig.3A, left) 5-HT

increased the frequency of the subthreshod oscillations from 8.6 to 14.2 Hz (Fig. 3B, left). This frequency increase occured over the entire voltage range where subthreshold Vm oscillations are exhibited, as shown in the graph of Fig 4A (same cell as in Fig. 3). In the same cell, held in normal Ringer at the level of conspicuous spike clustering (Fig. 3A, right), 5-HT was seen to increase the frequency of inter- and intra- spike clustering (Fig. 3B, right) whith the result that clustering appeared to be more pronounced. Preservation of clusters and the increase in their frequency of occurrence (inter-cluster frequency) were also seen over the entire voltage range examined (Fig 4B). Modulation of the frequency of rhythmic behavior was observed in all cells responsive to 5-HT. On average, 5-HT increased the frequency of subthreshold membrane potential oscillations by 65% from 8.5±1.9 Hz to 14.0±3.5 Hz (n=15).

SPIKE TRAIN AND ACTION POTENTIAL PROPERTIES

As already briefly mentioned in Chap. V, 5-HT produced differential effects on spike-train adaptation and the associated slow afterhyperpolarization (sAHP) following the train of spikes in SCs and non-SCs. In SCs, 5-HT reduced adaptation and the sAHP in every cell examined (Fig. 5A), irrespective of the sign of membrane potential changes induced. This effect, however, was only observed in response to intermediate and large current-pulse amplitudes (larger than about 0.4 nA). On average, 5-HT reduced the sAHP (see methods for evaluation of sAHP amplitude) by 73%, from 4.7±2.4 to 1.4±0.9 (n=9), even though more spikes were elicited in 5-HT in response to the same current pulse as in control. Contrary to the case with SCs, in non-SCs, 5-HT never affected the spike-train adaptation nor the sAHP for all current-pulse amplitudes considered. (fig 5B).

In SCs and non-SCs, 5-HT affected the single spike action potential waveform and fast afterhyperpolarization (fAHP) in a similar manner (see methods for evaluation of fAHP amplitude). In 18/24 SCs and in 9/15 non-SCs the fAHP was reduced (by 43±7% in SCs, n=18; by 40±8% in non-SCs, n=9), and the spike duration increased. This increase in

spike duration solely resulted from a reduced rate of action potential repolarization, since no significant 5-HT effect was detected on action potential amplitude and rate of rise (Fig. 5C).

DISCUSSION

The results presented in this chapter reveal rather feeble effects of 5-HT on the intrinsic membrane properties of MEC layer II neurons, in accordance with the proposed modulatory role of the serotonergic system in brain function. Although modest, 5-HT actions were specific and differentially regulated various aspects of the SCs' and non-SCs' electroresponsiveness.

In SCs, 5-HT caused a variable membrane response consisting of a hyperpolarization and/or depolarization of a few millivolts associated with an apparent input resistance decrease, while in non-SCs, 5-HT produced only the hyperpolarizing response. In both SCs and non-SCs, a small number of cells were unresponsive to 5-HT. These characteristics agree well with previous reports of 5-HT actions in the CNS. Although some purely hyperpolarizing responses have been described (Khateb et al. 1993; Aghajanian and Lakoski 1984; Leonard and LLinás 1994; Luebke et al. 1992), mixed and/or biphasic responses to 5-HT prevail in the hippocampus proper (Andrade and Nicoll 1987; Colino and Haliwell 1987; Yakel et al. 1988), the dentate gyrus (Baskys et al. 1989), the neocortex (Andrade and Chaput 1991a; Araneda and Andrade 1991) and subcortical nuclei (Bobker and Williams 1989; Stevens et al. 1992; Yakel et al. 1988). Nearly all these studies recounted a small proportion of 5-HT insensitive cells.

As with the case with SCs and non-SCs of the MEC, all the above-mentioned 5-HT hyperpolarizing responses were accompanied by an increase in apparent input conductance. This 5-HT inhibitory effect has been shown in other cells to result from activation of the 5-HT_{1A} receptor subtype mediating an increase in an inwardly rectifying

potassium current (Andrade and Chaput 1991a; Hoyer et al. 1994). Depolarizing 5-HT responses have been shown to be associated either with a conductance decrease resulting from inhibition of Ca^{2+} dependent and Ca^{2+} independent potassium conductances (Andrade and Nicoll 1987; Araneda and Andrade 1991; Colino and Haliwell 1987; Davies et al. 1987; Sheldon and Aghajanian 1991), or with a conductance increase (Stevens et al. 1992; Yakel et al. 1988), resulting from enhancement of the mixed cationic, hyperpolarization activated inward rectifier Ih (Bobker and Williams 1989; Larkman and Kelly 1992; McCormick and Pape 1990). A variety of 5-HT receptor subtypes including the $5HT_{2A}$, $5HT_{2C}$, $5HT_4$ and a subtype of the $5HT_1$ have been proposed for the mediation of the 5-HT depolarization. In the present study, ionic mechanisms of the 5-HT depolarizing response exhibited by SCs were not investigated, however, the apparent input resistance decrease associated with the 5-HT depolarization, coupled to the presence, in SCs, of a prominent Ih current (Chap. IV) could suggest a modulation by 5-HT of the mixed cationic inward rectifier in SCs. Although the exact identity of the 5-HT receptor subtype and the associated second messenger pathway modulating Ih are still unresolved (Bobker and Williams 1990; however see McCormick and Pape 1990; Takahashi and Berger 1990), an increase in intracellular cyclic adenosine monophosphate (cAMP) was found to mimic the 5-HT depolarization and modulation of Ih. In SCs, perfusion with membrane permeant analogs of cAMP (Chap. V) did not induce any membrane depolarization while still affecting other parameters known to be cAMP-sensitive (see later in the discussion).

In an attempt to pharmacologically isolate the 5-HT induced depolarization, preliminary experiments with the compound 2-methyl-5-HT were performed. While 2-methyl-5HT is regarded as the prototypical $5\text{-}HT_3$ receptor subtype agonist, activating a ligand gated ion channel to mediate a rapid depolarization, it can also bind with relatively high affinity to $5\text{-}HT_4$ receptors positively coupled to adenylyl cyclase, whose activation generally results in a slow depolarization (Hoyer et al. 1994). Perfusion with 2-methyl-5-

HT in SCs caused a response as variable as that of 5-HT (n=13), including depolarizations (n=4), hyperpolarizations (n=3), no change in Vm (n=3), and no response (n=3). In non-SCs, no response to 2-methyl-5-HT was observed (n=4). The absence of clear cut effects can probably be explained by the recent observation that 2-methyl-5-HT can also inhibit neuronal firing through 5-HT_{1A} receptor activation (Haddjeri and Blier 1995). The nature of the 5-HT induced depolarization in SCs thus remains to be investigated.

Not surprisingly, 5-HT was found to affect the rhythmic properties of SCs. In essence, this modulation was exactly opposite to that of the cholinergic agonist carbachol (Chap. V). 5-HT increased the frequency of the subthreshold membrane potential oscillations, accentuated spike clustering, and increased the instantaneous firing frequency within each cluster. This 5-HT effect does not seem to result from a non-specific effect such as decreased membrane time constant due to the Rin decrease observed with 5-HT, but rather to a specific conductance change. This is indicated by the fact that in the above mentioned experiments, when 2-methyl-5-HT produced a depolarization accompanied by a decrease in Rin, no change in the frequency of the subthreshold oscillations was observed (n=2).

While the importance of the ascending cholinergic system in regulating specific aspects of electroencephalographic activity and behavior is no longer to be demonstrated (see Chap. V), the exact role of the ascending serotonergic projections in this respect has been difficult to define. In behaving animals, neocortical fast activity and limbic theta rhythm persist following blockade of central muscarinic cholinergic transmission, and evidence suggests that this type of activity may depend on serotonergic input (reviewed in Vanderwolf 1988). Nevertheless, studies involving pharmacological manipulations of 5-HT transmission have reported contradictory findings on modulation of hippocampal theta (Robertson et al. 1991; Vertes et al 1994). In addition, depletion of forebrain 5-HT was found to have little effect on the frequency and morphology of hippocampal theta (Vanderwolf et al. 1989) and on behavioral tasks requiring intact hippocampal function

(Richter-Levin and Segal 1989; Riekkinen Jr et al. 1990). Here, the increase in frequency of the SCs' rhythmic activity following serotonergic receptor activation, mirrored, in every respect, the decrease effected by cholinergic receptor activation. While, at present, the specific link between limbic theta or fast activity and the 5-HT system is not entirely clear, the present study suggests that layer II neurons of the EC possess the ability to tightly regulate emergent network oscillatory properties, depending on the relative importance of cholinergic and serotonergic tone during various brain states.

In both SCs and non-SCs, 5-HT was found to affect action potential waveform by reducing the fAHP and increasing spike duration. 5-HT actions on potassium currents responsible for action potential repolarization have not been described. 5-HT, however, was observed to decrease high voltage activated Ca^{2+} currents (Foehring 1996). A reduction in Ca^{2+} currents is expected to inhibit Ca^{2+}-dependent K^+ currents and therefore to reduce the fAHP and increase action potential duration.

5-HT, unexpectedly, was found to modulate spike-train adaptation and associated sAHP in SCs but not in non-SCS. The negative finding in non-SCS is surprising since the I_{AHP} current underlying adaptation and sAHP is a ubiquitous target for serotonin regulation in the vertebrate CNS (hippocampus: Andrade and Nicoll 1987; dentate gyrus: Baskys et al. 1989; association cortex: Araneda and Andrade 1991; piriform cortex: Sheldon and Aghajanian 1991; human neocortex: McCormick and Williamson 1989). In addition to serotonin, all other monoamines including norepinephrine (McCormick and Williamson 1989), dopamine (Pedarzani and Storm 1995) and histamine (Haas and Konnerth 1983), also suppress I_{AHP}. I_{AHP} regulation at the cortical level was thus postulated as the principal mechanism by which the ascending monoaminergic systems change the functional state of the brain (Nicoll et al. 1990). The effect of monoamines on I_{AHP} is known to be mediated via channel phosphorylation, following a rise in cAMP and subsequent activation of protein kinase A (Pedarzani and Storm 1993; Pedarzani and Storm 1995; Torres et al. 1995).

In non-SCs, it cannot be argued that insensitivity of the sAHP to 5-HT solely results from absence, in those cells, of the serotonergic receptor subtype positively linked to adenylyl cyclase that would modulate I_{AHP} ($5HT_4$: Andrade and Chaput 1991b). Increasing intracellular cAMP directly by perfusion with membrane permeant analogs of cAMP and thus bypassing neurotransmitter receptor activation did not affect adaptation and sAHP in non-SCs while it suppressed both in SCs (Chap. V). It therefore seems that, in non-SCs, the dogma that monoamines increase cortical excitability by suppressing the main current responsible for limiting responsiveness to sustained stimuli does not hold. Recalling that cholinergic receptor activation drastically affected spike train characteristics in non-SCs but not in SCs (Chap. V) the present finding again points to additional potential for control, by layer II neurons, of network dynamics, depending on the specific interactions between cholinergic and serotonergic systems.

REFERENCES

Aghajanian, G. K. and Lakoski, J. M. Hyperpolarization of serotonergic neurons by serotonin and LSD; studies in brain slices showing increased K^+ conductance. *Brain Res.* 305: 181-185, 1984.

Altman, H. J. and Normile, H. J. What is the nature of the role of the serotonergic nervous system in learning and memory: prospects for development of an effective treatment strategy for senile dementia. *Neurobiol. Aging.* 9: 627-638, 1988.

Andrade, R. and Chaput, Y. The electrophysiology of serotonin receptor subtypes. In: *Serotonin Receptor Subtypes: Basic and clinical aspects*, edited by S. J. Peroutka. New-York: Wiley-Liss, Inc., 1991a, 103-124

Andrade, R. and Chaput, Y. 5-hydroxytryptamine$_4$-like receptors mediate the slow excitatory response to serotonin in the rat hippocampus. *J. Pharmacol. Exp. Ther.* 257: 930-937, 1991b.

Andrade, R. and Nicoll, R. A. Pharmacologically distinct actions of serotonin on single pyramidal neurones of the rat hippocampus recorded *in vitro*. *J. Physiol.* 394: 99-124, 1987.

Araneda, R. and Andrade, R. 5-Hydroxytryptamine$_2$ and 5-hydroxytryptamine$_{1A}$ receptors mediate opposing responses on membrane excitability in rat association cortex. *Neuroscience.* 40: 399-412, 1991.

Assaf, S. Y. and Miller, J. J. The role of a raphe serotonin system in the control of septal unit activity and hippocampal desynchronization. *Neuroscience.* 3: 539-550, 1978.

Baskys, A., Niesen, C. E., Davies, M. F., and Carlen, P. L. Modulatory actions of serotonin on ionic ocnductances of hippocampal dentate granule cells. *Neuroscience.* 29: 443-451, 1989.

Bobker, D. H. and Williams, J. T. Serotonin augments the cationic current I_h in central neurons. *Neuron.* 2: 1535-1540, 1989.

Bobker, D. H. and Williams, J. T. Ion conductances affected by 5-HT receptor subtypes in mammalian neurons. *Trends Neurosci.* 13: 169-173, 1990.

Colino, A. and Haliwell, J. V. Differential modulation of three separate K-conductances in hippocampal CA1 neurons by serotonin. *Nature (London).* 328: 73-77, 1987.

Davies, F. M., Deisz, R. A., Prince, D. A., and Peroutka, S. J. Two distinct effects of 5-hydroxytryptamine on single cortical neurons. *Brain Res.* 423: 347-352, 1987.

Foehring, R. C. Serotonin modulates N- and P- type calcium currents in neocortical pyramidal neurons via a membrane-delimited pathway. *J. Neurophysiol.* 75: 648-659, 1996.

Haas, H. L. and Konnerth, A. Histamine and noradrenaline decrease calcium-activated potassium conductance in hippocampal pyramidal cells. *Nature (London).* 302: 432-434, 1983.

Haddjeri, N. and Blier, P. Pre- and post-synaptic effects of the 5-HT_3 agonist 2-methyl-5-HT on the 5-HT system in the rat brain. *Synapse.* 20: 54-67, 1995.

Haigler, H. J. and Aghajanian, G. K. Lysergic acid diethylamide and serotonin: a comparison of effects on serotonergic neurons and neurons receiving a serotonergic input. *J. Pharmacol. Exp. Ther.* 188: 688-699, 1974.

Hoyer, D., Clarke, D. E., Fozard, J. R., Hartig, P. R., Martin, G. R., Mylecharane, E. J., Saxena, P. R., and Humphrey, P. A. International union of pharmacology classification of receptors for 5-hydroxytryptamine (serotonin). *Pharmacol. Rev.* 46: 157-203, 1994.

Hoyer, D. and Martin, G. R. Classification and nomenclature of 5-HT receptors: a comment on current issues. *Behav. Brain Res.* 73: 263-268, 1996.

Jacobs, B. L. and Azmitia, E. C. Structure and function of the brain serotonin system. *Physiol. Rev.* 72: 165-229, 1992.

Jacobs, B. L. and Jones, B. E. The role of central monoamine and acetylcholine systems in sleep-wakefulness states: mediation or modulation. In: *Cholinergic-Monoaminergic Interactions in the Brain*, edited by L. L. Butcher. New-York: Academic Press, 1978, 271-290.

Khateb, A., Fort, P., Alonso, A., Jones, B. E., and Mühlethaler, M. Pharmacological and immunohistochemical evidence for serotonergic modulation of cholinergic nucleus basalis neurons. *Eur. J. Neurosci.* 5: 541-547, 1993.

Larkman, P. M. and Kelly, J. S. Ionic mechanisms mediating 5-hydroxytryptamine- and noradrenaline-evoked depolarization of adult rat facial motoneurones. *J. Physiol. (London).* 456: 473-490, 1992.

Leonard, C. S. and LLinás, R. Serotonergic and cholinergic inhibition of mesopontine cholinergic neurons controlling REM sleep: an *in vitro* electrophysiological study. *Neuroscience.* 59: 309-330, 1994.

Luebke, J. I., Greene, R. W., Semba, K., Kamondi, A., McCarley, R. W., and Reiner, P. B. Serotonin hyperpolarizes cholinergic low-threshold burst neurons in the rat laterodorsal tegmental nucleus *in vitro*. *Proc. Natl. Acad. Sci. USA.* 89: 743-747, 1992.

McCormick, D. and Pape, H.-C. Noradrenergic and serotonergic modulation of a hyperpolarization-activated cation current in thalamic relay neurones. *J. Physiol. (London).* 431: 319-342, 1990.

McCormick, D. A. and Williamson, A. Convergence and divergence of neurotransmitter action in human cerebral cortex. *Proc. Natl. Acad. Sci. USA.* 86: 8098-8102, 1989.

Meltzer, H. Multiple roles and actions of serotonin systems. *J. Clin. Psychiatry.* 52: (suppl) 3, 1991.

Nicoll, R. A., Malenka, R. C., and Kauer, J. A. Functional comparison of neurotransmitter receptor subtypes in mammalian central nervous system. *Physiol. Rev.* 70: 513-565, 1990.

Pedarzani, P. and Storm, J. F. PKA mediates the effects of monoamine transmitters on the K^+ current underlying the slow spike frequency adaptation in hippocampal neurons. *Neuron.* 11: 1023-1035, 1993.

Pedarzani, P. and Storm, J. F. Dopamine modulates the slow Ca^{2+}-activated K^+ current I_{AHP} via cyclic AMP-dependent protein kinase in hippocampal neurons. *J. Neurophysiol.* 74: 2749-2753, 1995.

Richter-Levin, G. and Segal, M. Spatial performance is severely impaired in rats with combined reduction of serotonergic and cholinergic transmission. *Brain Res.* 477: 404-407, 1989.

Richter-Levin, G. and Segal, M. The effects of serotonin depletion and raphe grafts on hippocampal electrophysiology and behavior. *J. Neurosci.* 11: 1585-1596, 1991.

Riekkinen Jr, P., Sirviö, J., and Riekkinen, P. Interaction between raphe dorsalis and nucleus basalis magnocellularis in spatial learning. *Brain Res.* 527: 342-345, 1990.

Robertson, B., Baker, G. B., and Vanderwolf, C. H. The effects of serotonergic stimulation on hippocampal and neocortical slow waves and behavior. *Brain Res.* 555: 265-275, 1991.

Saudou, F. and Hen, R. 5-Hydroxytryptamine receptor subtypes in vertebrates and invertebrates. *Neurochem. Int.* 25: 503-532, 1994.

Segal, M. The action of serotonin in the rat hippocampal slice preparation. *J. Physiol.* 303: 432-439, 1980.

Sheldon, P. and Aghajanian, G. K. Excitatory responses to serotonin (5-HT) in neurons of the rat prirform cortex: evidence for mediation by 5-HT_{1C} receptors in pyamidal cells and 5-HT_2 receptors in interneurons. *Synapse.* 9: 208-218, 1991.

Sizer, A. R., Kilpatrick, G. J., and Roberts, M. H. T. A post-synaptic depressant modulatory action of 5-hydroxytryptamine on excitatory amino acid responses in rat entorhinal cortex *in vitro*. *Neuropharmacology.* 31: 531-539, 1992.

Stevens, D. R., McCarley, R. W., and Greene, R. W. Serotonin$_1$, and serotonin$_2$ receptors hyperpolarize and depolarize separate populations of medial pontine reticular formation neurons *in vitro*. *Neuroscience*. 47: 545-553, 1992.

Takahashi, T. and Berger, A. J. Direct excitation of rat spinal motoneurones by serotonin. *J. Physiol. (London)*. 423: 63-76, 1990.

Törk, I. Anatomy of the serotonergic system. *Ann. NY Acad. Sci.* 600: 9-35, 1990.

Torres, G. E., Chaput, Y., and Andrade, R. Cyclic AMP and Protein Kinase A mediate 5-hydroxytryptamine type 4 receptor regulation of calcium-activated potassium current in adult hippocampal neurons. *Molecular Pharmacol.* 47: 191-197, 1995.

Trulson, M. E. and Jacobs, B. L. Raphe unit activity in freely moving cats: correlation with level of behavioral arousal. *Brain Res.* 163: 135-150, 1979.

Vanderwolf, C. H. Cerebral activity and behavior: control by central cholinergic and serotoninergic systems. *Int. Rev. Neurobiol.* 30: 225-340, 1988.

Vanderwolf, C. H. and Baker, G. B. Evidence that serotonin mediates non-cholinergic neocortical low voltage fast activity, non cholinergic hippocampal rhythmical slow activity and contributes to intelligent behavior. *Brain Res.* 374: 342-356, 1986.

Vanderwolf, C. H., Leung, L. W. S., Baker, G. B., and Stewart, D. J. The role of serotonin in the control of cerebral activity: studies with intracerebral 5,7-dihydroxytryptamine. *Brain Res.* 504: 181-191, 1989.

Vertes, R. P., Kinney, G. G., Kocsis, B., and Fortin, W. J. Pharmacological suppression of the median raphe nucleus with serotonin1A agonists, 8-OH-DPAT and buspirone, produces hippocampal theta rhythm in the rat. *Neuroscience.* 60: 441-451, 1994.

Waterhouse, B. D., Moises, H. C., and Woodward, D. J. Interaction of serotonin with somatosensory cortical neuronal responses to afferent synaptic inputs and putative neurotranmitter. *Brain Res. Bull.* 17: 507-518, 1986.

Wenk, G., Hughey, D., Boundy, V., Kim, A., Walker, L., and Olton, D. Neurotransmitters and memory: role of cholinergic, serotonergic, and noradrenergic systems. *Behav. Neurosci.* 101: 325-332, 1987.

Yakel, J. L., Trussel, L. O., and Jackson, M. B. Three serotonin responses in cultured mouse hippocampal and striatal neurons. *J. Neurosci.* 8: 1273-1285, 1988.

Figure 1. 5-HT induced effects in SCs and non-SCs. *A*: In a non-SC, bath application of 5-HT (30 μM) for the duration indicated by bar, caused a hyperpolarization of 3 mV and a decrease in Rin of 25%, as assessed at the control membrane potential. Trace interrupted for duration indicated under dashed bar. *B*: In a SC, 5-HT (15 μM) caused a biphasic response consiting of a depolarization of 2.5 mV followed by a hyperpolarization to the control membrane potential. The Rin decrease was 33% when assessed at the control membrane potential, just before trace interruption. *C*: In another SC, 5-HT (30 μM) perfusion resulted in no change in the membrane potential. Rin decrease was 25%.

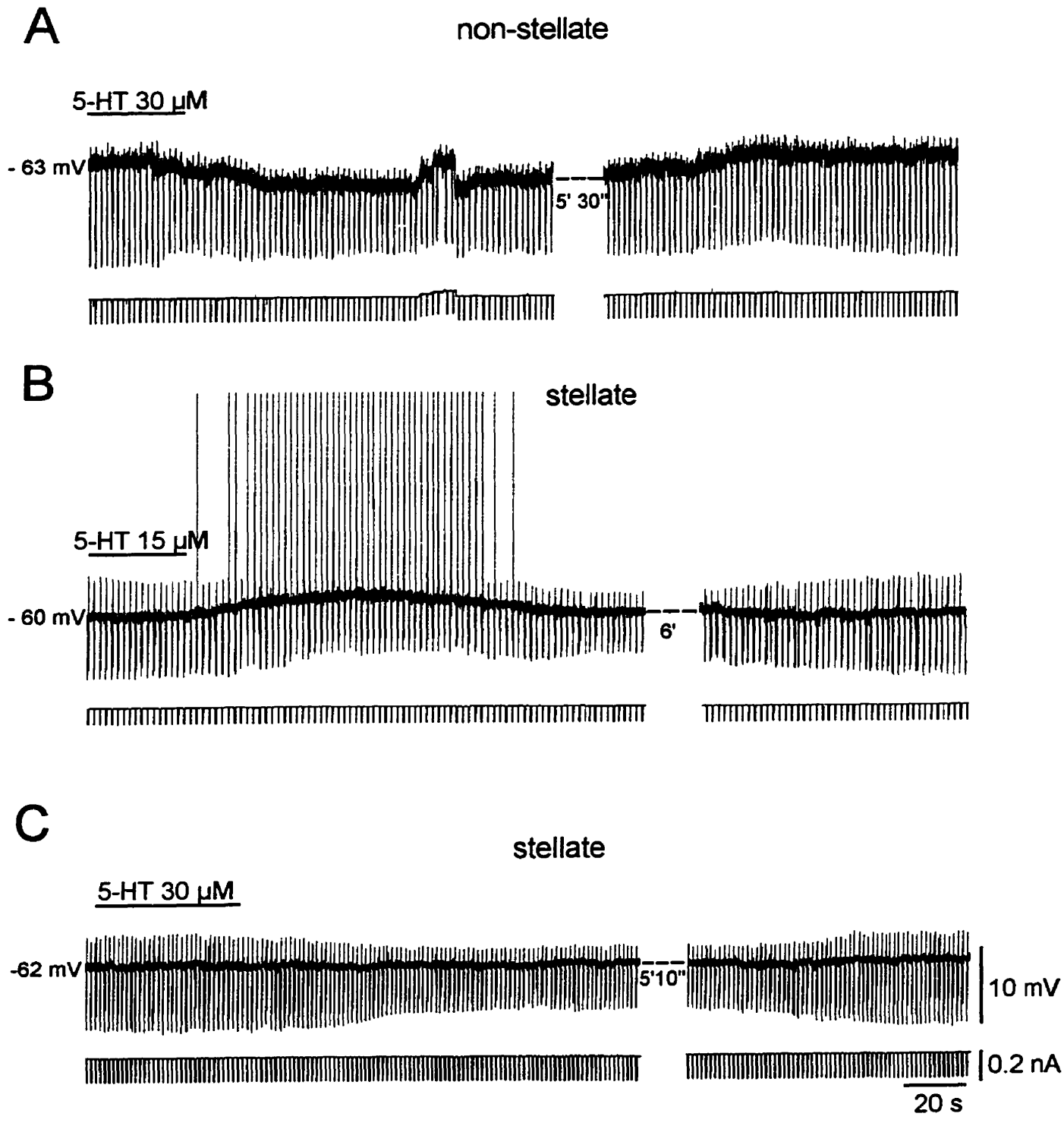
A
non-stellate
5-HT 30 µM
- 63 mV
5' 30"
B
stellate
5-HT 15 µM
- 60 mV
6'
C
stellate
5-HT 30 µM
-62 mV
5'10"
10 mV
0.2 nA
20 s

Figure 2. In SCs, 5-HT does not abolish rhythmic activity. *A*: In a SC held at the membrane potential where subthreshold oscillations and spike clusters are prominent, 5-HT (30 μM) produced a 3 mV hyperpolarization. At this hyperpolarized membrane potential subthreshold oscillations where no longer present as shown by the reduced noise in the recording. Depolarization to the control level by d.c. current injection restored rhythmic activity (arrow at 2). *B*: Expanded traces at moments indicated by arrows in *A*. Before 5-HT, membrane potential oscillations at a frequency of 11.5 Hz are interspersed with spike clusters (left). During 5-HT, d.c. depolarization to control level revealed that the frequency of the membrane potential oscillations increased to 21.0 Hz. Rin decrease was 24% (middle). Following washout of 5-HT, frequency of subthreshold oscillations is restored back to control levels (right).

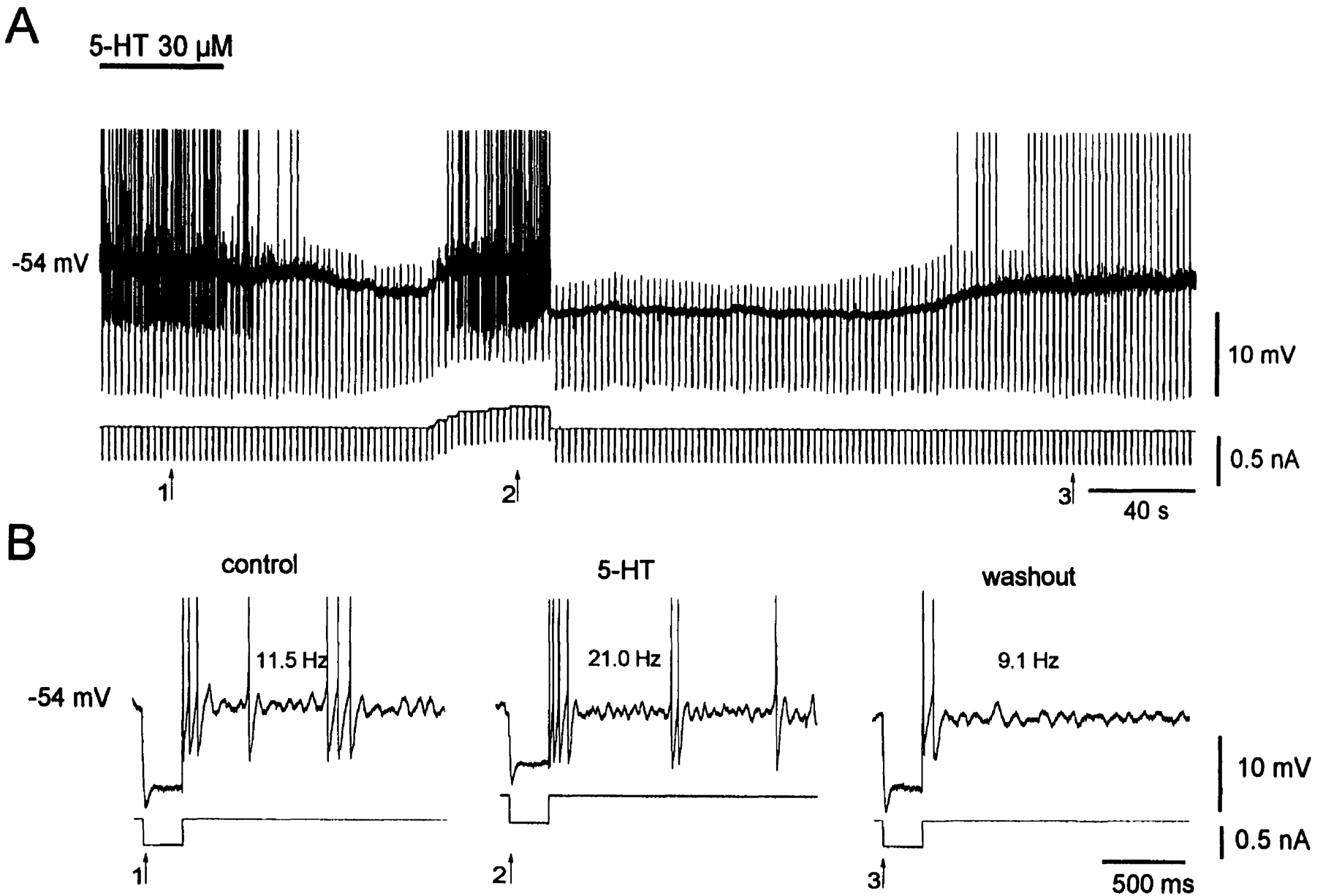
A
5-HT 30 µM
-54 mV
10 mV
0.5 nA
1
2
3
40 s
B
control
5-HT
washout
11.5 Hz
21.0 Hz
9.1 Hz
-54 mV
10 mV
0.5 nA
1
2
3
500 ms

Figure 3. 5-HT increases the frequency of all aspects of rhythmic activity in SCs. *A*: In normal Ringer, a SC held at - 53 mV by d.c. current injection displays subtrheshold membrane potential oscillations at a frequency of 8.6 Hz (left). At -52 mV the same SC exhibits conspicuous spike clustering (right). *B*: During perfusion with 5-HT (30 μM), the frequency of subthreshold oscillations is raised to 14.2 Hz, measured at the same membrane potential as in control (left). In 5-HT, spike clusters are preserved and appear even more prominent. Within clusters, instantaneous firing frequency is increased, and between clusters, frequency of occurrence of clusters is increased, relative to control (right). *C*: Following washout of 5-HT, frequency of rhythmic activity is restored to about control levels.

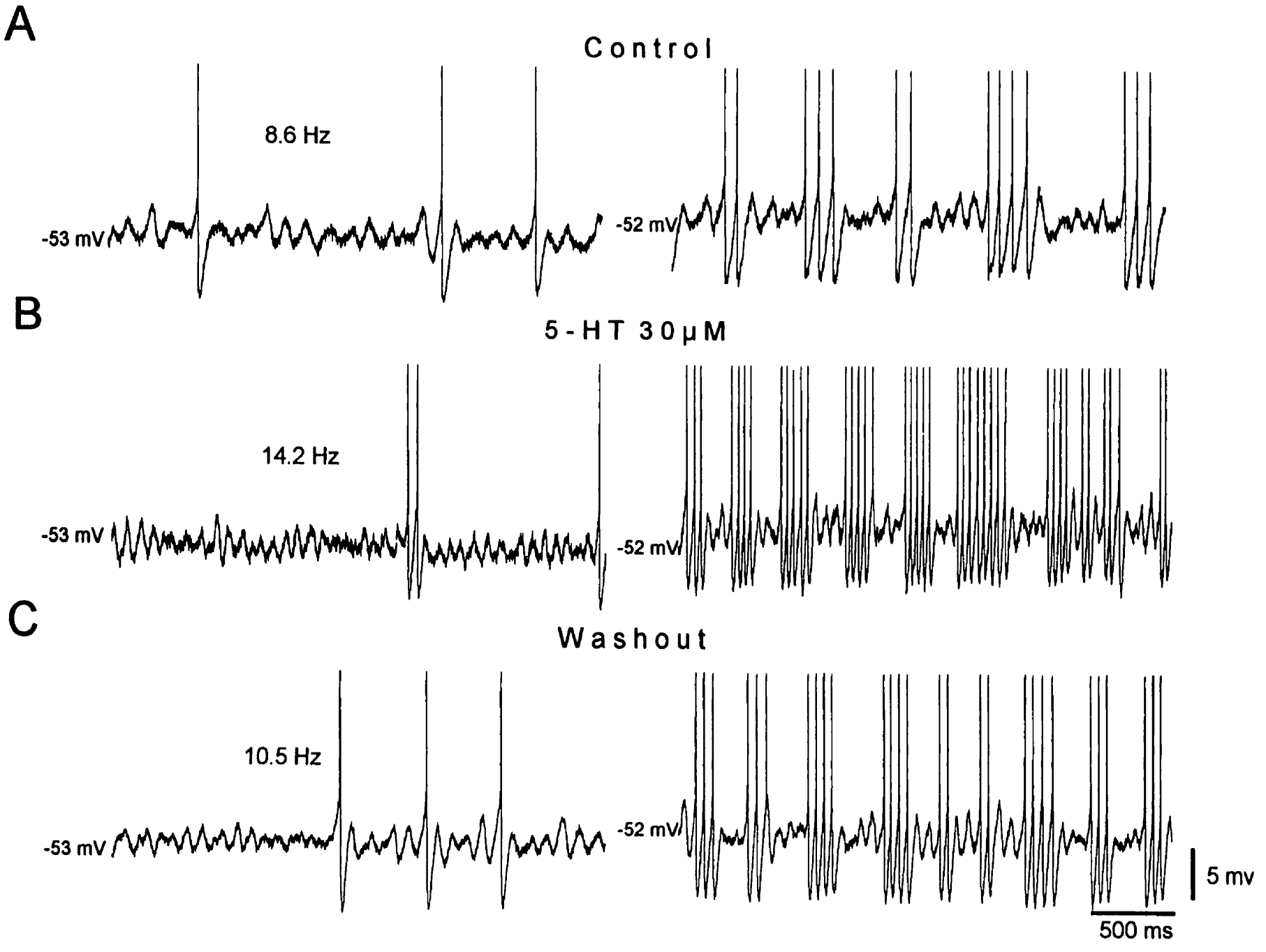
A
Control
8.6 Hz
-53 mV
-52 mV
B
5-HT 30µM
14.2 Hz
-53 mV
-52 mV
C
Washout
10.5 Hz
-53 mV
-52 mV
5 mv
500 ms

Figure 4. 5-HT-induced increase in frequency occurs over the entire voltage range over which rhythmic activity is displayed. *A*: In the same SC as in Fig. 3, frequency of subthreshold membrane potential oscillations *versus* membrane potential in control (●) and 5-HT (▲). *B*: Frequency of occurrence of spike clusters (intercluster frequency) *versus* membrane potential measured over a 3 s period in control (●) and 5-HT (▲).

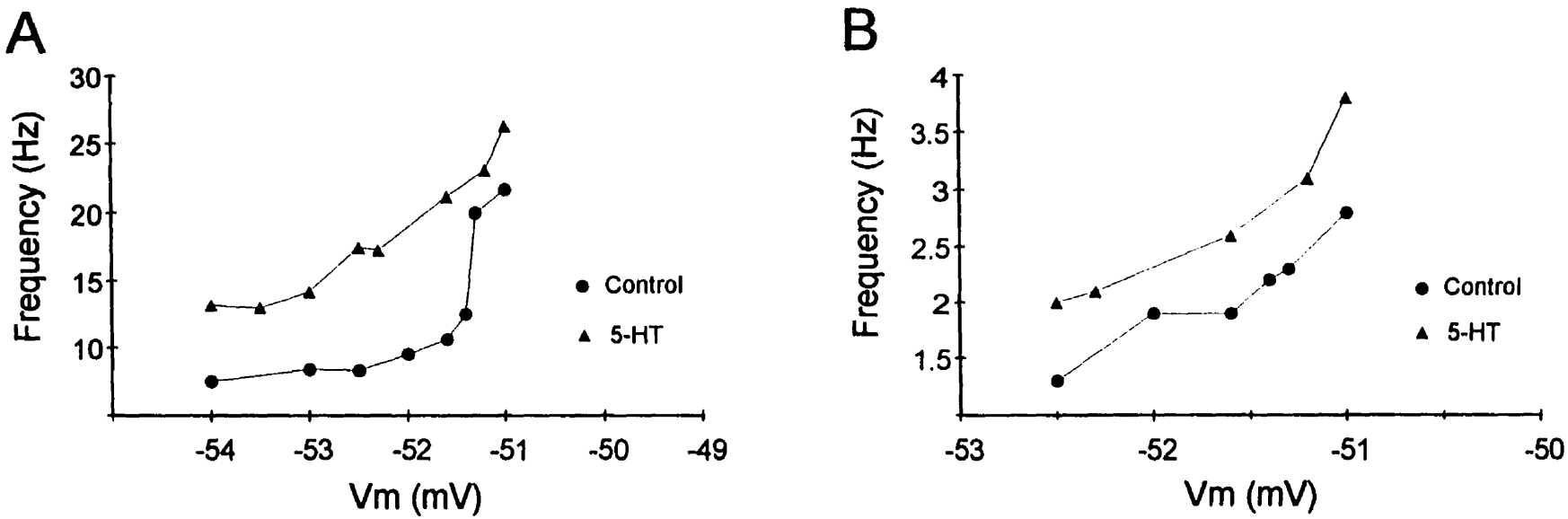
A
Frequency (Hz)
30
25
20
15
10
-54
-53
-52
-51
-50
-49
Vm (mV)
Control
5-HT
B
Frequency (Hz)
4
3.5
3
2.5
2
1.5
-53
-52
-51
-50
Vm (mV)
Control
5-HT

Figure 5. 5-HT effects on single spike and spike train characteristics. *A*: In a SC, 5-HT (15 μM) suppressed the prominent adaptation in firing frequency exhibited in response to a 0.8 nA current pulse, and reduced the sAHP following the train of spikes from 8.7 mV to 4.3 mV, even though many more spikes were elicited in 5-HT in response to the same current pulse. *B*: In a non-SC, 5-HT (30 μM) affected neither adaptation nor sAHP in response to a 0.5 nA current pulse. *C*: In a SC (top) and a non SC(bottom), 5-HT decreased fAHP and increased spike duration without affecting spike amplitude and rate of rise. 5-HT trace delimited by arrow. A single spike was elicited in response to a threshold current pulse in control and 5-HT.

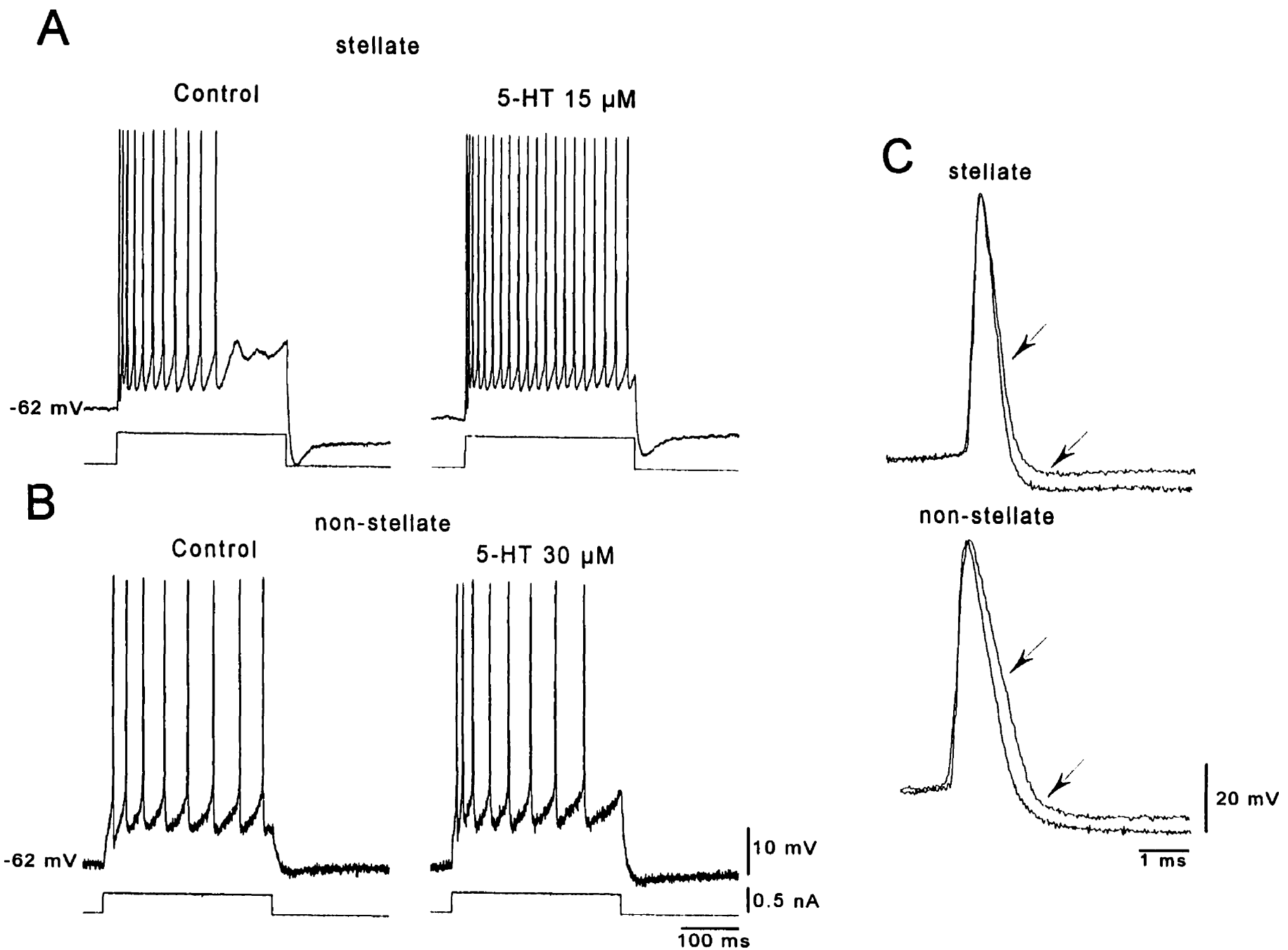
A
stellate
Control
5-HT 15 μM
-62 mV
B
non-stellate
Control
5-HT 30 μM
-62 mV
10 mV
0.5 nA
100 ms
C
stellate
non-stellate
20 mV
1 ms

CHAPTER VIII

GENERAL CONCLUSIONS AND DISCUSSION

The main objective of the present work was to determine the intrinsic electrophysiological properties of medial entorhinal cortex layer II neurons, to refine our understanding of the role of the entorhinal cortex within the medial temporal lobe. It was found that layer II neurons are endowed with a rich intrinsic electroresponsiveness which invalidates the notion that they are simple relay cells linking the neocortex to the hippocampal formation. In addition, the cellular mechanisms uncovered may provide a parsimonious explanation as to how the entorhinal cortex would implement the network properties required to achieve the normal and pathological functions it has been linked with.

LAYER II NEURONS CONSTITUTE TWO PARALLEL INFORMATION PROCESSING CHANNELS

This is the main recurring theme concluding each individual section of the present work. Projection neurons fell into two distinct morphological types (Chapter II) each endowed with vastly different electroresponsive properties (Chapter III), each differentially modulated by the cholinergic (Chapter V) and serotonergic (Chapter VII) systems. Without exact knowledge of the respective afferents to, and target structures of, these two channels, and of the synaptic interactions between them, attribution of a precise significance to the presence of those two channels is purely speculative. Yet, it appears as if the processing and integrative capabilities of layer II neurons are compounded, with the result that tremendous potential exists for reshaping of afferent stimuli before they are conveyed to the hippocampal formation.

THE MAJORITY OF LAYER II NEURONS DISPLAY A ROBUST RHYTHMIC BEHAVIOR

The stellate cells, the major constituents of layer II, exhibit subthreshold membrane potential oscillations and a firing pattern constituted by rhythmic spike clusters paced by intervening subthreshold oscillations. This rhythmic behavior is a robust and most likely relevant phenomenon in entorhinal cortex function: once manifested upon depolarization,

it remains sustained; it is present over a broad range of input stimuli; it persists following neurotransmitter receptor activation; its frequency can be modulated by membrane voltage and by neurotransmitters. Relation of rhythmic activity with the limbic theta rhythm has already been discussed (Chapter III and V). Here, it will be considered within the broader issue of the function of temporal correlation in neural activity.

For a long time it was assumed that information was coded by a neurons's mean firing rate (rate code model). An alternate view is presently emerging as a result of new theoretical and experimental approaches, which holds that information is contained in the firing pattern of a neuron (temporal code model) (Ferster and Spruston 1995). It is thus the precise timing of action potential discharge that carries the message. Hopfield (1995) has shown how the presence of an ongoing subthreshold membrane potential oscillation allows a neuron to recode analogue information - for example, a constant input stimulus - into the time domain - a precise firing pattern. The spike clusters displayed by the stellate cells upon d.c. depolarization are such an example. A network of individual encoders such as that constituted by the stellate cells interconnected via the net of recurrent axon collaterals that they possess (Chaper II) may thus implement temporally correlated firing between different stellate cell populations receiving different inputs from sensory and association cortices. Synchronous activity of neuronal populations is viewed and experimentally investigated as an efficient mechanism for binding the multiple, spatially distributed, feature representations extracted by the nervous system, into a unified and coherent experience (Singer and Gray 1995). Similarly, in memory acquisition, binding between multiple aspects of a particular event is needed to constitute a unique memory trace. Stellate cells may thus be perfectly suited to enhance response saliency by promoting synchronous firing within a particular neuronal assembly by the above mentioned mechanism, before transmission to the hippocampus. The frequency modulation effected by neurotransmitters may serve to modulate the degree of synchronization (Lampl and Yarom 1993), which would temporarily engage or disengage individual neurons from a

particular neuronal assembly thus permitting flexibility in the association of neuronal activity.

REFERENCES

Ferster, D. and Spruston, N. Cracking the neuronal code. *Science.* 270: 756-757, 1995.

Hopfield, J. J. Pattern recognition computation using action potential timing for stimulus representation. *Nature.* 376: 33-36, 1995.

Lampl, I. and Yarom, Y. Subthreshold oscillations of the membrane potential: a functional synchronizing and timing device. *J. Neurophysiol.* 70: 2181-2186, 1993.

Singer, W. and Gray, G. Visual feature integration and the temporal correlation hypothesis. *Ann. Rev. Neurosci.* 18: 555-586, 1995.

IMAGE EVALUATION TEST TARGET (QA-3)

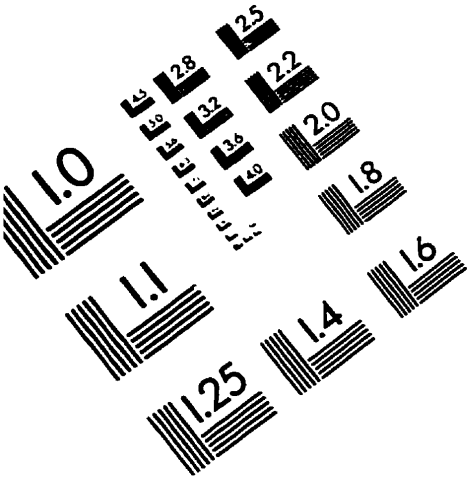

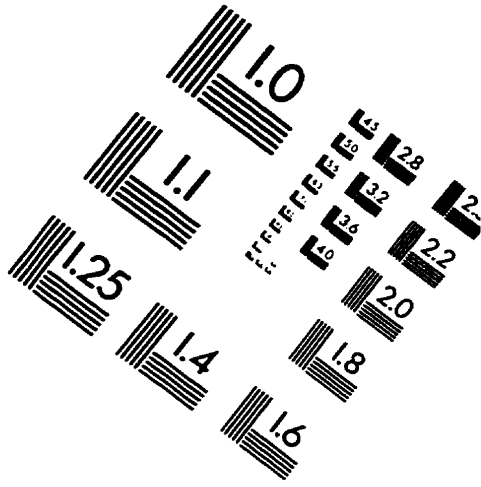

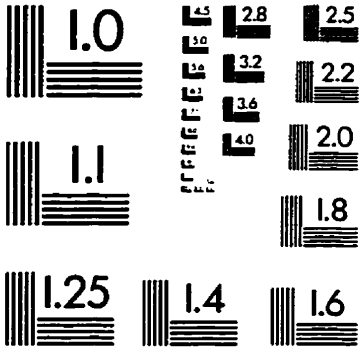

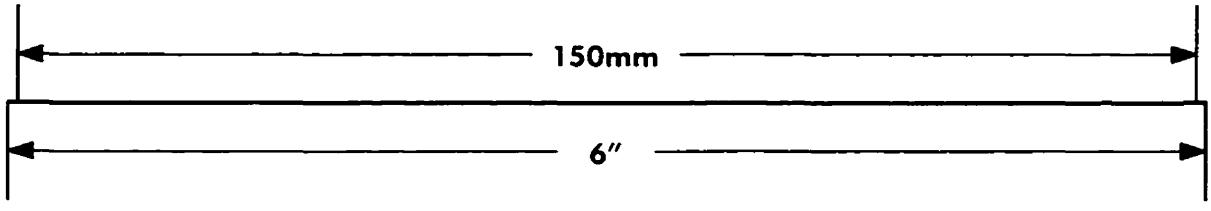

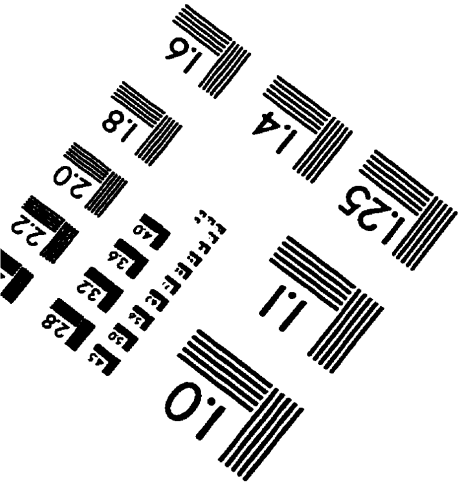

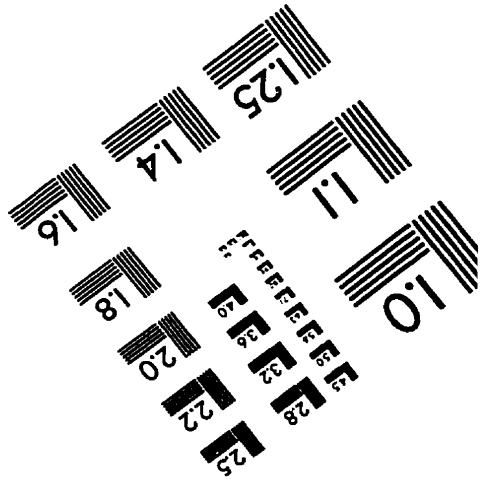

APPLIED IMAGE, Inc
1653 East Main Street
Rochester, NY 14609 USA
Phone: 716/482-0300
Fax: 716/288-5989